F. W. Klaiber, T. J. Wipf, C. M. Streeter

Testing of Old Reinforced Concrete Bridges

December 1997

Sponsored by the
Project Development Division of the
Iowa Department of Transportation and the
Iowa Highway Research Board

Iowa DOT Project HR-390

Iowa Department of Transportation

Final

REPORT

IOWA STATE UNIVERSITY
OF SCIENCE AND TECHNOLOGY

Department of Civil and Construction Engineering

The opinions, findings, and conclusions expressed in this publication are those of the authors and not necessarily those of the Project Development Division of the Iowa Department of Transportation or the Iowa Highway Research Board.

F. W. Klaiber, T. J. Wipf, C. M. Streeter

Testing of Old Reinforced Concrete Bridges

Sponsored by the
Project Development Division of the
Iowa Department of Transportation and the
Iowa Highway Research Board

Iowa DOT Project HR-390

Final

REPORT

IOWA STATE UNIVERSITY
OF SCIENCE AND TECHNOLOGY

Iowa Department of Transportation

Department of Civil and Construction Engineering

ABSTRACT

According to data obtained from the National Bridge Inventory (NBI), there are over 12,000 reinforced concrete bridges within the state of Iowa on the county road system. Of these 12,000 bridges, over 1,900 are considered structurally deficient based on traditional analytical rating methods. Current rating practices are based on the procedures outlined in the Manual for Maintenance Inspection of Bridges [1] which typically underestimate the load carrying capacity of existing bridges. Since the cost of replacing all these bridges is prohibitive, a procedure needs to be incorporated which gives a more accurate assessment of each bridges actual safe load carrying capacity. The objective of this research project was to service load test a representative sample of old reinforced concrete bridges (some them historic and some of them scheduled for demolition so that individual components could be obtained for laboratory testing) with the results being used to create a database so the performance of similar bridges could be predicted.

The types of bridges tested included two reinforced concrete open spandrel arches, two reinforced concrete filled spandrel arches, one reinforced concrete slab bridge, and one two span reinforced concrete stringer bridge. The testing of each bridge consisted of applying a static load at various locations on the bridges and monitoring strains and deflections in critical members. The load was applied by means of a tandem axle dump truck with varying magnitudes of load. At each load increment, the truck was stopped at predetermined transverse and longitudinal locations and strain and deflection data were obtained. The strain data obtained were then evaluated in relation to the strain values predicted by traditional analytical procedures and a carrying capacity of the bridges was determined based on the experimental data.

The response of a majority of the bridges tested was considerably lower than that predicted by analysis. Thus, the safe load carrying capacities of the bridges were greater than that predicted by the analytical models, and in a few cases, the load carrying capacities were found to be three or four times greater than calculated values. However, the test results of one bridge were lower than that predicted by analysis and thus resulted in the analytical rating being reduced. The results of the testing verified that traditional analytical methods, in most instances, are conservative and that the safe load carrying capacities of a majority of the reinforced concrete bridges are considerably greater than what one would determine on the basis of analytical analysis alone.

In extrapolating the results obtained from diagnostic load tests to levels greater than those placed on the bridge during the load test, care must be taken to ensure safe bridge performance at the higher load levels. To extrapolate the load test results from the bridges tested in this investigation, the method developed by Lichtenstein [2] in NCHRP Report 12-28(13)A was used.

TABLE OF CONTENTS

LIST OF FIGURES

LIST OF TABLES

1. INTRODUCTION

1.1. Background

In recent years, due to increases in legal load limits, an increasing number of the nations bridges need to carry loads greater than for which they were designed. To accommodate the heavier traffic, many of the bridges have either been strengthened or replaced. However, in many instances, the heavier traffic has been restricted by load postings. In the evaluation of these bridges, simplified models or conservative analysis techniques were used to determine their structural adequacy. Consequently, some bridges that possessed a reserve load carrying capacity may have been rated structurally inadequate. To obtain a better estimate of a bridge's load carrying capacity, nondestructive load testing is required.

Nondestructive load tests encompass both proof load tests and diagnostic load tests. Proof load tests are full scale load tests in which the structure remains functional during and after the test. This type of test consists of applying a target or predetermined maximum static and/or dynamic load to a given bridge. Testing is terminated when the target load has been reached or when the bridge begins to experience nonlinear behavior. Typically, the behavior of the material in the structure remains within the linear elastic range. Results from this test are used to obtain the maximum static load carrying capacity of the bridge.

Diagnostic tests are full scale load tests which are used to obtain behavioral responses of a bridge's structural components under service load conditions. Static and/or dynamic loading is applied to determine deflections, strains, impact factors, etc. Results from this type of testing are used in conjunction with the analytical rating to establish the load rating of a bridge.

The current bridge rating practice in the United States follows the procedures outlined in the American Association of State Highway Transportation Officials'(AASHTO) Manual for Maintenance Inspection of Bridges [1]. In this manual, bridge rating procedures are based on a thorough field inspection and a detailed analytical rating by a qualified engineer. This manual does not provide any guidelines for determining load capacity by nondestructive load

testing. Physical testing has typically shown that there is significantly greater strength than that predicted by traditional analytical methods.

The use of nondestructive load testing is a procedure that may be used by agencies not specialized in physical bridge testing to improve or remove postings of older bridges. By obtaining dependable estimates of a bridge's load carrying capacity, bridge owners can plan for repair or replacement. The cost of performing these types of tests and allowing the bridge to remain in service is far less than repairing or replacing the given bridge.

Nondestructive load testing is a particularly reliable method in determining the load carrying capacity of older reinforced concrete bridges. Due to the lack of as built bridge plans, the location, type, and size of reinforcement are typically unknown. Because of this, the analytical rating is more of a conservative estimate rather a bridge's actual load carrying capacity. To assess the actual load carrying capacity of Iowa's historic and non-historic reinforced concrete bridges, a questionnaire was sent to county engineers in each of the 99 counties to determine if they had any older reinforced concrete bridges which were scheduled for replacement and could be service load tested. Of the 61 counties that responded to the questionnaire, more than 20 county engineers said they had old reinforced concrete bridges that were scheduled to be replaced in the next five years and could be load tested. An example of the questionnaire used is presented in Appendix A.

1.2. Objective

The overall objective of this research project was to service load test a representative sample of old reinforced concrete bridges and to show that through the use of diagnostic load testing in conjunction with the analytical rating procedures, a more accurate safe load carrying capacity of the bridges could be attained. Also, in the cases of those bridges that were scheduled for replacement, demolition documentation consisting of photographs and video footage would be obtained and the condition of critical components would be assessed. Actual material strengths would be obtained from specimens taken from the demolished bridges.

1.3. Scope

The scope of this investigation involved selecting a minimum of five old reinforced concrete bridges from the counties that responded to the questionnaire. Selection of the bridges was made through consultation with a project advisory committee (PAC). Because the primary objective of this project was to show how diagnostic load testing can be used to estimate a bridge's actual load capacity, various types of concrete bridges were selected for testing. The results obtained could then be applied to as broad a range of bridges as possible.

This investigation also included developing theoretical ratings for each bridge based on standard AASHTO procedures and comparing that with the experimental rating obtained from the service load tests.

In the case of the bridges that were to be removed, a thorough inspection of critical components and tests to determine material strengths were conducted. The field inspection included assessing extent of corrosion and loss of section of reinforcing, concrete deterioration and cover, condition of connections, and loss of bond between concrete and reinforcing steel. Because the primary concern of this project was the superstructure, the condition and load carrying capacity of the substructure was not considered in the overall assessment of the bridge's actual load carrying capacity.

1.4. Research Program

From consulting with the PAC which consisted of county engineers and Iowa Department of Transportation (Iowa DOT) personnel, four types of old reinforced concrete bridges were selected for service load testing. The types selected consisted of both historic and non-historic bridges. The four types chosen include:

- Reinforced concrete open spandrel arch - historic
- Reinforced concrete filled spandrel arch- historic
- Reinforced concrete slab
- Reinforced concrete stringer

Using the four types of bridges selected as a guide, six bridges were chosen to be tested. The bridges tested included:

- Concrete open spandrel arch - Marsh Arch Bridge I (Bridge I)
- Concrete open spandrel arch - Marsh Arch Bridge II (Bridge II)
- Concrete slab bridge (Bridge III)
- Concrete filled spandrel arch - Luten Arch Bridge (Bridge IV)
- Concrete stringer bridge - two span (Bridge V)
- Concrete filled spandrel arch (Bridge VI)

Of the six bridges tested, the two Marsh Arch Bridges were scheduled for replacement. From each Marsh Arch bridge, concrete cores from the deck and reinforcing steel from the deck and hangers were obtained for laboratory testing. Also, a concrete floor beam was removed from Marsh Arch Bridge I for testing.

The diagnostic load test for each bridge consisted of applying a static load at various predetermined locations and monitoring strains and deflections in critical components. Loading for each bridge was accomplished by means of a tandem axle dump truck and was applied in a series of increments (i.e. additional material was added to the truck bed).

Before each bridge was tested, a theoretical load rating was calculated. Each bridge was load rated using the Load and Resistance Factor Rating (LRFR) method and the standard AASHTO HS20-44 and Type 3 vehicles. These two types of rating vehicles were selected to show the rating difference between the standard HS loading and that of a more typical loading. Because the test bridges were one lane and had short spans, the variable spacing dimension for the HS20-44 vehicle was chosen to be the minimum of 4270 m (14 ft). This particular wheel spacing was shown to be the critical loading case for each of the bridges tested. Wheel configuration and weight distribution for each of these vehicles is presented in Figure 1.1.

1.5. Literature Review

Load testing of bridges has been conducted in the United States and Europe since the middle of the 19th century. These early tests were primarily conducted to verify new designs and to determine ultimate load carrying capacities. In recent years however, agencies have begun to use load testing as a tool to evaluate the load carrying capacity of existing structures

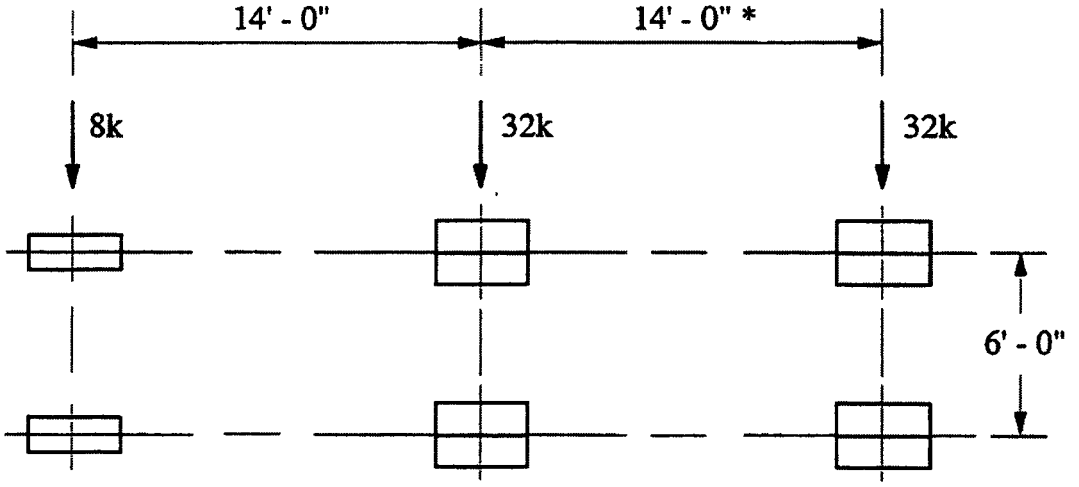

* Variable spacing(14 - 30ft)

a. Vehicle HS20-44

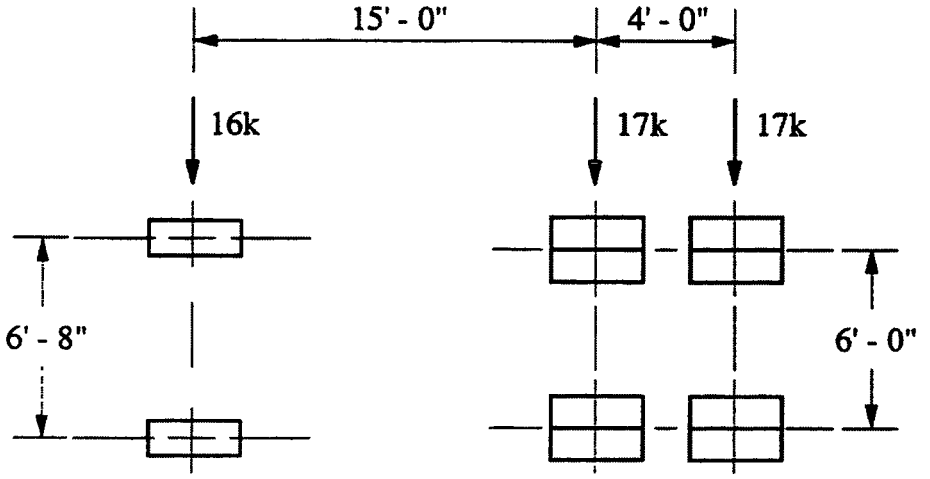

b. Vehicle Type 3

Figure 1.1. Wheel configuration and weight distribution of rating vehicles.

and to modify load ratings which were obtained from traditional analytical methods.

In the United States, several states have begun to implement nondestructive load testing procedures to determine or confirm the ratings of their existing bridges. Most notably are Florida and Alabama which have already instituted nondestructive load testing programs for rating of their existing bridges. Florida has two specially built tractor trailor vehicles for testing and a van which houses the data acquisition equipment [3]. The test vehicles are equipped with boom cranes which place standard-size concrete blocks onto the flat bed trailors. This setup allows the load to be placed in gradual known increments. The test vehicles are able to place a minimum test load equivalent to a standard HS20 rating vehicle multiplied by 2.86 to account for impact and a live load factor.

Like Florida, the Alabama Department of Transportation (ALDOT) also has two specially built test vehicles [4]. The test trucks have a tri-axle configuration with the front axle able to be raised when the vehicle is unloaded. This configuration was selected because it most commonly produces the worst case loadings and because it also similar to the ALDOT standard tri-axle dump truck. Each test vehicle is equipped with a boom crane which allows 32 load blocks of 8,400 N (1,900 lbs) each to be placed in two layers on the beds of the trucks. The gross weight of each truck can be varied from 178,000 N (40,000 lbs) to 446,000 N (105,800 lbs). Data from each test is obtained by means of a data acquisition unit housed within a separate van.

Besides the United States, Canada and Switzerland have also been using load testing as a means of evaluating their new and existing bridges. In Ontario, over 250 bridges have been load tested in the last 24 years [5]. Most of these tests were more of a proof test where the bridges were subjected to high loads in order to verify load carrying capacities and to modify load postings. Ontario's requirements for load testing of existing bridges are presented in the Ontario Highway Bridge Design Code, however no specific testing guidelines or procedures are presented.

Like Canada, Switzerland has also performed numerous load tests of their bridges. However, a majority of the tests have only been conducted on new bridges as a requirement

for acceptance before it is opened to traffic [5]. The tests consist of loading each of the bridges with four to eight dump truck type vehicles of 250 KN (56,200 lbs) each and monitoring deflections at various locations. The results are then compared to the analytical predictions made by the designer.

Along with the testing which has been conducted in Canada and Switzerland, numerous proof and diagnostic load tests have also been performed in the United States which show the conservative nature of traditional analytical ratings. These test have been conducted on both steel and reinforced concrete bridges.

In a study conducted by Chajes et al. [6], a diagnostic load test was performed on a steel girder and slab bridge in order to improve the initial analytical rating which resulted in the bridge having to be posted and partially restricted to truck traffic. The bridge in question was located in Delaware and consisted of three simply supported spans measuring 12,800 mm (42 ft) wide, and 6,930 mm (22 ft 9 in), 19,510 mm (64 ft), and 6,930 mm (22 ft 9 in) long respectively. Each span contained nine noncomposite steel girders. Using the BRASS program, initial rating factors were determined which required the bridge to be posted. The testing was conducted using a three axle tandem vehicle at a constant loading of 22 KN (50,000 N). The test vehicle was driven across the bridge at 8 km/h (5 mph) in three transverse positions approximately 3,050 mm (10 ft) apart.

Results from the testing indicated that there was composite action between the slab and girders and that a degree of restraint was occurring at the bearings. Using these results, new composite section properties were determined and then verified using a finite element model. After rerating the bridge using both the finite element model and the revised BRASS program, it was determined that the bridge may no longer need to be posted. Before the load test, the inventory, operating, and posting rating factors for a HS20T rating vehicle were 0.76, 1.27, and 0.93 respectively. After the load test, the rating factors were increased to 1.21, 2.01, and 1.47 respectively using the BRASS program and 1.11, 2.42, and 1.55 respectively using the finite element model.

A similar study was conducted by Boothby and Craig [7]. In their investigation, a historic steel pony truss was tested in order to determine if the initial posting could be raised

in order to permit emergency vehicles to cross. The test bridge had a span of 27.18 m (89 ft) and a roadway width of 4.42 m (14 ft 6 in.). The roadway consisted of a 75 mm (3 in.) glued-laminated treated timber deck supported by steel stringers and beams. In its most recent inspection, the bridge was given a sufficiency rating of of 17.9 on a scale of 100.

Before testing, the bridge was rated in accordance with the Manual for the Maintenance Inspection of Bridges. The rating resulted in an inventory rating of 41.8 kN (4.7 tons) and an operating rating of 73.0 kN (8.2 tons) with the floor beams being the controlling member.

Testing of the bridge consisted of applying a known weight in four increments at various longitudinal and transverse locations. The load was applied by means of a single axle dump truck. Strains were observed in the truss, a floor beam, stringers, and hangers and deflections were obtained at the midspan.

Results from the testing revealed that the stresses in the trusses remained low for all load increments and that the floor beam was the critical member. Using the test data, the bridge was rerated using the allowable stress method. The inventory and operating ratings of the bridge were increased to 96.8 kN (10.8 tons) and 138 kN (15.5 tons) respectively. The increased rating allowed the bridge to remain in service without undertaking any costly repairs.

Similar benefits have also been realized in reinforced concrete bridges. However, a majority of the testing which has been performed has been proof load testing. This type of testing is typically conducted on reinforced concrete bridges because the lack of known structural details and materials properties which are needed for diagnostic load testing.

In a study conducted by Beal [8], [9], as quoted in Pinjarkar [3], two reinforced concrete T-beam bridges were subjected to service load tests. In addition, one was also subjected to an ultimate load test. The first bridge (Hannacroix Creek Bridge) was constructed in 1930 and consisted of seven beams spanning 11,430 mm (37.5 ft). At the time of testing , the bridge was in poor condition which resulted in a condition rating of 2 to 3 based on a scale of 1 to 7. The second reinforced concrete T-beam bridge (Roeliff Jansen Kill Bridge) tested was also constructed in 1930. This particular bridge spanned 12,040 mm

(39.5 ft) and was in better condition than the Hannacroix bridge.

The service load tests were performed on the two bridges using a dump truck with a rear axle load of 142,345 N (32,000 lbs). The truck was positioned in various locations to monitor the midspan behavior of each beam.

The ultimate load test was conducted on the Hannacroix Creek Bridge and was conducted using hydraulic jacks. The jacks were resisted by cables embedded in the bedrock beneath the bridge. During the tests, strains, displacements, and end rotations were monitored. Strains were monitored in four tension reinforcing bars and one compression reinforcing bar.

Results from the testing revealed that the service load stresses in the rebars were well below those calculated by analytical methods. At the test load, the stress in the tension bars was 8 MPa (1,200 psi) which is considerably lower than the 40 MPa (5,800 psi) calculated. Also, the ultimate load test of the Hannacroix Creek Bridge showed no reduction in load capacity despite its deteriorated condition.

From the test results, it was concluded that T-beam bridges have reserve strength despite their deteriorated condition and that the deterioration commonly observed is mainly cosmetic and has no effect on the overall load capacity of the bridge. Only excessive loss of cover and area of tension steel are potentially serious problems.

In addition to the articles presented here on the benefits derived from load testing of existing bridges, Pinjarkar et al. [3] provides references and synopses of over 250 articles from around the world published in the past thirty years on the load testing of existing steel, reinforced concrete, post-tensioned concrete, prestressed concrete, timber, cast iron, and masonry bridges. However, even with all of the testing which has been conducted, no specific guidelines have been published by AASHTO to guide bridge owners in conducting nondestructive load tests and applying results obtained from such tests. Because of this, states which have begun conducting nondestructive load tests have implemented their own guidelines and procedures which may differ from state to state.

Recently, a study was conducted by Prinjarkar et al. [3] in conjunction with the National Cooperative Highway Research Program (NCHRP) to develop guidelines and

methodology for nondestructive load testing of highway bridges. The report includes criteria for selecting test methods, a description of test procedures, and discusses the economic benefits achieved from load testing, the risks, and criteria for selecting candidate bridges.

The evaluation of the results obtained from load testing and the enhancement of the analytical rating is one of the most difficult tasks in conducting a load test. Care must be taken when extrapolating to loads greater than those placed on the bridge during the load test. In an NCHRP study conducted by Lichtenstein [2], a procedure was developed to assist the bridge owner in evaluating the results obtained from load testing and extrapolating those results to loads greater than those placed on the bridge during the test. This procedure involves calculating a test benefit, if any, from measured strains, then reducing that value based on such conditions as lack of redundancy, frequency of inspection, the anticipated behavior of the bridge at higher loads, etc. This particular procedure was utilized in evaluating the bridges in this research project. For a more complete discussion of this procedure, see Sec. 1.7.

1.6. Test Equipment and Procedures

1.6.1. Test Equipment

The testing procedure for each bridge consisted of obtaining strains and deflections in critical components and locations. Since the procedure for each bridge was identical, the same test setup and data acquisition system were used.

To determine strains in critical bridge components, 120 ohm electrical resistant bonded strain gages were used. Where the strain gages were bonded to steel, strain gages with a gage length of 13 mm (1/2 in.) were used. When the strain gages were bonded to the concrete, strain gages with a gage length of 57 mm (2 1/4 in.) and 114 mm (4 1/2 in.) were used. The only bridge in which the 114 mm (4 1/2 in.) strain gages were used was the concrete stringer (Bridge V). The 114 mm (4 1/2 in.) strain gages have a longer gage length which improves the accuracy of the strain readings. The more accurate strain readings were needed to calibrate the finite element model of the bridge; this model was used to predict the

structural behavior of the concrete stringer bridge.

Before the strain gages could be applied to the concrete, the concrete surface at the gage locations had to be prepared properly. The preparation involved the application of a two part epoxy compound "patch" to fill any voids in the surface of the concrete, thus ensuring full contact between the surface of the concrete and gage.

To prevent the attached gages from being contaminated with dirt and moisture, a rubber patch was applied to cover and seal the gages. The patch was then covered with foil tape and sealed with silicone caulk.

Deflections in each bridge were obtained by means of Celesco PT-101 displacement transducers (potentiometers) mounted on tripods at various locations underneath the bridges. The wires from the Celescos were attached to hooks which were screwed into wooden blocks mounted on the underside of the bridges. Figure 1.2 shows the typical mounting configuration of the deflection transducers

Data from the various tests was recorded by means of a Hewlett Packard Data Acquisition System (DAS).

Figure 1.2. Typical setup of displacement transducers.

1.6.2. Test Procedures

The testing of each of the six bridges consisted of applying a static load at various predetermined transverse and longitudinal locations on the bridges and monitoring strains and deflections in critical components. The same testing procedure was used on all six bridges.

Loading of each bridge was accomplished by means of a tandem axle dump truck. The trucks used were supplied by the counties in which the bridges were located and by the Iowa DOT. Because the trucks came from a variety of sources, the wheel configurations and weight distributions varied from test to test The exact truck weights and dimensions are presented within the following chapters.

The load was applied to the bridges in a series of increments. For all the test bridges, the first load increment consisted of an empty truck; subsequent load increments varied as a function of the amount of weight added. Weight for the various load increments consisted of aggregate supplied by local quarries or county storage sites. The total weight of the loaded trucks was determined using scales at the quarries or local grain elevator scales.

The trucks were positioned transversely on the bridges in three lanes for each test. In the first and third lanes, the trucks were positioned as close to the curb as possible. In the second lane, the trucks were centered on the bridges.

1.7. Research Method

As stated previously, the scope of this project dealt with determining an estimate of a bridges load carrying capacity through diagnostic load testing. Determining a bridges load carrying capacity from diagnostic load tests is accomplished by subjecting a given bridge to a known applied load and determining the strains in critical components. The measured strains are then compared to theoretical strains predicted from an analytical model subjected to the same loading. If the measured strains are less than the theoretical strains, a test benefit is derived and the bridge possess a reserve capacity. Conversely, if the measured strains are greater than the theoretical strains, the bridge has less capacity than predicted. When a benefit is obtained from testing, it should be approached with caution. The results should not

be extrapolated to loads which are higher than loads placed on the bridge unless methods which ensure that the bridge is going to respond at the expected levels are incorporated. It should also be noted that diagnostic load tests are only applicable to bridges with known "as built" structural details and material properties. If these items are unknown, a proof load test should be conducted.

For this project, the results obtained from the six diagnostic load tests were extrapolated using the guidelines and method developed by Lichtenstein [2]. This particular method involves both quantitative and qualitative factors which are considered simultaneously in modifying the analytical rating of the bridges.

The first step in utilizing this method is to developed a theoretical load rating for the bridge. In developing the load rating, a thorough field inspection should be conducted and "as built" plans should be obtained. Using this information, an analytical model can be constructed which closely approximates the conditions encountered in the field. The more accurate and detailed the model, the better the theoretical load rating will be. The model is then used to determine individual member capacities and the responses due to dead and live loads . In determining the live load effects, the rating vehicle should be positioned so as to produce the maximum effect in the critical components. After capacities and dead and live load effects have been determined, the theoretical rating factors are calculated. The rating factors are determined using either the allowable stress method, load factor method, or load and resistance factor rating (LRFR) method. If the rating factor is greater than or equal to one, no further analysis is needed. However, if the rating factor is less than one, this rating method may be used in conjunction with a diagnostic load test to either decrease or increase the rating.

After a diagnostic load test has been conducted, the following equation is used to modify the theoretical load rating:

$$RF_T = RF_c \times K \qquad (1)$$

where:

RF_T = The load rating factor after the results from the diagnostic load test have been applied.

RF_c = The theoretical load rating factor obtained from the analytical model.

K = An adjustment factor based on the comparison of the measured test behavior with that obtained from the analytical model.

The adjustment factor 'K' used in the preceding equation (Eqn. 1) is a function of the results obtained from the diagnostic load test and of the expected response of the bridge at higher load levels. It is determined from the following equation:

$$K = 1 + K_a \times K_b \tag{2}$$

where:

K_a = A factor obtained from the comparison of the results obtained from the theoretical model with those obtained with from the load test.

K_b = A factor which takes into account the frequency of inspections, the presence of special structural features such as redundancy, and the ability of the test team to explain the results obtained for from the load test.

In relating the measured test results with the results obtained from the theoretical model, the following equation is used:

$$K_a = \frac{\varepsilon_c}{\varepsilon_T} - 1 \tag{3}$$

where:

ε_T = The maximum measured strain in the component being considered.

ε_c = The theoretical strain produced by the test vehicle at the exact positioning and loading as produced the actual test strain.

The factor K_b can be thought of as a safety factor which reduces K_a to account for items such as non redundant members, the lack of inspections, and members not performing adequately at the higher load levels. It is defined as follows:

$$K_b = K_{b1} \times K_{b2} \times K_{b3} \quad (4)$$

K_{b1} is a factor which takes into account the behavior of the bridge beyond the test load level and also the magnitude of the theoretical test load effects in comparison to the rating load effects. This factor is assigned a value between 1 and 0 where 1 indicates that the behavior of the bridge at the higher rating load level will be the same as the behavior exhibited at the test load level and the responses predicted by the analytical model at the test load level are similar to the responses predicted at the initial load rating level . This is determined by loading the analytical model with 1.33 times the rating vehicle gross load and ensuring that linear behavior is present in the bridge components at the higher load level. A value of 0 indicates that the behavior of the bridge can not be extrapolated to levels beyond the rating load level. Table 1.1 is provided as a guidance in selecting a value for K_{b1}. The letters T and W refer to the gross loading effects in the critical members produced by the test vehicle and the rating vehicle, respectively.

The factor T/W is presented in Table 1.1 to ensure that the test vehicle is similar in magnitude and exhibits a response similar to that of the rating vehicle.

The factor K_{b2} is a function of the type and interval of inspections. This factor is included to ensure that any change in the condition of the bridge while operating at the higher

Table 1.1. Values for K_{b1}.

Can member behavior be extrapolated to 1.33W ?		Magnitude of test load			K_{b1}
Yes	No	$\frac{T}{W} < 0.4$	$0.4 \le \frac{T}{W} \le 0.7$	$\frac{T}{W} > 0.7$	
x		x			0
x			x		0.8
x				x	1.0
	x	x			0
	x		x		0
	x			x	0.5

Table 1.2. Values for K_{b2}.

Inspection		K_{b2}
Type	Frequency	
Routine	between 1 & 2 years	0.8
Routine	less than 1 year	0.9
In-Depth	between 1 & 2 years	0.9
In-Depth	less than a year	1.0

rating level will be diagnosed in time to reduce the load rating to levels which do not endanger the bridge. Values for K_{b2} are presented in Table 1.2.

The factor K_{b3} is included to account for sudden failure of the bridge due to fracture or fatigue of critical members and the absence of redundant members. This factor is included so the test team will evaluate all failure modes before the load rating is extrapolated to higher levels. Table 1.3 provides guidance in selecting values for this factor.

The preceding method was developed to give the engineer a level of comfort when extrapolating loads to levels higher than those predicted by analytical methods. A flowchart is presented in Figure 1.3 as a guide for determining the theoretical rating factors and applying the diagnostic load test procedure. The steps presented in the flowchart are illustrated in an example problem in Sec. 1.7.1.

Table 1.3. Values for K_{b3}.

Fatigue Controls		Redundancy		K_{b3}
No	Yes	No	Yes	
	x	x		0.7
	x		x	0.8
x		x		0.9
x			x	1.0

To obtain the rating factors for the bridges in this project, the LRFR method was used. Unlike the allowable stress and load factor methods which calculate both an inventory and operating rating, the LRFR method only calculates one rating factor. This method resulted from the culmination of work conducted by Imbsen et. al. [10] in the early 80's and was later adopted by AASHTO and presented in a guide specification [11].

The LRFR method is a limit states approach to load rating which applies reduction and load factors to the nominal strength and dead and live loads, respectively. This method is expressed by the following equation:

$$RF = \frac{\phi R_n - \gamma_d D}{\gamma_L L(1+I)} \tag{5}$$

where:

RF = Rating factor

ϕ = Resistance factor

R_n = Nominal resistance

γ_d = Dead load Factor

D = Nominal dead load

γ_L = Live load factor

L = Nominal live load

I = Live load impact factor

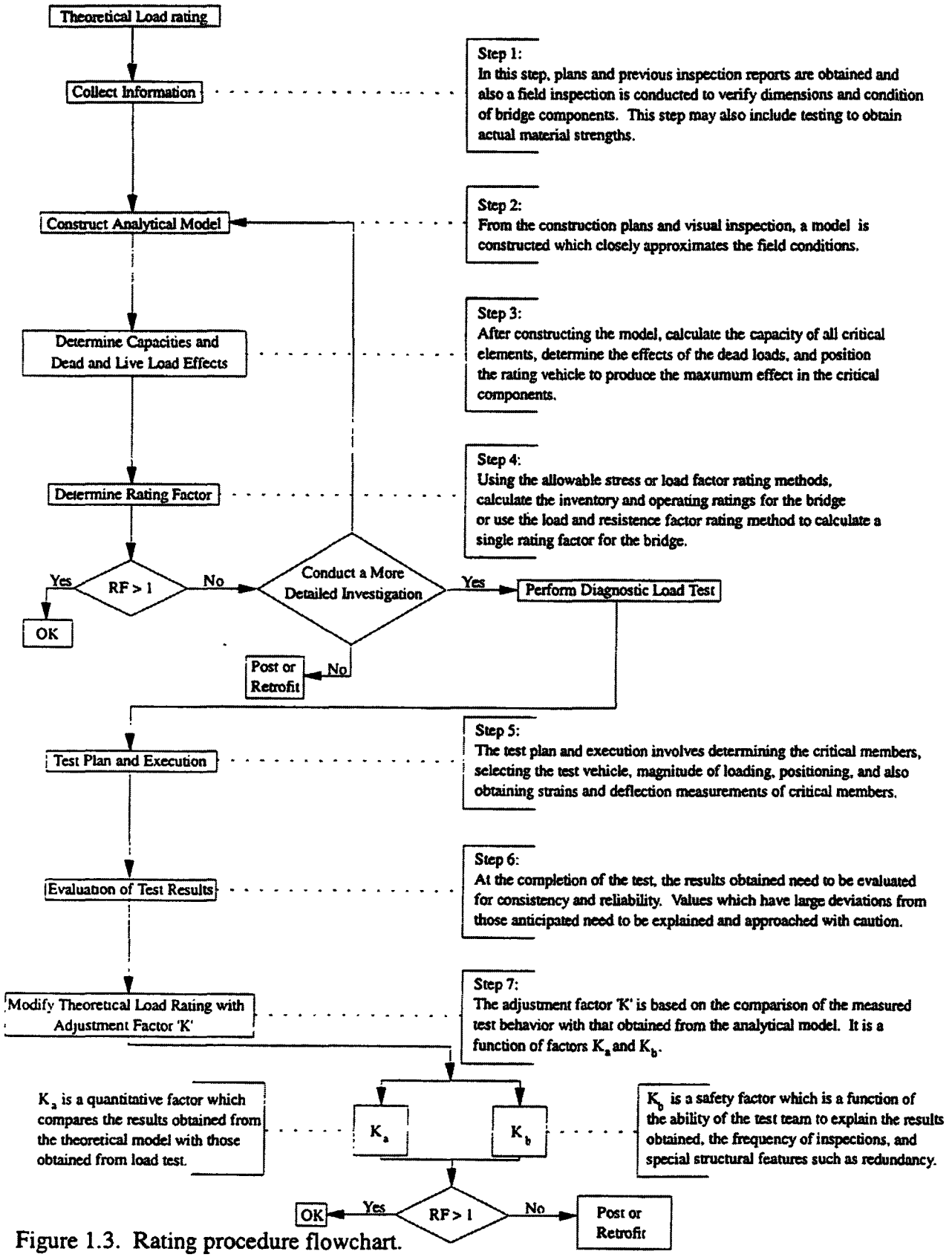

Figure 1.3. Rating procedure flowchart.

The resistance factor for each bridge is dependent on the condition of the superstructure, the presence (or absence) of redundancy, the degree of inspection, and the type of maintenance. For reinforced concrete, the resistance factor ranges from 0.95 for a bridge in good to fair condition with redundant members, careful inspection, and vigorous maintenance to 0.55 for a bridge which is heavily deteriorated, has no redundant members, estimated inspection, and intermittent maintenance.

The dead load factor is assigned a constant value of 1.2 and is increased by 20 % when overlays are present. The live load factor is assigned a value ranging from 1.3 to 1.8. The magnitude of this factor is dependent on the average daily truck traffic (ADTT) and the enforcement of overload restrictions.

The impact factor is determined by the condition of the wearing surface. It is assigned value ranging from 0.1 for a wearing surface in good to fair condition to 0.3 for a wearing surface in critical condition. This deviates from other rating procedures where the impact factor is determined by the span of the bridge.

The load rating of the bridge is then determined by multiplying the rating factor by the gross load of the rating vehicle. The load rating is determined from the following equation:

$$\text{Load rating} = RF \times W \tag{6}$$

where:

W = gross load of rating vehicle (tons)

In determining the theoretical rating factors for each bridge, the same material strengths and properties were assumed for each bridge unless laboratory testing was conducted to determine actual values. The concrete strength was assumed to be 28 MPa (4,000 psi) and the modulus of elasticity was determined using the following equation $E_c = 5{,}000\sqrt{f_c'}$ ($57{,}000\sqrt{f_c'}$). The strength of the reinforcing steel and the modulus of elasticity were assumed to be 228 MPa (33,000 psi) and 200,000 MPa (29,000,000 psi), respectively.

1.7.1. Example Problem

In this section, a sample problem is presented to illustrate the various calculations of the diagnostic load testing method explained in Sec 1.7. The sample problem is a single span, simply supported reinforced concrete T-beam girder bridge. The following steps coincide with the steps presented in the rating procedure flowchart in Figure 1.3.

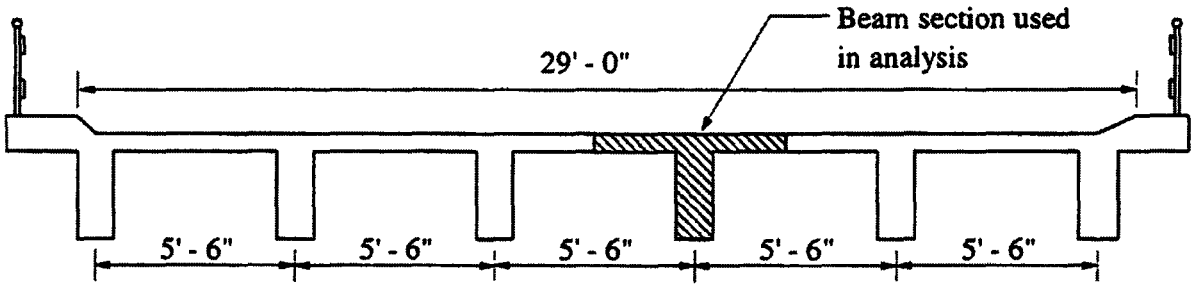

a. Bridge cross-section

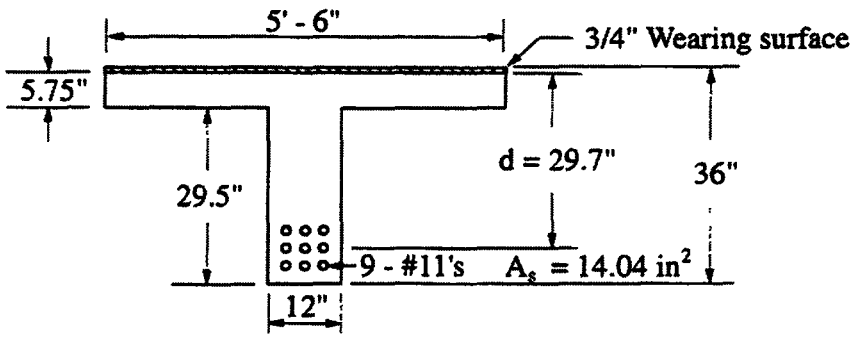

b. Girder cross-section

Figure 1.4. Cross-section of example T-beam girder bridge.

Step 1: Collection of Information

Bridge data:

Span, c-c bearings, L = 50 ft

Concrete:

Compressive strength, $f'_c = 3{,}000$ psi

unit weight = 150 lb/ft^2

Reinforcing steel:

Grade 40 steel, $f_y = 40{,}000$ psi

A_s = 9 - #11 bars

$A_s = (9)(1.56) = 14.04$ in^2/beam

Girder spacing = 5.5 ft

Slab depth = 6.5 in. (includes wearing surface)

Wearing surface = 0.75 in.

Effective thickness of slab = 5.75 in.

Structurall girder depth = 29.7 in.

Stem width = 12 in.

Site conditions:

- Heavy volume roadway (ADTT > 1000) with significant sources of overloads without effective enforcement.
- Wearing surface is rough with significant deterioration and the superstructure is in poor condition with areas of heavy deterioration.
- Maintenance is intermittent and inspections are performed every one to two years.
- Support conditions consist of the girders resting directly on the abutments.

Step 2: Construct analytical model

- The first step in constructing the model is to determine support conditions. Since the girders of the bridge are not physically attached to the abutments and bearing pads are present, the individual girders will be modeled as simply supported beams.
- Since the deck and beams were cast monolithically, one needs to determine how much of the slab is effective in the T-beam flange (see Fig. 1.4a).

According to Section 8.10.1 of AASHTO's Standard Specification for Highway Bridges [12]:

- The total width of slab effective as a T-girder flange shall not exceed one-fourth of the span length of the girder.

and

- The effective flange width overhanging on each side of the web shall not exceed six times the thickness of the slab or one-half the clear distance to the next web.

Effective slab width:

$w \leq 1/4L$

$w \leq (1/4)(50) = 12.5$ ft

$$\text{Overhanging flange width} = \frac{(12.5 - 1)}{2} = 5.75 \text{ ft}$$

Effective flange width:

$f \leq 6t$ where t is the slab thickness and f is the distance from face of beam to edge of slab.

$f \leq 6(5.75) = 34.5$ ft

or

$f \leq$ one-half the clear distance to the next web

$f \leq (1/2)(4.5)$

$f \leq 2.25$

$f = 2.25$ ft < 5.75

Therefore, $f = 2.25$ ft controls.

Final width of slab effective as a T-beam = 2.25 + 1 + 2.25 = 5.5 ft (see Fig. 1.4b)

Since 5.5 ft < the effective slab width w = 5.75 ft, 5.5 ft controls

Step 3: Determine the capacity and dead and live load effects.

- The live load effects for this bridge will be determined using an AASHTO HS20 rating vehicle.

Capacity:

- The T-beam section used in determining the moment capacity of the beam is presented in Figure 1.4 (b).
- In this example, it is assumed that the capacity of the girders is controlled by the ultimate moment strength and thus only moment calculations are presented. In an actual bridge analysis problem, the slab, shear, bearing, etc. should also be checked to determine the controlling mode of failure.
- The first step in determining the moment capacity of the T-beam section is to calculate the effective depth of the compressive stress block, a. If the depth of the stress block is less than the effective thickness of the slab, one can treat the slab as a rectangular section of width 5.5 ft.

$$a = \frac{A_s f_y}{0.85 f_c' b}$$

$A_s = 14.04\ in^2$ $\quad$ b = effective width = 5.5 ft or 66 in.

$f_y = 40{,}000$ psi $\quad$ $f_c' = 3{,}000$ psi

$$a = \frac{(14.04)(40{,}000)}{(0.85)(3000)(66)} = 3.34 \text{ in.} < 5.75 \text{ in.}$$

Since the depth of the compressive stress block a, is less than the effective slab depth, the cross section behaves as a rectangular beam with a width of 66 in.

- Determine if the section is controlled by the yielding of the tension steel.

$\rho \le \rho_{max}$

$$\rho = \frac{A_s}{bd} = \frac{14.04}{(66)(29.7)} = 0.00716$$

$$\rho_{max} = 0.75\rho_b = (0.75)\frac{0.85\beta_1 f_c'(87{,}000)}{f_y(87{,}000 + f_y)} = 0.0279$$

$$\rho = 0.0716 < \rho_{max} = 0.0279$$

Therefore, the cross section is controlled by the yielding of the tension steel and not compression failure of the concrete.

- Calculate the nominal moment capacity of the beam.

$M_n = A_s f_y (d - a/2)$

$$M_n = \frac{(14.04)(40{,}000)(29.7 - \frac{3.34}{2})}{(12)(1000)} = 1{,}312 \text{ ft-k}$$

Dead Load:

Deck weight: (6.5/12)(5.5)(0.150)	= 0.45 k/ft/beam
Girder weight: (12/12)(29.5/12)(0.150)	= 0.37 k/ft/beam
Curbs, railings, etc. weight:	= 0.18 k/ft/beam
	= 1.00 k/ft/beam

$$M_D = \frac{wL^2}{8} = \frac{(1.00)(50)^2}{8} = 312.5 \text{ ft-k}$$

Live load:

Maximum moment per wheel line produced by HS20 rating vehicle:

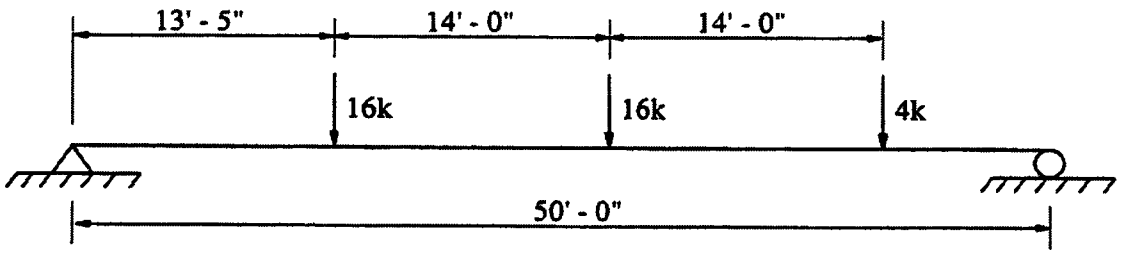

From above loading,
M_{HS20} = 314 ft-k per wheel line

Distribution factor:

$DF = \frac{S}{6.0}$ where S equals the stringer spacing in feet.

$$DF = \frac{5.5}{6.0} = 0.92$$

Live load moment:

$$M_{LL} = M_{HS20} \times DF = (314)(0.92) = 289 \text{ ft-k}$$

Step 4: Determine the rating factor

- To determine the rating factor for this bridge, the LRFR method presented previously will be used.

$$RF_c = \frac{\phi M_n - \gamma_d M_D}{\gamma_L M_{LL}(1+I)}$$

ϕ = 0.70 (Redundant structure, heavy deterioration, careful inspection, intermittent maintenance)

γ_D = 1.2

γ_L = 1.80

I = 0.2 (wearing surface rough and heavily deteriorated)

$$RF_c = \frac{(0.70)(1312) - (1.2)(312.5)}{(1.80)(289)(1.2)} = 0.87$$

Gross weight of HS20 rating vehicle = 36 tons

Rating = (0.87)(36) = 31 T

When the rating factor is less than one, the bridge owner has four options. First, the bridge may be posted for reduced loads. Secondly, the bridge may be retrofitted to increase its carrying capacity. Thirdly, a more detailed analytical model can be developed and the bridge rerated. Finally, the bridge owner may choose to perform a diagnostic load test or a proof load test to obtain a better estimate response of the critical members. For this example bridge, the fourth option will be selected: a diagnostic load test.

Step 5: Test plan and execution

- From the theoretical load rating, it was determined that the critical component of the bridge was the girders.

- To measure the maximum response of the girders under the test loading, strains and deflections were measured at the centerline of each of the six girders.
- Testing of the bridge consisted of applying a static load at various longitudinal and transverse locations to produce maximum moments and deflections in the girders. The load was applied by means of tandem axle dump truck in four load increments. The wheel configuration of the test vehicle matched that of the Type 3 vehicle presented in Figure 1.1.

Step 6: Evaluation of test results

- A maximum strain of 75 microstrain was measured at the center of the two middle girders (see Fig 1.4a). As expected, the maximum strain occurred when the test vehicle was positioned to produce maximum moment in the two girders.
- The maximum strain was lower than was theoretically predicted yet was consistent for the various loading increments.

Step 7: Modify the theoretical load rating

- Using the results obtained from the diagnostic load test, the theoretical load rating can be modified. The modification of the theoretical load rating is accomplished by means of an adjustment factor 'K' which based on the comparison of the measured test behavior with that obtained from the analytical model. The modified rating factor takes the following form:

$$RF_T = RF_c K$$

where:

RF_T = the rating factor obtained by including the results from the load tests

RF_c = the rating factor obtained from the theoretical calculations

$K = 1 + K_a K_b$

- The first step in modifying the existing load rating is to determine the magnitude of the factor K_a (Eqn. 3).

Factor K_a:

$$K_a = \frac{\varepsilon_c}{\varepsilon_T} - 1$$

- To determine K_a , the theoretical maximum strain produced in the girder by the test vehicle used in the field test is calculated.
- To obtain the theoretical strain in the girder, the equivalent concrete section, location of the neutral axis, and uncracked moment of inertia has to be calculated.

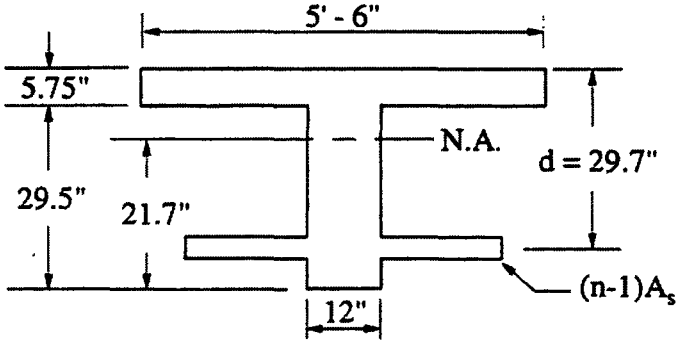

Equivalent concrete section:

$E_s = 29{,}000{,}000$ psi

$E_c = 3{,}600{,}000$ psi

$$n = \frac{E_s}{E_c} = 8$$

$(n-1)A_s = (8-1)(14.04) = 98.28$ in^2

Location of the neutral axis:

$$N.A. = \frac{\sum A\bar{y}}{\sum A}$$

$$= \frac{(5.75)(66)(32.38) + (29.5)(12)(14.75) + (98.28)(5.55)}{(5.75)(66) + (29.5)(12) + 98.28}$$

= 21.7 in.

Uncracked moment of inertia:

$$I_g = \frac{bh^3}{12} + Ad^2$$

$$= 1/12(66)(5.75)^3 + (66)(5.75)(10.68)^2 + 1/12(12)(29.5)^3 + (29.5)(12)(6.95)^2 + (98.28)(16.15)^2 = 112{,}737 \text{ in}^4$$

Theoretical moment produced by the test vehicle:

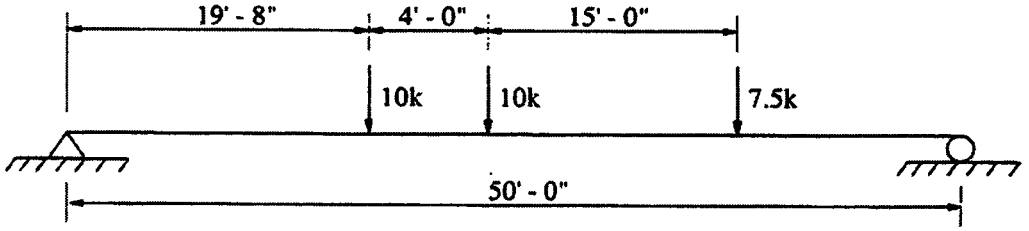

$M_{test\ vehicle}$ = 269 ft-k per wheel line

Distribution factor:

DF = 0.92 (see previous calculations)

Test load moment:

$M_T = M_{T\ est\ vehicle}$ x DF

$M_T = (269)(0.92) = 247$ ft-k

Theoretical stress:

$$\sigma_c = \frac{M_T y}{I_g} = \frac{(247)(12)(1000)(21.7)}{112{,}737} = 570 \text{ psi}$$

Theoretical and test strains:

$$\varepsilon_c = \frac{\sigma_c}{E_c}$$

ε_c = calculated theoretical strain in concrete

$$\varepsilon_c = \frac{570}{3{,}600{,}00} = 1.58 \times 10^{-4} \text{ in./ in.}$$

$$\varepsilon_T = 7.5 \times 10^{-5} \text{ in./in.}$$

ε_T = strain produced from test vehicle

$$K_a = \frac{\varepsilon_c}{\varepsilon_T} - 1 = \frac{1.58 \times 10^{-4}}{7.5 \times 10^{-5}} - 1 = 1.11$$

- The final step in the modification of the theoretical load rating is to determine the magnitude of the factor K_b (Eqn. 4).

Factor K_b:

$$K_b = K_{b1} K_{b2} K_{b3}$$

K_{b1}: depends on the relationship between the test vehicle effect and the gross rating load effect

$$K_{b1} = \frac{T}{W} = \frac{M_T}{M_{LL}(1+I)}$$

$$\frac{T}{W} = \frac{247}{289(1.2)} = 0.72$$

From Table 1.1, with T/W >0.7 and the member behavior expected to remain the same at 1.33 times the gross rating effect

$K_{b1} = 1.0$

K_{b2}: From Table 1.2, with routine inspections between one and two years

$K_{b2} = 0.8$

K_{b3}: From Table 1.3, fatigue is not a factor in this type of bridge and redundancy is provided for by the multiple girders

$K_{b3} = 1.0$

$K_b = (1.0)(0.8)(1.0)$

$K_b = 0.8$

Modified rating:

$RF_T = RF_c(1+K_aK_b) = (0.87)[1 + (1.11)(0.8)] = 1.64$

Gross weight of HS20 rating vehicle = 36 tons

Rating = (1.64)(36) = 59 T

As a result of the diagnostic load test, the rating of the bridge increased from 31 tons to 59 tons.

2. BRIDGE I: REINFORCED CONCRETE OPEN SPANDREL ARCH

2.1. Bridge Description

The first bridge to be service load tested was a one lane reinforced concrete open spandrel arch (Marsh Arch) located on a secondary county road (Deer Ave.) in southwest Boone County over Beaver Creek. Average daily traffic was approximately 75 vehicles and consisted mainly of local traffic. At the time of testing, this bridge was listed on the Iowa Historic Bridge Inventory and was one of 11 Marsh Arch bridges still remaining within the state. Built in 1914, this particular type of reinforced concrete open spandrel arch was developed and patented by James B. Marsh in the early 20th century. Because of this, bridges of this type are historically known as Marsh Arch Bridges. The items which made these bridges unique included: the concept of hanging the deck from the arch, the use of both reinforcing steel and structural steel, and the idea of allowing the deck to move independent of the arch. Figure 2.1 illustrates the layout of this type of bridge. All dimensions listed were obtained from field measurements.

Bridge I had a clear span of 27,430 mm (90 ft) and a roadway width from the inside of curb to the inside of curb of 4,700 mm (15 ft - 5 in.). The bridge deck was 5,385 mm (17 ft -8 in.) wide and 205 mm (8 in.) thick. Reinforcing consisted of two layers of 19 mm (3/4 in.) square reinforcing bars spaced at 150 mm (6 in.) on center in the longitudinal direction and 15 mm (1/2 in.) round reinforcing bars spaced at 305 mm (12 in.) on center in the transverse direction. In addition to this reinforcement, there was a series of 19 mm square reinforcing bars placed in a crossing pattern on top of the longitudinal and transverse reinforcement. Due to faulty placement or design, no longitudinal reinforcement was provided in the top portion of the deck in the negative moment regions. Figure 2.2 illustrates the reinforcement in the deck.

The deck was supported by nine transverse reinforced concrete beams spaced at 2,745 mm (9 ft) on center. The seven interior beams were supported by hangers (see Fig. 2.1a & b) which were in turn attached to the arch. The remaining two end beams were located between the arches and were provided not only to support the deck but to tie the arches together.

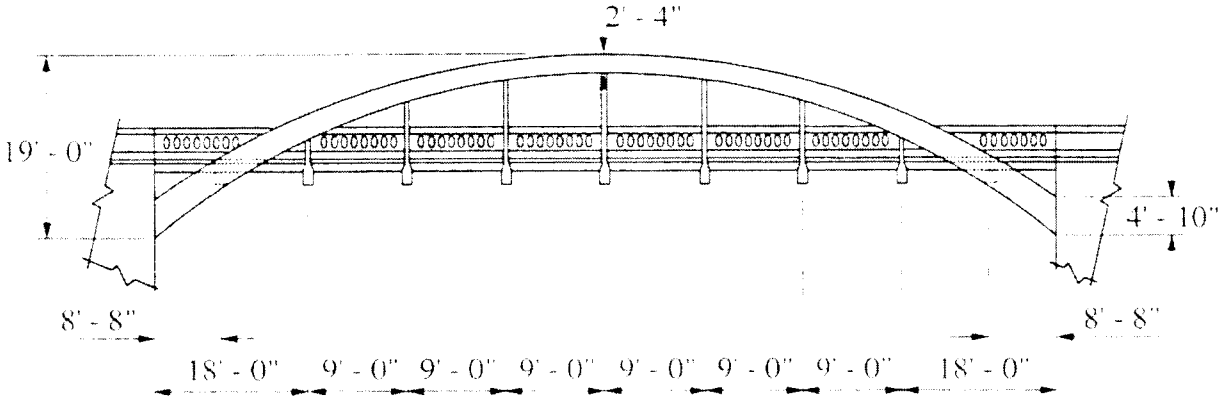

a. Elevation

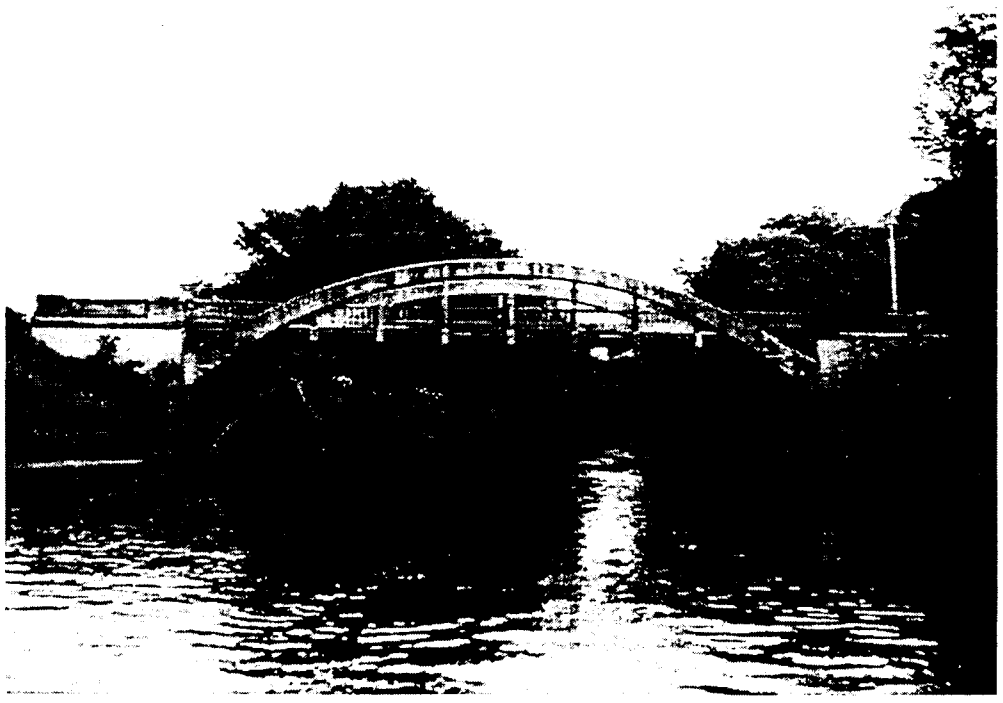

b. Photograph of bridge profile

Figure 2.1. Bridge I: Layout.

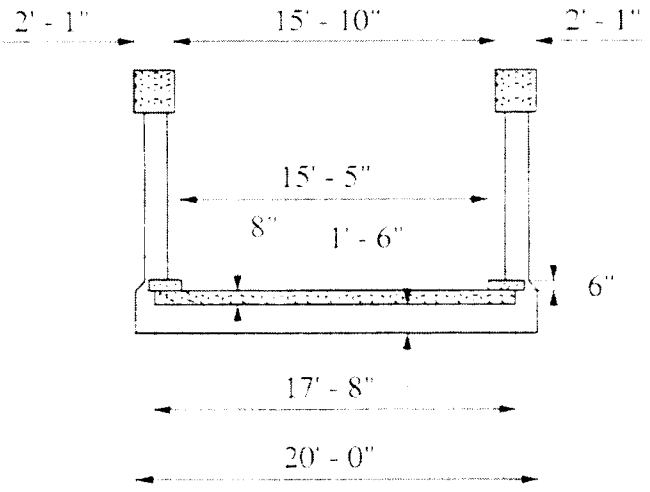

c. Typical cross section

d. Photograph of Bridge I looking South.

Figure 2.1. Continued.

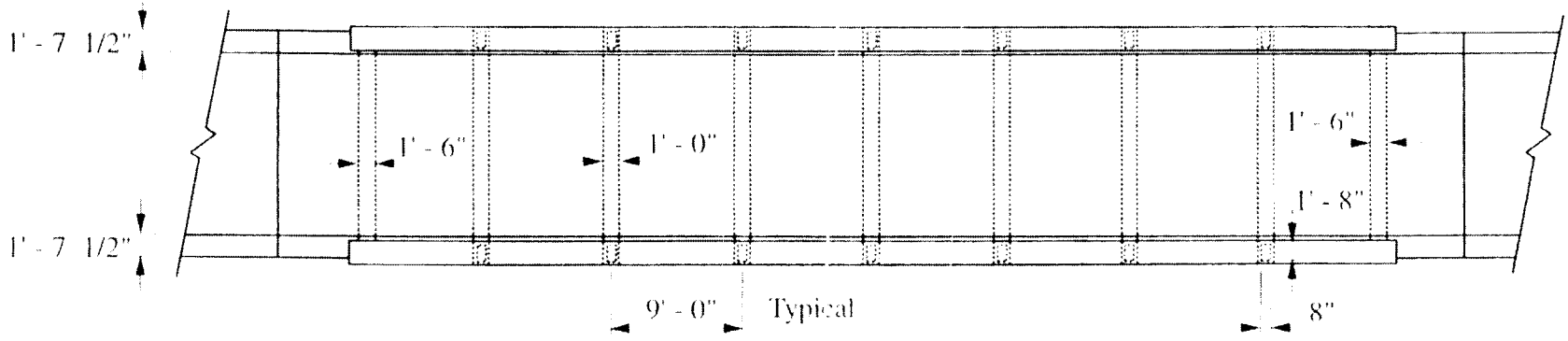

e. Plan view

f. Aerial photograph

Figure 2.1. Continued.

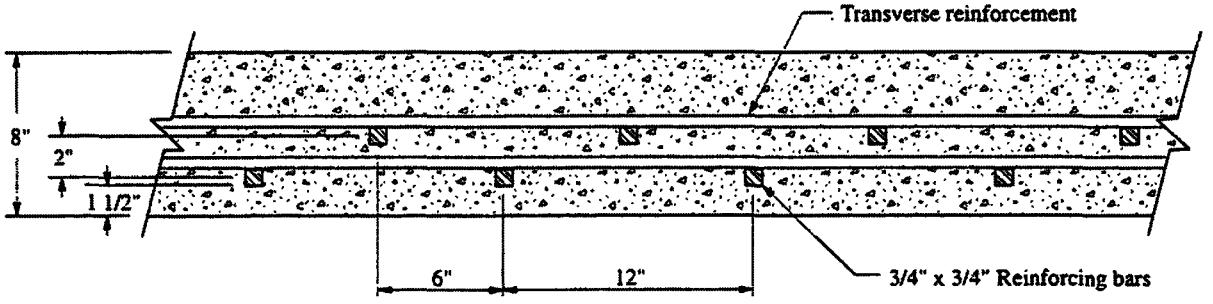

a. Longitudinal reinforcement

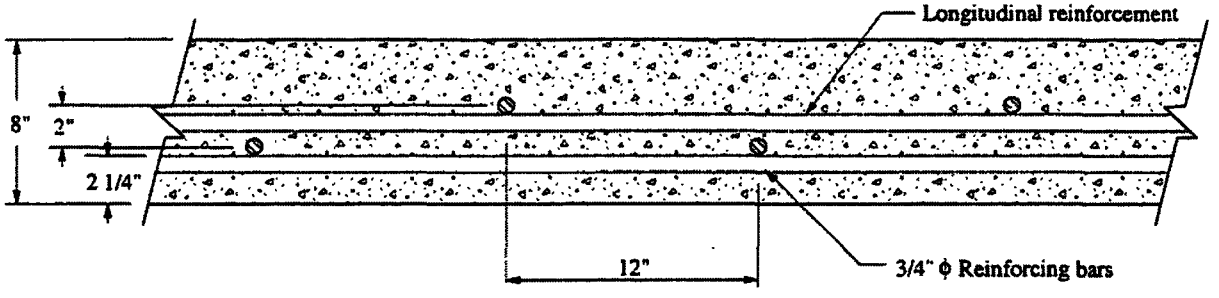

b. Transverse reinforcement

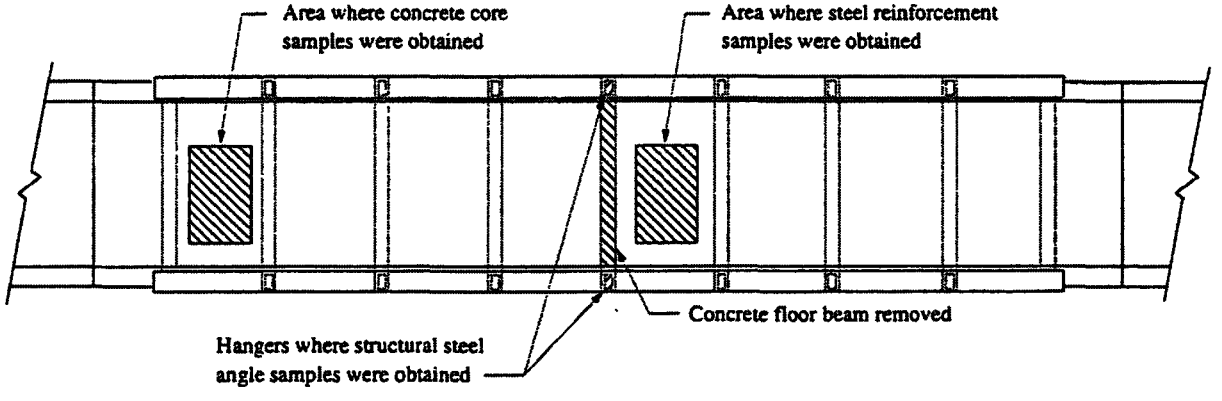

c. Crossing reinforcement

Figure 2.2. Bridge I: Deck reinforcement.

Since these beams were attached to the arches, a construction joint was provided between the beams and the deck to allow the deck to move independent of the arches.

The interior transverse beams had a depth from the bottom of the deck to the bottom of the beams of 460 mm (18 in.), a width of 305 mm (12 in.), and total length of 6,095 mm (20 ft). The end transverse beams which tied the arches had a depth from the bottom of the deck to bottom of the beams of 510 mm (20 in.), a width of 460 mm (18 in.), and a length of 4,825 mm (15ft 10in.).

Reinforcing for the interior beams consisted of two 2 1/2 in. x 2 1/2 in. x 1/4 in. structural steel angles and two 26 mm (1 1/8 in.) diameter steel rods. To provide for shear reinforcement, the 26 mm steel rods were bent up at a 15 degree angle beginning at 1,855mm (6ft - 1in.) from the edge of the beam. No stirrups were provided for additional shear reinforcement. In addition to the reinforcement in the bottom portion of the beams, two 19 mm (3/4 in.) square reinforcement bars were provided in the top of the beams.

Reinforcement in the end beams consisted of four 19 mm (3/4 in.) square reinforcing bars in the bottom of the beams and four in the top. Each bar was extended into the arches for development. The configuration of the transverse reinforced concrete beams and the reinforcement used is presented in Figure 2.3.

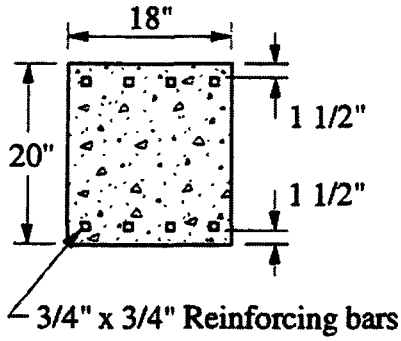

a. Reinforcement in end beams

Figure 2.3. Bridge I: Configuration and reinforcing details in transverse floor beams.

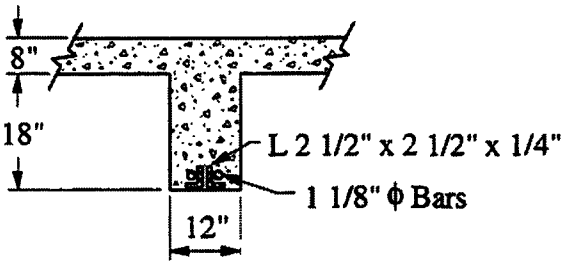

b. Reinforcement at centerline of interior beams

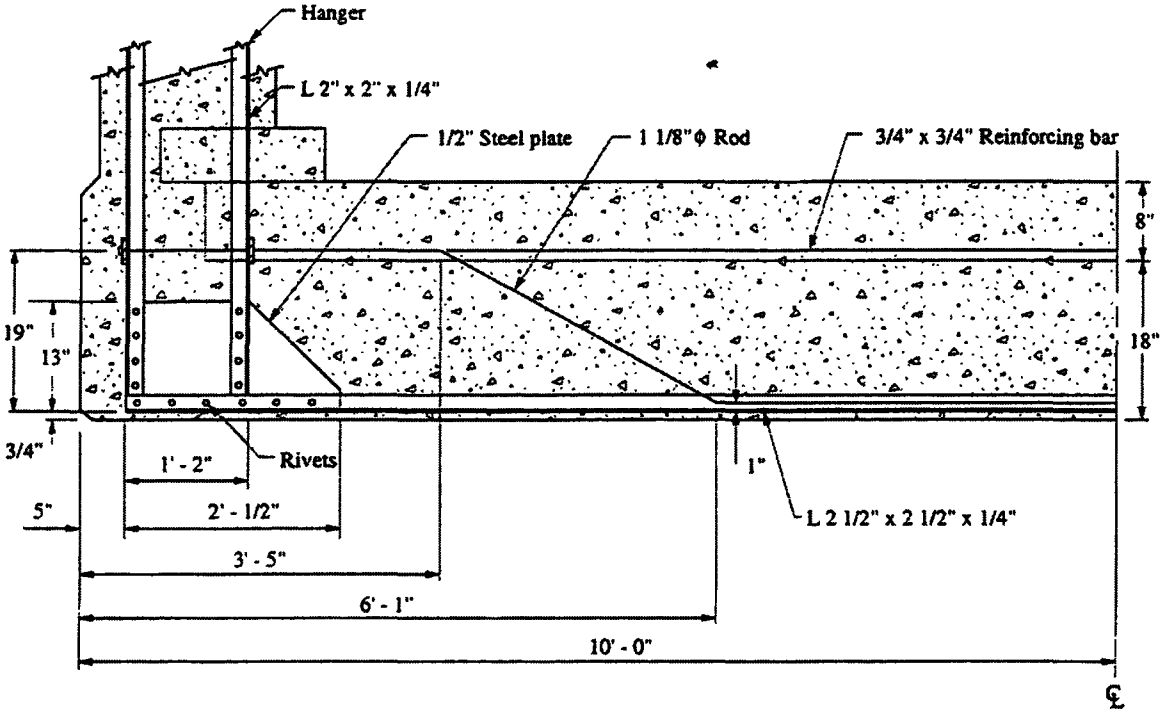

c. Half section detail of interior beams

Figure 2.3. Continued.

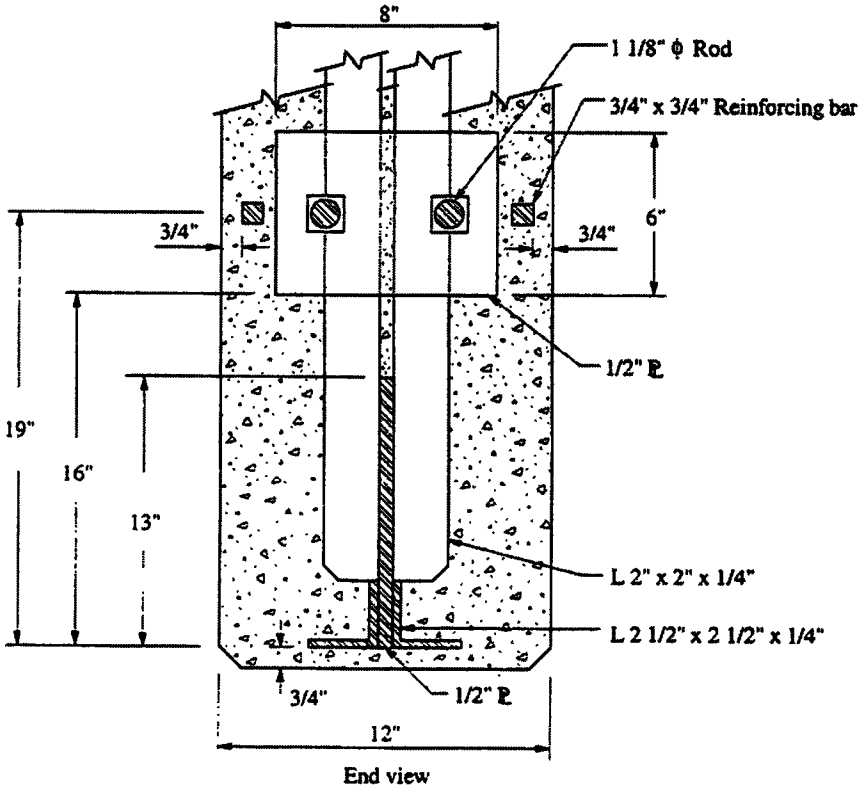

d. End view of interior beams

Figure 2.3. Continued.

The hangers which supported the deck and beams were composed of structural steel encased in concrete. Each hanger had a depth of 500 mm (20 in.) and a width of 205 mm (8 in.); reinforcing in the hangers consisted of four 2 in. x 2 in. x 1/4 in. structural steel angles (see Fig. 2.4).

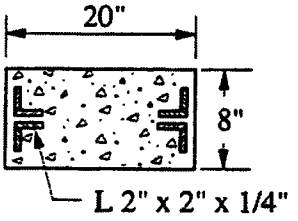

Figure 2.4. Bridge I: Configuration and reinforcing details of hangers.

The final and most important component of this bridge is the arches. Each arch had a rise of 5,790 mm (19 ft), a constant width of 635 mm (25 in.) along its length, and a thickness of 710 mm (28 in.) at the crown and 1,475 mm (58 in.) at the abutments. Shown in Figure 2.5 are reinforcing details within each arch; it consisted of four structural steel angles 3 in. x 3 in. x 5/16 in. which were tied together by steel lattice.

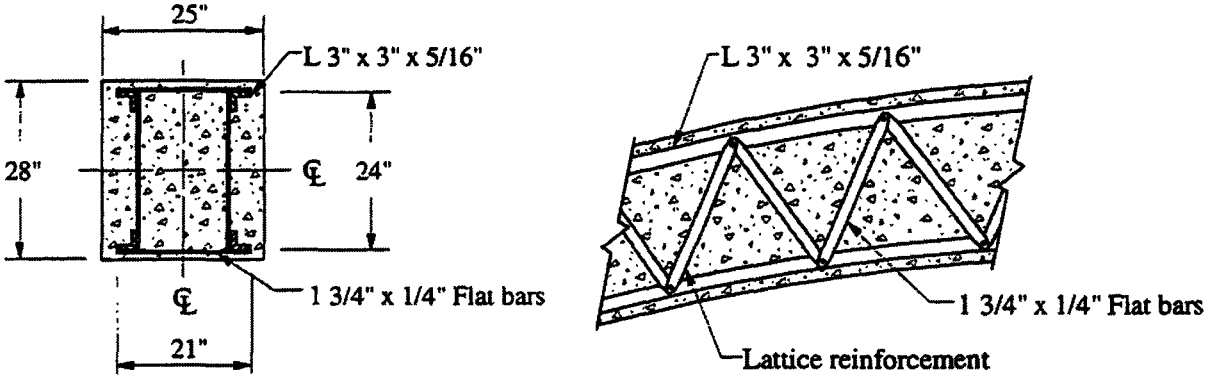

a. Cross-section at crown

b. Profile

Figure 2.5. Bridge I: Configuration and reinforcing details of arches.

2.1.1. Condition Assessment

Before service load testing the bridge, a visual inspection of the major components was conducted and previous inspection reports were obtained. From the latest inspection conducted in 1995, the deck and superstructure were given a condition rating of 3 based on a scale of 0-9 where 0 represents failed condition and 9 represents excellent condition. The bridge was also posted for 15 tons and one lane.

From the visual inspection conducted by the researchers, it was determined that the arches had severe spalling along their entire lengths. The spalling was so severe at the abutments, on the underside at the crown, and at the juncture of the railings that the reinforcement was exposed. In the areas where the concrete had spalled and exposed the

steel reinforcing, corrosion and pitting of the steel was noted. Several pictures of the deterioration in the arches are presented in Figure 2.6.

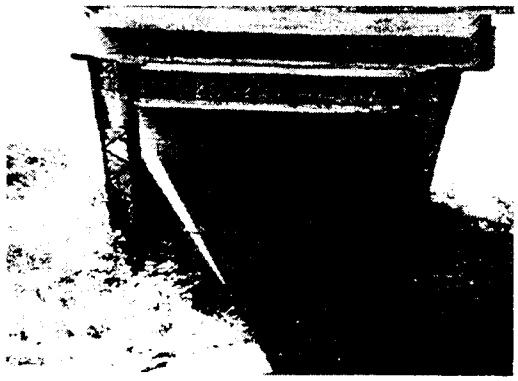

a. Deterioration at north abutment

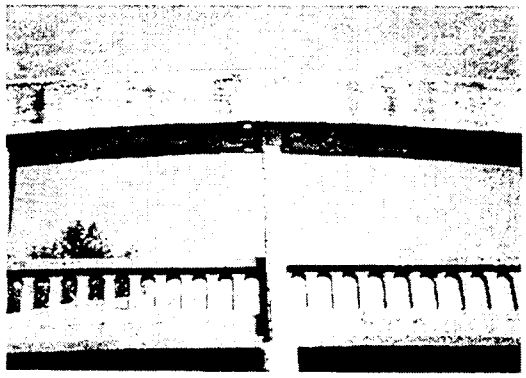

b. Deterioration at crown of west arch

c. Deterioration at juncture of railings

Figure 2.6. Bridge I: Photographs of arch deterioration.

Typical deterioration within the hangers is shown in Figure 2.7. In a majority of the hangers, the concrete had delaminated on the inside (road side) and outside (stream side) faces, and in a few cases, a significant amount of the concrete was missing. On the hangers where the concrete had fallen off and the steel reinforcing was exposed, pitting, corrosion, and an extensive loss of section were noted. From the steel samples removed from the hangers for testing, the average loss of section area per angle was determined to be 15 percent.

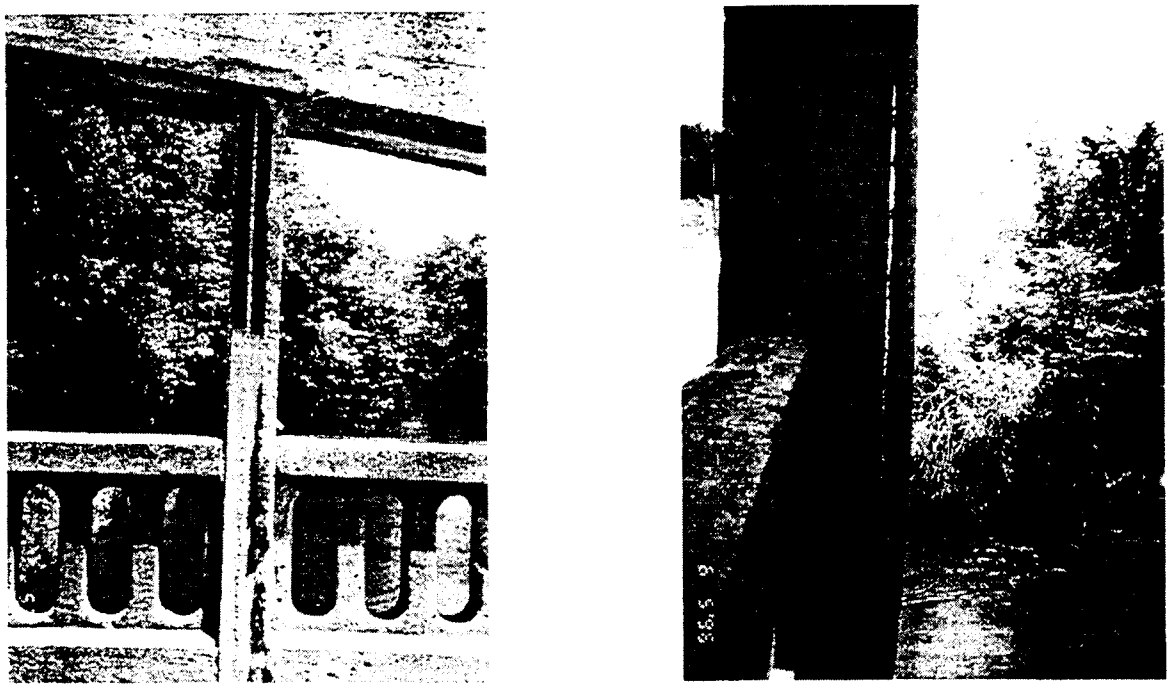

a. Exposed reinforcement

b. Delaminated concrete

Figure 2.7. Bridge I: Photographs of hanger deterioration.

Of all the components, the deck had the worst deterioration. A section of approximately 9,145 mm (30 ft) in length located within the center portion of the bridge had sustained a loss of over 25 mm (1 in.) of the wearing surface and showed extensive cracking and crumbling from numerous freeze-thaw cycles. A photograph of the deteriorated section is presented in Figure 2.8.

Figure 2.8. Bridge I: Photograph of deck deterioration.

The last major component to be visually inspected was the transverse floor beams. In all of the beams, the deterioration was most prevalent along the bottom. Concrete delamination had occurred along their entire lengths and in a few locations the concrete was missing. The exposed steel was corroded and pitted. Figure 2.9 shows typical deterioration of the beams. The reinforcing steel which remained encased in concrete was in good condition and showed no signs of deterioration

The wear and deterioration of this bridge can be attributed to many factors. Because entrained air had not been developed when this bridge was built, the concrete experienced severe spalling from continuous freeze-thaw cycles. Also, because the quality control of the concrete mix was not as stringent as it is today, the aggregate gradation consisted of large amounts of course aggregates. In some areas of the bridge, the concrete mix contained aggregate which exceeded 76 mm (3 in.) in diameter. An excessive amount of course aggregate leads to a highly porous mix which allows water to penetrate. The adverse of effects of water penetration are clearly seen in the hangers. Water penetrated

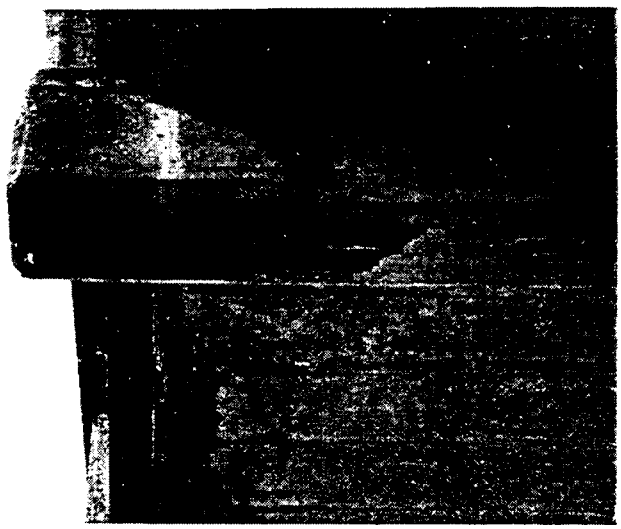

Figure 2.9. Bridge I: Photograph of beam deterioration.

through the concrete and began corroding the reinforcing steel. When steel begins to corrode it expands and delaminates the concrete cover. No petrographic study was conducted on the concrete.

This bridge has been periodically inspected. However, in the past 25 years, the only repairs that have been undertaken have been to the deck. In these repairs, asphalt was added to several areas of the deck to improve the riding surface, thus keeping the bridge in operating condition. These repairs obviously did not improve the structural integrity of the bridge.

2.2. Demolition

One of the major factors in selecting this bridge for testing was the fact that it was scheduled for replacement and material samples could be obtained for laboratory testing. Two months after the service load testing was completed, demolition of the bridge began. Prior to the demolition, material samples were removed from the bridge; see Figure 2.10 for the locations of where the samples were taken. The material samples collected included: seven concrete cores from the deck, five pieces of reinforcing steel from the deck, two sections of structural steel angles from the hangers, and an entire concrete floor beam. The

concrete core samples were obtained from the end of the deck where the concrete was not as deteriorated. The reinforcing steel samples were obtained from the center portion of the bridge and the structural steel angle samples were obtained from the center hangers. The concrete floor beam was removed from the center of the bridge.

To document the demolition, the process was video taped and photographed. Over two hours of video footage were obtained of various stages of the demolition process. Also, over 70 photographs were taken of various reinforcing and connection details and of different stages of the demolition.

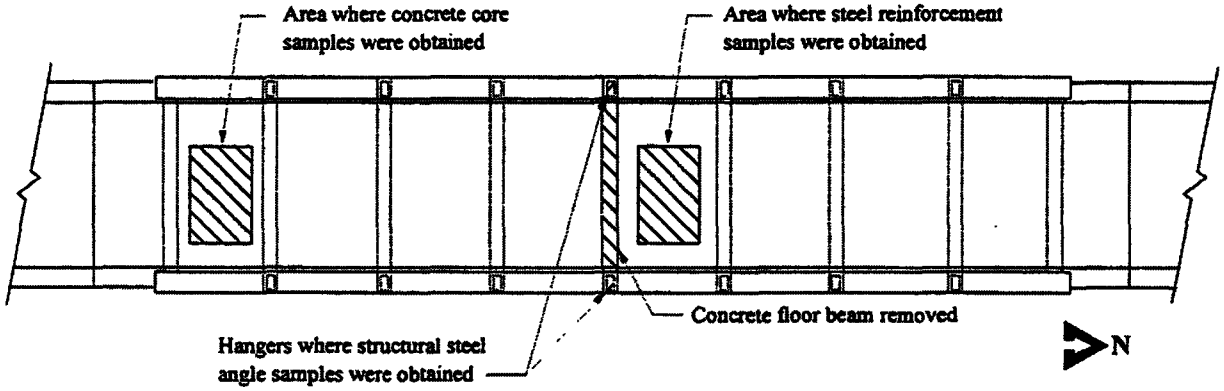

Figure 2.10. Bridge I: Locations of material samples.

2.3. AASHTO Rating

As a result of the bridge demolition, the condition of the various components and the exact locations and amounts of reinforcement were determined. Also, from the laboratory testing of the material samples, actual material strengths were attained. With this information, a more precise theoretical load rating of the bridge could be determined.

The components that were analyzed to obtain an overall rating for the bridge included: the floor beams, deck, hangers, and arches. The rating vehicles were positioned to produce maximum shear and moment in the floor beams, deck and arches and maximum axial force in the hangers. In rating the various components, the procedures outlined in The Manual for Maintenance Inspection of Bridges [1] and Guide Specifications for Strength

Evaluation of Existing Steel and Concrete Bridges [11] were followed. The material strengths determined from the laboratory testing were used for the concrete and steel. The modulus of elasticity of the concrete was determined using the equation, $E_c = 5{,}000\sqrt{f'_c}$ ($57{,}000\sqrt{f'_c}$); the modulus of elasticity of the steel was taken as 200,000 MPa (29,000,000 psi). The LRFR method rating explained in Sec. 1.7 was used to obtain the rating factors.

The calculations used to determine the rating factors of each of the components are presented in Appendix B. It should noted that the calculations are only presented for the critical mode of failure. Using the HS20 rating vehicle, the rating of the bridge was governed by the deck; however, using the Type 3 rating the vehicle the rating of the bridge was governed by the floor beams. The overall rating of the bridge was governed by the deck. A summary of the theoretical load ratings for the various components is presented in Table 2.1.

Table 2.1. Bridge I: Theoretical Load Rating Summary.

	Vehicle HS20 AASHTO LRFR		Vehicle Type 3 AASHTO LRFR	
	Rating Factor	Rating (tons)	Rating Factor	Rating (tons)
Slab:	0.94	39.8	1.50	37.5
Beams:	1.18	42.5	1.43	35.8
Hangers:	2.19	78.8	2.64	66.0
Arches:	4.14	149.0	5.18	129.5

Indicates controlling component

2.4. Test Setup and Procedures

To modify the load rating of the bridge, strains produced by the test vehicle were monitored in the arches, hangers, and beams. Also, to observe the general structural behavior of the bridge, deflections at various locations were obtained.

Deflections in the bridge were monitored at the centerlines of beam B5 and deck panels S6, S7, and S8; refer to Figure 2.11 for the location of the deflection transducers. Also, deflections were monitored at the ends of beams B3, B5, and B7. These locations were selected to observe the behavior of the arches, deck panels and center beam as the test vehicle

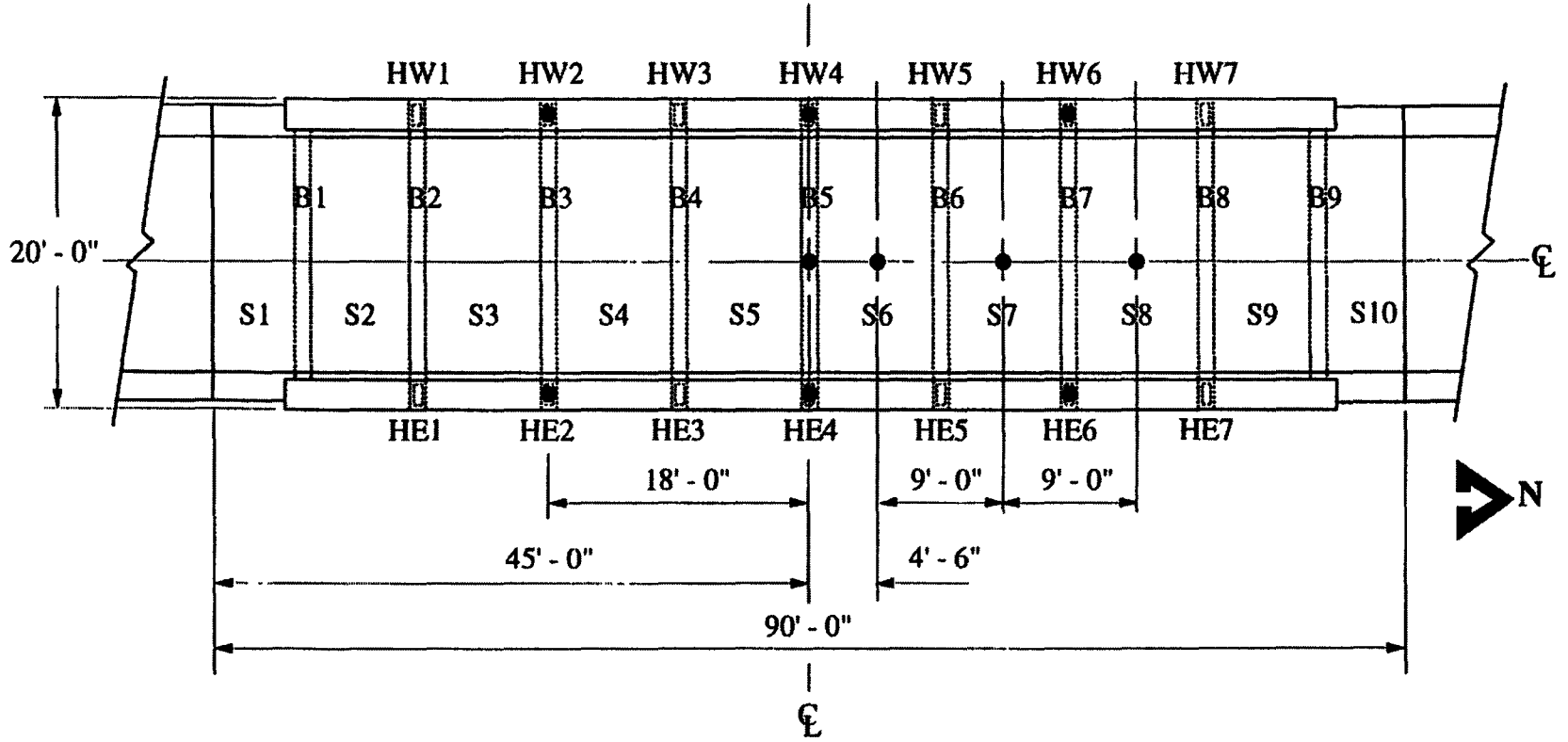

- ● Deflection transducer locations
- Bx Beam numbers (x = 1 - 9)
- Sx Deck panel numbers (x = 1 - 10)
- HWx West hanger numbers (x = 1 - 7)
- HEx East hanger numbers (x = 1 - 7)

Figure 2.11. Bridge I: Location of deflection transducers.

moved across the bridge. All deflections in the bridge were obtained using the equipment and setup described Sec. 1.6.1.

Strains in the arches, hangers, and beams were monitored at the center of the bridge. The centerline location of the bridge was chosen to obtain strain data from the various components because this was the critical location for each of the elements. Due to the presence of small cracks and general concrete deterioration on the underside of the deck panels, no strain gages were attached to the slab.

Strains were monitored in hangers HW4 and HE4 (see Fig. 2.11). Because the concrete had fallen off the faces of the hangers, strain gages were applied to each of the four exposed structural steel angles in each hanger.

Strains were monitored at the crown of all four sides of the two arches. One strain gage was bonded to the top face and one was bonded on each of the side faces. On the bottom face of each arch, the concrete had fallen off and strain gages were bonded to each of the exposed steel angles.

Strains in beam B5 were observed at the centerline of the member. As with the other two components, the concrete had fallen off exposing two structural steel angles to which strain gages were bonded. Strain gage locations for the three elements are presented in Figure 2.12. The strain gages used and the application process were described in Sec. 1.6.1.

The type of vehicle and loading process used in testing the bridge were described in Sec. 1.6.2. For this bridge, the loading was applied in three increments. In the first load increment, the test vehicle had a gross vehicle weight of 115,655 N (26,000 lbs). In load increments two and three, the test vehicle had a gross vehicle weight of 160,170 N (36,000 lbs) and 231,310 N (52,000 lbs) respectively. The magnitude of the load increments and wheel configuration of the test vehicle are presented in Figure 2.13; a photograph of the test vehicle is presented in Figure 2.14.

To observe the structural behavior of the bridge, the test vehicle was stopped at beams B1 through B9 and deck panels S6, S7, and S8 and data readings were taken; Figure 2.15 shows the stopping locations of the test vehicle. The lane positioning of the test vehicle was described in Sec. 1.6.2 and is shown in Figure 2.16. The test vehicle was positioned on the

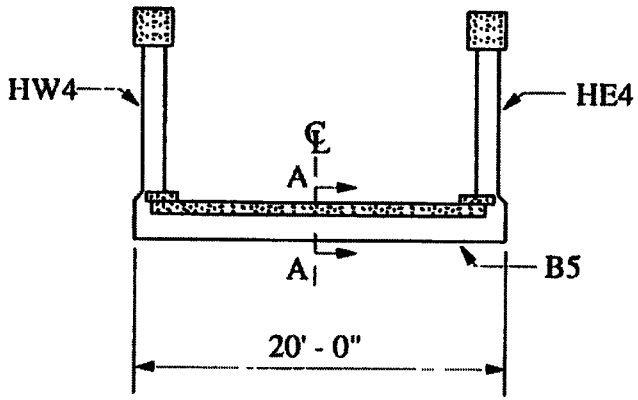

a. Cross section at centerline of bridge

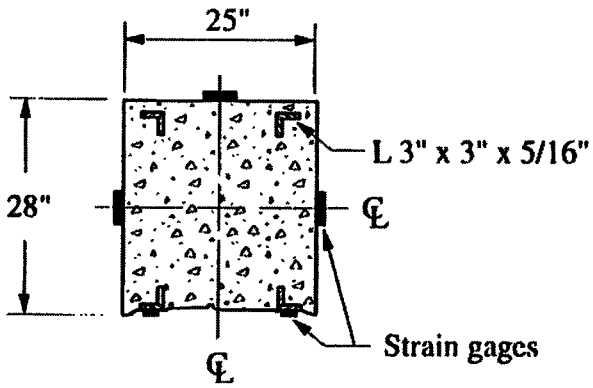

b. Location of strain gages at crown of arches

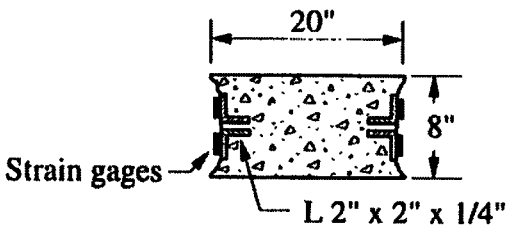

c. Location of strain gages on hangers HW4 and HE4

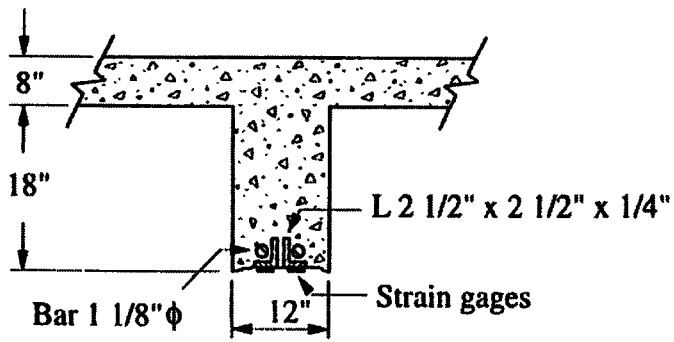

d. Section A-A

Figure 2.12. Bridge I: Location of strain gages at centerline of bridge.

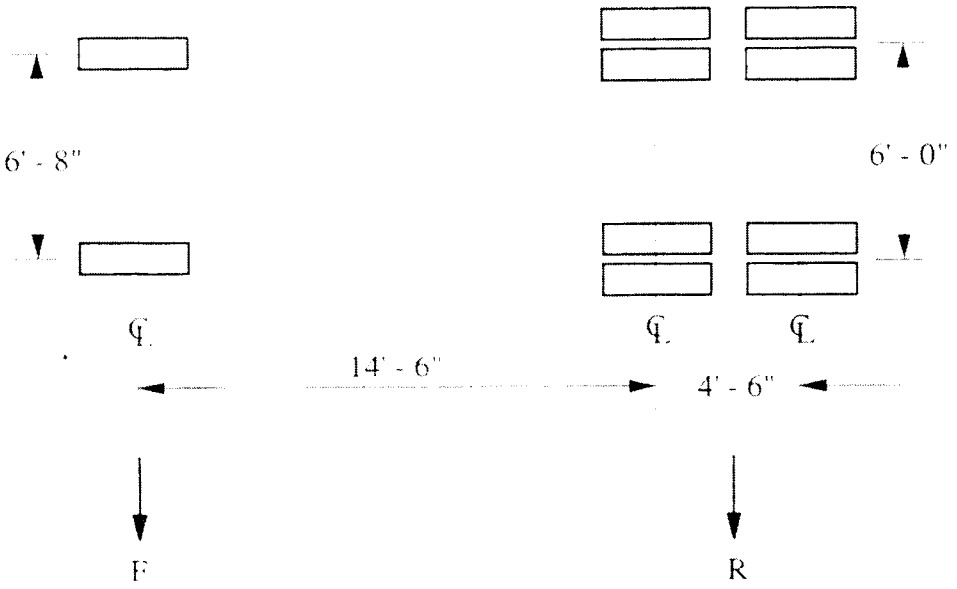

Load Increment	F (kips)	R (kips)	Total Load (kips)
1	12.0	14.0	26.0
2	12.0	24.0	36.0
3	14.0	38.0	52.0

Figure 2.13. Bridge I: Wheel configuration and weight distribution in test vehicle.

Figure 2.14. Bridge I: Photograph of test vehicle on bridge.

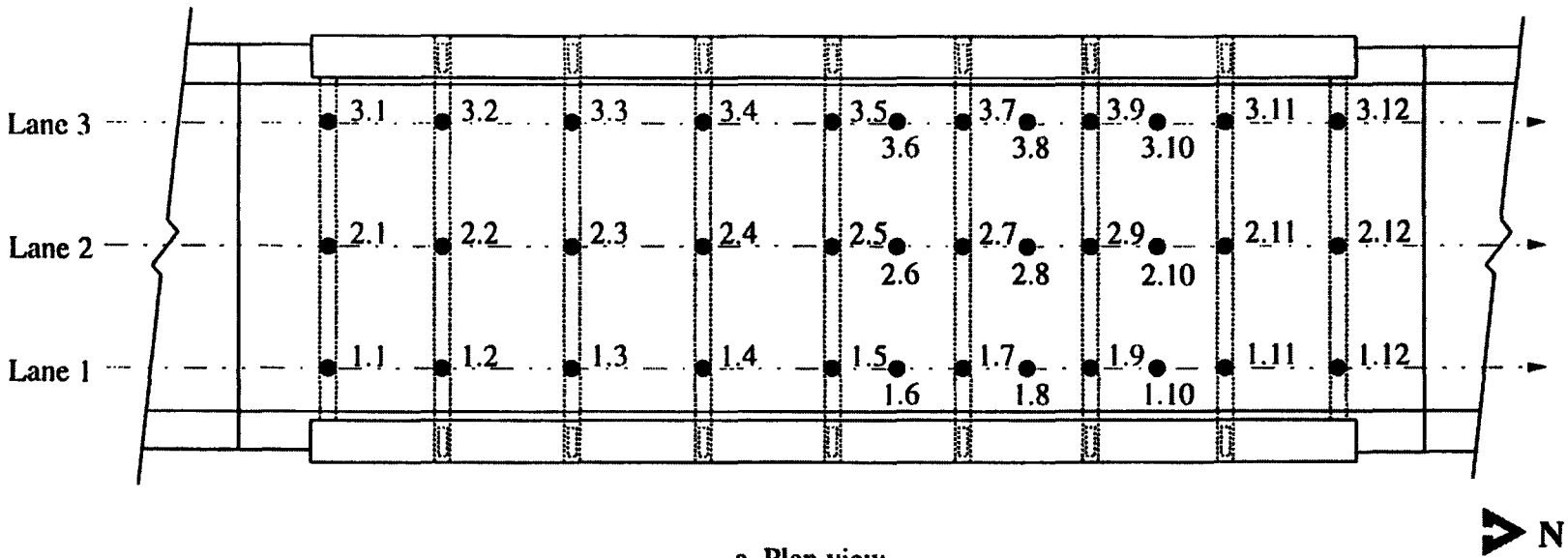

a. Plan view

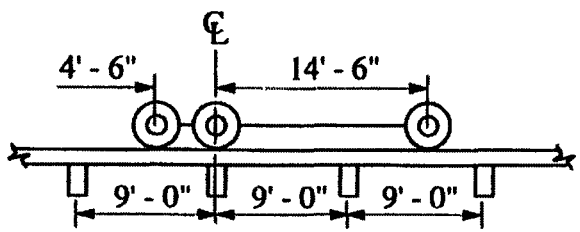

b. Truck position on beams

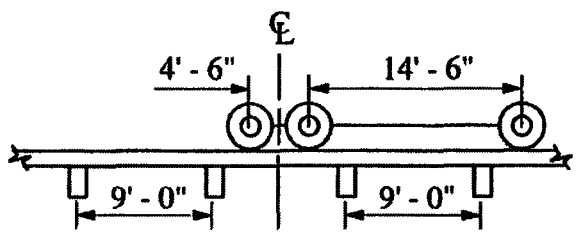

c. Truck position on deck panels.

Figure 2.15. Bridge I: Longitudinal location of test vehicle for various tests.

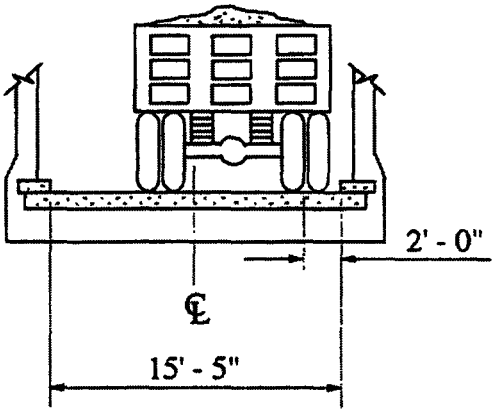

a. Lane 1

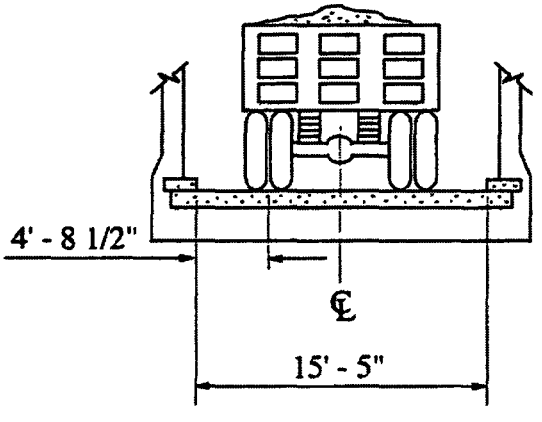

b. Lane 2

Figure 2.16. Bridge I: Transverse location of test vehicle on bridge.

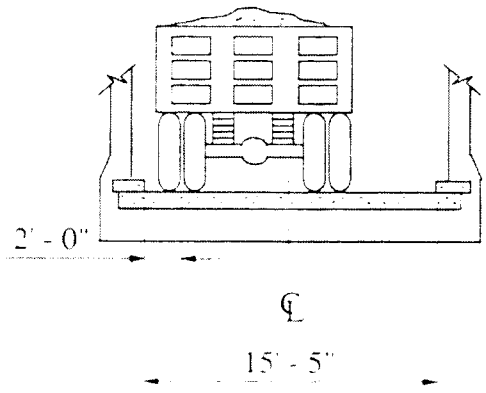

c. Lane 3

d. Photograph of test vehicle in Lane 3

Figure 2.16. Continued.

beams with the front wheel of the rear tandem centered over the members. The test vehicle was positioned on the deck panels with the tandem wheels centered on the panels.

2.5. Material Specimens

As previously described, material samples were obtained from the bridge before it was demolished. The samples that were obtained for laboratory testing included: concrete cores from the deck, structural steel reinforcing from the hangers, reinforcing steel from the deck, and a concrete floor beam.

2.5.1. Test Equipment and Procedures

2.5.1.1. Concrete Core Samples

To determine the compressive strength of the concrete, seven 102 mm (4 in.) diameter cores were obtained from the deck. Due to the irregularities in the deck, the lengths of the cylinders varied.

To prepare the cylinders for testing, the ends were cut to a obtain a smooth surface and capped using a sulfur mortar according to American Society of Testing and Materials (ASTM) C 617 [13].

The testing of the cylinders was conducted according to ASTM C 39 [14] and C 42 [15]. The specimens were compressed at a constant rate of 0.24 MPa/s (35 psi/s) using an universal testing machine.

2.5.1.2. Concrete Floor Beam

To obtain the nominal capacity and to observe the failure mechanism, a concrete floor beam was removed from Bridge I for testing. The transverse beam that was removed (see Fig. 2.10 for location of beam) was the one that was monitored for strains and deflections during the diagnostic load test.

Because a concrete saw was not available, the floor beam was removed using a wrecking ball and an acetylene torch. Removal was accomplished by having the wrecking

ball tap along each side of the beam in order to break away the concrete and expose the reinforcing in the deck. Care was taken to leave the part of the deck that was effective as the flange of the T-beam and also not to damage the beam. Once the concrete had been broken away the acetylene torch was used to cut the reinforcing bars in the deck; final removal was accomplished by cutting the hangers from the beam.

Removal of the beam using the wrecking ball left a varying width of deck connected to the beam. To obtain a constant width of section for testing purposes, the overhanging portion of the deck was reformed and new concrete added. The portion of the deck that was reformed extended out 610 mm (2 ft) from each side of the beam and had a thickness of 205 mm (8 in.) which matched the original thickness of the deck. The deck was extended 610 mm from each side of the beam to provide the width of slab effective as a T-beam flange, as required in the Standard Specifications for Highway Bridges Sec. 8.10.1.1 [12] for a beam length of 6,095 mm (20 ft). Thus, the total width of beam flange after the addition of the new concrete was 1,525 mm (5 ft). A photograph of the concrete beam with form work in place is presented in Figure 2.17.

To prepare the existing slab for the new concrete, the uneven edges were hosed and scrubbed with water to remove any laitance. Because the longitudinal reinforcement from the existing slab was still in tact and the exposed faces were adequately roughened, no bonding agents were used. One problem with placing new concrete against old concrete is matching the compressive strengths of the two mixes. The average compressive strength of the existing concrete was obtained from the cores removed form the deck and was determined to be 30 MPa (4,320 psi) To match the compressive strength of the existing concrete, a standard C4 concrete mix supplied by a local concrete plant was used for the new flange section. This mix had a compressive strength of 28 MPa (4,000 psi) on the day in which the beam was tested. The compressive strength of the new concrete was obtained from 152 mm x 305 mm (6 in. x 12 in.) cylinders which were cast the same day the flange of the beam was cast. Photographs of the beam after pouring and form removal are shown in Figure 2.17c and d, respectively.

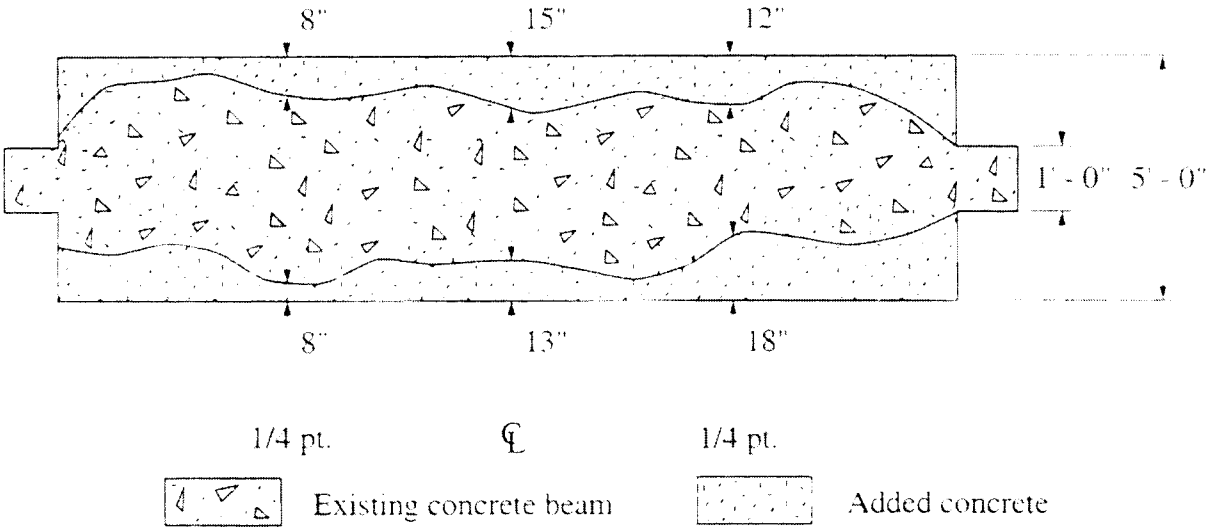

a. Plan view of added concrete

b. Photograph of concrete floor beam and form work

Figure 2.17. Bridge I: Schematic of concrete floor beam and slab.

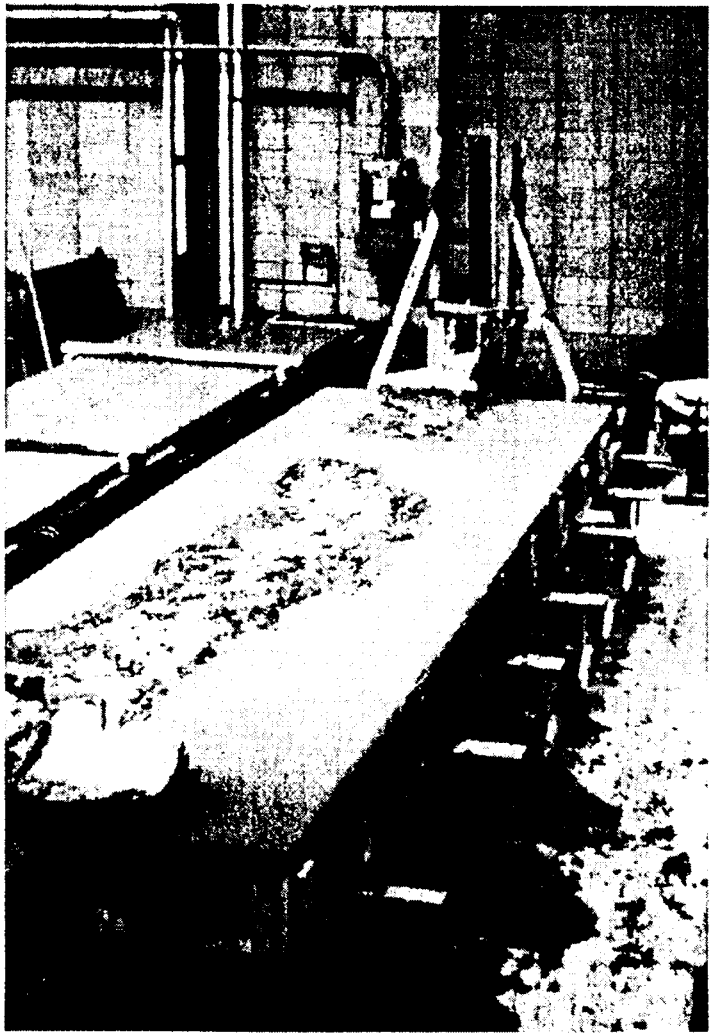

c. Beam after concrete placement

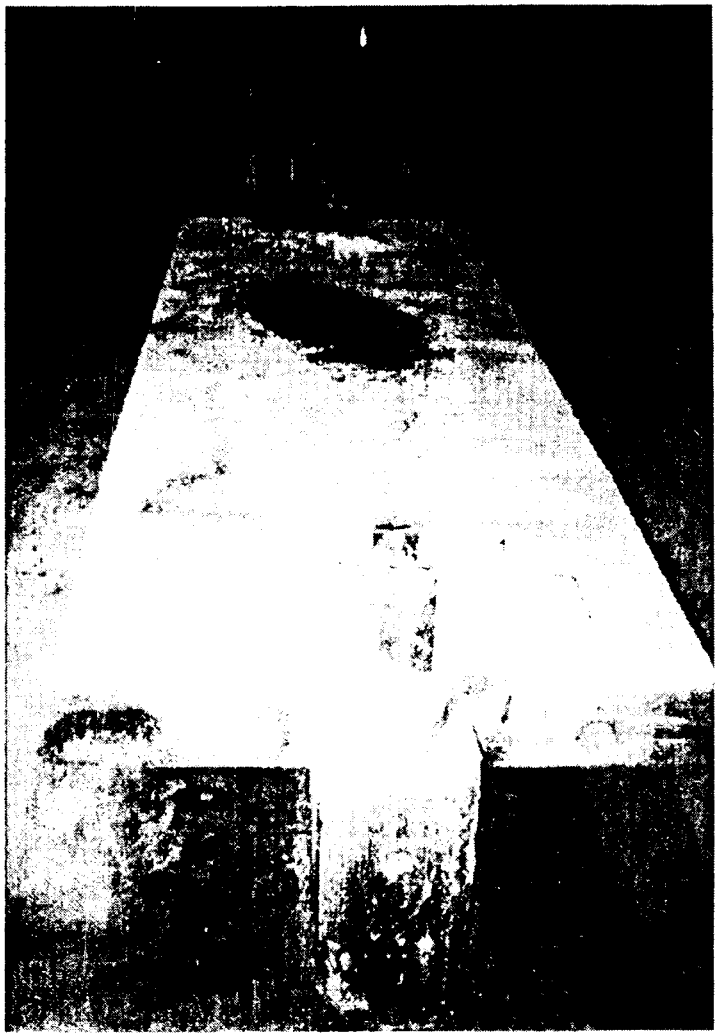

d. Beam after form removal

Figure 2.17. Continued.

During the removal of the beam from the bridge, a large diagonal crack developed towards the west end of the beam. To obtain the maximum moment in the beam and prevent premature shear failure, two external stirrups shown in Figure 2.18a were added. The legs of the stirrups consisted of 16 mm (5/8 in.) Dywidag bars. The legs were attached to the deck by drilling holes through the flange and fastening the Dywidag bars with nuts and washers. Two C8x11.5 steel channels were used to connect the legs across the bottom of the beam. As shown in Figure 2.18a, the two external stirrups were 180 mm (7 in.) apart across the diagonal crack.

Testing of the beam consisted of applying two point loads having an area of 92, 905 mm^2 (1 ft^2) along the centerline of the beam. The point loads were postioned to produce maximum moment in the beam and also to simulate the rear wheels of the standard rating vehicles presented in Figure 1.1.

Loading of the beam was accomplished by means of two 533,785 N (120,000 lbs) hydraulic rams spaced 1,830 mm (6 ft) apart. The loading frame consisted of two W12x87 steel beams centered on top of the hydraulic rams. The beams were then secured to the laboratory floor by means of 29 mm (1 1/8 in.) Dywidags. Support conditions for the beam consisted of a pin and a roller and were spaced at 205 mm (8 in.) from the ends of the beam. Figure 2.18 shows the configuration of the beam test.

During the testing of the beam, strains and deflections were monitored at various locations. Three strain gages were applied on top of the deck at the centerline of the beam. The gages were place transversely across the deck at 381 mm (15 in.) spacings. Also, strain gages were placed on the bottom of the beam web at the centerline of the beam. The concrete at this location had fallen off and one strain gage was bonded to each of the two exposed structural steel angles. The strain gages used and surface preparation are described in Sec.1.6.1.

The magnitude of the applied load was measured using a 222,410 N (50,000 lb) load cell at each load point. Deflections in the beam were monitored at the quarter points and the centerline. Deflection transducers were attached to the edges of the flange at the centerline of the beam to monitor the rotation of the beam as it was being loaded. Sec. 1.6.1 describes the

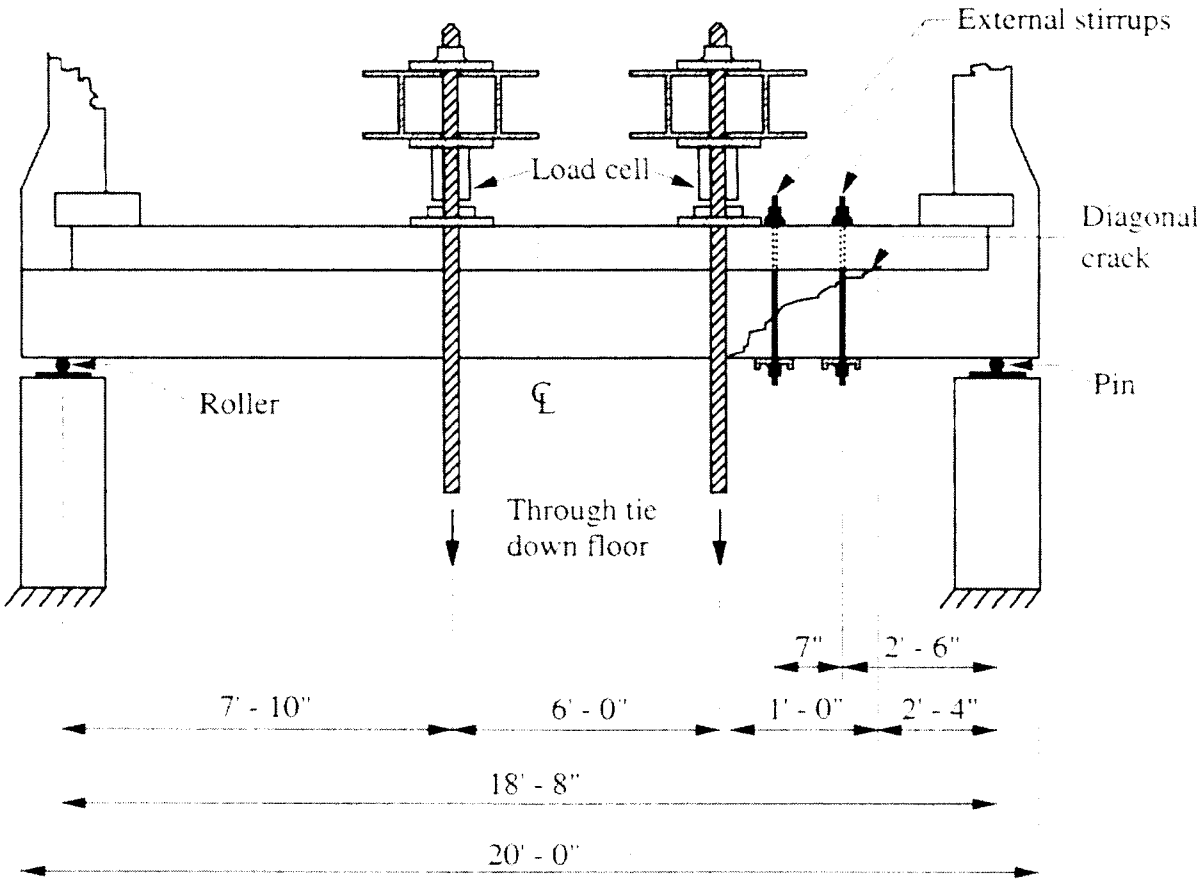

a. Test configuration

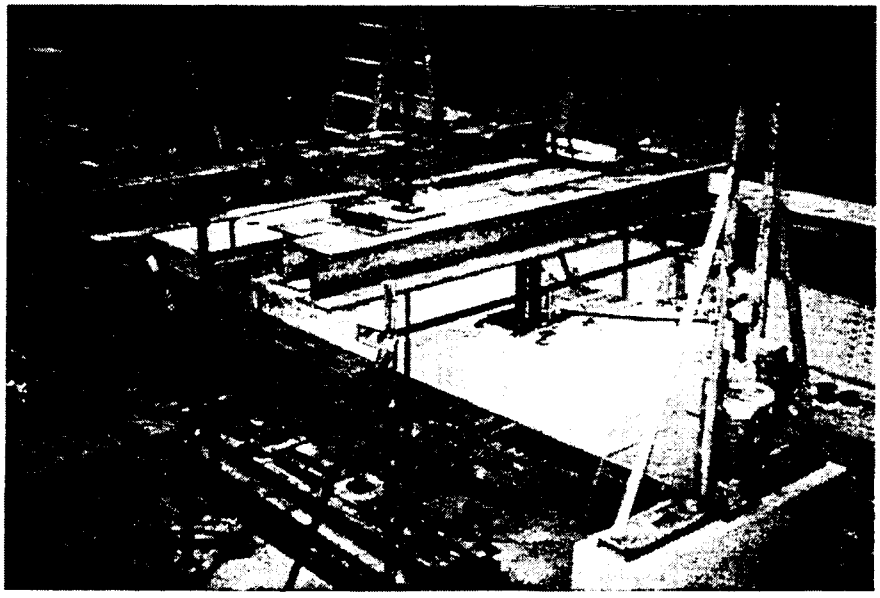

b. Photograph of test configuration

Figure 2.18. Bridge I: Beam test setup.

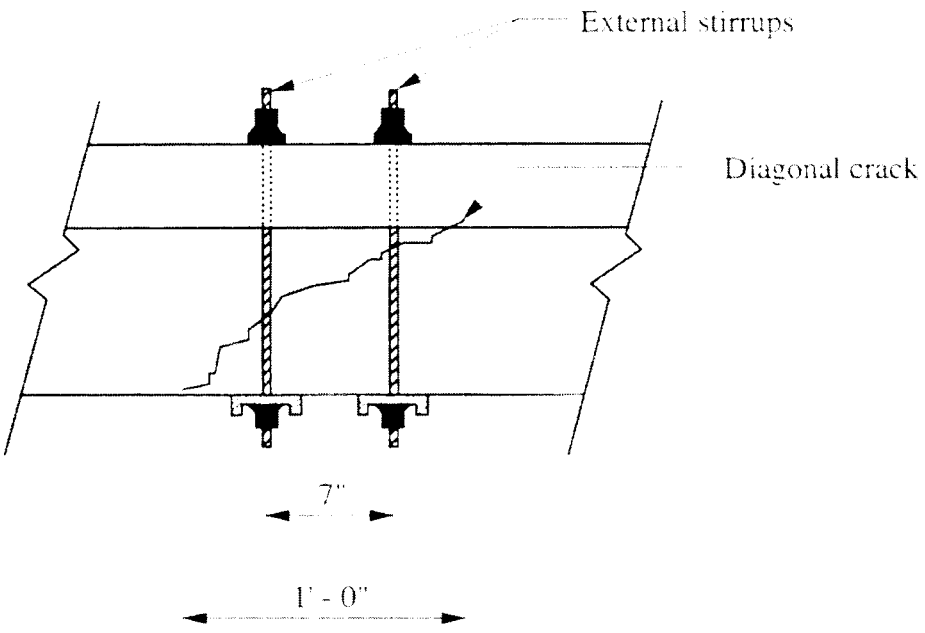

c. Cracked section

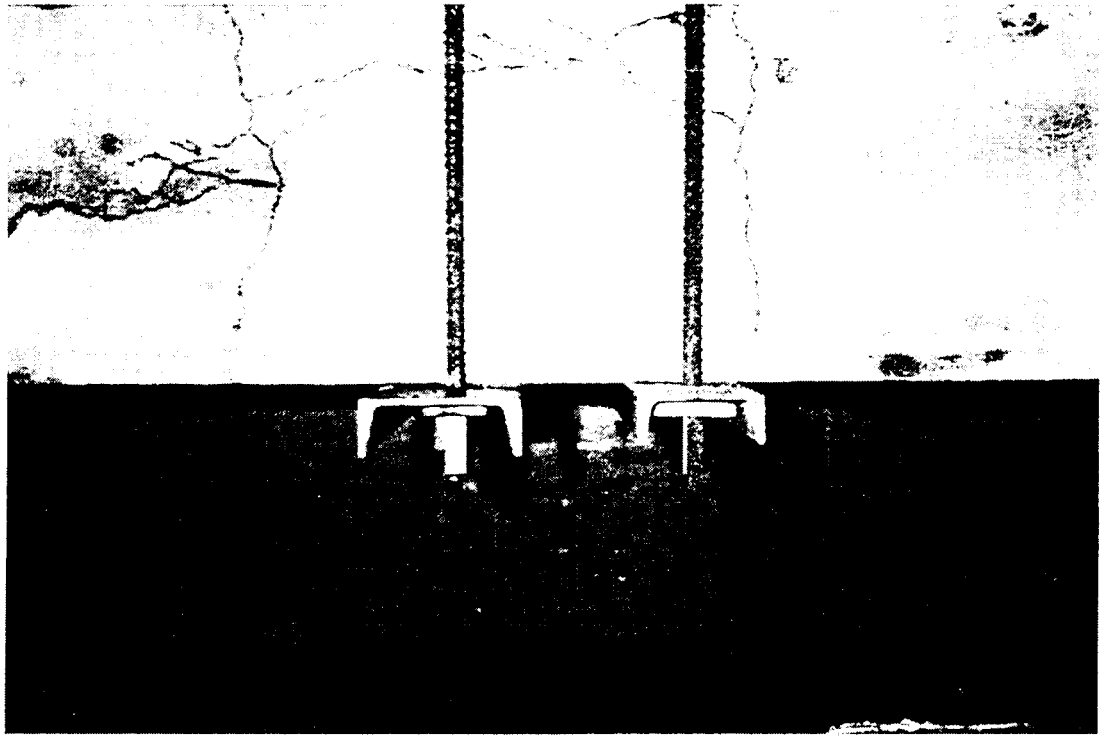

d. Photograph of external stirrup

Figure 2.18. Continued.

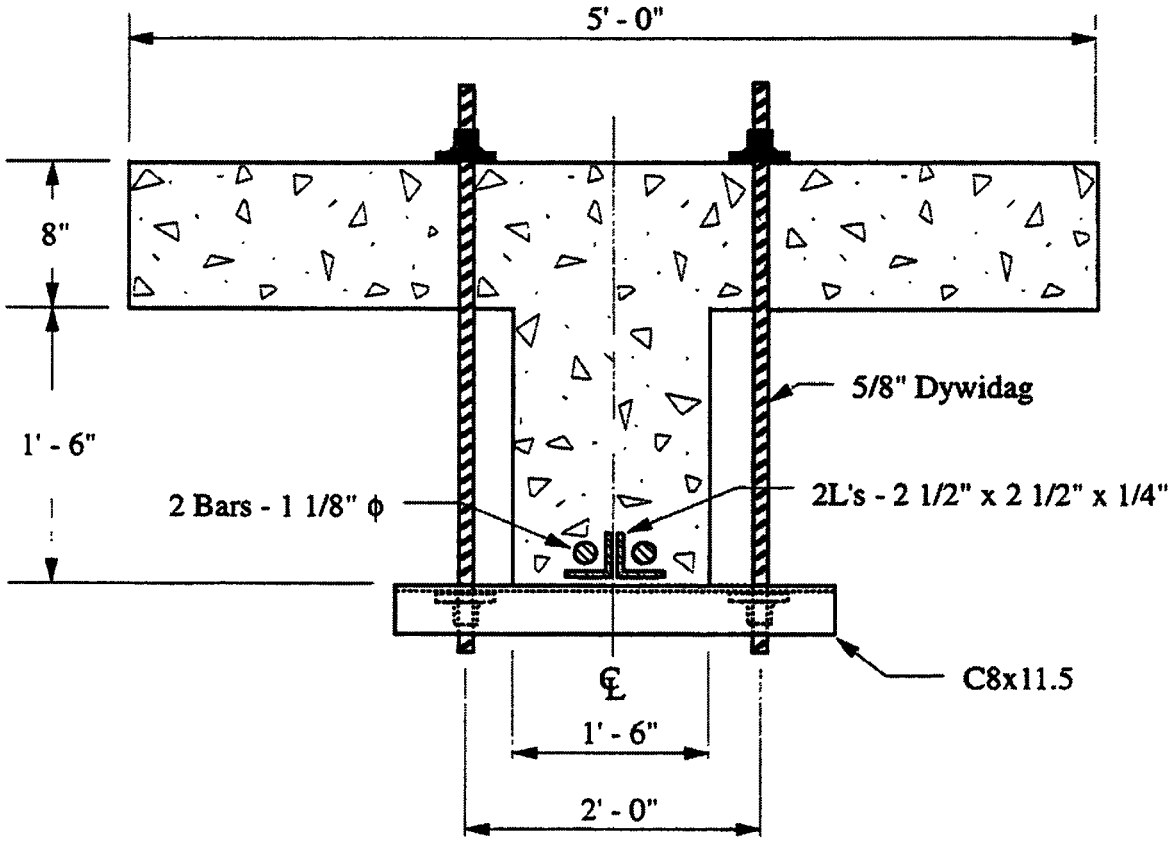

e. External stirrup configuration

Figure 2.18. Continued.

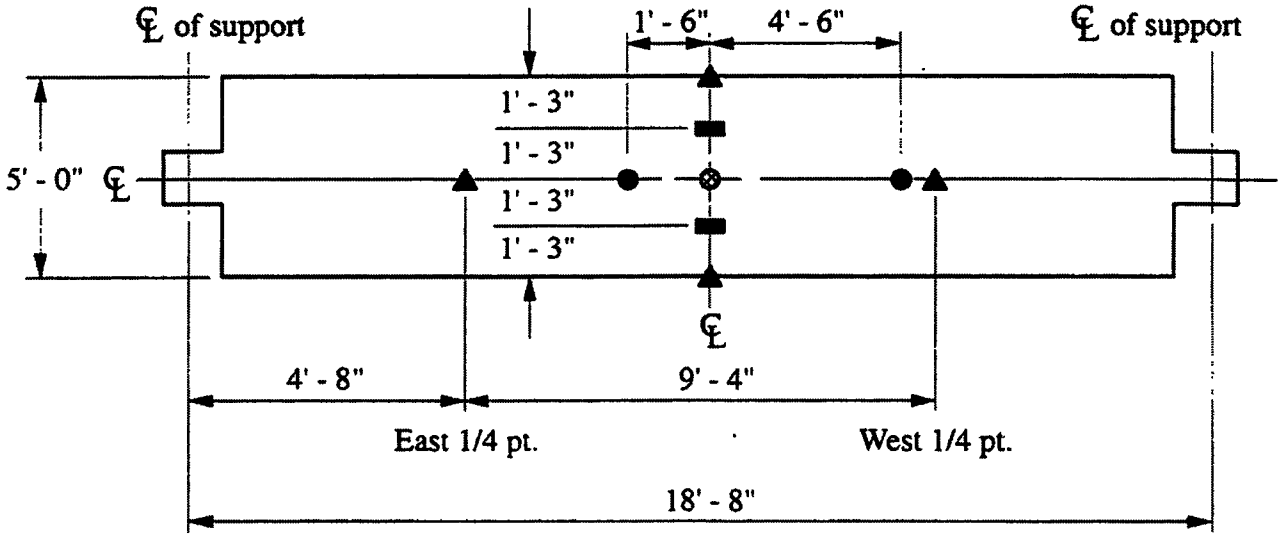

▲ Deflection transducers
▬ Strain gages
⊗ Deflection transducers and strain gages
● Load points

a. Plan view of gaging locations

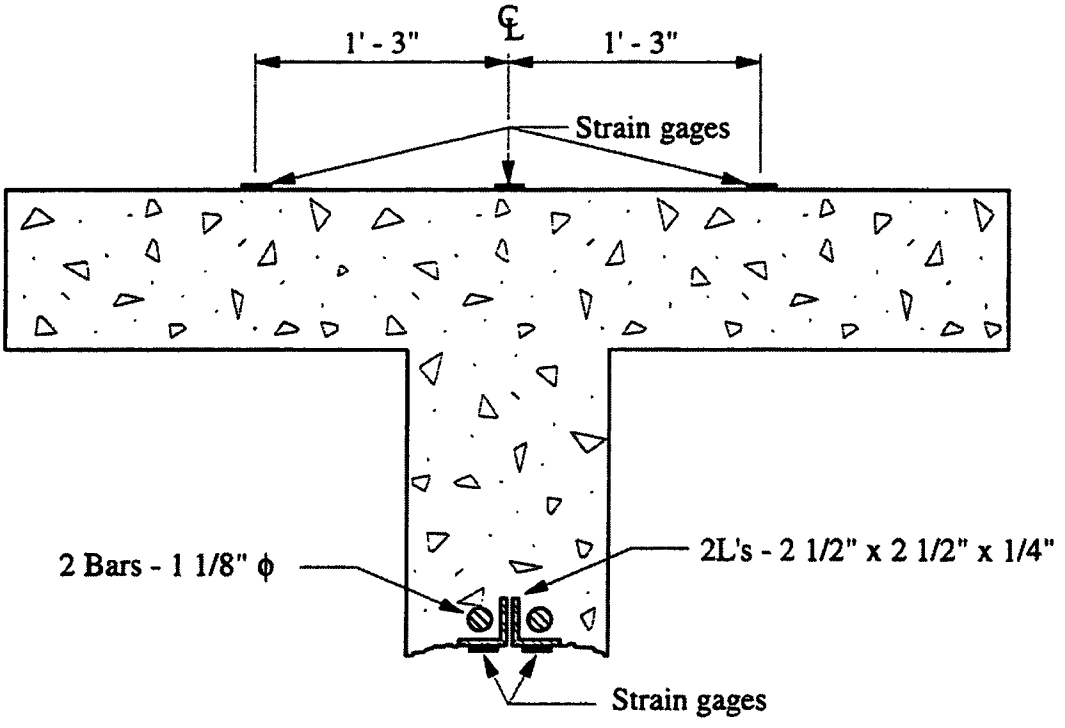

b. Location of strain gages at centerline

Figure 2.19. Bridge I: Location of strain gages and deflection transducers on test beam.

setup and deflection transducers used in the testing. Figure 2.19 shows the locations of the strain gages and deflection transducers in the test beam.

Loading of the beam was applied in two cycles at a constant rate using a hand pump. In the first cycle, the beam was loaded until the tension steel began to yield and then was unloaded. Strain, deflection, and load readings were taken during the first cycle at 2,225 N (500 lb) increments using a DAS. Prior to reloading the beam, the external stirrup was removed to determine if the diagonal crack would result in shear failure of the beam. The load was then reapplied in the preceding increments until the tension steel yielded and compression failure of the concrete was observed in the flange. The removal of the external stirrup did not have any effect on increasing the load carrying capacity of the beam. The resulting failure was in bending rather than shear.

2.5.1.3. Steel Samples

To obtain the yield strength of the reinforcing steel in the bridge, structural steel angle specimens were removed from the center hangers and reinforcing steel specimens were removed from the deck. Also, the reinforcing bars in the test beam were obtained following the laboratory testing. Refer to Figure 2.10 for the locations where the specimens were obtained.

Two of the four structural steel angles in hangers HW4 and HE4 were removed for testing. The specimens were over 1,220 mm (4 ft) long and were removed using an acetylene torch. To obtain specimens for testing, coupons were obtained from the legs of the angles.

Five reinforcing steel specimens were removed from the deck. The specimens obtained were over 1,220 mm (4 ft) long and were removed using an acetylene torch. As with the structural steel specimens, the reinforcing bars were cut into 455 mm (18 in.) lengths and then milled to remove any pitting or corrosion.

A 915 mm (3 ft) section from each of the two reinforcing bars in the test beam were removed. The two specimens were cut into 460 mm (18 in.) lengths and then milled to remove any pitting or rusting.

Testing of each of the specimens was conducted according to ASTM A 370 [16]. The specimens were loaded in tension at a constant rate of 379 MPa/min (55,000 psi/min) using an universal testing machine. Strain in the specimens was monitored using an extensometer. The load and strain data were obtained using a DAS; specimens were loaded until failure occurred.

2.6. Results and Discussion

2.6.1. Bridge I

The response exhibited by the various bridge components during the diagnostic load test was lower than anticipated. The strains obtained were well below the elastic limit of the material and the deflections were on the order of one to two millimeters (0.04 in. - 0.08 in.).

The strains obtained at the centerline of beam B5 were significantly lower than the yield point of the reinforcement for all three load increments. At load positions 1.5, 2.5, and 3.5 the strains remained linear elastic for the three load increments. The maximum tensile strain obtained was 143 microstrain and occurred during the last load increment when the test vehicle was located at load position 2.5. The theoretical strain calculated in the beam using the same load increment and load position was determined to be 399 microstrain. This is over two times the actual strain produced by the test vehicle yet both are still significantly lower than the yield strain (1,379 microstrain) of the reinforcement. The strains at the centerline of the beam for the three load increments and three vehicle positions is presented graphically in Figure 2.20.

The centerline deflection of beam B5 was also extremely small; the response of the beam remained linear as the weight of the test vehicle was increased. At load positions 1.5, 2.5, and 3.5, the centerline deflections remained the same for the three load increments. The deflections ranged from a low of 0.5 mm (0.02 in.) at the first load increment to a maximum of 1.8 mm (0.07 in.) at the third load increment. Figure 2.21 illustrates the centerline deflection of the for the three load increments and load positions.

The centerline deflections of deck panels S6, S7, and S8 were essentially the same magnitude as the centerline deflections of beam B5. In all three deck panels, the response

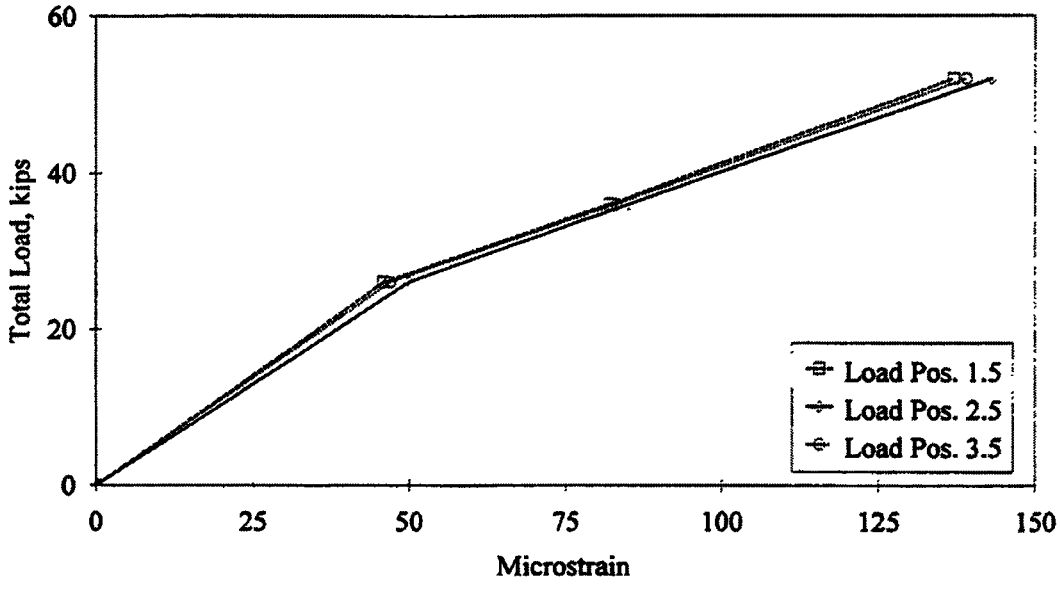

Figure 2.20. Bridge I: Bottom strain at centerline of beam B5.

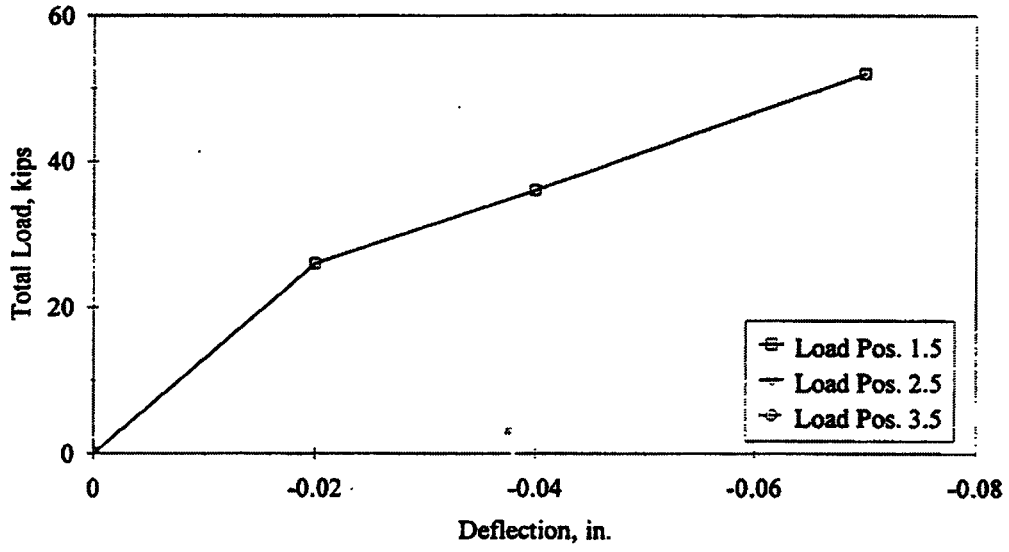

Figure 2.21. Bridge I: Centerline deflection of beam B5.

remained linear for the three load increments. Maximum deflections in panels S6, S7, and S8 occurred when the test vehicle was located at load positions 2.6, 2.8, and 2.10, respectively. Panels S6 and S7 had maximum deflections of 2 mm (0.08 in.) while panel S8 had a maximum deflection of 1.8 mm (0.07 in.). The deflections of panel S7 remained the same for the three load increments. The centerline deflections of the three panels are presented graphically in Figure 2.22. The anomaly in the graph of panel S8 (Fig. 2.22c) at load position 3.10 was caused by a malfunctioning deflection transducer at the time the data were taken.

As with the beam, the strains in hangers HE4 and HW4 were well below the yield strain of the steel. The response of the hangers remained linear for the three load increments. Also, as the weight of the test vehicle was increased, bending was observed in both HE4 and HW4. The extent of the bending increased with each load increment The bending of the hangers resulted from the rotation of the ends of beam B5. At load position 1.5 and load increments one , two, and three, the maximum tensile strain in the two angles on the inside face of hanger HE4 was 27, 43, and 69 microstrain, respectively. At the same load increments and position, the tensile strain in the two angles on the outside face of the hanger was 10,8, and 8 microstrain, respectively.

The same behavior was observed in hanger HW4. At load position 3.5 and load increments one, two, and three, the maximum tensile strain in the two angles on the inside face of hanger HW4 was 19, 39, and 70 microstrain, respectively. At the same load increments and position, the tensile strain in the two angles on the outside face of the hanger was 4,1, and 4 microstrain respectively.

Overall, the maximum strain values of 69 and 70 microstrain obtained from hangers HE4 and HW4 respectively are significantly lower than the yield strain of the reinforcement. The maximum strains in hangers HE4 and HW4 are presented in Figure 2.23 for load positions 1.5, 2.5, and 3.5 and the three loading increments.

The strains measured at the crowns of both arches were similar in magnitude to the strains measured in the floor beam and hangers; linear behavior was observed in each arch for the three load increments. The maximum strain at the crown of the east arch was obtained

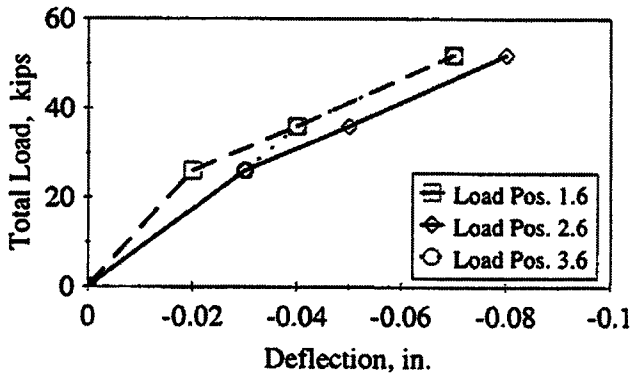

a. Deck panel S6

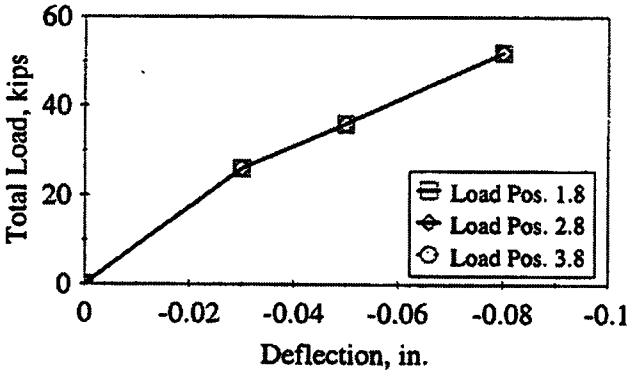

b. Deck panel S7

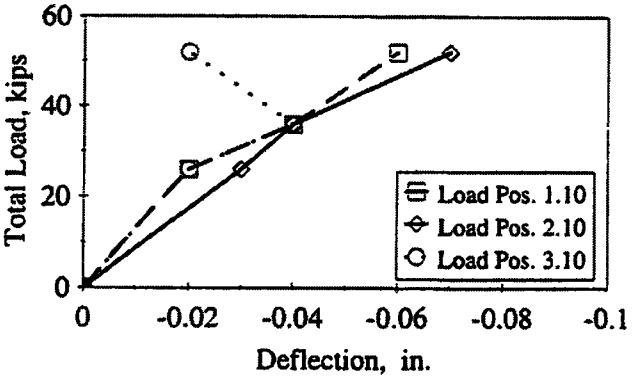

c. Deck panel S8

Figure 2.22. Bridge I: Centerline deflection of deck panels.

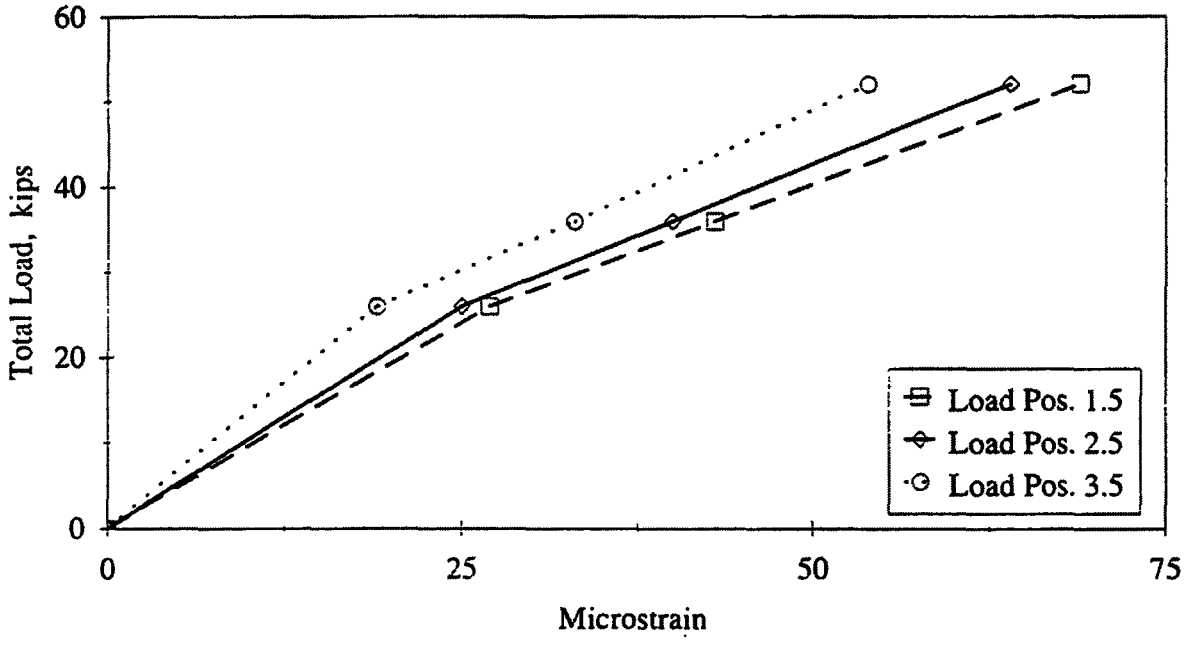

a. Hanger HE4

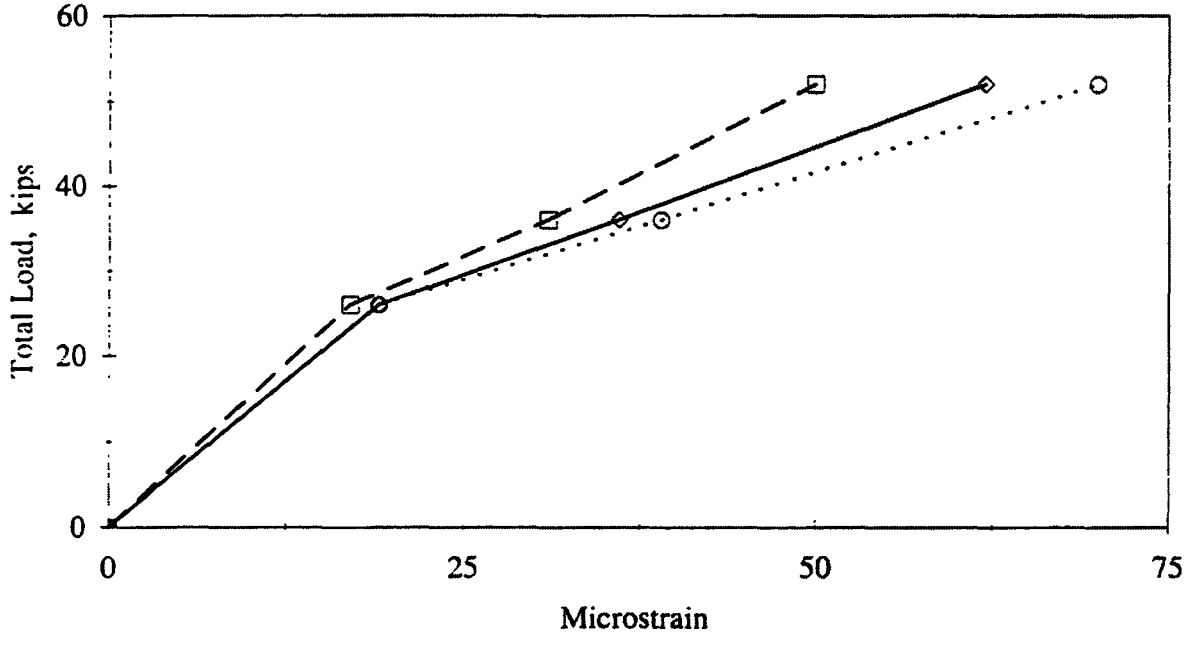

b. Hanger HW4

Figure 2.23. Bridge I: Strain in hangers.

when the test vehicle was located at load position 1.5, and the maximum strain at the crown of the west arch was obtained when the test vehicle was located at load position 3.5. Bending of the arches at the crowns was observed when the test vehicle was in these two positions. Compression was observed in the concrete on the top and side faces while tension was observed in the steel reinforcement on the bottom face. At load position 1.5 and load increments one, two, and three, the compressive concrete strain in the top face of the east arch was 24, 35, and 52 microstrain, respectively. While the tensile strain in the reinforcement at the bottom face of the east arch was 3, 10, and 17, respectively.

The behavior at the crown of the west arch mirrored that of the east arch. When the test vehicle was located at load position 3.5, the compressive concrete strain at the top face of the arch was 20, 30, and 46 microstrain for the three load increments, respectively. The tensile strain in the reinforcement at the bottom face of the arch was 2, 8, and 14 microstrain for the same three load increments. Bottom face strains in the east and west arches for the three load increments are presented in Figure 2.24.

The strains measured in the crowns of the east and west arches were significantly lower than strains at which compression failure in the concrete or yielding of the steel occurs. Compression failure of concrete is typically taken at 3000 microstrain which is significantly higher than the 52 microstrain obtained from the top face of the east arch. The maximum strain in the reinforcing steel was 17 microstrain which is significantly lower than the yield strain of steel.

As the test vehicle moved across the bridge, the deflections of the east and west arches were maximum at the crowns. The maximum deflection at the crown of the east arch was 0.8 mm (0.03 in.) and occurred at load increment three when the test vehicle was located at load position 1.5. The maximum deflection at the crown of the west arch was 1 mm (0.04 in.) and occurred at the same load increment when the test vehicle was located at load position 3.5. It should be noted that the deflections obtained included the deformations in hangers HW4 and HE4 since the deflection transducers were attached to the bottom of the beams and not directly to the arches. At deflection transducer locations HW2, HE2, HW6, and HE6, no deflection of the east or west arches was observed for all load positions and

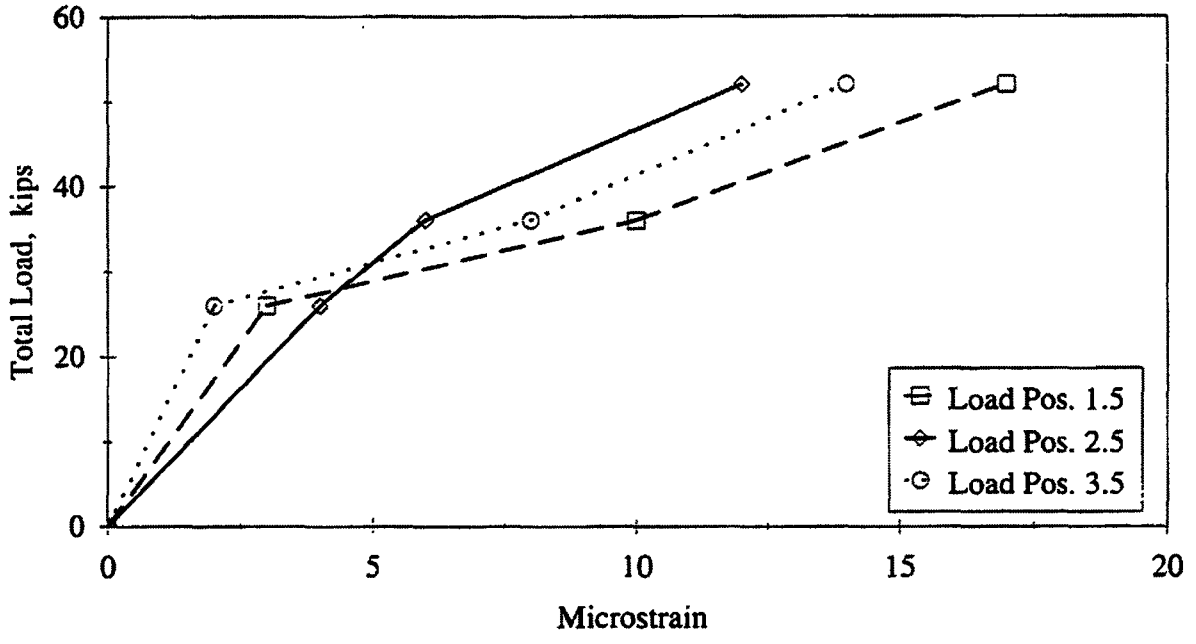

a. East arch

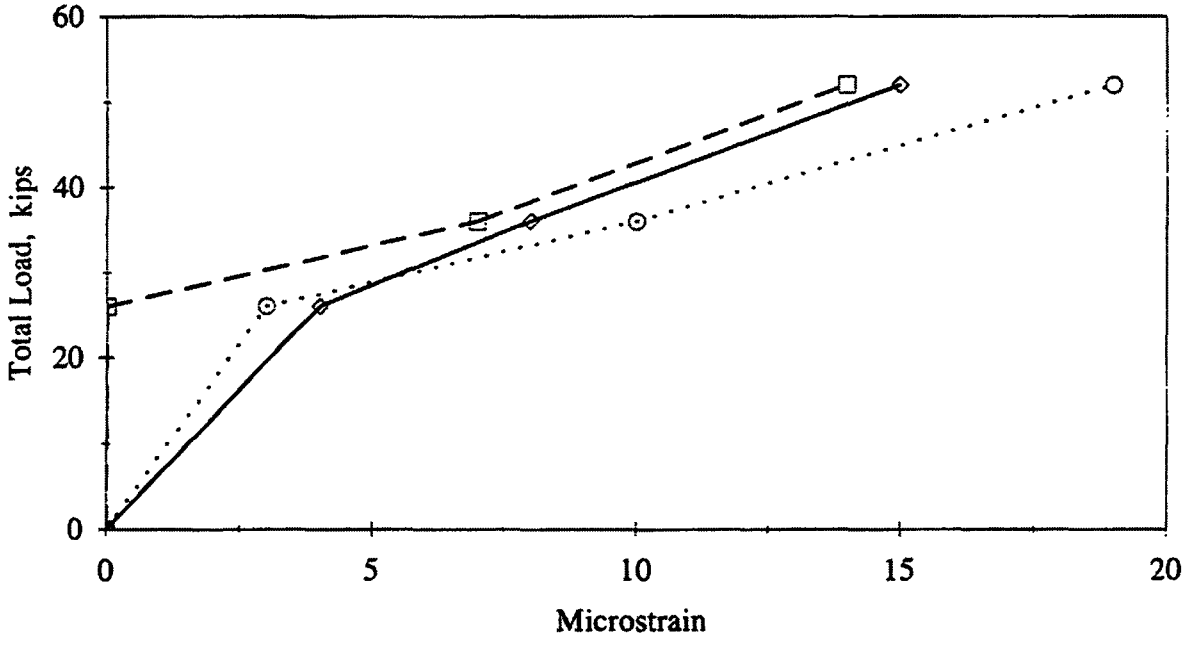

b. West arch

Figure 2.24. Bridge I: Strain at crown of arches.

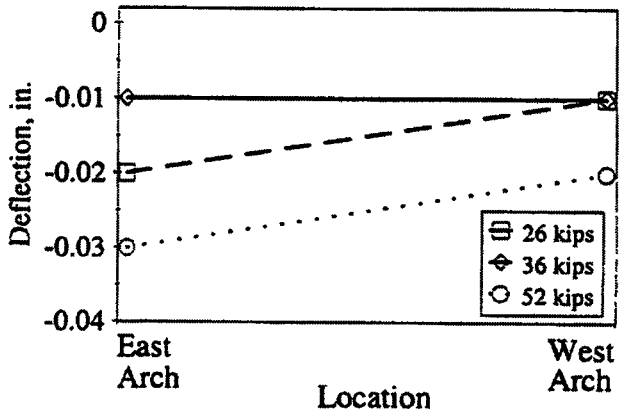

a. Load position 1.5

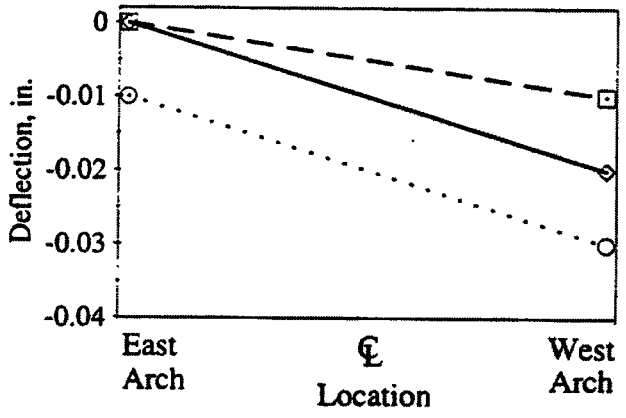

b. Load position 2.5

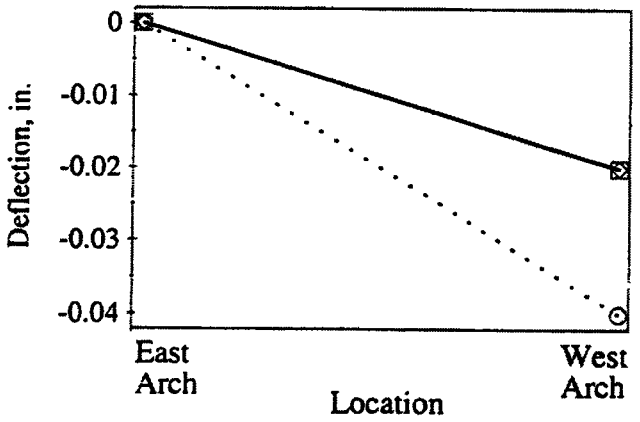

c. Load position 3.5

Figure 2.25. Bridge I: Deflection at crown of arches.

increments. Figure 2.25 shows the deflection at the crowns of the east and west arches for load increments one, two, and three and load positions 1.5, 2.5, and 3.5.

2.6.2. Concrete Core Samples

From the seven concrete cores obtained from the deck of the bridge, the average compressive strength was determined (see data in Table 2.2). The results of the testing ranged from a low of 24 MPa (3,410 psi) to a high of 33 MPa (4,790 psi) with an average compressive strength of 33 MPa (4,320 psi). This is considerably higher than the 22.8 MPa (3,300 psi) which is the assumed value when the compressive strength of the concrete is unknown [1]. The average compressive strength of the in situ concrete is higher than the assumed value which was expected since concrete continues to gain strength over time.

Table 2.2. Bridge I: Results of concrete compressive strength tests.

Specimen	Compressive Strength Psi
A	3,410
B	3,690
C	4,440
D	4,470
E	4,710
F	4,710
G	4,790
Average	4,320
Standard Deviation	546

1 psi = 0.00689 MPa

2.6.3. Concrete Floor Beam

The results from the beam test revealed that the nominal flexural strength was less than that predicted by analytical methods and the mode of failure was due to bending and not shear.

As previously mentioned, the test beam was loaded twice. The first test was conducted to determine the nominal flexural strength of the beam. The nominal flexural strength of the beam was reached when the tension reinforcing steel yielded. Yielding of the steel occurred when the total applied load had reached 407,790 N (91,000 lbs) or 202,395 N (45,500 lbs) per load point. This was one and a quarter times the total weight of the HS20-44 (320,270 N (72,000 lbs)) rating vehicle and almost twice the total weight of the Type 3 (222,410 N (50,000 lbs)) rating vehicle. The actual nominal flexural strength of the beam was calculated to be 405,390,180 N-mm (299,000 ft-lb). The theoretical nominal flexural strength was calculated to be 417,592,560 N-mm (308,000 ft-lb) using the strength design method. The material strengths obtained from the laboratory testing were used to calculate the theoretical nominal flexural strength of the beam.

The second test was conducted to determine if the external stirrups provided additional shear capacity. Prior to reloading the beam, both external stirrups (see Fig. 2.18c) were removed. The beam was then reloaded to a maximum total applied load of 511,546 N (115,000 lbs) or 255,773 N (57,500 lbs) per load point. The beam behaved as it did during the first load cycle and failed in flexure. No changes were observed at the location of the external stirrups; it was concluded that the beam had adequate shear strength and the external stirrups were not required.

The centerline strains at the top of the deck and bottom of the web remained linear until the total applied load had reached 407,790 N (91,000 lbs). At this point, yielding of the tension reinforcement was observed. The centerline strains at the top of the deck and bottom of the web are presented in Figure 2.26.

The maximum deflection at the centerline of the beam was obtained during the second test. A deflection of 110 mm (4.3 in.) was obtained when the total applied load was 511,545 N (115,000 lbs). At this load, the concrete in the top of the deck had a compression failure. At the load at which the tension reinforcing steel yielded (407,790 N (91,000 lbs)), the beam centerline deflection was 13 mm (0.5 in.). The deflections of the beam quarter points and centerline are presented in Figure 2.27.

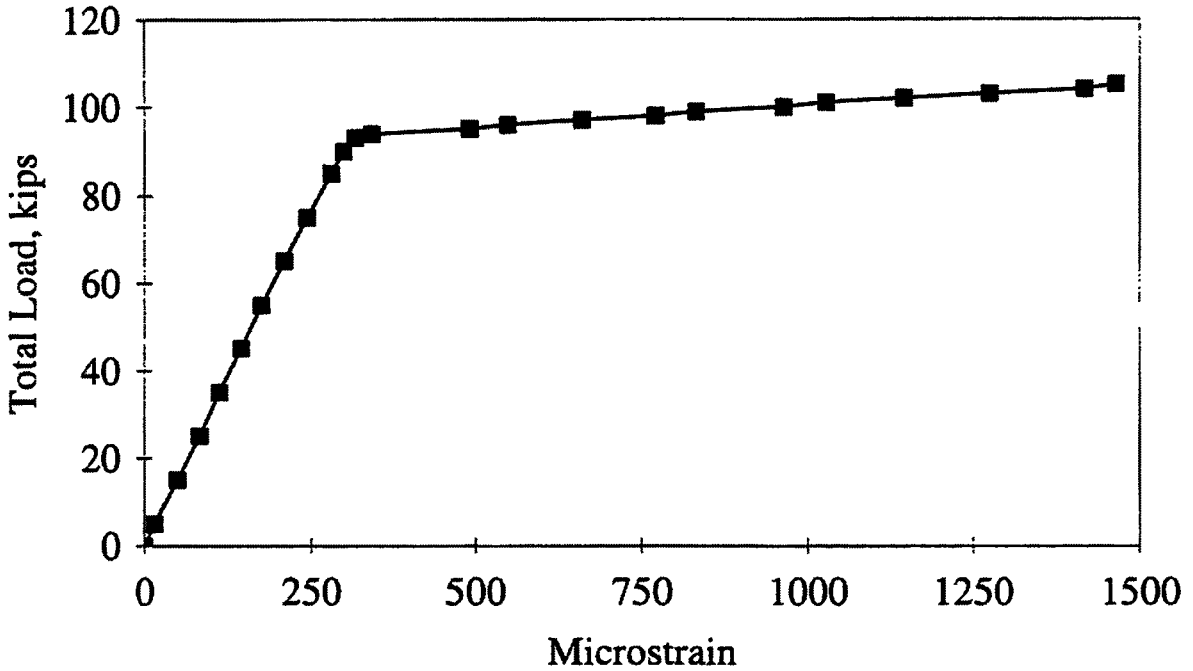

a. Centerline of deck

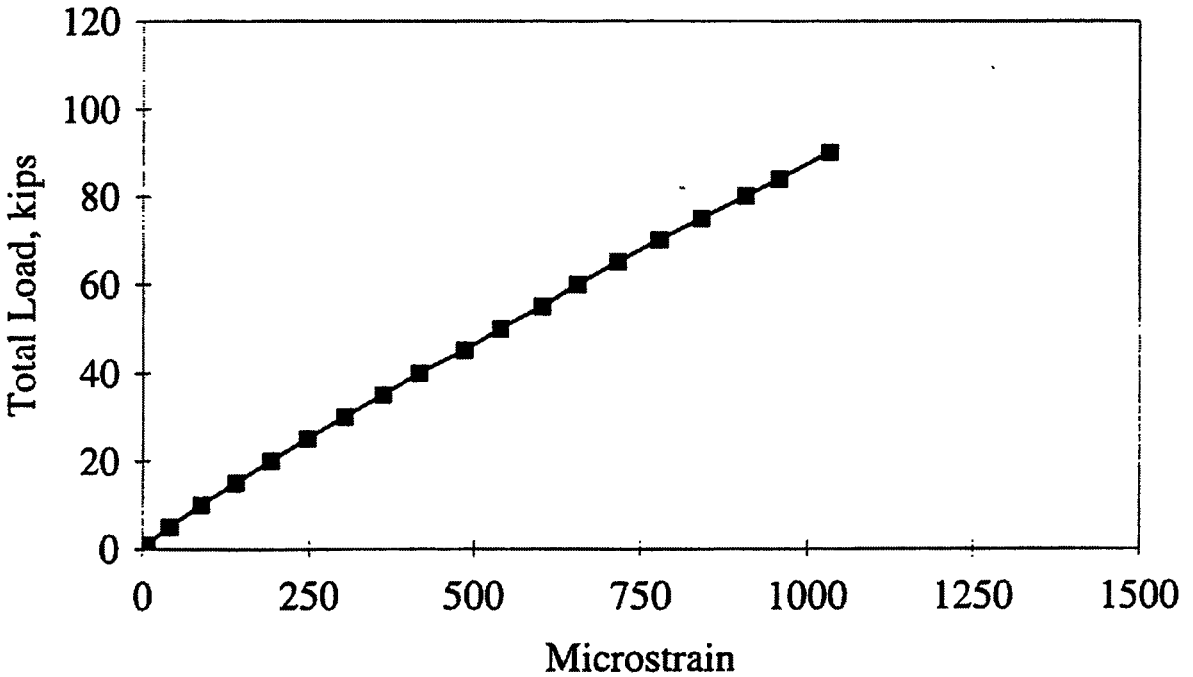

b. Bottom of web

Figure 2.26. Bridge I: Test beam strains.

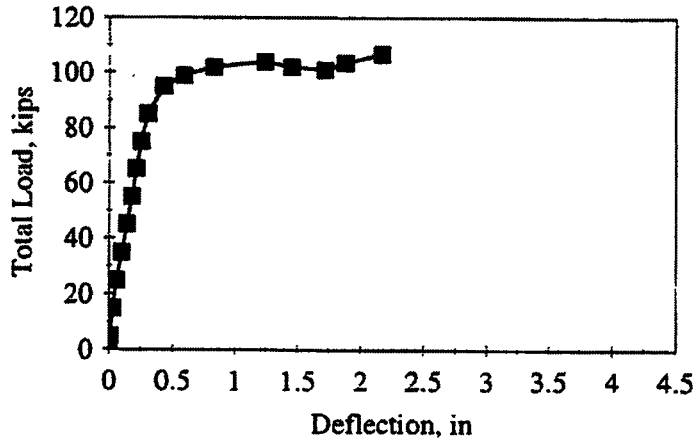

a. East quarter point

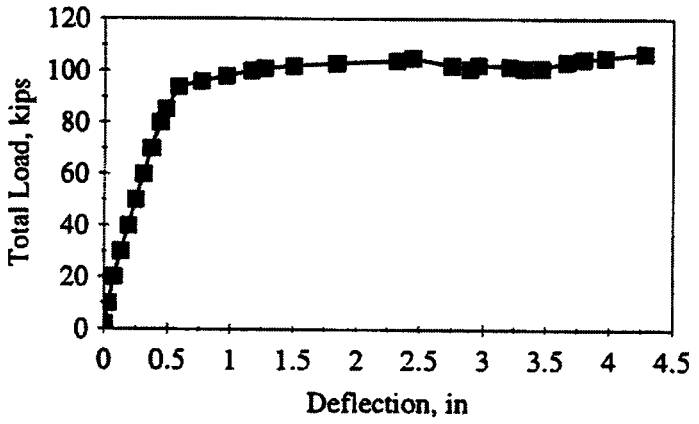

b. Centerline

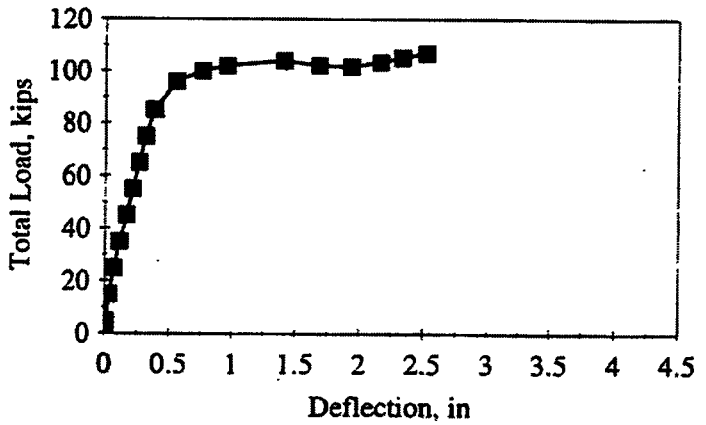

c. West quarter point

Figure 2.27. Bridge I: Test beam deflections.

2.6.4. Steel Samples

Results of the tensile tests performed on the structural steel specimens are presented in Table 2.3. The yield stresses of the steel specimens obtained for laboratory testing were greater than the assumed values for the period in which the bridge was built.

The average yield stress of the three structural steel specimens obtained from the hangers was 276 MPa (40,000 psi), and ranged from a low of 272 MPa (39,500 psi) to a high of 277 MPa (40,200 psi). For unknown steel in structures built between 1905 and 1936, the assumed minimum yield strength of the steel is 207 MPa (30,000 psi) [1].

Table 2.3. Bridge I: Tensile test results of reinforcing obtained from hangers.

Specimen	Yield Strength psi	Ultimate Strength psi	Young's Modulus psi
HW4N	40,200	51,600	28,100,000
HW4S	39,500	54,100	27,000,000
HE4S	40,200	50,800	25,500,000
Average	40,000	52,200	26,900,000
Standard Dev.	404	1,720	1,300,000

1 psi = 0.00689 MPa

Results of the tensile tests performed on the five reinforcing steel specimens obtained from the deck are presented in Table 2.4. Results ranged from a low of 252 MPa (36,500 psi) to a high of 324 MPa (47,000 psi) with an average yield strength of 285 MPa (41,400 psi). The assumed yield strength of structural grade reinforcing steel in structures built prior to 1954 is 228 MPa (33,000 psi) [1].

The last specimens to be obtained and tested were two 29 mm (1 1/8 in.) diameter reinforcing bars from the floor beams. The average yield strength obtained from the two bars was 234 MPa (33,900 psi). The assumed yield strength of the bars is the same as that for the reinforcing steel in the deck. Results of these tensile tests are presented in Table 2.5.

Overall, the yield strength of the structural and reinforcing steel was greater than the assumed values at the time the bridge was built. Typical stress-strain curves for the steel specimens tested are presented Figure 2.28.

2.6.5. Modified Rating

Using the strains obtained from the diagnostic load test, the theoretical load rating was modified using the procedure presented in Sec 1.7. The load rating of the beams and hangers increased while the rating for the arches decreased. The load rating for deck remained unchanged since no strain data was obtained.

Table 2.4. Bridge I: Tensile test results of reinforcing obtained from deck.

Specimen	Yield Strength psi	Ultimate Strength psi	Young's Modulus psi
S6A	42,300	58,700	29,800,000
S6B	42,800	51,500	28,800,000
S6C	47,000	66,100	29,100,000
S6D	36,500	52,400	28,500,000
S6E	38,500	57,200	29,600,000
Average	41,400	57,180	29,200,000
Standard Dev.	4,080	5,850	541,000

1 psi = 0.00689 MPa

Table 2.5. Bridge I: Tensile test results of reinforcing obtained from test beam.

Specimen	Yield Strength psi	Ultimate Strength psi	Young's Modulus psi
Bar A	33,400	49,800	28,900,000
Bar B	34,300	51,400	29,500,000
Average	33,900	50,600	29,200,000
Standard Dev.	640	1,130	424,300

1 psi = 0.00689 MPa

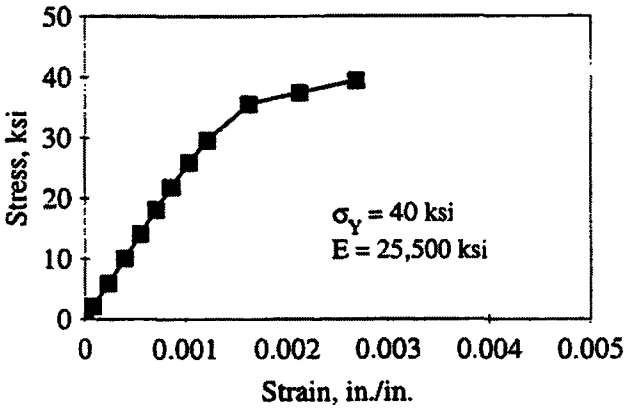

a. Structural steel in hangers

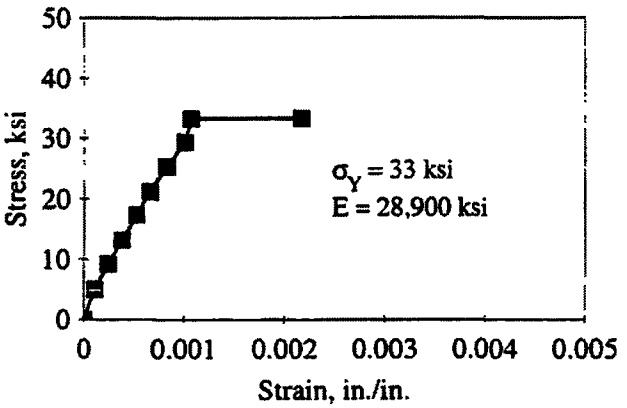

b. Reinforcing steel in beams

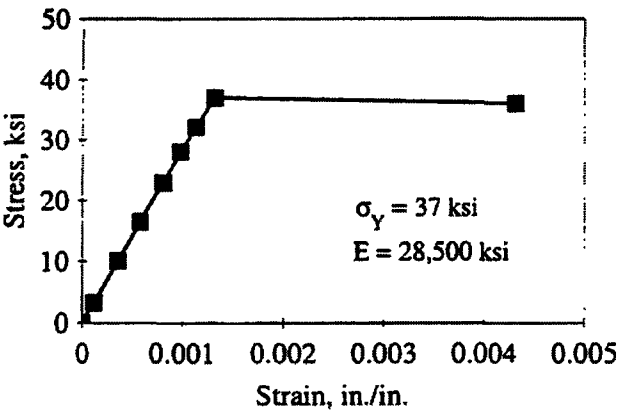

c. Reinforcing steel in deck

Figure 2.28. Bridge I: Typical stress-strain curves of bridge reinforcing.

The rating of the beams increased from 373,650 N (42 tons) to 916,333 N (103 tons) for the HS20-44 vehicle. For the Type 3 rating vehicle, the rating of the beams increased from 311,376 N (35 tons) to 773,991 N (87 tons).

The rating of the hangers increased from 693,923 N (78 tons) to 1,743,703 N (196 tons) for the HS20-44 rating vehicle. For the type 3 rating vehicle, the rating increased from 587,165 N (66 tons) to 1,459,017 N (164 tons).

Finally, the rating of the arches decreased from 1,325,570 N (149 tons) to 676,130 N (76 tons) for the HS20-44 rating vehicle and decreased from 1,147,640 N (129 tons) to 587,165 N (66 tons) for the Type 3 rating vehicle. The decrease in the rating of the arches can be explained by the presence of a greater load distribution to other parts of the bridge than was predicted by the analytical model. A summary of the theoretical and modified rating for each component is presented in Table 2.6. The modified rating calculation for this bridge is presented in Appendix B.

The overall rating of the bridge was governed by the deck since no strain data was obtained to modify its theoretical load rating. Using the HS20 rating vehicle, the bridge would still require load posting but using the Type 3 rating vehicle no load posting would be necessary.

Table 2.6. Bridge I: Rating Summary.

	Vehicle HS20				Vehicle Type 3			
	AASHTO LRFR		Modified Rating		AASHTO LRFR		Modified Rating	
	RF_c	R(tons)	RF_T	R(tons)	RF_c	R(tons)	RF_T	R(tons)
Slab:	0.94	33.8			1.50	37.5		
Beams:	11.18	42.5	2.87	103.3	1.43	35.8	3.48	87.0
Hangers:	2.19	78.8	5.47	196.9	2.64	66.0	6.59	164.8
Arches:	4.14	149.0	2.11	76.0	5.18	129.5	2.64	66.0

indicates controlling component

3. BRIDGE II: REINFORCED CONCRETE OPEN SPANDREL ARCH

3.1. Bridge Description

Like Bridge I, Bridge II was also a Marsh Arch Bridge. Built in 1919, Bridge II was one lane and was located approximately one mile north of Bridge I on secondary county (350th St.) road over Beaver Creek in southwest Boone County. Average daily traffic for this structure was 40 vehicles which consisted of local traffic. At the time of testing, this bridge was also listed in the Iowa Historic Bridge Inventory. The layout and dimensions of the bridge are presented in Figure 3.1; dimensions listed were obtained from field measurements.

Bridge II had a clear span of 25,910 mm (85 ft) and a roadway width from the inside of curb to the inside of curb of 5,180 mm (17 ft). The bridge deck was 5,490 mm (18 ft) wide and 205 mm (8 in.) thick. The layout of the reinforcement in the deck is presented in Figure 3.2. Reinforcing in the longitudinal direction consisted of two layers of bars. The reinforcing in the bottom layer consisted of 15 mm (5/8 in.) square bars on 150 mm (6 in.) centers. Reinforcing in the top layer was located 75 mm (3 in.) above the bars in the bottom layer and consisted of 15 mm (1/2 in.) diameter bars on 150 mm (6 in.) centers. The reinforcement in the transverse direction consisted of 15 mm (1/2 in.) diameter bars on 610 mm (24 in.) centers.

The deck was supported by 10 transverse concrete beams spaced at 2,620 mm (8 ft - 7 in.) on center. The eight interior beams were attached to the hangers and the two end beams were located between the arches. The end beams were provided to support the deck and to tie the arches together. As in Bridge I, there was a construction joint between the end beams and the deck which allowed the deck to move independent of the arches.

The depth of the interior beams varied from the center of the bridge to the edge of the deck due to the deck camber. At the centerline, the beams had a depth of 533 mm (21 in.) measured from the bottom of the deck to the bottom of the beams. At the edge of the bridge, the beams had a depth of 457 mm (18 in.) measured from the bottom of the deck to the bottom of the beams.

Unlike the interior beams, the end beams were T-shaped. The flange had a thickness

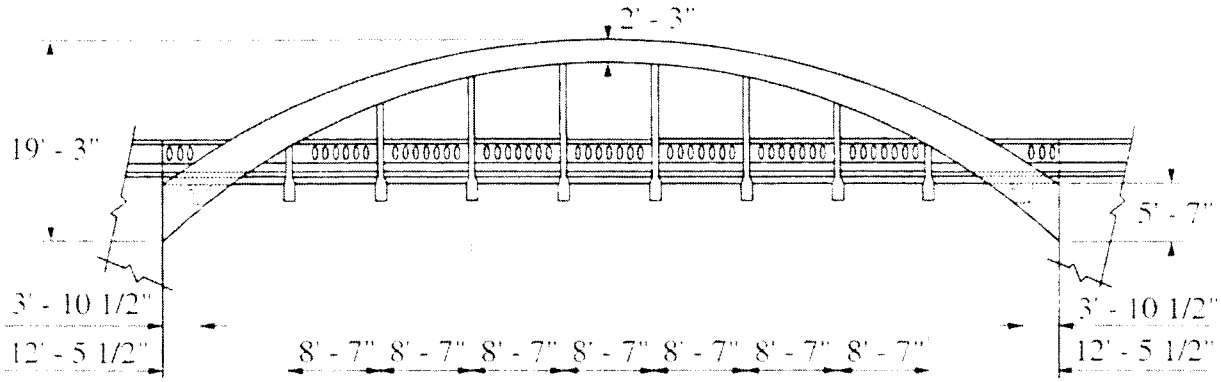

a. Elevation

b. Photograph of bridge profile.

Figure 3.1. Bridge II: Layout.

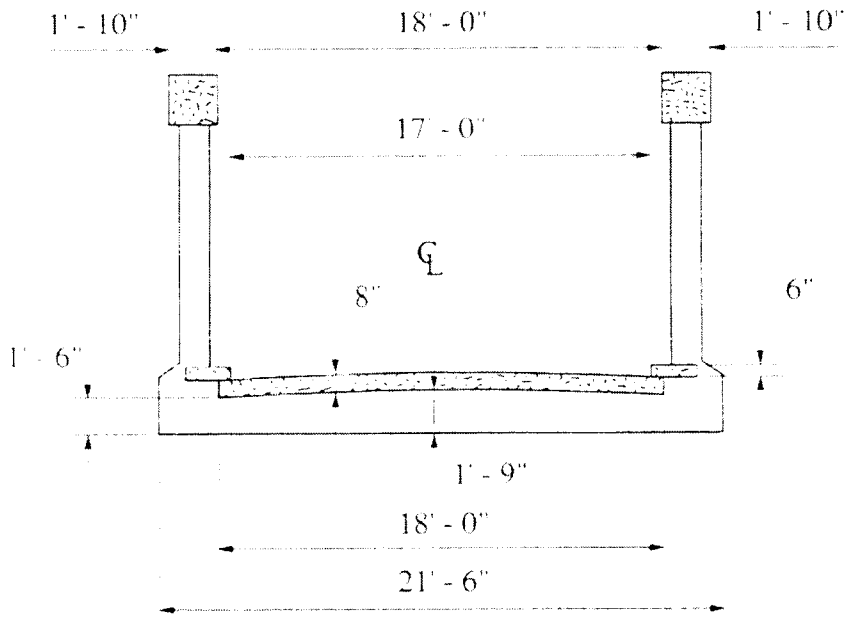

c. Typical cross section

d. Photograph of Bridge II looking East.

Figure 3.1. Continued.

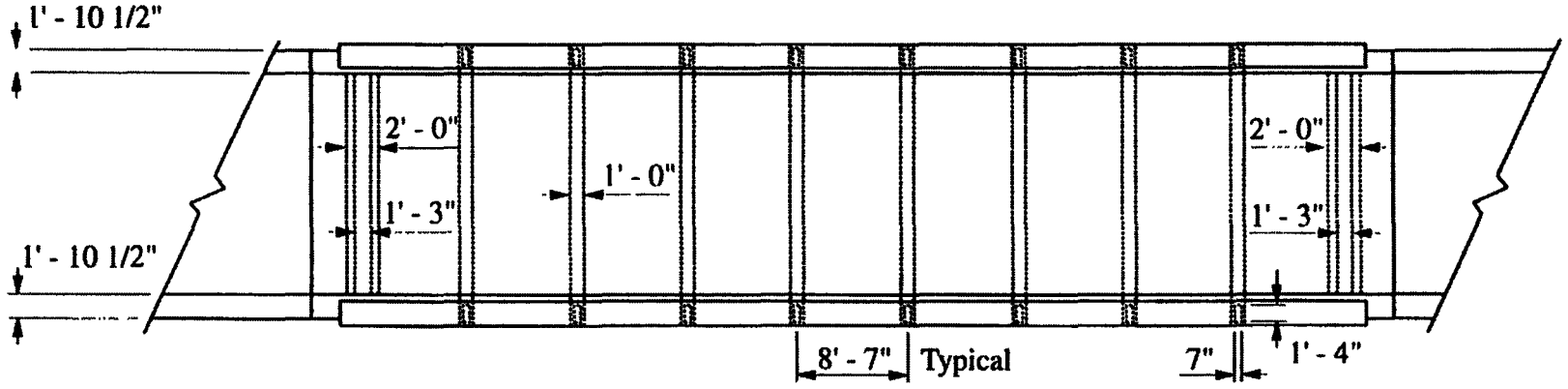

e. Plan View

Figure 3.1. Continued.

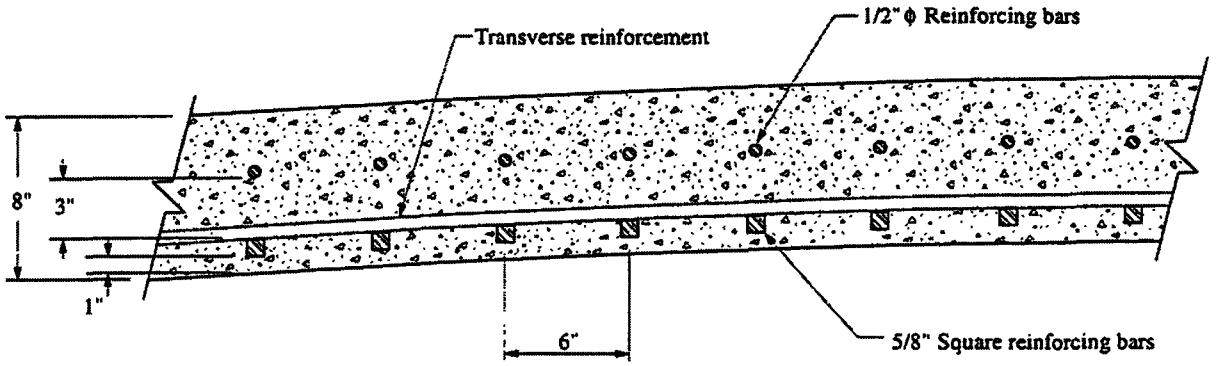

a. Longitudinal reinforcement

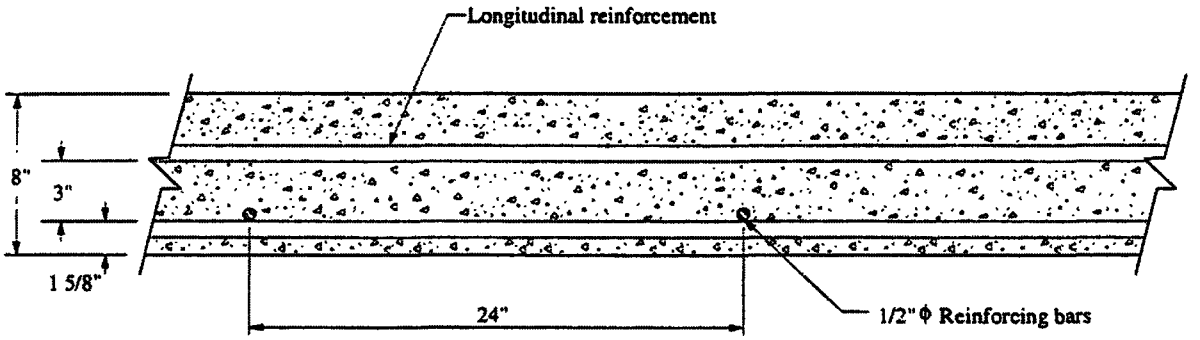

b. Transverse reinforcement

Figure 3.2. Bridge II: Deck reinforcement.

of 305 mm (12 in.) and width of 610 mm (24 in.). The web had a depth and a width of 381 mm (15 in.).

Reinforcing for the interior beams consisted of two 2 1/2 in. x 2 1/2 in. x 1/4 in. structural steel angles and two 25 mm (1 in.) square bars. The 25 mm bars were bent up at an angle and

terminated in a 90 degree hook at the end of the beam to provide shear reinforcement and development.

Reinforcing in the end beams consisted four 29 mm (1 1/8 in.) square reinforcing bars in the bottom of the web and four 19 mm (3/4 in.) square reinforcing bars in the top. To provide for shear reinforcement, two of the 29 mm (1 1/8 in.) bars in the web were bent up at an angle and extended into the arches for development. The configuration and reinforcing in the interior and end beams are presented in Figure 3.3.

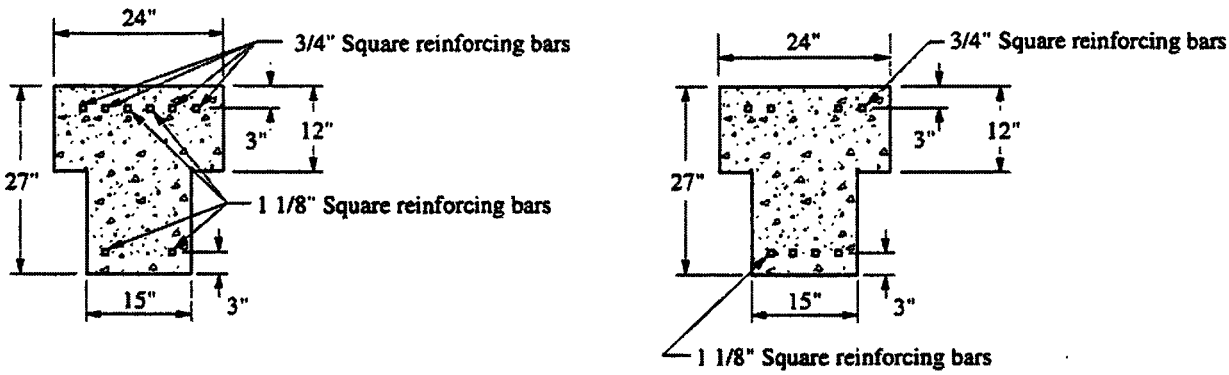

a. End section of end beam

b. Centerline of end beam

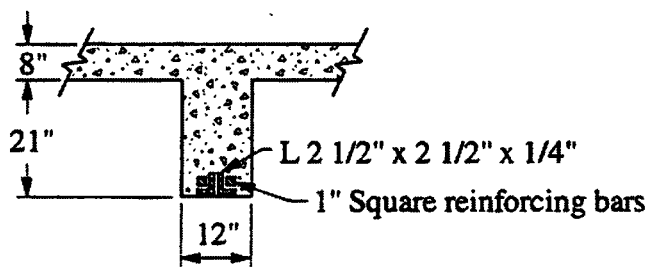

c. Centerline of interior beams

Figure 3.3. Bridge II: Configuration and reinforcing details of transverse floor beams.

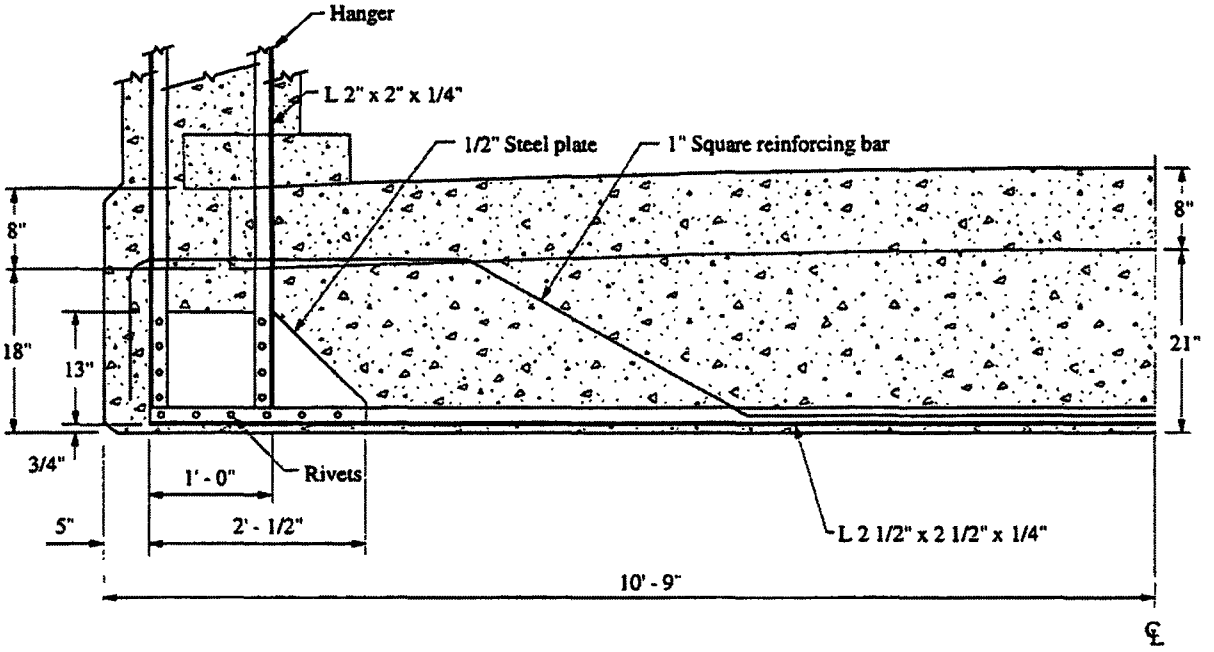

c. Half section detail of interior beams

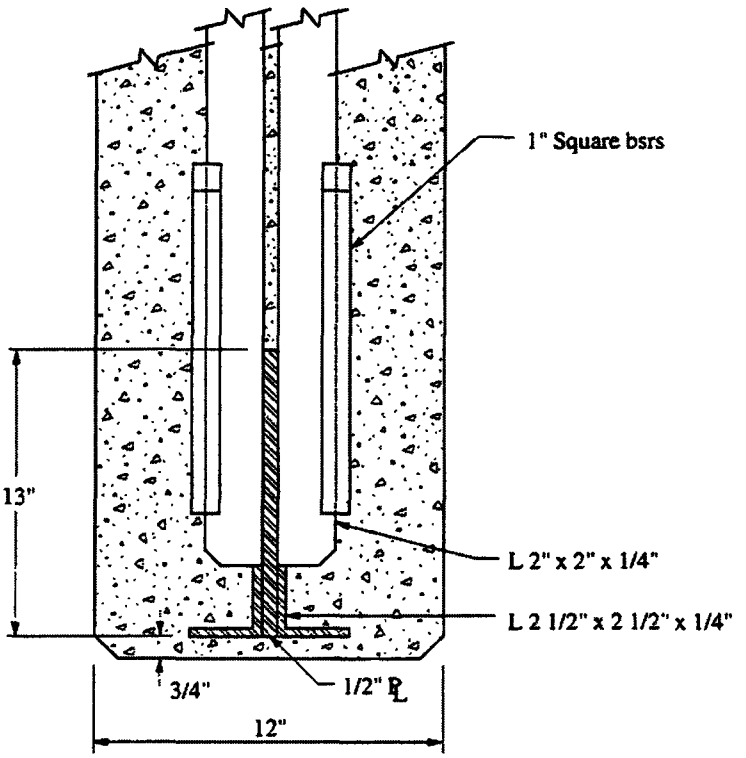

d. End view of interior beams

Figure 3.3. Continued.

As in Bridge I, the hangers were constructed of four 2 in. x 2 in. x 1/4 in. structural steel angles encased in concrete. The hangers had a depth of 406 mm (16 in.) and a width of 178 mm (7 in.). The configuration and reinforcing details of the hangers are presented in Figure 3.4.

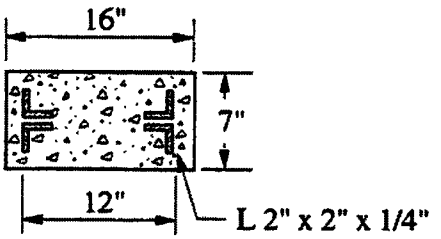

Figure 3.4. Bridge II: Configuration and reinforcing details of hangers.

The two arches had a rise of 5,870 mm (19ft - 3in.), a constant width of 560 mm (22 in.), and thickness of 685 mm (27 in.) at the crown and 1,700 mm (5ft - 7in.) at the abutments. Reinforcing consisted of four structural steel angles 3 in. x 3 in. x 5/16 in. which were tied together by a series of steel lattice work. Figure 3.5 shows the configuration and reinforcing details of the arches.

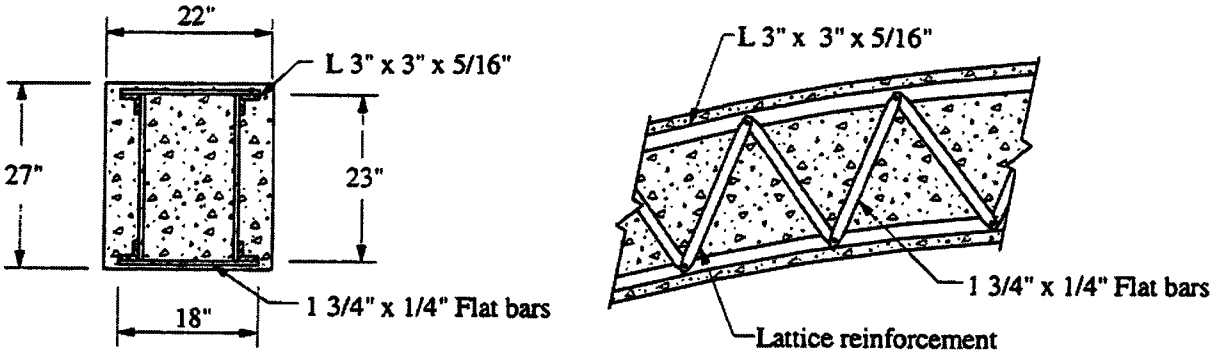

a. Cross-section at centerline

b. Profile

Figure 3.5. Bridge II: Configuration and reinforcing details of arches.

3.1.1. Condition Assessment

The condition assessment for the bridge involved a thorough visual inspection of all the components by the researchers and the obtaining of the previous inspections reports. From the most recent inspection conducted in 1995, the deck was given a condition rating of 3 and the superstructure was given a condition rating of 5. The condition rating is based on a scale which ranges from 0-9 where 0 represents failed condition and 9 represents excellent condition. Due to the narrow roadway and the poor condition of the deck and superstructure, the bridge was posted for one lane and 15 tons

From the visual inspection conducted by the researchers, the arches, hangers, and beams were in much better condition than those of Bridge I; however, the deck was significantly more deteriorated. The arches showed severe scaling and spalling along their entire lengths. The reinforcement in the south arch was exposed at the bottom face near the crown and at the east abutment. Photographs of typical arch deterioration are shown in Figure 3.6.

a. Spalling and of south arch

b. Deterioration at east abutment

Figure 3.6. Bridge II: Photographs of arch deterioration.

Unlike the condition of the hangers on Bridge I, only two hangers on Bridge II showed any deterioration. On the one hanger, the concrete had delaminated on the outside face (stream side). On another hanger, the concrete had completely fallen off the inside face (road side) exposing the reinforcing. Where the reinforcing was exposed, small amounts of pitting and corrosion were noted. Photographs of the hanger deterioration are shown in Figure 3.7.

a. Delaminated concrete

b. Exposed reinforcement

Figure 3.7. Bridge II: Photographs of hanger deterioration.

Of all the components, the deck showed the worst deterioration; photographs of the deck deterioration are shown in Figure 3.8. Approximately 75 mm (3 in.) of wearing surface had been lost in the middle two thirds of the bridge. Due to the loss of section in the deck, the top reinforcing bars were exposed at various locations. Also, along the bottom edges of the deck, the reinforcing bars were exposed the entire length of the bridge. The exposed reinforcing bars in the top and bottom of the deck were corroded and pitted.

a. Exposed reinforcement at top of deck

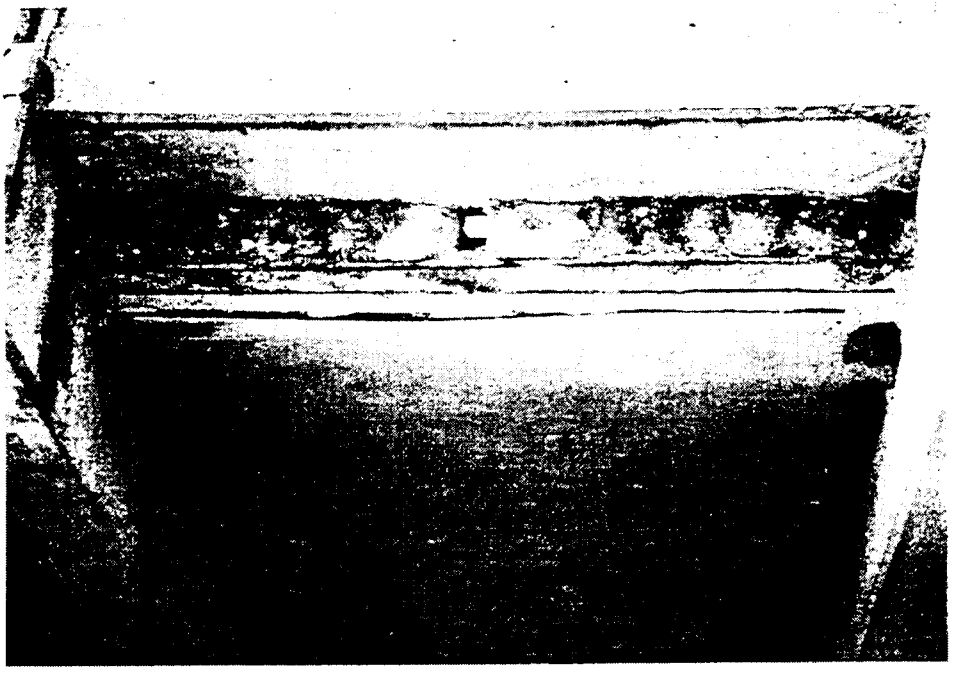

b. Exposed reinforcing at bottom edge of deck

Figure 3.8. Bridge II: Photographs of deck deterioration.

The floor beams showed no observable signs of deterioration. The concrete was sound and no delamination or exposed reinforcement was noted.

As discussed in Sec. 2.1.1, the deterioration of the concrete can be attributed to many factors. These include: the lack of air entrainment, poor mix design and control, poor aggregate gradation, insufficient cover, etc.

As was previously discussed, this bridge was also periodically inspected. The only repairs made to this bridge in the past 25 years were to the deck - asphalt was added to several areas of the deck to improve the riding surface. These repairs kept the bridge in operation, however, obviously did not improve the structural integrity of the bridge.

3.2. Demolition

As with Bridge I, this bridge was also demolished. Demolition began approximately 11 months after the diagnostic load testing was completed. Prior to the demolition, material samples were removed from the bridge for laboratory testing. The samples collected included: three concrete cores from the deck, three sections of reinforcing steel from the deck, and two sections of structural steel angles from two different hangers. The locations from where the material samples were obtained are presented in Figure 3.9.

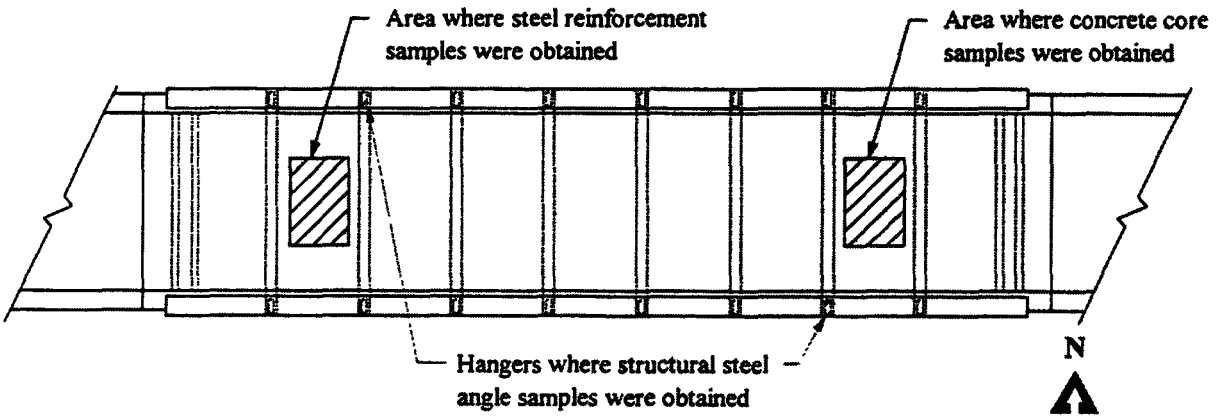

Figure 3.9. Bridge II: Material sample locations.

To document the demolition, the process was video taped and photographed. Over two hours of video footage were obtained of various stages of the demolition process. Also, over 20 photographs were taken of various reinforcing and connection details and of different stages of the demolition.

3.3. AASHTO Rating

As a result of the demolition of the bridge, the condition of the various components and the exact locations and amounts reinforcement were determined. Also, from the laboratory testing of the material samples, actual material strengths were attained. With this information, a more precise theoretical load rating of the bridge could be determined.

The components that were analyzed to obtain an overall rating for the bridge included: the floor beams, deck, hangers, and arches. The rating of the bridge was controlled by the deck for the HS20 and Type 3 rating vehicles. The procedures followed to obtain the rating factors for the various components were discussed in Sec. 2.3. The calculations used to determine the rating factors of each of the components are presented in Appendix B. A summary of the theoretical load rating is presented in Table 3.1.

Table 3.1. Bridge II: Theoretical load rating summary.

	Vehicle HS20 AASHTO LRFR		Vehicle Type 3 AASHTO LRFR	
	Rating Factor	Rating (tons)	Rating Factor	Rating (tons)
Slab:	0.79	28.4	1.30	32.5
Beams:	1.65	59.4	1.79	44.8
Hangers:	3.21	115.6	3.50	87.5
Arches:	4.17	150.1	4.79	119.8

indicates controlling component

3.4. Test setup and Procedures

Strains produced by the test vehicle were monitored in the arches, hangers, and beams. Also, to observe the general structural behavior of the bridge, deflections at various locations were obtained.

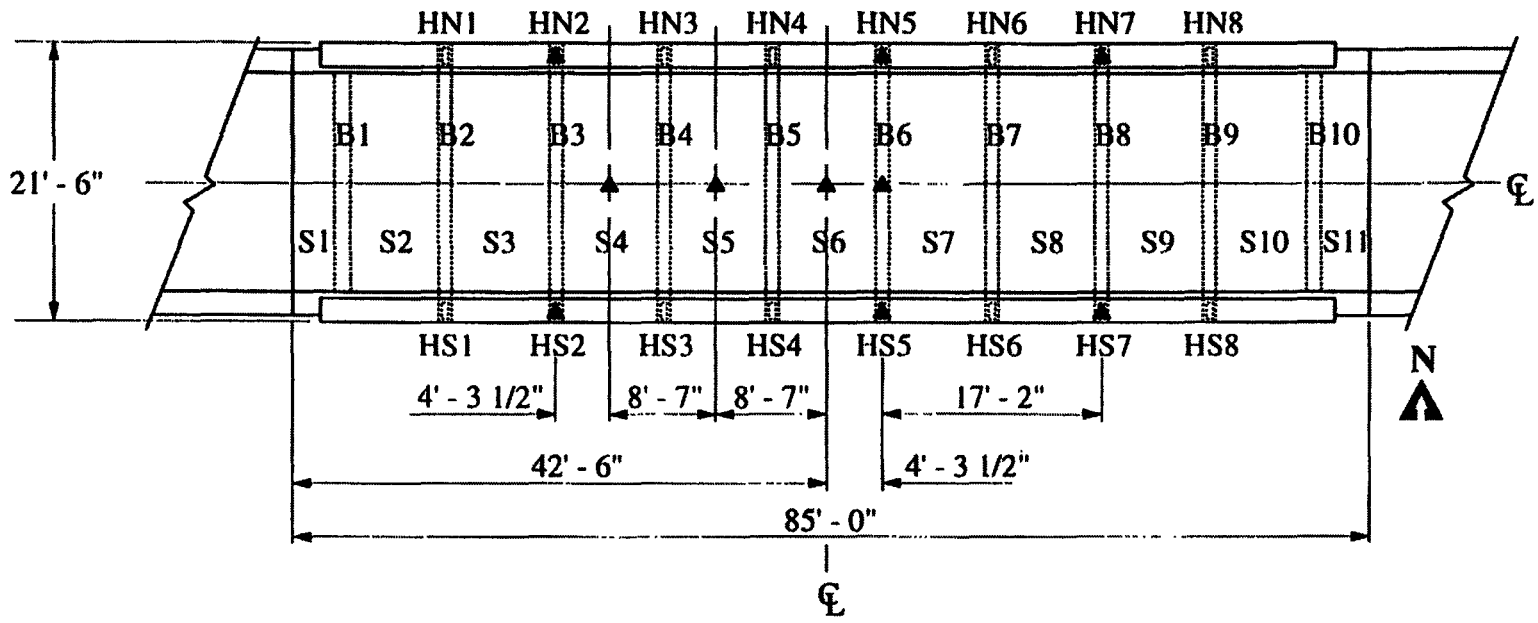

▲ Deflection transducer locations
Bx Beam numbers (x = 1 - 10)
Sx Deck panel numbers (x = 1 - 11)
HNx North hanger numbers (x = 1 - 8)
HSx South hanger numbers (x = 1 - 8)

Figure 3.10. Bridge II: Location of deflection transducers.

Deflections in the bridge were monitored at the centerlines of beam B6 and deck panels S4, S5, and S6; see Figure 3.10 for the locations of the deflection transducers. Also, deflections were monitored at the ends of beams B3, B6, and B8. These locations were chosen to observe the behavior of the arches, deck panels and center beam as the test vehicle moved across the bridge. All bridge deflections were obtained using the equipment and setup described in Sec 1.6.1.

Strains were monitored at the crowns of the arches, at the centerline of beam B6, and at the inside and outside faces of hangers HN5 and HS5; see Figure 3.11 for the location of the strain gages on the various components. Strains were not monitored in the deck due to the excessive deterioration on the underside of the individual deck panels.

Strains were monitored at the crowns of the arches since they were determined to be the most critical sections. Three strain gages were attached to each arch - one strain gage on the center of the top face and one on the center of each side face.

Strains in beam B6 were monitored at the centerline of the member. Since no concrete deterioration was present in the beam, one strain gage was bonded to the concrete in the center of the beam.

The strain gages for hangers HN5 and HS5 were bonded to the structural steel angles within each hanger. Before the strain gage could be attached, the concrete cover on the inside and outside faces of the two hangers had to be removed. Once removed, strain gages were bonded to two exposed angles located diagonally across from each other (see Fig. 3.11c). The types of strain gages used and the application process were discussed in Sec. 1.6.1.

The type of vehicle and loading process used in testing the bridge were described in Sec. 1.6.2. For this bridge, the loading was applied in three increments. In the first load increment, the test vehicle had a gross vehicle weight of 115,655 N (26,000 lbs). In load increments two and three, the test vehicle had a gross vehicle weight of 162,360 N (36,500 lbs) and 238,425 N (53,600 lbs), respectively. The magnitude of the load increments and wheel configuration of the test vehicle presented in Figure 3.12; a photograph of the test vehicle is shown in Figure 3.13.

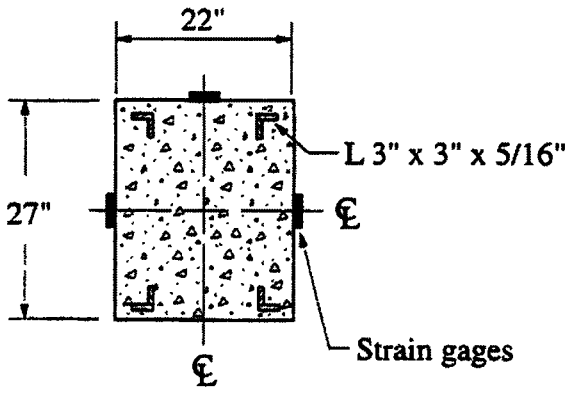

a. Location of strain gages at crown of arches

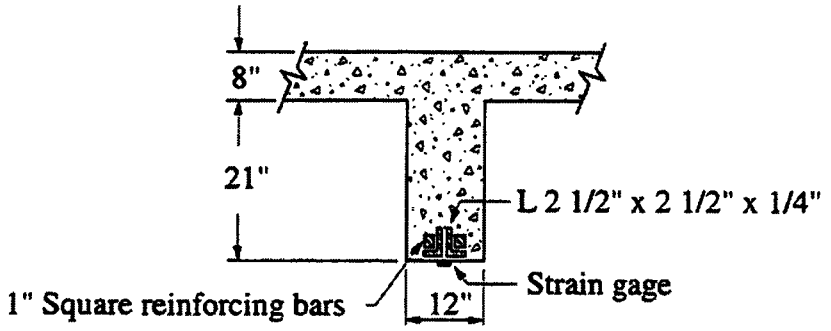

b. Centerline cross-section of beam B6

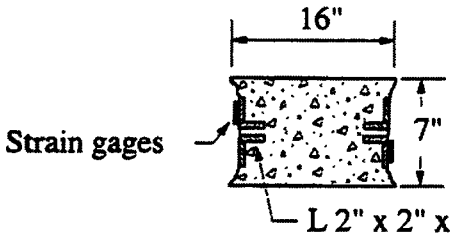

c. Location of strain gages on hangers HN5 and HS5

Figure 3.11. Bridge II: Location of strain gages on various bridge components.

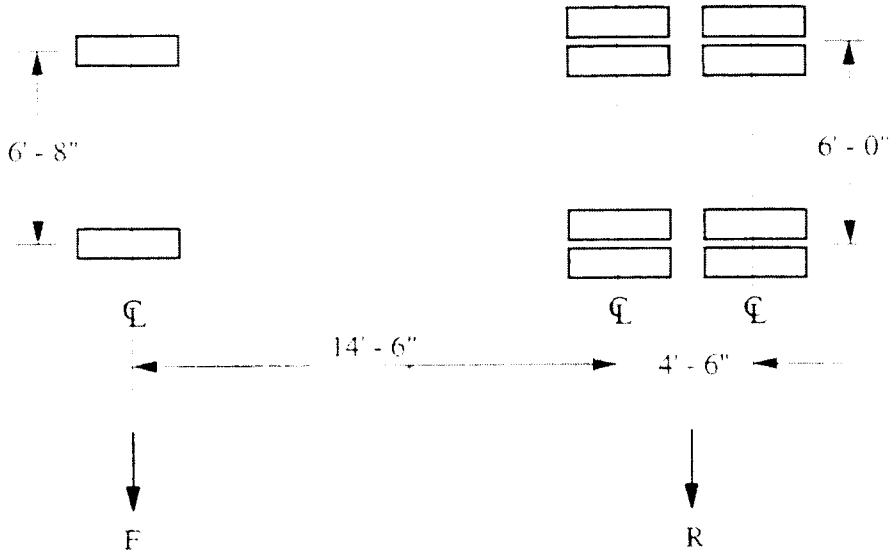

Load Increment	F (kips)	R (kips)	Total Load (kips)
1	12.0	14.2	26.2
2	11.8	24.7	36.5
3	14.6	39.0	53.6

Figure 3.12. Bridge II: Wheel configuration and weight distribution in test vehicle.

Figure 3.13. Bridge II: Photograph of test vehicle on bridge.

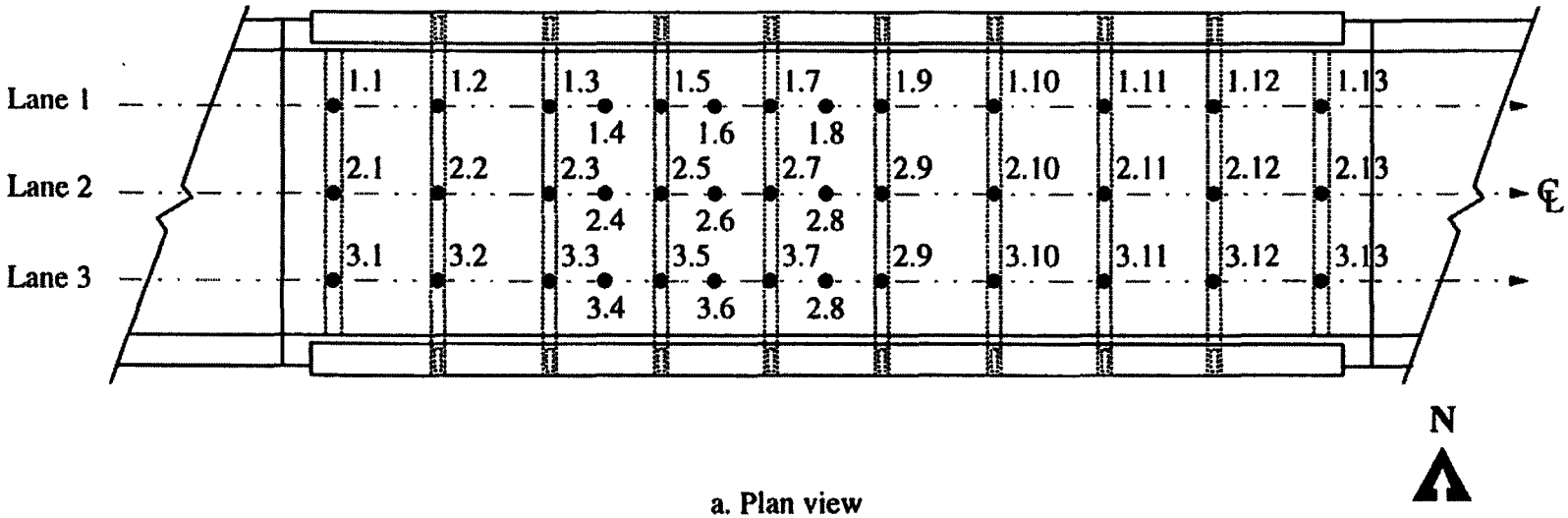

a. Plan view

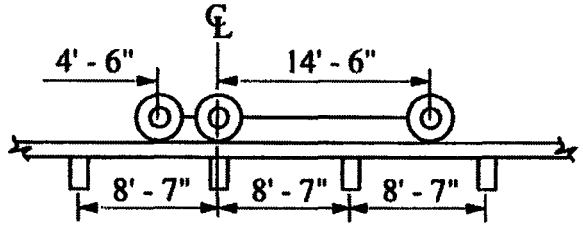

b. Truck position on beams

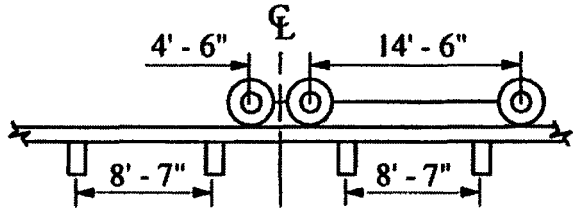

c. Truck position on deck panels

Figure 3.14. Bridge II: Longitudinaal location of test vehicle for various tests.

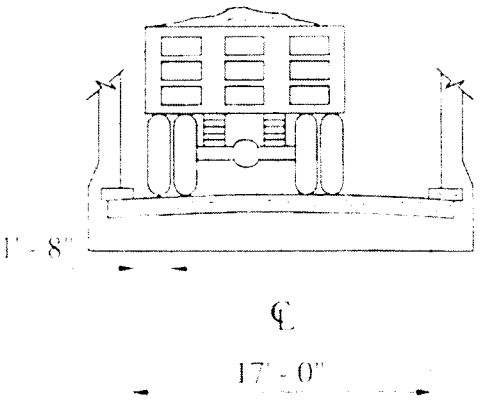

a. Lane 1

b. Photograph of test vehicle in Lane 1

Figure 3.15. Bridge II: Transverse location of test vehicle on bridge.

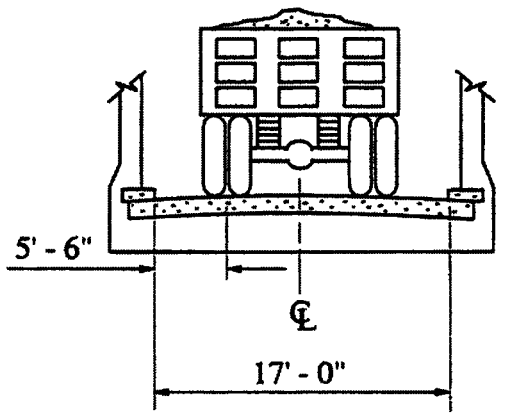

c. Lane 2

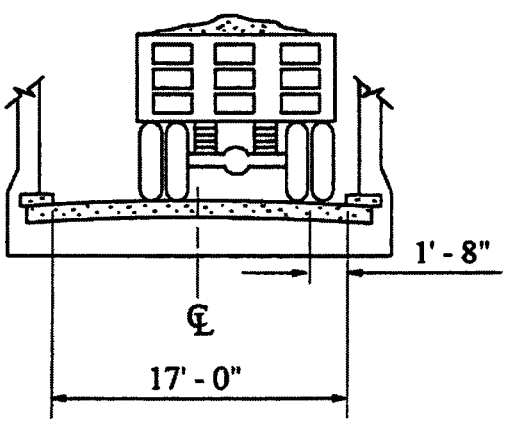

d. Lane 3

Figure 3.15. Continued.

To observe the structural behavior of the bridge and obtain maximum strains in the various components, the test vehicle was stopped at beams B1 through B10 and deck panels S4, S5, and S6.. At each location, strain and deflection readings were taken. The test vehicle was positioned on the beams with the front wheel of the rear tandem centered over the members and on the deck panels with the tandem wheel centered on the panels. Figure 3.14 shows the various positions of the test vehicle; the lane positioning of the test vehicle was described in Sec. 1.6.2. and is shown in Figure 3.15.

3.5. Material Specimens

As previously described, material samples were obtained from the bridge before it was demolished. The samples that were obtained for testing consisted of concrete cores from the deck, structural steel reinforcing from the hangers, and reinforcing steel from the deck.

3.5.1. Test Equipment and Procedures

3.5.1.1. Concrete Core Samples

The compressive strength of the concrete was determined from three 102 mm (4 in.) diameter cores obtained from the deck. The lengths of the three specimens varied due to the deterioration of the deck. The specimen preparation and the test procedures followed were the same as those used for the concrete cores obtained from Bridge I. Refer to Sec. 2.5.1.1 for a description of the specimen preparation, test procedures, and the testing equipment.

3.5.1.2 Steel Samples

To obtain the yield strength of the reinforcing steel in the bridge, structural steel angle specimens were removed from the hangers and reinforcing steel specimens were removed from the deck. Refer to Figure 3.9 for the locations where the specimens were obtained.

Two of the four structural steel angles over 1,220 mm (4 ft) long in hangers HN2 and HS7 were removed for testing. From the four sections of structural steel angle, three 457 mm (18 in.) coupons were obtained from one of the legs of the angles. The final coupons were then milled to remove any pitting or corrosion.

Four 19 mm (3/4 in.) square reinforcing bars 1,220 mm (4 ft) long were removed from the deck. From the four specimens obtained, three were selected for testing; the three specimens were cut into 457 mm (18 in.) lengths and then milled to remove any pitting or corrosion. The testing procedures followed were the same as those used for the steel reinforcing specimens obtained from Bridge I. Refer to Sec. 2.5.1.3 for a description of the test procedures and equipment.

3.6. Results and Discussion

3.6.1. Bridge II

As was expected, the responses exhibited by the various components of Bridge II were also very small. The strains obtained were significantly lower than the elastic strain limits of the materials and the deflections were well below those which would cause any cracking in the concrete.

The maximum strains at the centerline of beam B6 were obtained when the test vehicle was located at load positions 1.9, 2.9, and 3.9. For all three load positions and increments, the strain in the beam remained linear. The linear response of the beam is shown in Figure 3.16 for the three load positions and increments. At load increment three, the strain in the beam ranged from a maximum of 53 microstrain at load position 3.9 to 51 and 47 microstrain at load positions 2.9 and 1.9, respectively. The same linear response was exhibited at load increments one and two. At load increment two and load positions 1.9, 2.9, and 3.9, the strain in the beam was 34, 39, and 38 microstrain, respectively. At load increment one, the strain in the beam was 24, 28, and 26 microstrain, respectively. The maximum recorded strain in the beam of 53 microstrain was 40% of 131 microstrain obtained from the analytical model using the same loading (configuration and magnitude).

Like the strains, the deflection at the centerline of beam B6 was maximum at load positions 1.9, 2.9, and 3.9 and remained linear for the three loading increments. At load position 1.9, the deflection ranged from 1.27 mm (0.05 in.) at load increment one to 3.56 (0.14 in.) at load increment three. At load position 2.9, the deflection ranged from 1.52 mm

(0.06 in.) at load increment one to a maximum of 4.06 mm (0.16 in.) at load increment three. At load position 3.9, the deflection response of the beam was similar to that obtained at load position 1.9 - 1.27 mm (0.05 in.) at load increment one to 3.30 mm (0.13 in.) at load increment three. Figure 3.17 shows the centerline deflection of the beam for the three load increments and positions.

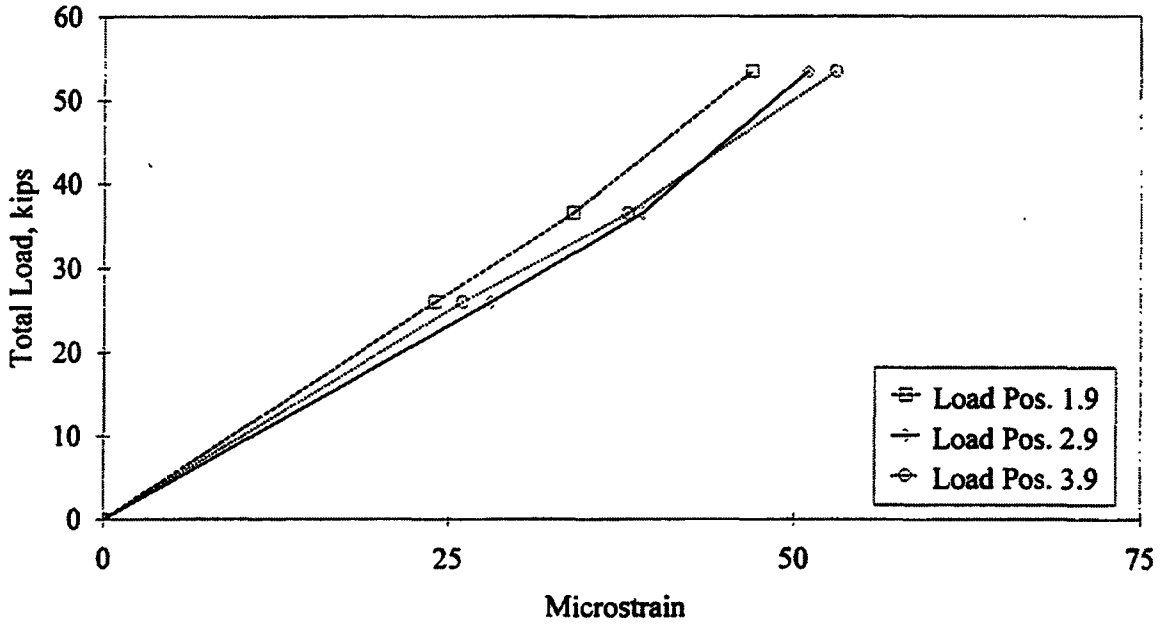

Figure 3.16. Bridge II: Bottom strain at centerline of beam B6.

Figure 3.18 shows the centerline deflection of each slab for the three load increments and position. The largest deflections in the bridge occurred at the centerline of deck panels S4, S5, and S6. For the three load increments, the deflection response of each slab remained linear and did not vary with the transverse positioning of the test vehicle. In panel S4, the largest deflection occurred at load increment three and load positions 1.4, 2.4, and 3.4. At load increment three, the deflections remained relatively constant and ranged from 3.30 mm (0.13 in.) at load position 1.4 to 3.56 mm (0.14 in.) and 3.30 mm (0.13 in.) at load positions 2.4 and 3.4, respectively. The same uniform response was exhibited at load increments one and two.

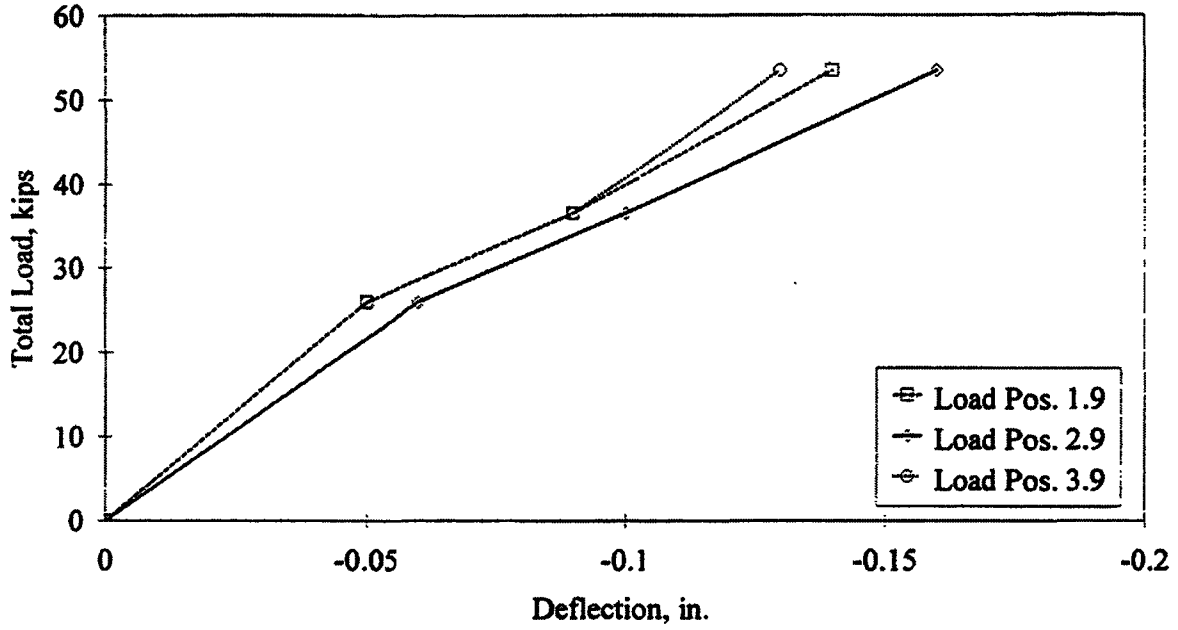

Figure 3.17. Bridge II: Centerline deflection of beam B6.

Slabs S5 and S6 exhibited the same response with S6 having slightly higher deflections for the three load increments. In panel S5, the largest deflection occurred at load increment three and load positions 1.6, 2.6, and 3.6; the deflections remained relatively constant and ranged from 4.06 mm (0.16 in.) at load position 1.6 to 4.06 mm (0.16 in.) and 3.81 mm (0.15 in.) at load positions 2.6 and 3.6, respectively.

In panel S6, the largest deflections also occurred at load increment three and load positions 1.8, 2.8, and 3.8; maximum deflections obtained were 4.32 mm (0.17 in.), 4.57 mm (0.18 in.), and 3.81 mm (0.15 in.), respectively. The same uniform response was also exhibited at load increments one and two.

The response of hangers HN5 and HS5 was similar to those in Bridge I. The strains remained linear and well below the yield strain of the material for all three load increments. Also, as the loading increased, bending perpendicular to the roadway was observed in both hangers. The bending resulted from the deflection of beam B6 and the subsequent rotation of the ends. At load position 1.9 and load increments one, two, and three, the maximum tensile

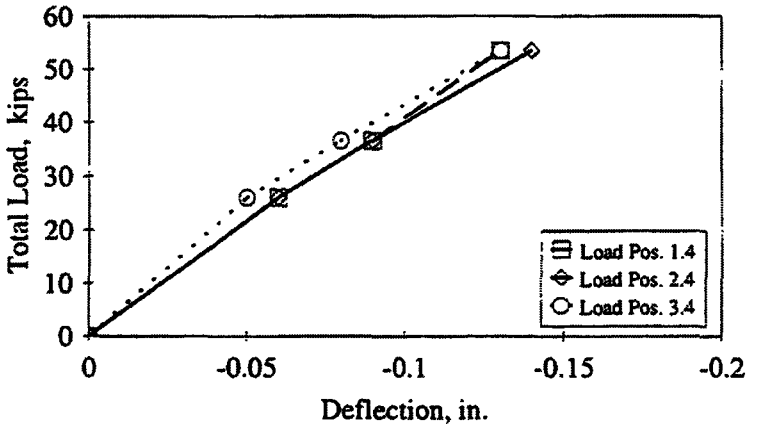

a. Deck panel S4

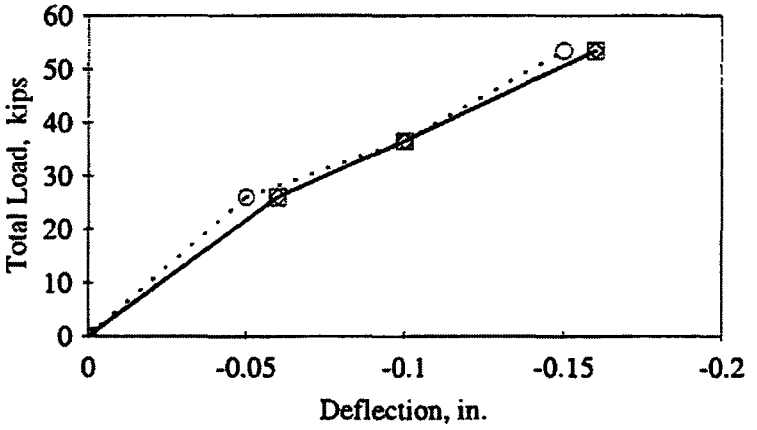

b. Deck panel S5

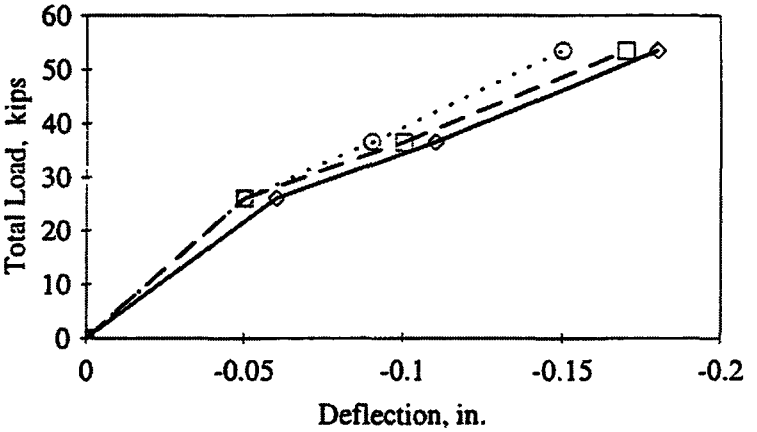

c. Deck panel S6

Figure 3.18. Bridge II: Centerline deflection of deck panels.

strain in HN5 was 41, 64, and 95 microstrain, respectively; this strain occurred in the angle on the inside face of the hanger. At the same load increments and position, the strain in the angle on the outside face of the hanger was -4, 1, and 11 microstrain, respectively.

The same behavior was observed in hanger HS5. At load position 3.9 and load increments one, two, and three, the maximum tensile strain which occurred in the angle on the inside face of HS5 was 36, 60, and 90 microstrain, respectively. At the same load increments and position, the strain in the angle on the outside face of the hanger was -2, -1, and 7 microstrain, respectively.

Overall, the maximum strain values of 95 and 90 microstrain obtained from hangers HN5 and HS5, respectively are significantly lower than the 1,441 microstrain required to yield the reinforcement. The strains in hangers HN5 and HS5 are presented in Figure 3.19 for load positions 1.9, 2.9, and 3.9 and the three loading increments.

Like the magnitude of the strains in the beam and hangers, the magnitude of the strains in the arches remained well below the elastic limit of the material. The largest strains at the crown of the north and south arches were obtained when the test vehicle was located at load positions 1.9 and 3.9 respectively. At these load positions, bending was observed in both arches. At load position 1.9 and load increments one, two, and three, the compressive strain in the concrete at the top face of the north arch was 19, 30, and 51 microstrain, respectively. At the same load positions for the three load increments, the average compressive strain in the north and south faces of the arch was 8, 10, and 15 microstrain.

The behavior of the crown of the south arch mirrored that of the north arch with the magnitude of the strains being slightly smaller. At load position 3.9 and load increments one, two, and three, the compressive strain in the concrete at the top face of the arch was 14, 26, and 34 microstrain, respectively. At the same load positions for the three load increments, the average compressive strain in the north and south faces of the arch was 8, 13, and 16 microstrain. The strain in the top faces of the north and south arches for the three load increments are presented in Figure 3.20.

The strains measured in the crowns of the north and south arches were significantly lower than the strains at which compression failure of the concrete occurs. Compression

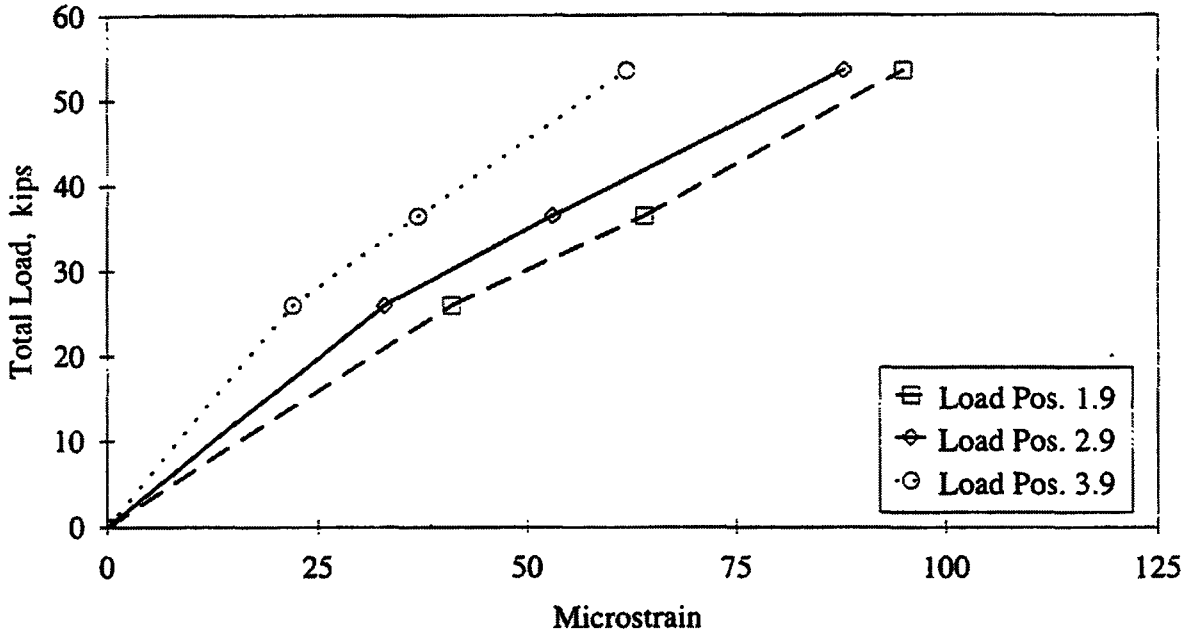

a. Hanger HN5

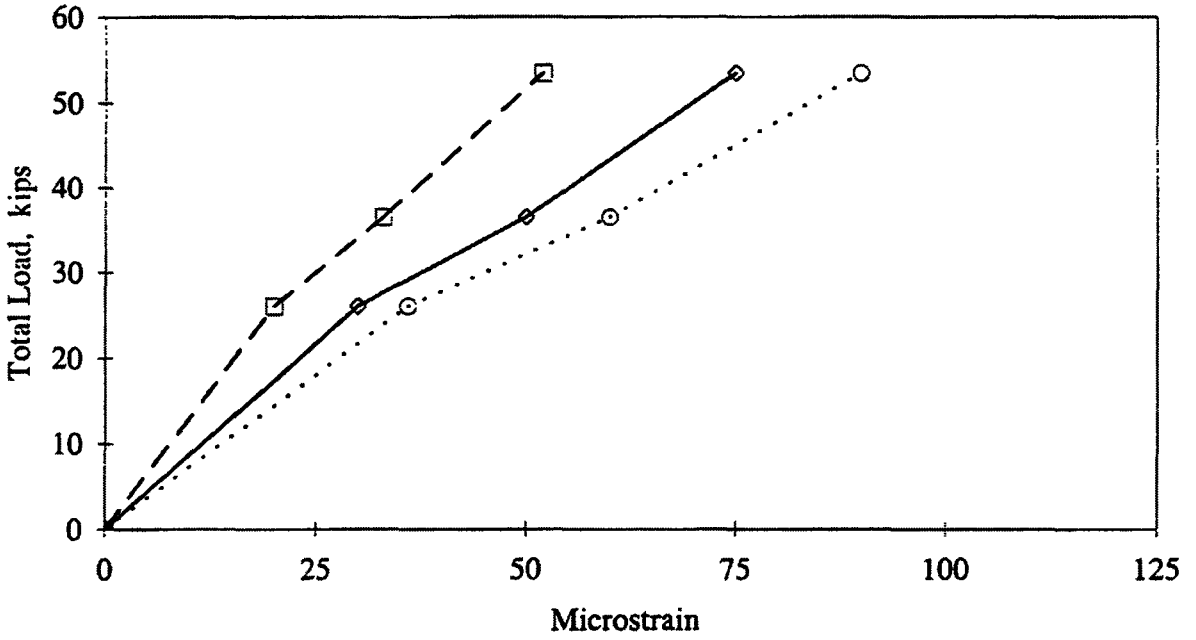

b. Hanger HS5

Figure 3.19. Bridge II: Strain in hangers.

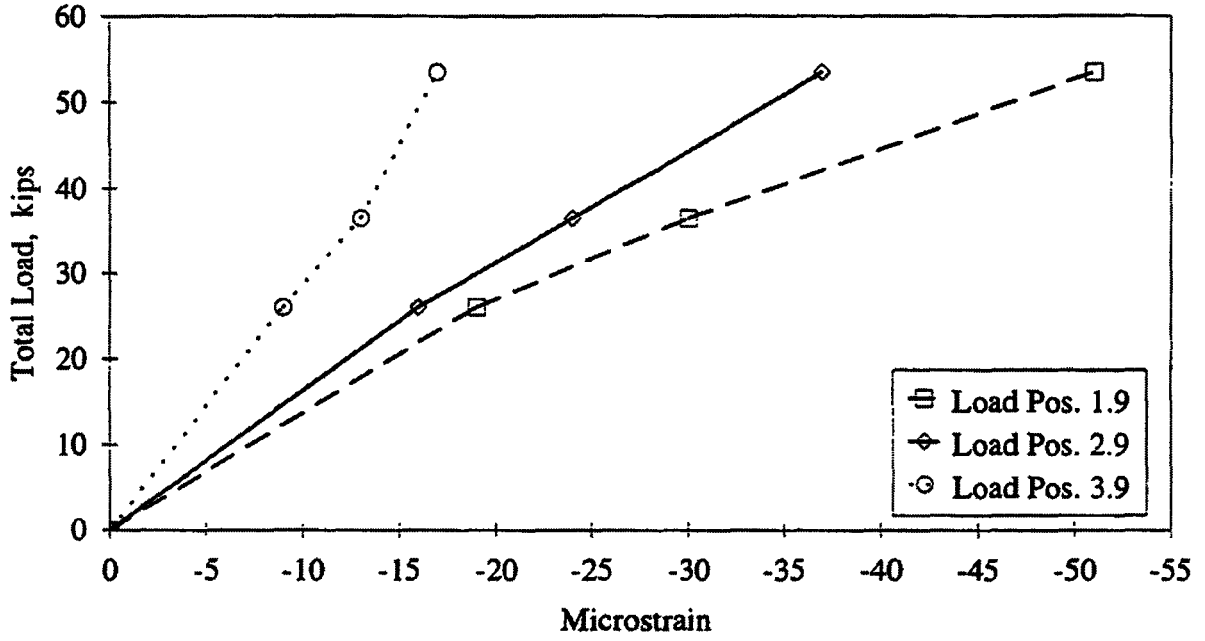

a. North arch

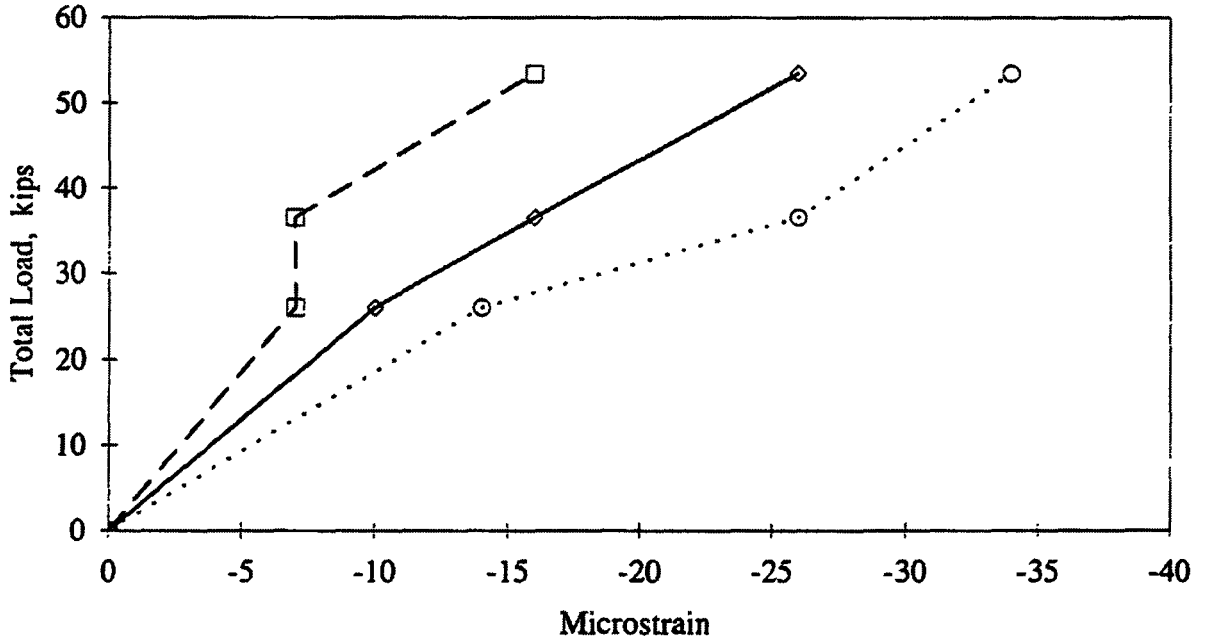

b. South arch

Figure 3.20. Bridge II: Strain at crown of arches.

failure of concrete is typically taken at 3,000 microstrain which is considerably higher than the 51 microstrain obtained from the top face of the north arch.

As the test vehicle moved across the bridge, deflections in the north arch were obtained at HN2, HN5, and HN7; similarly, deflections in the south arch were obtained at HS2, HS5, and HS7. The largest deflection of the north arch occurred at location HN2 when the test vehicle was at load position 1.3. At load increments one, two, and three, the deflection of the north arch at HN2 was 1.02 mm (0.04 in.), 1.52 mm (0.06 in.), and 2.29 mm (0.09 in.), respectively. At load position 1.9, the deflections at HN5 were 0.76 mm (0.03 in.), 1.27 mm (0.05 in.) and 1.78 mm (0.07 in.), respectively. At load position 1.11, deflections at HN7 were 0.76 mm (0.03 in.), 1.27 mm (0.05 in.), and 1.78 mm (0.07 in.), respectively.

The magnitude of the deflections of the south arch were similar for all three load increments. Like the north arch, the maximum deflection occurred at HS2 when the test vehicle was at load position 3.3. At load increments one, two, and three, the deflection of the south arch at HS2 was 0.76 mm (0.03 in.), 1.52 mm (0.06 in.), and 2.03 mm (0.08 in.), respectively. At load position 3.9, the deflections at HS5 were 1.02 mm (0.04 in.), 1.27 mm (0.05 in.), and 2.03 mm (0.08 in.), respectively. At load position 3.11, deflections at HS7 were 0, 1.02 mm (0.04 in.), and 1.78 mm (0.07 in.), respectively. The defections of the north and south arches at HN2 and HS2 for the three load increments are presented in Figure 3.21. It should be noted that the deflections obtained include the very small deformations in the hangers since the deflection transducers were attached to the bottom of the beams and not directly to the arches.

3.6.2. Concrete Core Samples

From the three concrete cores obtained from the deck of the bridge, the average compressive strength was determined. The results of the tests ranged from a low of 30.7 MPa (4,450 psi) to a high of 31.9 MPa (4,630 psi) with an average compressive strength of 31.3 MPa (4,550 psi). This is considerably higher than the 22.8 MPa (3,300 psi) which is the assumed value when the compressive strength of the concrete is unknown [1]. The compressive strength results for the concrete core tests are presented in Table 3.2.

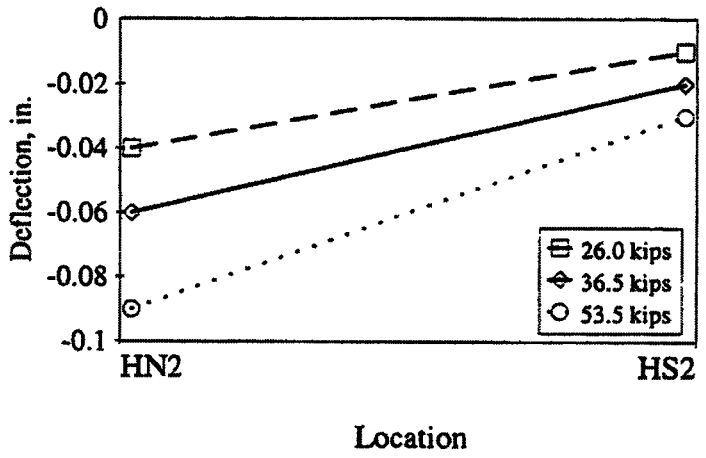

a. Load position 1.3

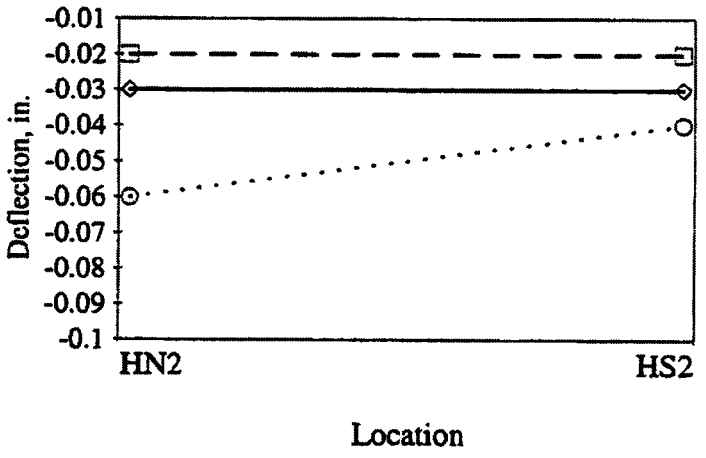

b. Load position 2.3

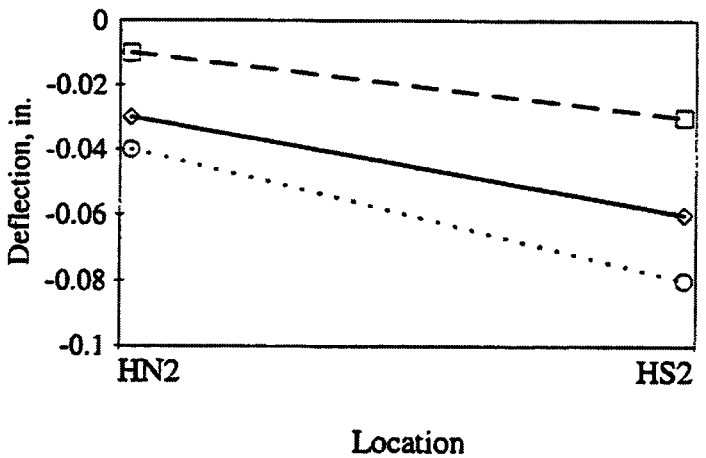

c. Load position 3.3

Figure 3.21. Bridge II: Deflection of arches.

Table 3.2. Bridge II: Results of concrete compressive strength tests.

Specimen	Compressive Strength psi
A	4,450
B	4,560
C	4,630
Average	4,550
Standard Deviation	91

1 psi = 0.00689 MPa

3.6.3 Steel Samples

The yield stress of the steel specimens was greater than the usually assumed values for steel from the period in which the bridge was built.

The average yield stress of the three structural steel specimens obtained from the hangers was 288 MPa (41,800 psi). The yield stress values ranged from a low of 280 MPa (40,600 psi) to a high of 301 MPa (43,700 psi). For unknown steel in structures built between 1905 and 1936, the assumed minimum yield strength of the steel is 207 MPa (30,000 psi) [1]. Results of the tensile tests performed on the structural steel specimens are presented in Table 3.3.

The average yield strength of the reinforcing steel was determined from the specimens obtained from the deck. Results from the tests ranged from a low of 310 MPa (44,900 psi) to a high of 361 MPa (52,400) with an average yield strength of 327 MPa (47,400 psi). The assumed yield strength of reinforcing steel in structures built prior to 1954 is 228 MPa (33,000 psi) [1]. Results of the tensile tests performed on the reinforcing steel specimens are presented in Table 3.4. The high modulus of elasticity values are a result of the extensometer malfunctioning at the time of testing.

Overall, the yield strength of the structural and reinforcing steel is considerably higher than the assumed values for unknown steel in structures built during this period. Typical stress-strain curves for the steel specimens are presented in Figure 3.22.

Table 3.3. Bridge II: Structural steel tensile test results.

Specimen	Yield Strength psi	Ultimate Strength psi	Young's Modulus psi
H1	41,100	62,400	30,900,000
H2	40,600	62,800	30,200,000
H3	43,700	62,500	29,300,000
Average	41,800	62,600	30,100,000
Standard Dev.	1,660	208	800,000

1 psi = 0.00689 MPa

Table 3.4. Bridge II: Tensile test results of reinforcing obtained from deck.

Specimen	Yield Strength psi	Ultimate Strength psi	Young's Modulus psi
R1	44,900	72,400	38,200,000*
R2	45,000	71,100	43,000,000*
R3	52,400	76,800	31,300,000
Average	47,400	73,400	
Standard Dev.	4,300	2,990	

1 psi = 0.00689 MPa

*Experimental error

3.7. Modified Rating

Using the strains obtained from the diagnostic load test, the theoretical load rating was modified using the procedure outlined in Sec. 1.7. Overall, the ratings of the beams, hangers, and arches increased while the rating for the deck remained unchanged since no strain data were obtained for this element.

The rating of the beams increased from 528 kN (59 tons) to 1,183 kN (133 tons) for the HS20-44 rating vehicle. For the Type 3 rating vehicle, the rating of the beams increased from 391 kN (44 tons) to 899 kN (101 tons).

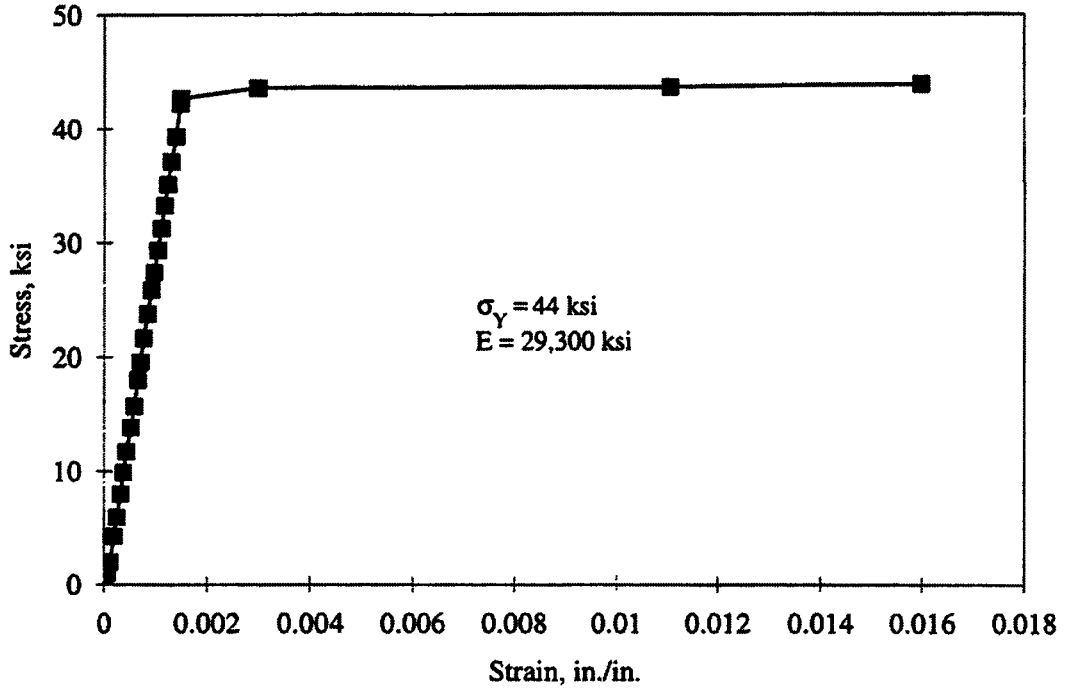

a. Structural steel in hangers (specimen H3)

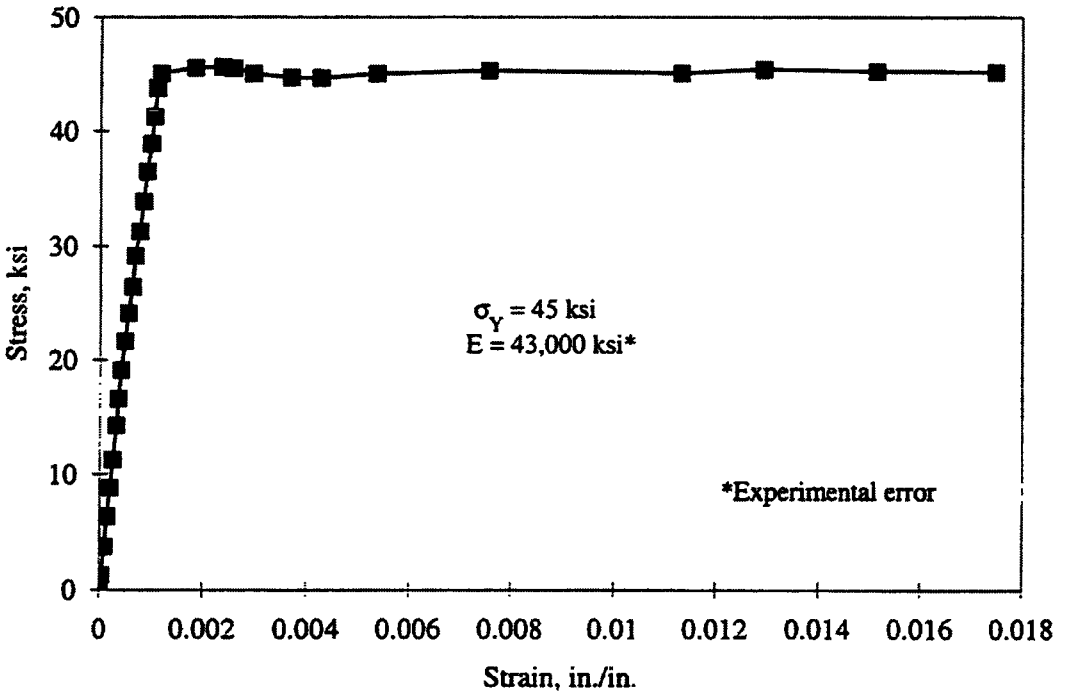

b. Reinforcing steel in deck (specimen R2)

Figure 3.22. Bridge II: Typical stress-strain curves of bridge reinforcing.

The rating of the hangers increased from 1,023 kN (115 tons) to 2,020 kN (227 tons) for the HS20-44 rating vehicle. For the Type 3 rating vehicle, the rating increased from 774 kN (87 tons) to 1,530 kN (172 tons).

Finally, the rating of the arches increased from 1,334 kN (150 tons) to 1,592 kN (179 tons) for the HS20-44 rating vehicle. For the Type 3 rating vehicle, the rating increased from 1,059 kN (119 tons) to 1,272 kN (143 tons). A summary of the theoretical and modified rating for each component is presented in Table 3.5. The modified rating calculations are presented in Appendix B.

The overall rating of the bridge was governed by the deck since no strain data were obtained to modify its theoretical load rating. The bridge would still require load posting for the HS20 vehicle; however, no load posting would be required for the Type 3 vehicle.

Table 3.5. Bridge II: Rating summary.

	Vehicle HS20				Vehicle Type 3			
	AASHTO LRFR		Modified Rating		AASHTO LRFR		Modified Rating	
	RF_c	R(tons)	RF_T	R(tons)	RF_c	R(tons)	RF_T	R(tons)
Slab:	0.79	28.4			1.30	32.5		
Beams:	1.65	59.4	3.72	133.9	1.79	44.8	4.04	101.0
Hangers:	3.21	115.6	6.32	227.5	3.50	87.5	6.89	172.3
Arches:	4.17	150.1	4.98	179.3	4.79	119.8	5.72	143.0

indicates controlling component

4. BRIDGE III: REINFORCED CONCRETE SLAB

4.1. Bridge Description

The third bridge to be service load tested was a reinforced concrete slab bridge. This particular bridge was located on a secondary county road (150th St.) in northeast Boone County over a tributary of Squaw Creek. The ADT for this structure was 35 vehicles as of 1987. Built in 1920, this bridge is one of nearly 1,000 slab bridges still remaining within the state of Iowa. Figure 4.1 shows the layout of this bridge; the dimensions shown were obtained from field measurements.

Bridge III had a clear span of 6,705 mm (22 ft) and a total width of 6,095 mm (20 ft). The roadway width from the inside of curb to the inside of curb was 5,590 mm (18ft - 4in.). The thickness of the deck varied from a maximum of 535 mm (21 in.) at the center to a minimum of 485 mm (19 in.) at the edges. The reinforcement details are shown in Figure 4.2. Reinforcement in the slab consisted of one layer of 19 mm (3/4 in.) square reinforcing bars spaced at 150 mm (6 in.) on center in the longitudinal direction and 13 mm (1/2 in.) round reinforcing bars spaced at 460 mm (18 in.) on center in the transverse direction. During construction, an asphalt felt material was placed on top of the abutments before the deck was cast to provided separation between the slab and the abutments. This separation allowed the deck to slip and rotate freely under applied loading which allowed the bridge to be designed as simply supported.

4.1.1. Condition Assessment

Prior to the diagnostic load test, previous inspection reports for the bridge were obtained and a thorough visual inspection was conducted by the researchers. The latest inspection conducted in 1993 showed a condition rating of 5 for the deck and a condition rating of 7 for the superstructure. The lower rating for the deck was due to exposed rebar on the bottom of the slab; the bridge was posted for narrow roadway.

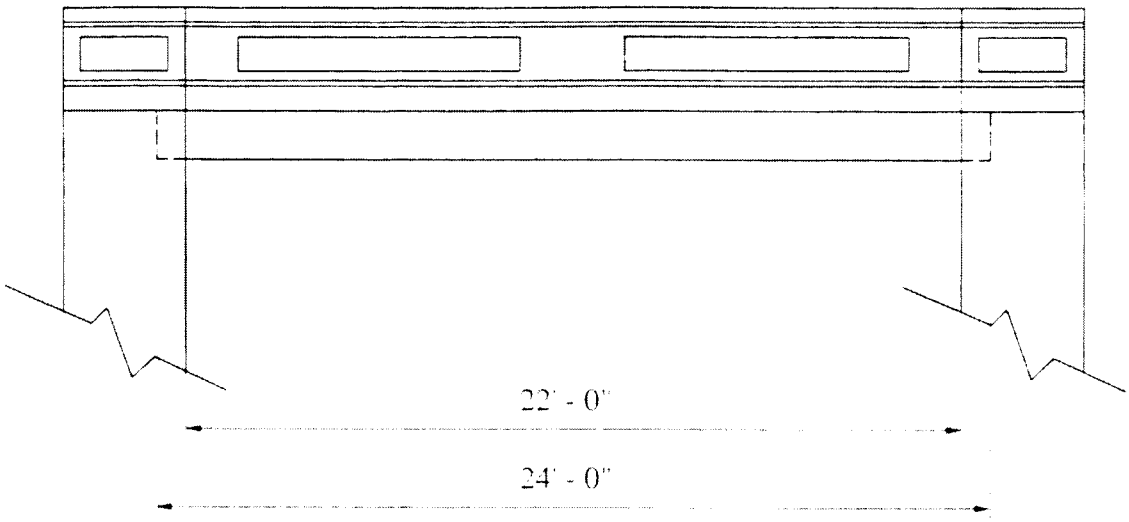

a. Elevation

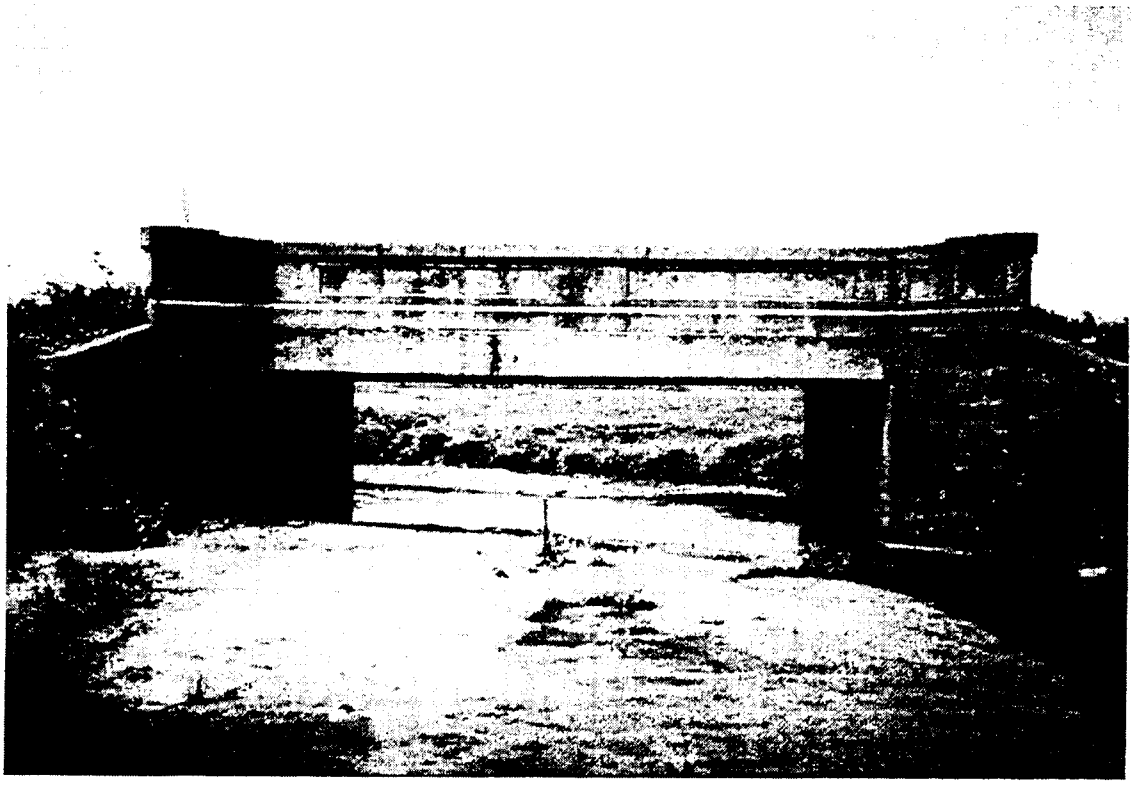

b. Photograph of bridge profile

Figure 4.1. Bridge III: Layout.

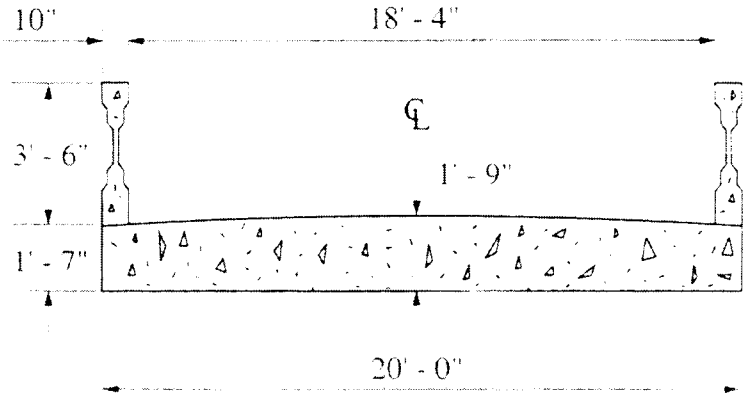

c. Typical cross section

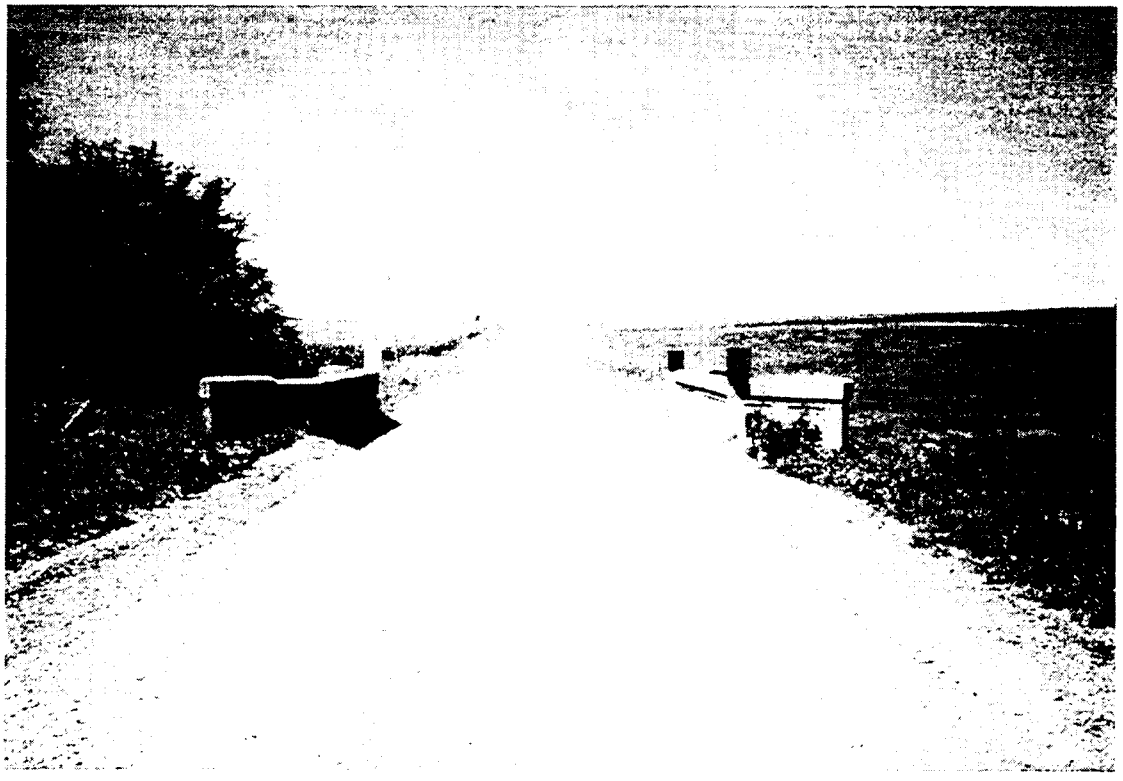

d. Photograph of Bridge III looking West

Figure 4.1. Continued.

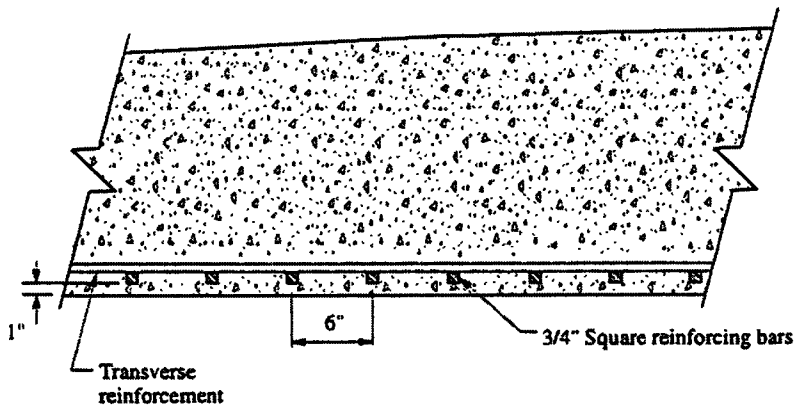

a. Longitudinal reinforcement

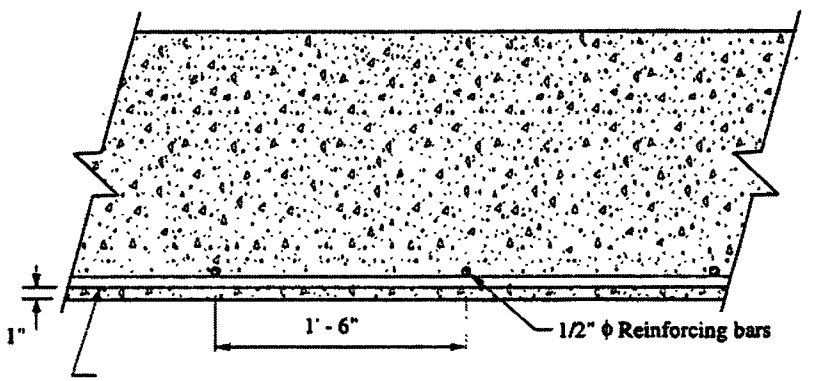

b. Transverse reinforcement

Figure 4.2. Bridge III: Slab reinforcement details.

At the time the visual inspection was conducted by the researchers, the deterioration in the bottom of the slab had not been repaired. Spalling of the concrete was observed at each of the four floor drain openings. At one of the openings, the spalling was so severe that a large section of the longitudinal reinforcing bars was exposed. The exposed reinforcing had moderate corrosion. The railings, wing walls and abutments were in good shape and showed no signs of serious deterioration. A photograph of the exposed reinforcement previously

Figure 4.3. Bridge III: Photograph of exposed reinforcement in slab.

described is shown in Figure 4.3.

4.2. AASHTO Rating

Using the information obtained from the visual inspection, the condition of the slab was assessed and the theoretical load rating factors were calculated . The vehicles and procedures used to obtain the rating factors were described in Secs. 1.4 and 1.7, respectively. The material strengths of the concrete and reinforcing steel were assumed to be 28 MPa (4,000 psi) and 228 MPa (33,000 psi), respectively. The modulus of elasticity of the concrete was determined using the equation $E_c = 5{,}000\sqrt{f'_c}$ ($57{,}000\sqrt{f'_c}$). The modulus of elasticity of the steel was taken as 200,000 MPa (29,000,000 psi). Using the HS20-44 rating vehicle, the slab was given a load rating of 0.61; with the Type 3 vehicle, the bridge had a load rating of 0.69. The calculations used to obtain the load ratings are presented in Appendix B. Table 4.1 shows the results of the theoretical load rating for the two rating vehicles.

Table 4.1. Bridge III: Theoretical load rating summary.

	Vehicle HS20 AASHTO LRFR		Vehicle Type 3 AASHTO LRFR	
	Rating Factor	Rating (tons)	Rating Factor	Rating (tons)
Slab	0.61	22.0	0.69	17.3

4.3. Test Setup and Procedures

To obtain material and general structural behavior, strains and deflections were monitored at various locations. A diagram of the strain gage and deflection transducer locations is shown in Figure 4.4. As can be observed, strain gages were bonded on the bottom of the slab at the centerline and near the west abutment. Also, one strain gage was bonded to the top of the south railing at the centerline. The strain gages were placed in order to obtain the maximum strain in the deck and to also observe strain behavior in the deck as the test vehicle was placed in various locations.

Two strain gages were placed on the bottom of the deck at a distance of 305 mm (1 ft) from the west abutment. The strain gages were placed transversely at the quarter points of the slab. These strain gages were added to determine if the deck was free to rotate under the applied loading. The types of strain gages used and the application process were discussed in Sec. 1.6.1.

The deflections of the bridge were monitored at the centerline and at the west quarter point. As shown in Figure 4.4a, three deflection transducers were mounted transversely across the bottom of the deck at the centerline. The same setup was used at the quarter point except that the deflections at the north edge and the center were the only ones obtained due to a malfunctioning deflection transducer at the south edge. The deflections were obtained using the equipment and setup described in Sec. 1.6.1.

The type of vehicle and loading process used in the testing the bridge were described in Sec.1.6.2. For this bridge, the loading was applied in three increments. In the first load increment, the test vehicle had a gross vehicle weight of 95,635 N (21,500 lbs). In load increments two and three, the test vehicle had a gross vehicle weight of 173,401 N (39,000

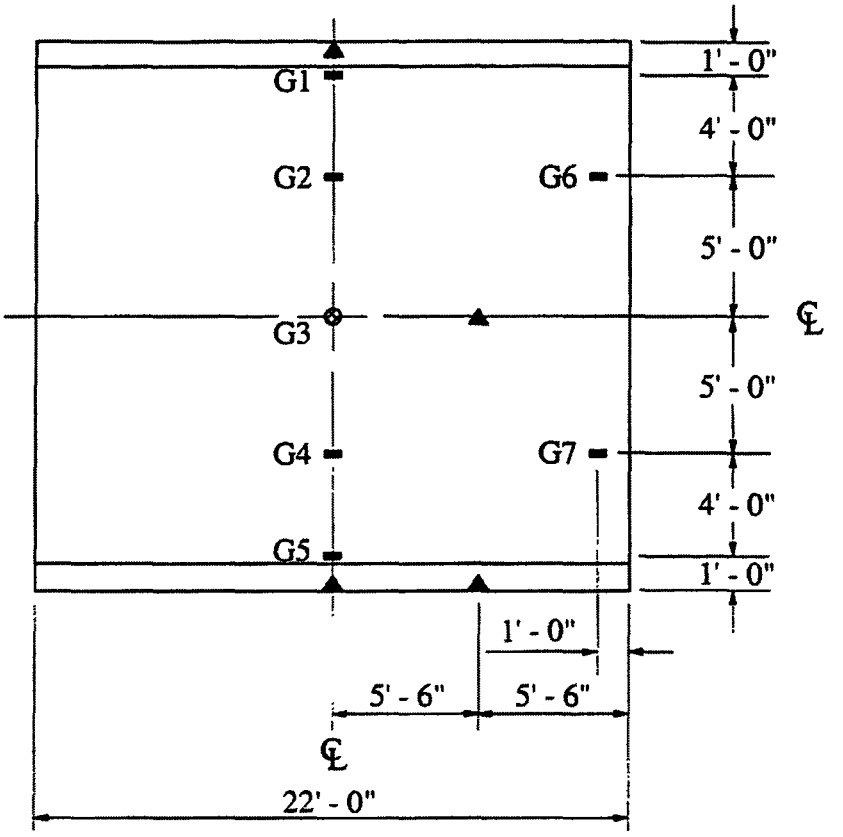

a. Plan view

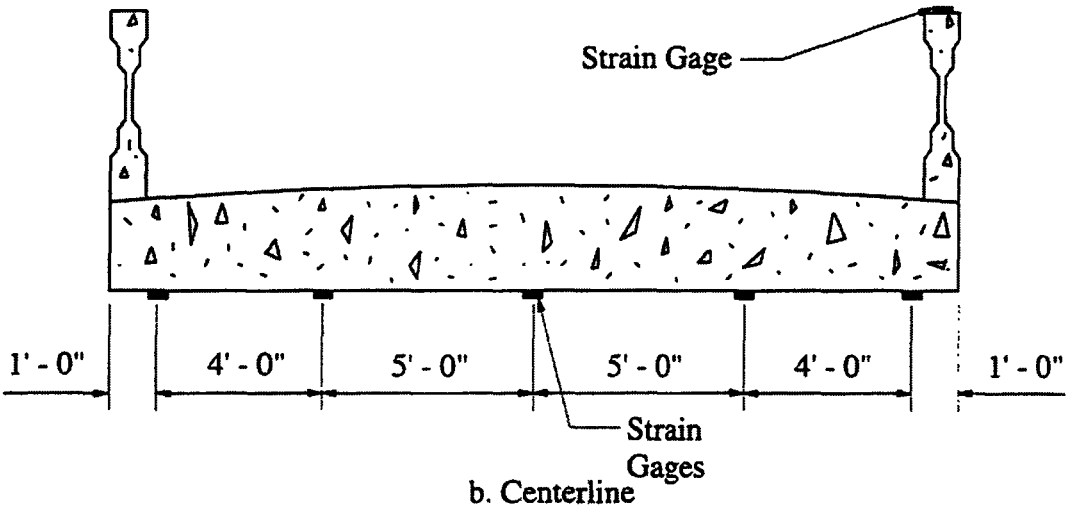

b. Centerline

Figure 4.4. Bridge III: Location of strain gages and deflection transducers.

lbs) and 307,815 N (69,200 lbs), respectively. The magnitude of the load increments and wheel configuration of the test vehicle are presented in Figure 4.5; a photograph of the test vehicle is shown in Figure 4.6.

The deflection and strain behavior of the bridge were observed by stopping the test vehicle at various longitudinal and transverse locations. Longitudinally, the test vehicle was stopped at the east quarter point, center, and west quarter point; these locations are shown in Figure 4.7. At each location, the test vehicle was positioned so that the front axle of the rear tandem was centered on the desired location. Once the vehicle had been positioned, strain and deflection readings were taken. The transverse lane positioning of the test vehicle was described in Sec. 1.6.2 and is shown in Figure 4.8.

4.4. Results and Discussion

The response of the bridge to the applied loading was linear for both strains and deflections. Also, the magnitude of the strains and deflections was extremely small which suggests that the structure has significant more strength than was predicted by the theoretical load rating in Sec. 4.3.

The strains at the centerline of the bridge varied depending on the placement of the test vehicle. With the test vehicle located at load position 1.2, the strains at G1 and G3 were maximum for the three load increments whereas the strains at G2, G4, and G5 remained small. The strains at G1 and G3 ranged from 3 microstrain at load increment one to 17 and 16 microstrain respectively for load increment three.

At load position 2.2, the maximum strain was recorded at G3 (center) for the three load increments. This is expected since the railings add stiffness to the edge of the deck which results in smaller strain readings at the edges. The strain values at G3 ranged from 5 microstrain at load increment one to 19 microstrain at load increment three.

The largest strain readings at G5 occurred when the load was in position 3.2. The strain ranged from 6 microstrain at load increment one to 28 microstrain at load increment three. The strains at G2 and G4 were the lowest for the three load positions and load

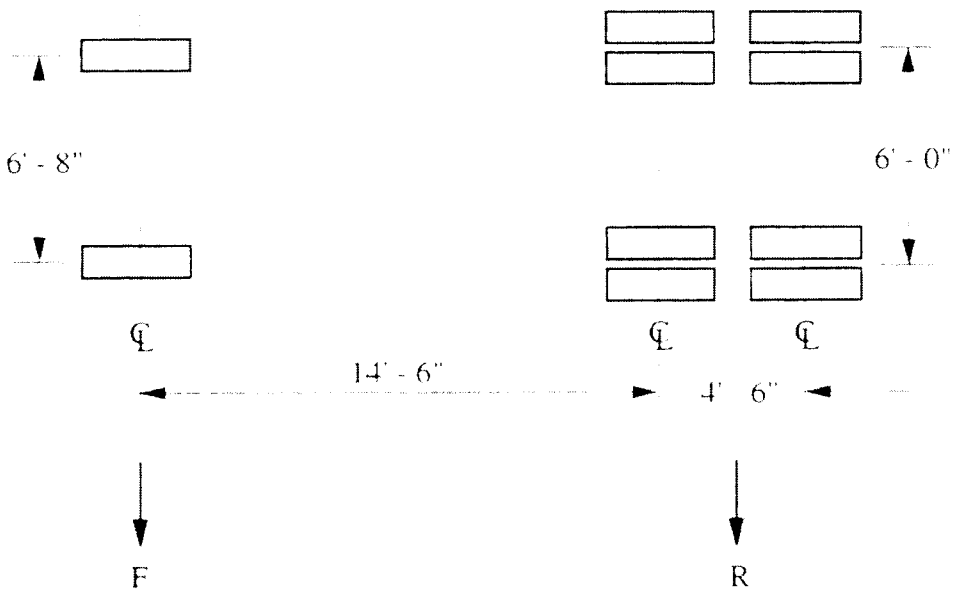

Load Increment	F (kips)	R (kips)	Total Load (kips)
1	9.3	12.2	21.5
2	12.9	26.1	39.0
3	17.4	51.8	69.2

Figure 4.5. Bridge III: Wheel configuration and weight distribution in test vehicle.

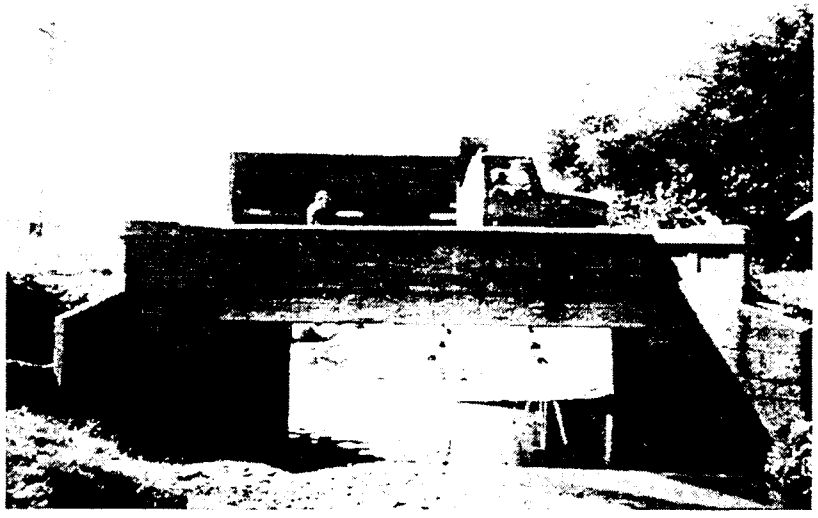

Figure 4.6. Bridge III: Photograph of test vehicle on bridge.

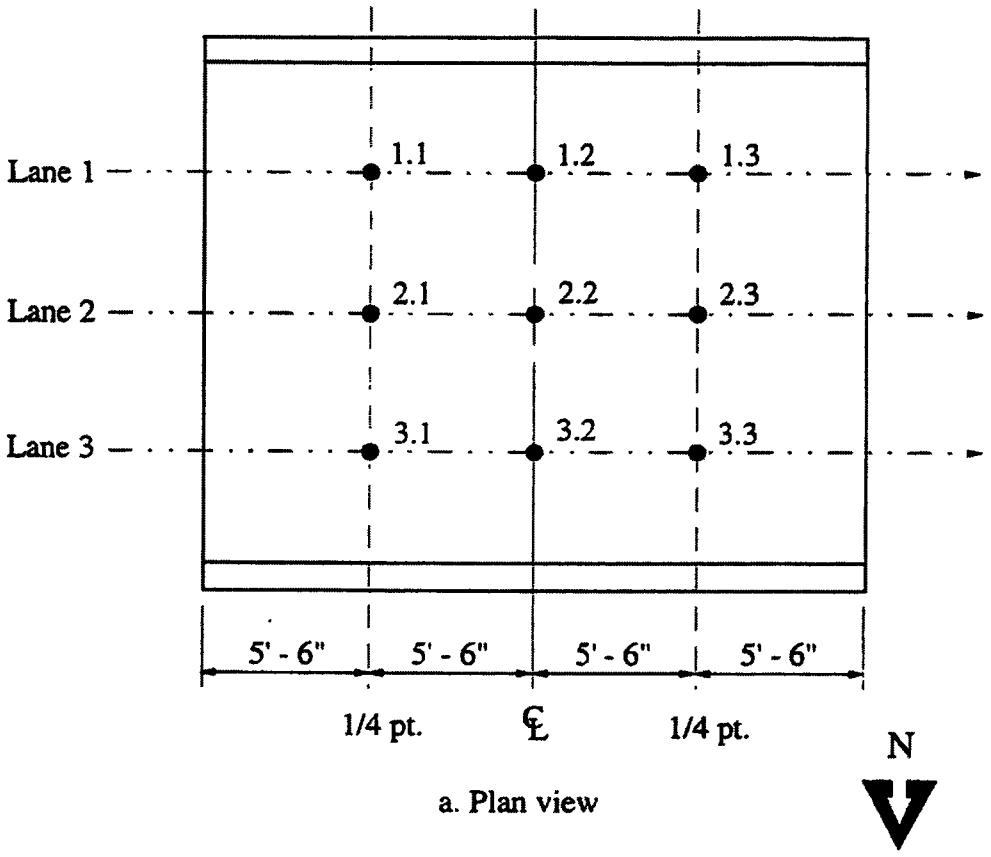

a. Plan view

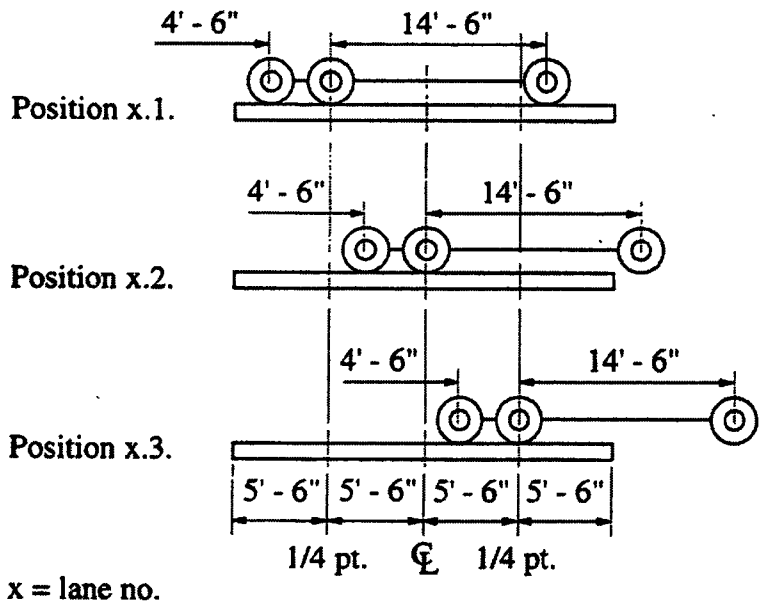

x = lane no.

b. Truck stopping position on deck.

Figure 4.7. Bridge III: Longitudinal location of test vehicle for various tests.

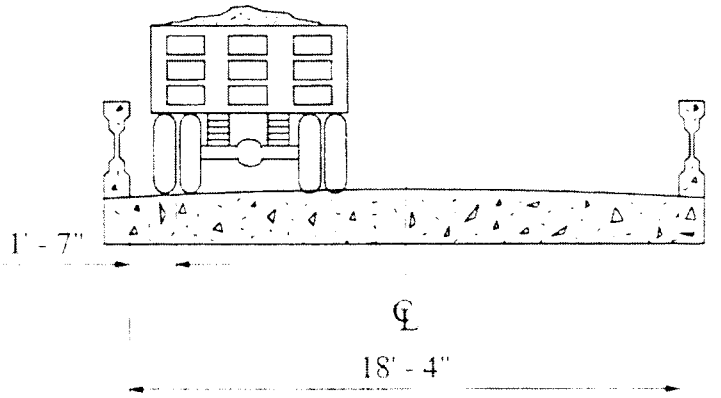

a. Lane 1

b. Photograph of test vehicle in Lane 1

Figure 4.8. Bridge III: Transverse location of test vehicle on bridge.

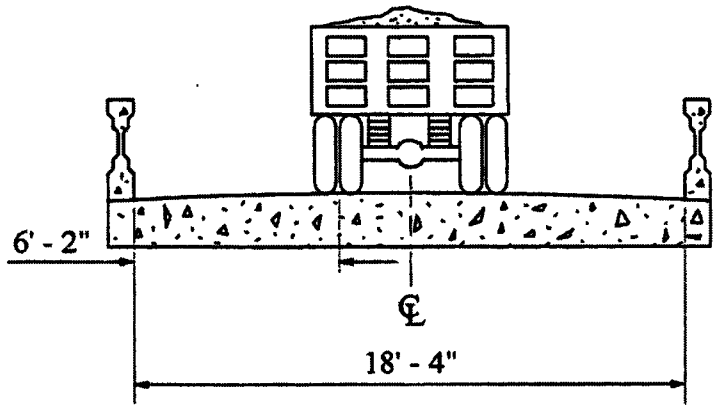

c. Lane 2

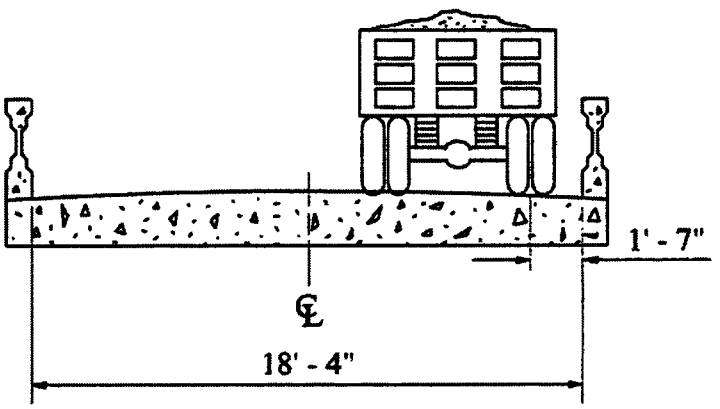

d. Lane 3

Figure 4.8. Continued.

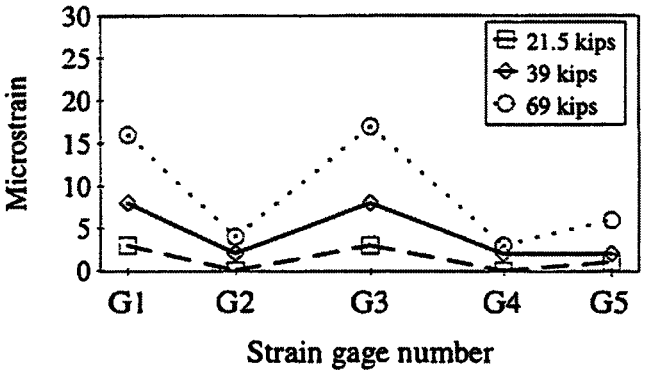

a. Load position 1.2

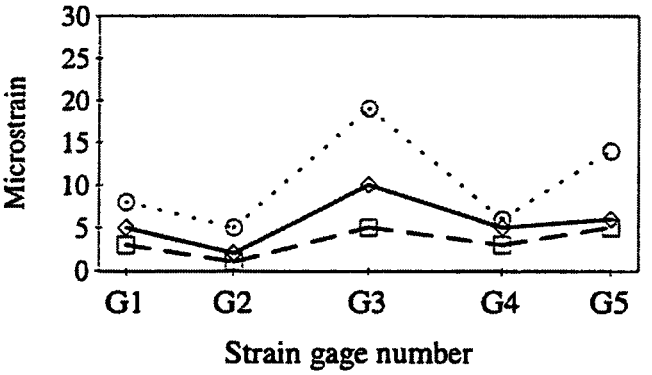

a. Load position 2.2

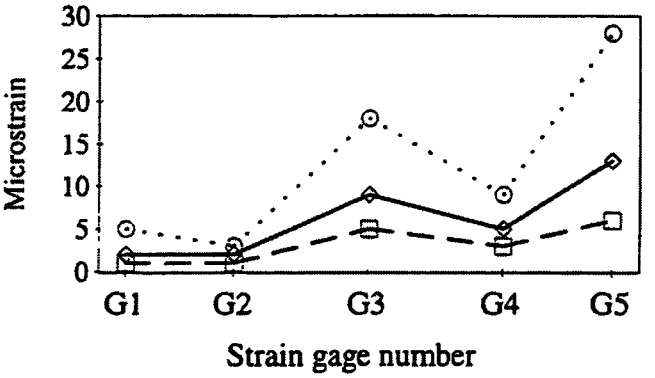

a. Load position 3.2

Figure 4.9. Bridge III: Longitudinal strains at bridge centerline.

increments. Figure 4.9 illustrates the distribution of the strains at the centerline of the slab for the three load increments and load positions 1.2, 2.2, and 3.2.

The response of the bridge was consistent for the three load increments and load positions. When the test vehicle was located in lanes one and three, maximum strains were recorded at the edges and when the test vehicle was located in lane two, maximum strains were recorded at the center. As shown by the graphs in Figure 4.9, the strains obtained were extremely small. The maximum strain recorded was 28 microstrain which is over 4.5 times smaller than the strain (130 microstrain) at which tensile cracks begin to form in concrete. The linear response exhibited by the slab is shown by Figure 4.10 which plots the strain at G3 verses the three load increments for load positions 1.2, 2.2, and 3.2.

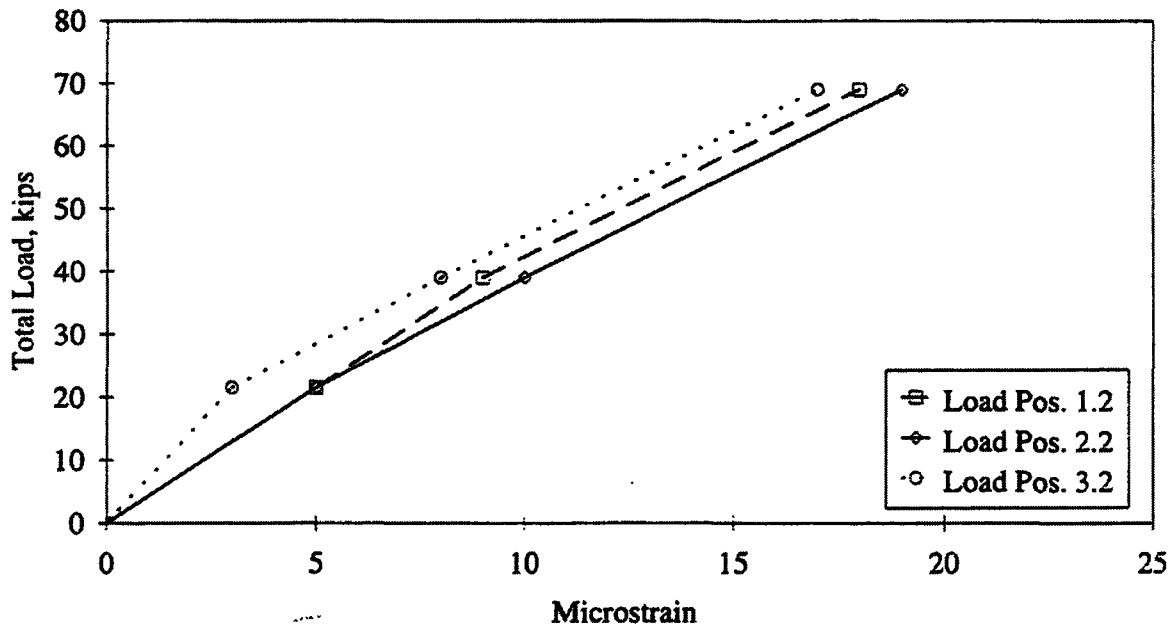

Figure 4.10. Bridge III: Strains at bridge centerline.

The strains recorded at G6 and G7 indicates that the slab was rotating at the abutments and was not fixed. For the three load increments and various load positions, the

strains at G6 and G7 remained positive. Thus, the analysis of the slab as a simply supported member is justified.

Like the strains, the deflections at the centerline of the slab were also very small. With the test vehicle located at load position 1.2, the deflection at the south edge of the slab ranged from a minimum of 0.03 mm (0.001 in.) at load increment one to a maximum of 0.30 mm (0.012 in.) at load increment three.

The maximum deflection of the slab was attained when the test vehicle was at load position 2.2 . The slab deflected 0.41 mm (0.016 in.) at load increment three. Also, at this load position, the stiffening affect of the railings was quite noticeable. At load increment three, the deflections at the north and south edges of the slab were 0.13 mm (0.005 in.) while at the center of the slab the deflection was 0.41 mm (0.016 in.).

The deflection of the north edge of the slab was similar to the deflection of the south edge of the slab. With the test vehicle located at load position 3.2, the deflection of the north edge ranged from a minimum of 0.03 mm (0.001 in.) at load increment one to a maximum of 0.28 mm (0.011 in.) at load increment three. Graphs showing the transverse deflection at the bridge centerline for load increments one, two, and three, and load positions 1.2, 2.2, and 3.2 are presented in Figure 4.11.

Graphs showing the deflections obtained from the center transducers at the centerline and west quarter point for the three load increment are presented in Figure 4.12. The deflection response of the bridge at the west quarter point was less than that at the centerline. At load increments one and two, no deflections were observed at the edge of the slab or at the centerline for load positions 1.3, 2.3, and 3.3. At load increment three and load positions 1.3, 2.3, and 3.3, the center deflection was 0.08 mm (0.003 in.), 0.15 mm (0.006 in.), and 0.05 mm (0.002 in.), respectively.

4.5. Modified Rating

Using the strain data obtained from the diagnostic load test and the procedure described in Sec 1.7., the theoretical load rating was modified. The test strain values used in the modified rating procedure were the strains at the centerline of the slab averaged for load

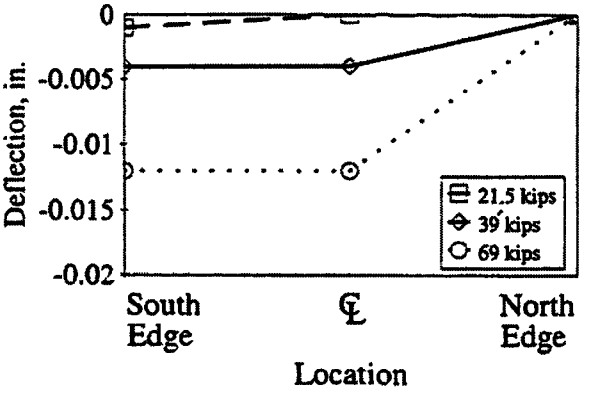

a. Load position 1.2

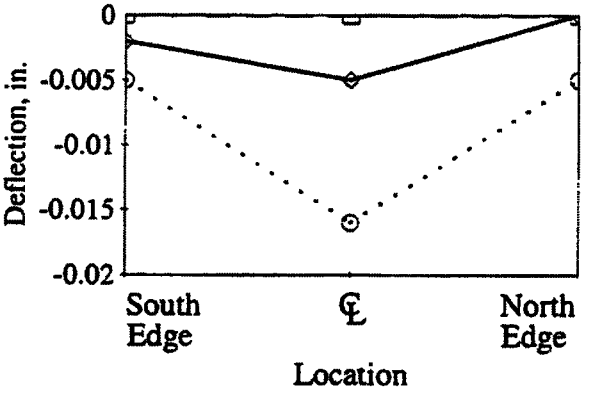

b. Load position 2.2

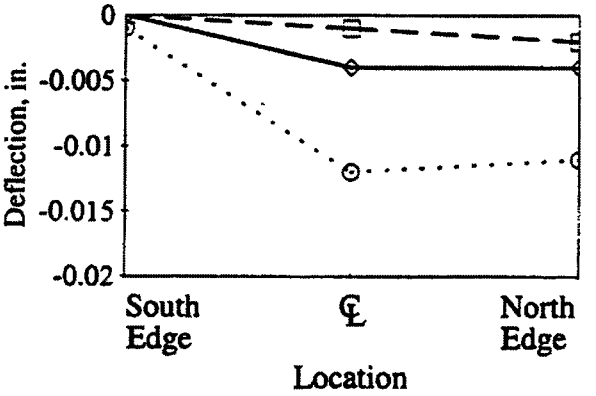

c. Load position 3.2

Figure 4.11. Bridge III: Deflections at bridge centerline.

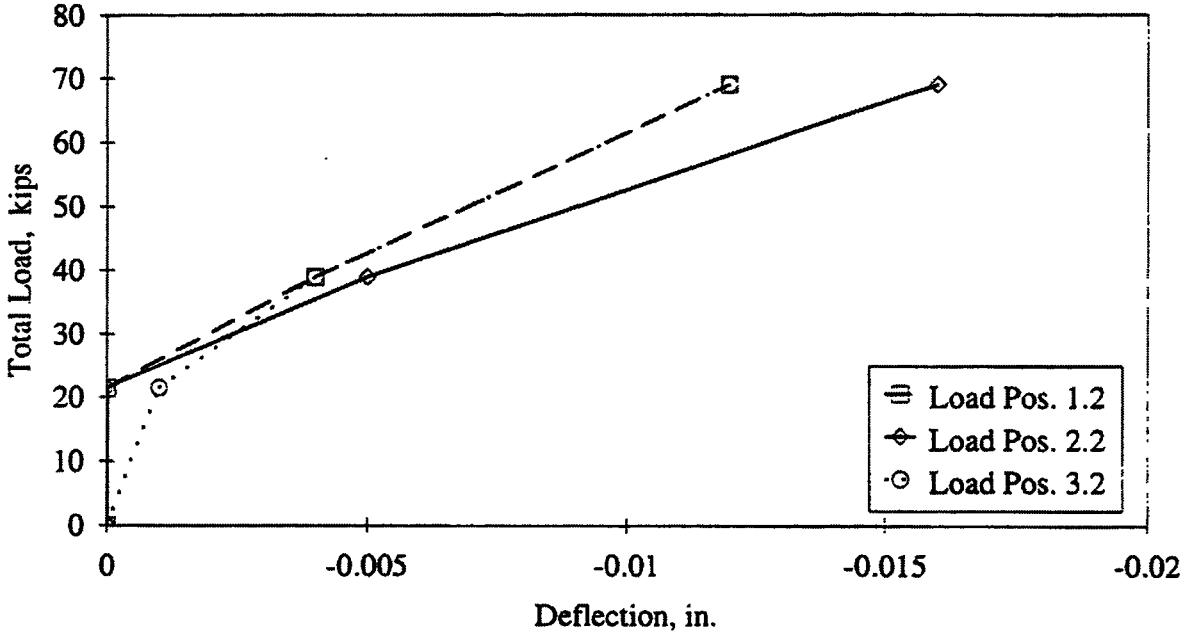

a. Centerline

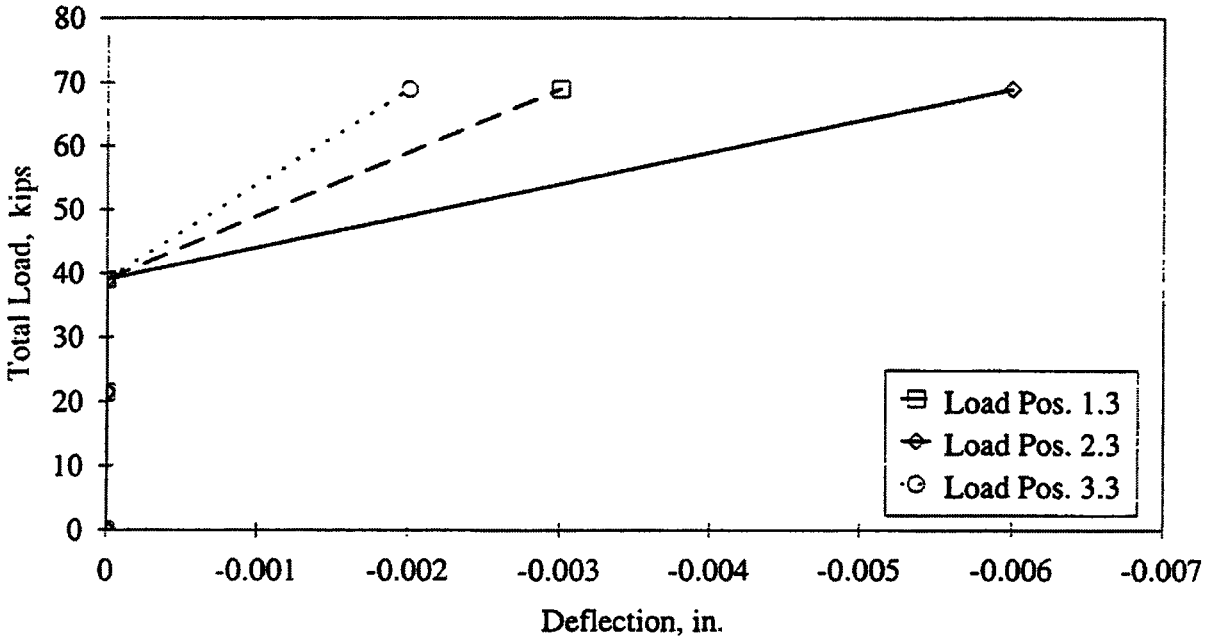

b. Quarter point

Figure 4.12. Bridge III: Longitudinal deflections.

increment three and load positions 1.2, 2.2, and 3.2. The largest of the three values was selected - 13 microstrain when the test vehicle was located at load position 3.2. For the same load position and load increment, the theoretical strain calculated in the bottom of the slab was 84 microstrain.

The large difference in the theoretical and test strain values can be explained by the presence of the railings. The addition of the railings adds considerable stiffness to the edges of the deck which results in smaller strain and deflection values. In the determining the theoretical strain in the bottom of the slab, the increased stiffness provided by the railings was neglected resulting in higher predicted strain.

The results obtained from the diagnostic load test allowed the theoretical load rating to be significantly increased. The rating of the slab increased from 195,720 N (22 tons) to 960,815 N (108 tons) for the HS20 rating vehicle. For the Type 3 rating vehicle, the rating of the slab increased from 151,240 N (17 tons) to 756,195 N (85 tons). A summary of the theoretical and modified rating is presented in Table 4.2. The rating calculations for the slab are presented in Appendix B.

The results of the diagnostic load test clearly indicate the conservative response predicted by traditional analytical procedures and standard ASSHTO rating methods. Without the diagnostic load test, the bridge would have to be posted for both the HS20 and Type 3 vehicles. In reality, the bridge has considerable reserve capacity.

Table 4.2. Bridge III: Rating Summary.

	Vehicle HS20				Vehicle Type 3			
	AASHTO LRFR		Modified Rating		AASHTO LRFR		Modified Rating	
	RF_c	R (tons)	RF_T	R (tons)	RF_c	R (tons)	RF_T	R (tons)
Slab	0.61	22.0	3.02	108.7	0.69	17.3	3.41	85.3

5. BRIDGE IV: FILLED REINFORCED CONCRETE SPANDREL ARCH

5.1. Bridge Description

The third type of bridge to be service load tested was a filled reinforced concrete spandrel arch located in the northwest corner of Marshall County over Minerva Creek. Like the previous bridges tested, Bridge IV was also one lane and located on a secondary county (140th St.) road. The ADT for the bridge was 40 vehicles. Constructed in 1912, this particular type of filled reinforced concrete spandrel arch bridge was designed and patented in the early 20th century by Daniel B. Luten and hence is known historically as a Luten Arch Bridge. What made this arch different from other arches built during this period was the implementation of a curved reinforced concrete slab which was located beneath the stream bed. The slab was provided to tie the abutments together and to reduce the thrust to the foundation allowing for smaller footings. At the time of testing, there were five Luten Arch Bridges remaining within the state of Iowa and all were listed on the Iowa Historic Bridge Inventory. The layout for this bridge is presented in Figure 5.1; all dimensions were obtained from field measurements.

Bridge IV had a clear span of 19,200 mm (63 ft), a rise of 2,740 mm (9 ft), and a total width of 5,180 mm (17 ft). The roadway measured 4,675 mm (15 ft - 4 in.) from the inside of curb to the inside of curb and had two reinforced concrete railings 915 mm (3 ft) high and 205 mm (8 in.) wide. Due to extensive damage, a portion of the north railing had been removed and replaced by a temporary railing consisting of four angle posts and a timber hand rail. The thickness of the arch at the crown, determined by drilling a series of cores, was 330 mm (13 in.).

Because of the age of Bridge IV, no as built plans or design drawings could be located. To determine the thickness of the arch ring at the abutments and the arrangement of the reinforcement, the remaining four Luten Arches in the state were researched. Of the four bridges, the layout and plans for the Luten Arch located in Story County most closely resembled the bridge being tested. The Story County Luten Arch was 3,960 mm (13 ft) longer, rose 1220 mm (4 ft) higher and had a crown thickness 75 mm (3 in.) greater than

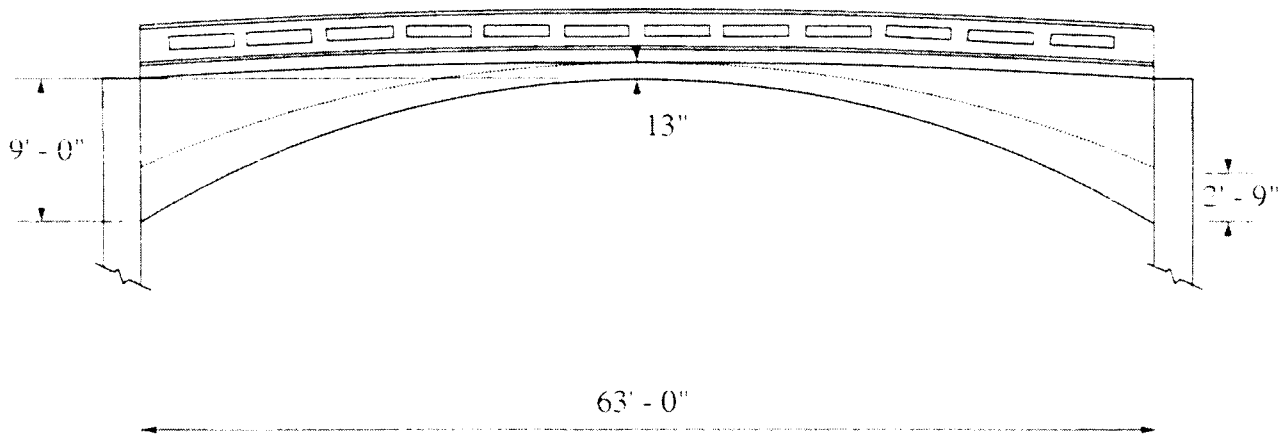

a. Elevation

b. Photograph of bridge profile

Figure 5.1. Bridge IV: Layout.

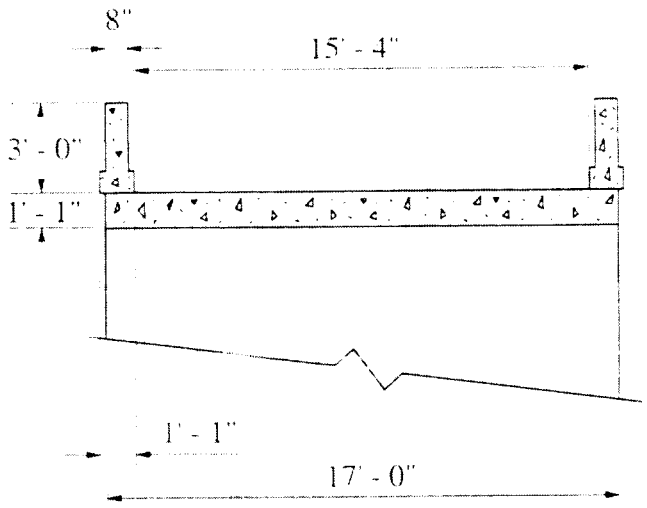

c. Centerline cross section

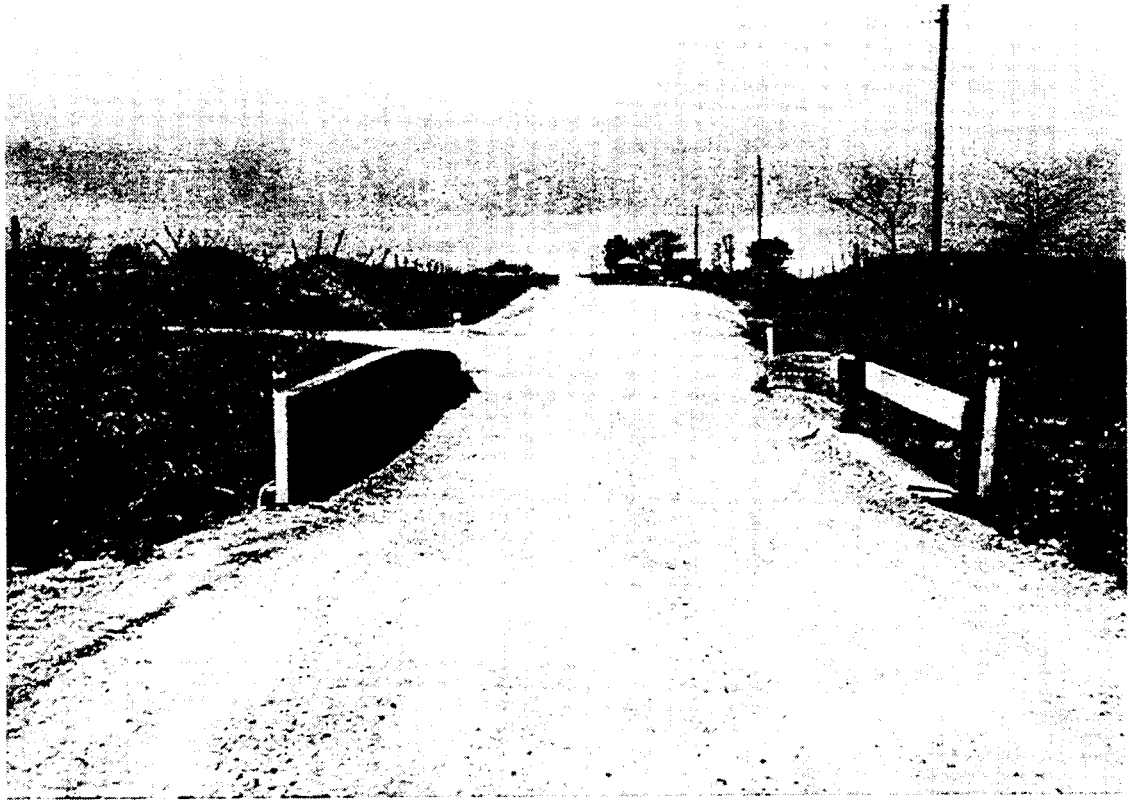

d. Photograph of Bridge IV looking West.

Figure 5.1. Continued.

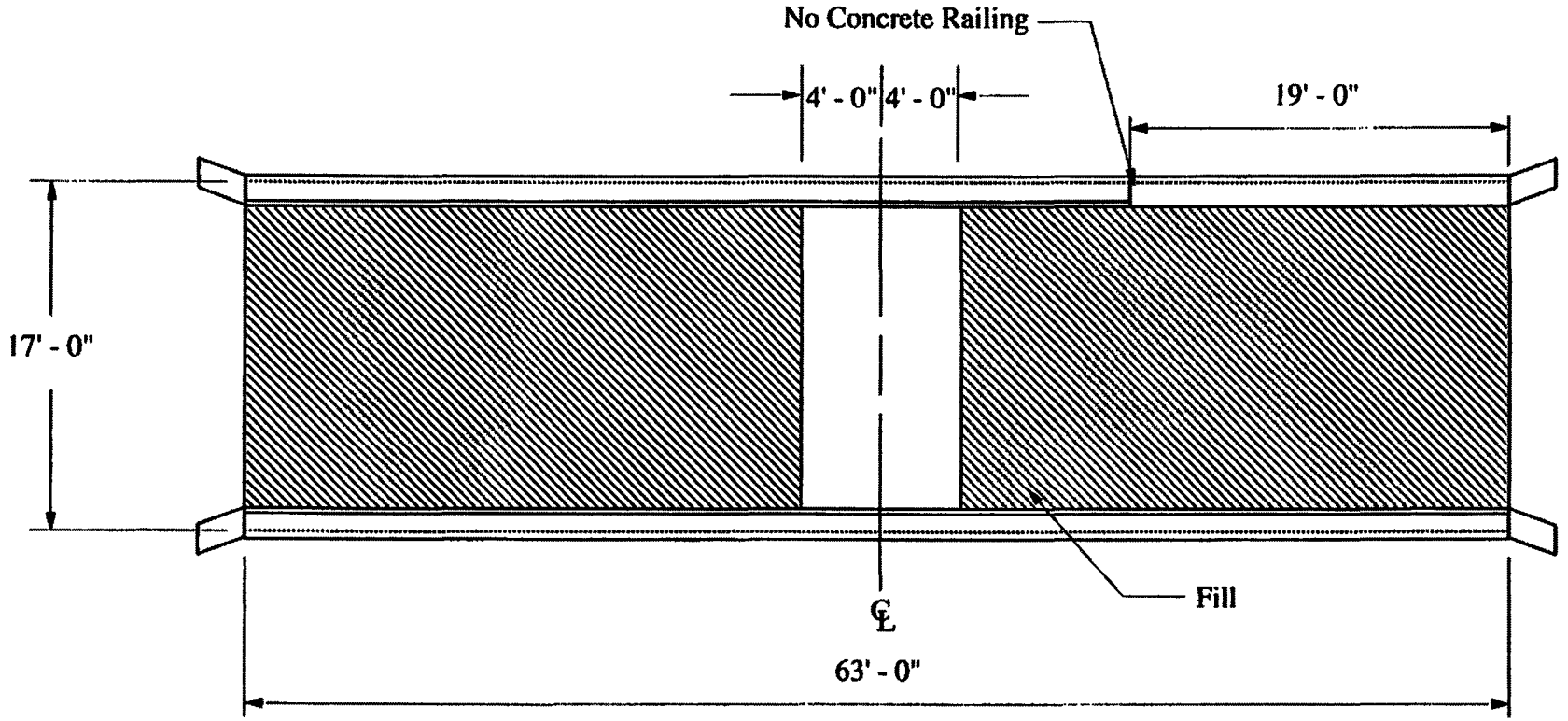

e. Plan View

Figure 5.1. Continued.

Bridge IV. Also, the thickness of the arch at the abutments was 1,040 mm (41 in.). Using these dimensions, the thickness of the arch ring at the abutments for Bridge IV was proportioned and assumed to be 840 mm (33 in.).

The reinforcement for the Story County Luten Arch consisted of two layers of 22 mm (7/8 in.) diameter bars spaced at 305 mm (12 in.) on center. The top bars were offset 150 mm (6 in.) from the bottom bars. The distance from the center of the bars to the to the top and bottom faces of the arch ring was 50 mm (2 in.). Due to extensive deterioration on the underside of Bridge IV, the reinforcing bars had become exposed in various areas. The exposed bars were undeformed, 19 mm (3/4 in.) in diameter, and spaced at 305 mm (12 in.) on center. Because this reinforcement spacing matched that of the reinforcement spacing of the Story County Luten Arch, the researchers assumed that there was also a layer of the same size bars in the top of the arch ring. These bars were assumed to be at the same spacing as the bottom bars and offset 150 mm (6 in.). Figure 5.2 shows the assumed reinforcement configuration in Bridge IV.

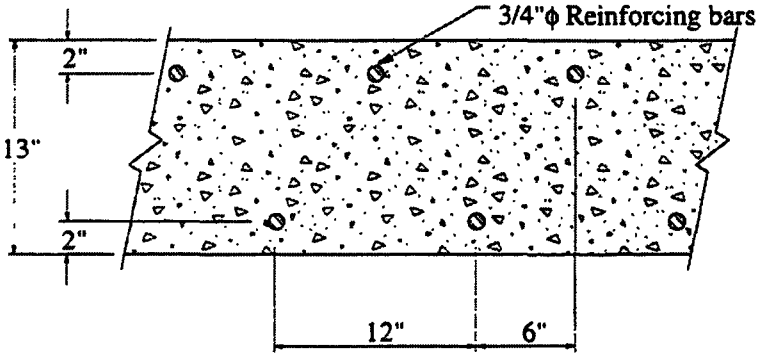

Figure 5.2. Bridge IV: Assumed configuration and reinforcing details at crown of arch.

Two spandrel walls were constructed along each side of the arch ring to retain the roadway material. Because no plans were available, the thickness of the walls were unknown. The fill material for the roadway was approximately 1,880 mm (6 ft - 2 in.) deep at the abutments and tapered with the shape of the arch to zero depth 1,220 mm (4 ft) from

the centerline of the arch. At the point where the fill material stopped, the top of the arch was exposed and became the roadway surface (see Fig. 5.1d).

5.1.1. Condition Assessment

Like in the previous bridges tested, old inspection reports were obtained and a thorough visual inspection was conducted by the researchers prior to the diagnostic load test. From the latest inspection conducted in 1994, the superstructure and the substructure were both given an overall condition rating of 4 which is considered poor on the rating scale used. Even with a low condition rating, the only recommended posting was for a one lane bridge.

The visual inspection of the bridge conducted by the researchers revealed considerable damage and deterioration at various locations. As previously mentioned, the north railing had been damaged to the point were a temporary replacement was needed. A photograph of the replacement railing is presented in Figure 5.3.

Figure 5.3. Bridge IV: Photograph of damaged railing.

Considerable damage and deterioration was also noted at the northwest wing wall. Due to extensive undermining from the stream, the wing wall had broken loose from the abutment and had begun sliding into the creek. A photograph of the damaged wing wall is

Figure 5.4. Bridge IV. Photograph of northwest wing wall.

presented Figure 5.4.

On the underside of the bridge, severe spalling was observed along the north edge and across the entire width of the arch at the crown. The spalling was so severe in certain locations that the reinforcing steel had become exposed. The exposed reinforcing steel was heavily corroded and had considerable loss of section. A typical photograph of the exposed reinforcing steel is presented in Figure 5.5.

Finally, the bottom of the stream was probed to determine if the reinforced concrete slab which tied the abutments together still remained. After digging at various locations, the slab could not be located. It was assumed that the slab was either not constructed or had been washed away.

5.2. AASHTO Rating

After conducting the visual inspection of the bridge and determining actual dimensions, an analytical model was constructed and analyzed using structural analysis

Figure 5.5. Bridge IV: Photograph of exposed reinforcing steel on underside of arch.

software. From the analytical model, the theoretical load rating factors for the vehicles described in Sec. 1.4 were calculated. The method and procedures used to obtain the rating factors were described in Sec. 1.7. Using the HS20-44 rating vehicle, a rating factor of 7.18 was calculated. Using the Type 3 rating vehicle , a rating factor of 8.39 was calculated. The large rating factors can be attributed to the wide distribution of the wheel loads through the deck as per AASHTO guidelines. The distribution of the load through the soil fill results in an area load over the arch. The effects obtained from an area load are considerably less than those of a point load under the same loading. In determining the magnitude of the distributed load onto the arch, the guidelines outlined in the Standard Specification for Highway Bridges [12] were followed. The calculations used to obtain the load rating factors are presented in Appendix B. Table 5.1 shows the results of the theoretical load rating for the two rating vehicles.

Table 5.1. Bridge IV: Theoretical load rating summary.

	Vehicle HS20 AASHTO LRFR		Vehicle Type 3 AASHTO LRFR	
	Rating Factor	Rating (tons)	Rating Factor	Rating (tons)
Arch	7.18	258.5	8.39	209.8

5.3. Test Setup and Procedures

To obtain material and general structural behavior, strains and deflections were monitored at various locations. The locations of the strain gages and deflection transducers are presented in Figure 5.6. Strain gages were bonded on the bottom of the arch at the centerline and at the east quarter point. The four centerline strain gages were placed uniformly across the arch beginning at 305 mm (1 ft) from the south edge. A strain gage was not placed at 305 mm (1 ft) from the north edge because of the severe spalling at this location.

Three strain gages were also located at the east quarter point of the arch. The strain gages were placed transversely at the quarter points and the centerline. The types of strain gages used and the application process were discussed in Sec. 1.6.1.

The bridge deflections were also monitored at the centerline and at the east quarter point of the arch. As shown in Fig. 5.6a, three deflection transducers were mounted transversely across the bottom of the arch at the crown and at the east quarter point. The deflections were obtained using the equipment and setup described in Sec. 1.6.1.

The type of vehicle and loading process used in the testing of the bridge were described in Sec. 1.6.2. For this bridge, the loading was applied in four increments: 117,000 N (26,300 lbs), 167,300 N (37,600 lbs), 221,100 N (49,700 lbs), and 271,300 N (61,000 lbs), respectively. The wheel configuration and load distribution in the test vehicle are presented in Figure 5.7, while a photograph of the test vehicle is shown in Figure 5.8.

The deflection and strain behavior of the bridge were observed by stopping the test vehicle at various longitudinal and transverse locations. Longitudinally, the test vehicle was stopped at the east quarter point, center, and west quarter point. At each location, the test vehicle was positioned such that the front axle of the rear tandem was centered on the

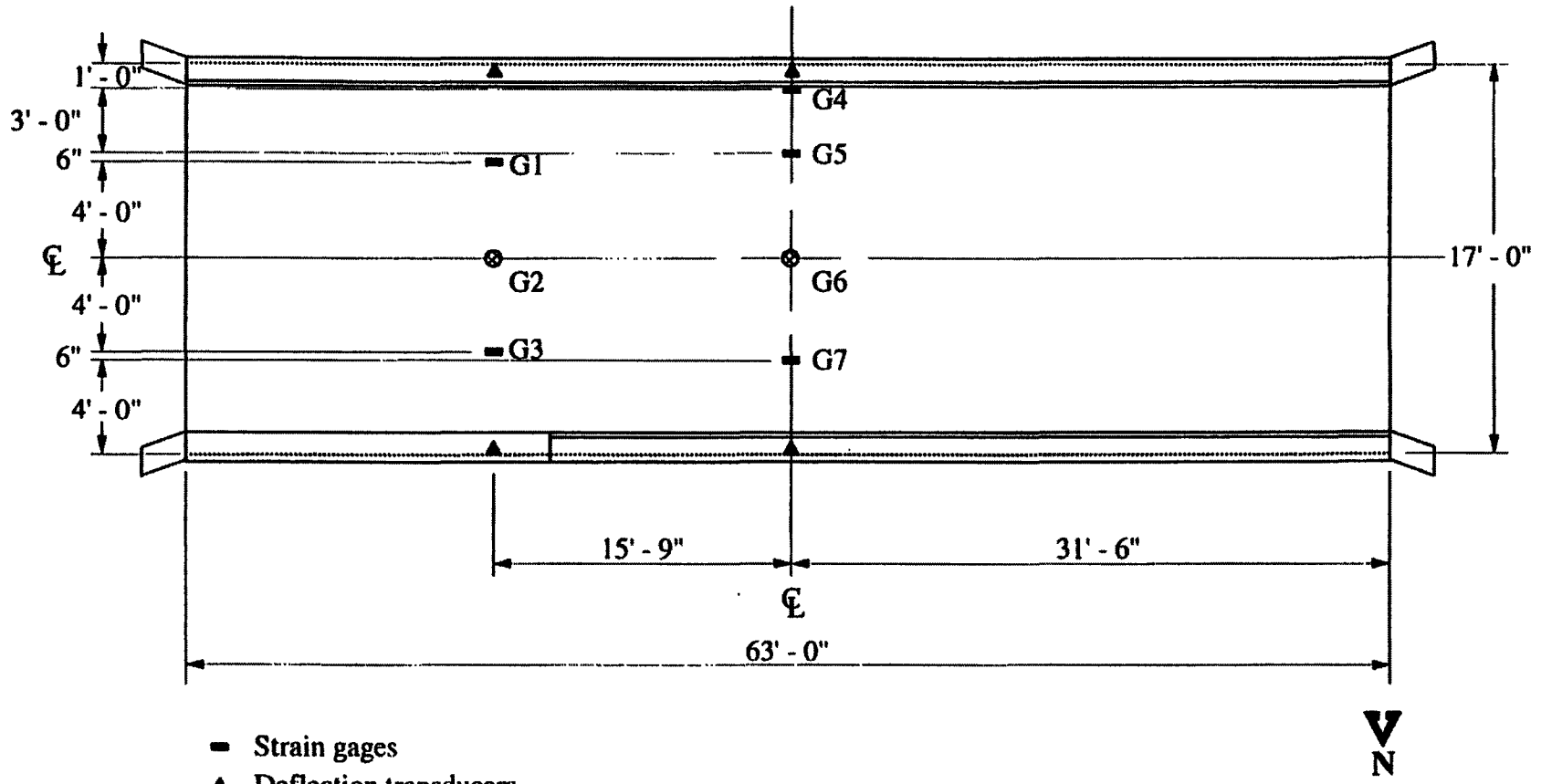

a. Plan view

Figure 5.6. Bridge IV: Location of strain gages and deflection transducers.

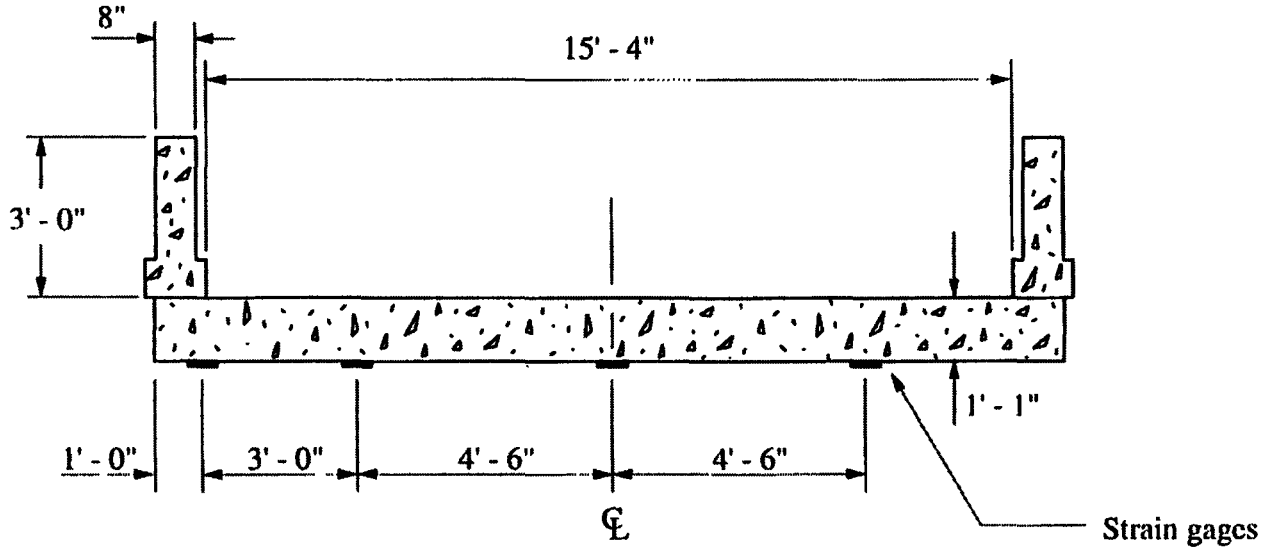

b. Centerline

Figure 5.6. Continued.

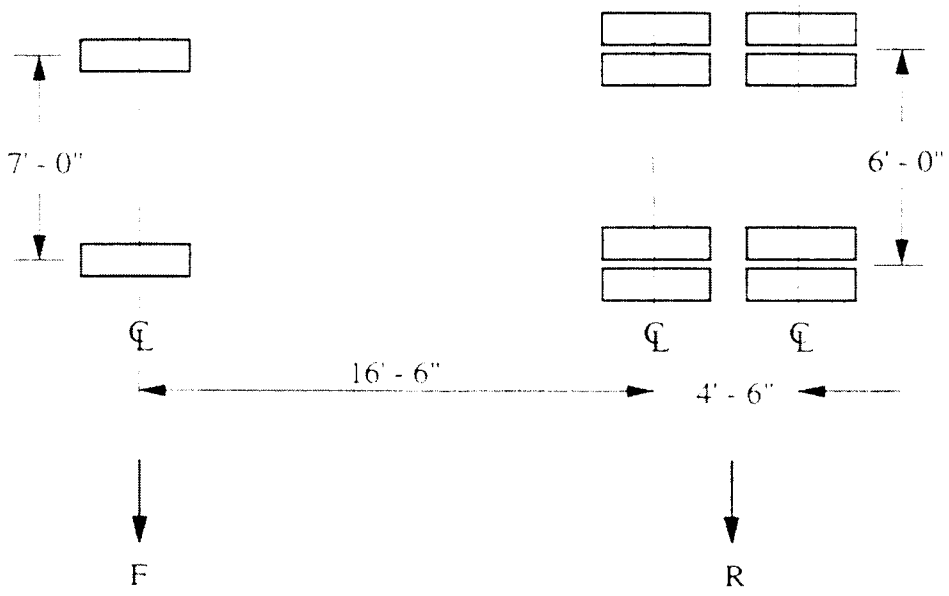

Load Increment	F (kips)	R (kips)	Total Load (kips)
1	12.2	14.1	26.3
2	14.2	23.4	37.6
3	16.7	33.0	49.7
4	18.7	42.3	61.0

Figure 5.7. Bridge IV. Wheel configuration and weight distribution in test vehicle.

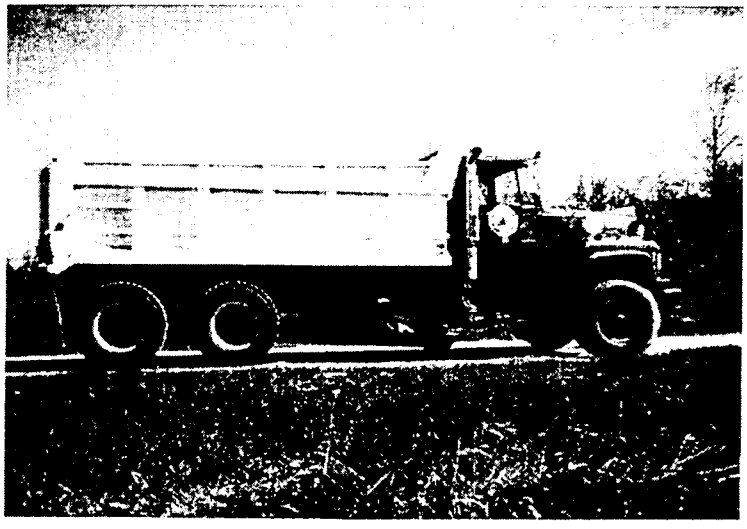

Figure 5.8. Bridge IV: Photograph of test vehicle.

stopping location. Once the vehicle had been positioned, strain and deflection readings were taken. The stopping locations for the various tests are shown in Figure 5.9. It should be noted that at the west 1/4 pt. the front axle of the test vehicle was off the bridge and the responses measured were a result of the rear tandem alone. The transverse lane positioning of the test vehicle was described in Sec 1.6.2 and is shown in Figure 5.10.

5.4. Results and Discussion

Both strains and deflections remained linear for the various loadings and were well below the elastic limit of the material (see Fig 5.12). This response was similar to the responses obtained from the previous bridges tested.

The maximum strains in the bridge occurred at the crown and varied across the width of the arch depending on the location of the test vehicle. At load position 1.2, the maximum strains were recorded at G4 for the four load increments. The strains ranged from a maximum of 58 microstrain at load increment four to 16 microstrain at load increment one. The strain then decreased to a minimum at G6 (center) and then increased at G7. The strain at G6 and G7 ranged from 25 microstrain and 31 microstrain respectively at load increment four to 7 microstrain and 12 microstrain respectively at load increment one.

The same strain behavior was also observed at load position 2.2. The highest strains were measured at the edges of the arch and the lowest were measured at the center. The maximum strains were measured at G4 and G7 while the smallest strains were measured at G6. The strains at G4 and G7 ranged from a maximum of 36 microstrain and 39 microstrain, respectively at load increment four to 11 microstrain and 14 microstrain at load increment one. At G6, the strains ranged from a maximum of 22 microstrain at load increment four to 7 microstrain at load increment one.

At load position 3.2, the strains were maximum along the loaded edge and then decreased to a minimum along the unloaded edge. At G7, the maximum strain ranged from 45 microstrain at load increment four to 16 microstrain and load increment one. The smallest strains were measured at G4 and ranged from 23 microstrain at load increment four to 7 microstrain at load increment one. The variation of the longitudinal strains across the crown

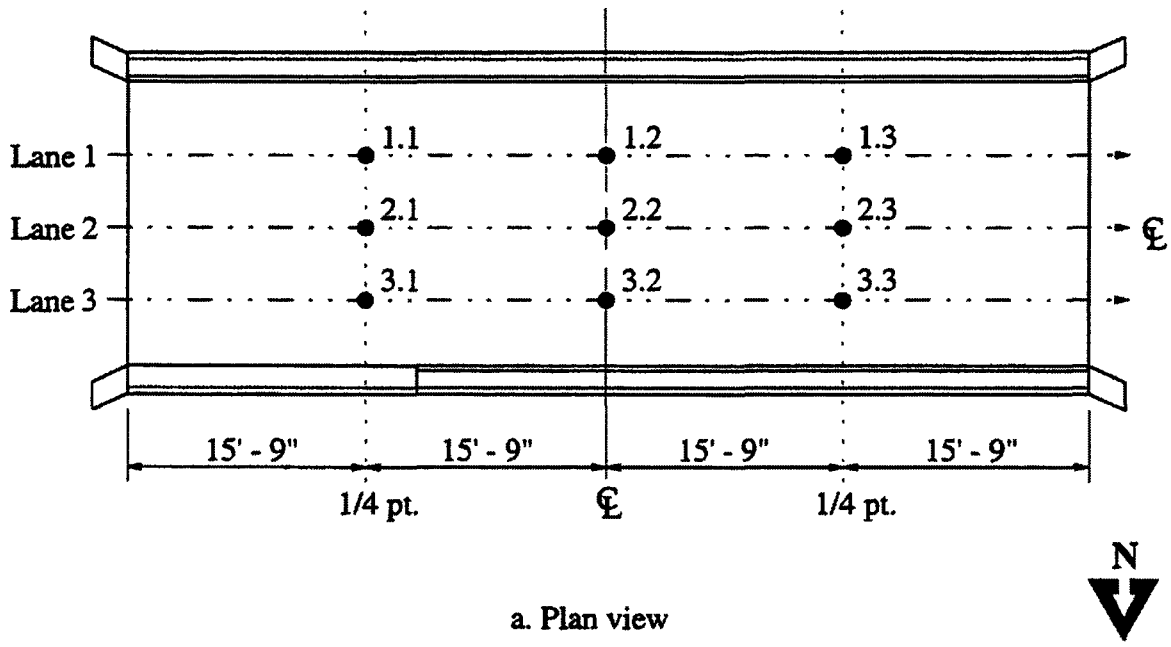

a. Plan view

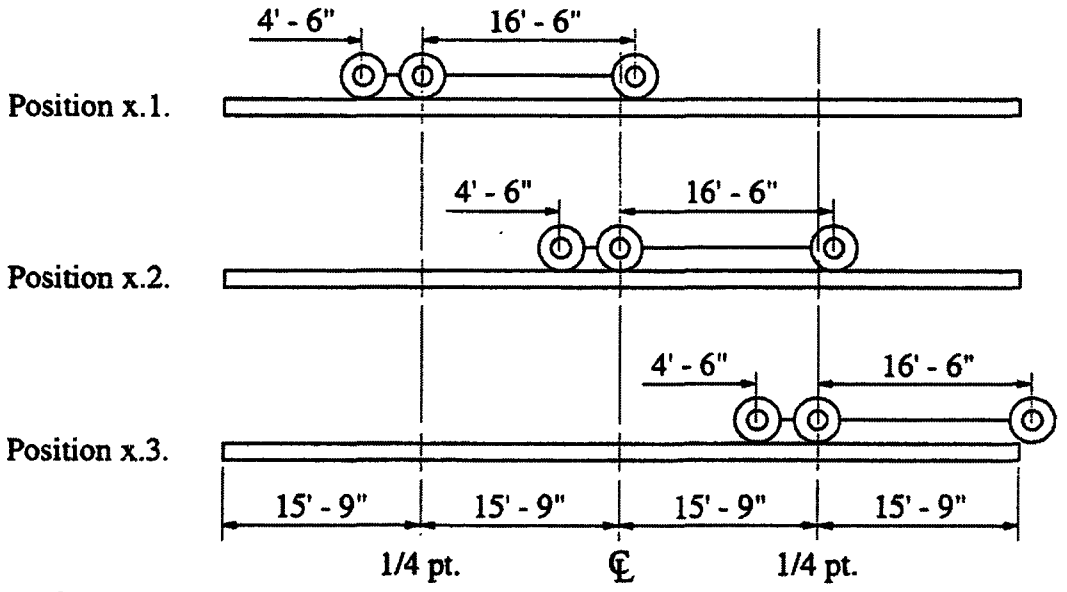

b. Truck stopping position on deck.

Figure 5.9. Bridge IV: Longitudinal location of test vehicle for various tests.

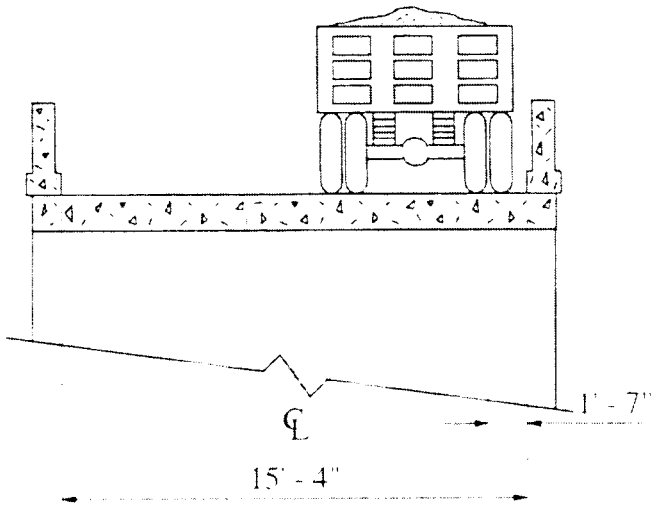

c. Lane 3

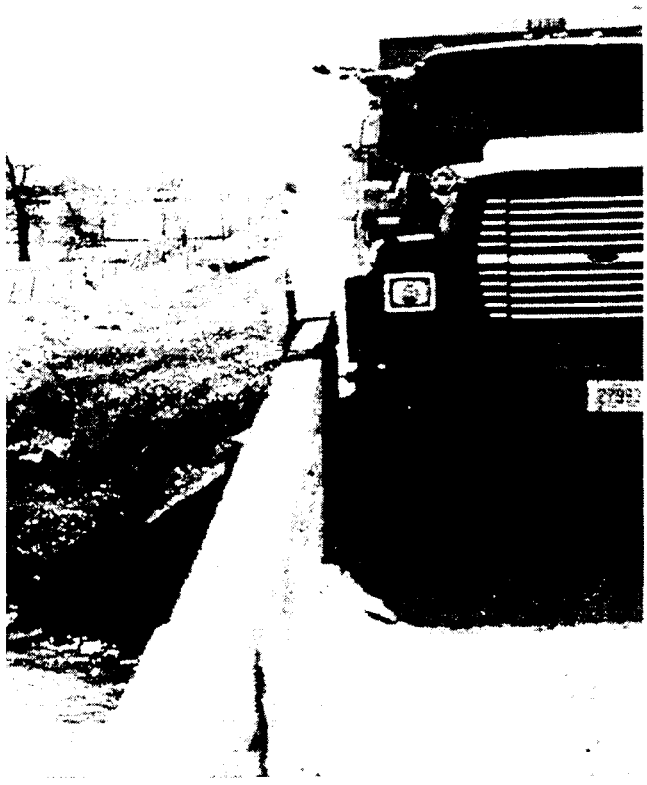

d. Photograph of test vehicle in Lane 3

Figure 5.10. Continued.

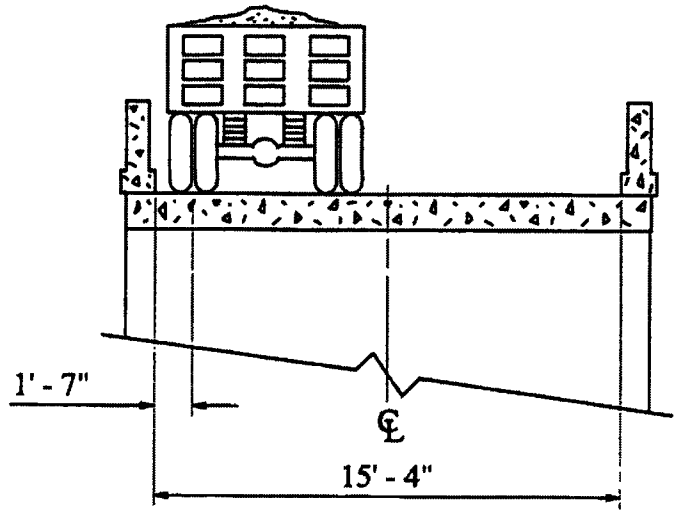

a. Lane 1

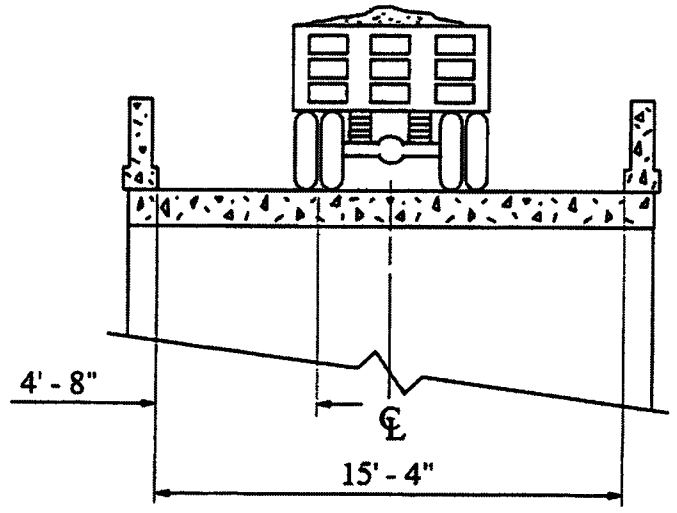

b. Lane 2

Figure 5.10. Bridge IV: Transverse location of test vehicle on bridge.

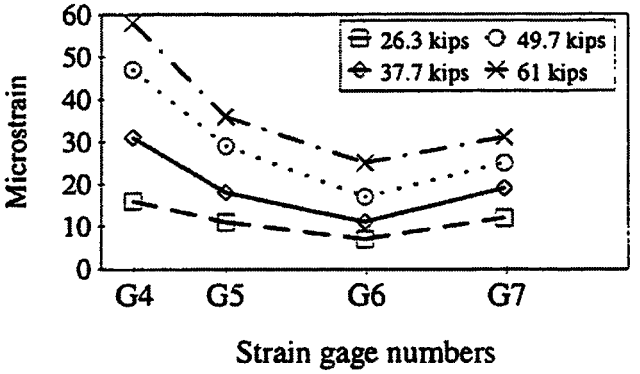

a. Load position 1.2

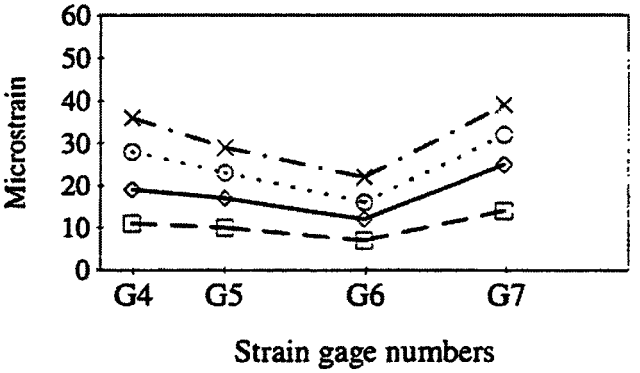

b. Load position 2.2

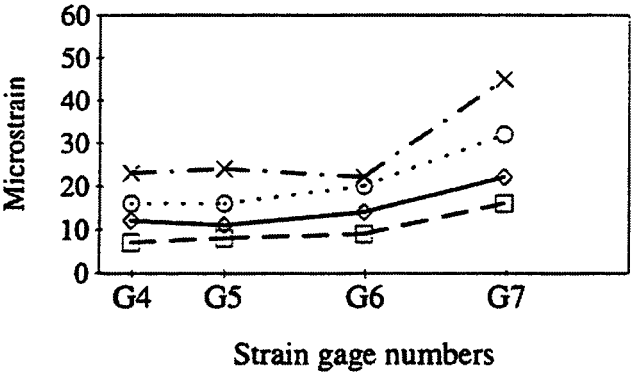

c. Load position 3.2

Figure 5.11. Bridge IV: Longitudinal strains at bridge centerline.

of the arch for the various load increments and positions is presented in Figure 5.11.

The strains measured at the east quarter point remained in the single digits for all load positions and load increments. For the various loadings and positions, compressive behavior was observed across the entire width of the arch. The strain values ranged from 0 microstrain at load increment one to 9 microstrain at load increment four. As in the strains at the crown of the arch, the strains at the quarter point were maximum near the edges (G1 and G3) and minimum at the center (G2).

Even though the response of the bridge was unexpected, the strains still remained linear for all loading positions and increments. Figure 5.12 shows the average strain values at the crown of the arch versus the four load increments. The maximum average strain of 38 microstrain occurred at load increment four and load position 1.2. This average strain value is approximately 1/4 the strain (approx. 130 microstrain) at which tensile cracks develop in concrete.

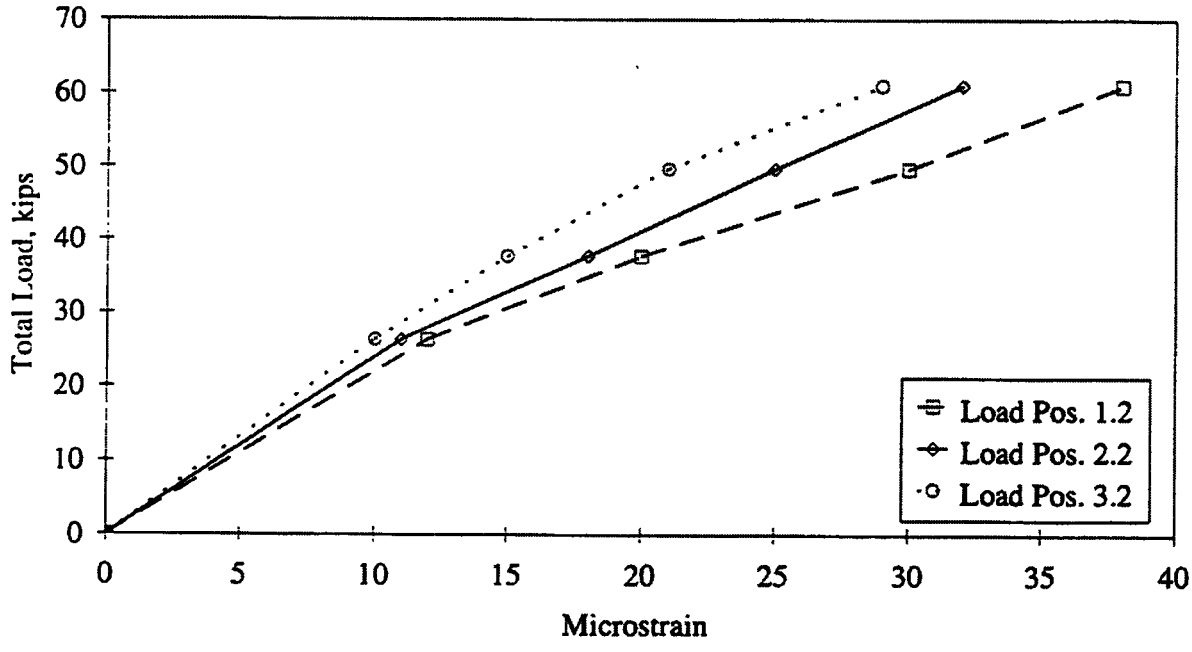

Figure 5.12. Bridge IV: Average strains at bridge centerline.

The deflection behavior of the bridge at the crown was similar to the behavior exhibited by the measured strains for the various loading positions and increments. At load positions 1.2 and 2.2, the edges of the arch had a higher deflection than the center. At load position 1.2, the maximum deflection occurred at the south edge and ranged from 0.53 mm (0.021 in.) at load increment one to 1.91 mm (0.075 in.) at load increment four. As in the strain readings, the deflection of the arch decreased at the center and then increased at the north edge. The deflections at the center and north edge of the arch ranged from 0 and 0.41 mm (0.016 in.), respectively, at load increment one to 0.81 mm (0.032 in.) and 1.07 mm (0.042 mm), respectively at load increment four.

The same response was observed at load position 2.2. The higher deflections occurred along the north and south edges while the deflections at the center were less. The deflections at the north edge, center, and south edge ranged from 0.56 mm (0.022 in.), 0, and 0.33 mm (0.013 in.), respectively, at load increment one to 1.70 mm (0.067 in.), 0.91 mm (0.036 in.), and 1.09 mm (0.043 in.), respectively, at load increment four.

At load position 3.2, the bridge exhibited a more normal response. The deflections were greatest along the north edge and then decreased to a minimum at the south edge for all load increments. The deflection at the north edge, center, and south edge ranged from 0.99 mm (0.039 in.) 0, and 0.10 mm (0.004 in.), respectively, at load increment one to 2.59 mm (0.102 in.), 1.09 mm (0.043 in.), and 0.66 mm (0.027 in.), respectively, at load increment four. The transverse deflection of the bridge for the various loading positions and increments is presented in Figure 5.13.

The deflection response of the bridge at the east quarter point remained consistent for the various loading positions and increments - maximum at the center and smaller at the edges.

The average deflection values at the crown and east quarter point versus the four load increments are shown graphically in Figure 5.14. As with the stain values, the deflection values remained linear at the crown and east quarter point for the various loading positions and increments.

The unexpected behavior of the bridge at load positions 1.2 and 2.2 may be

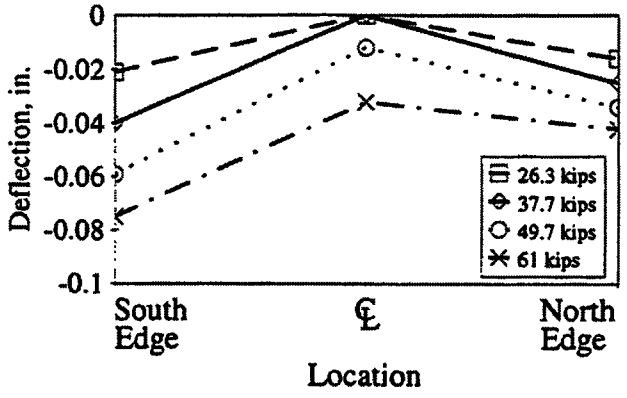

a. Load position 1.2

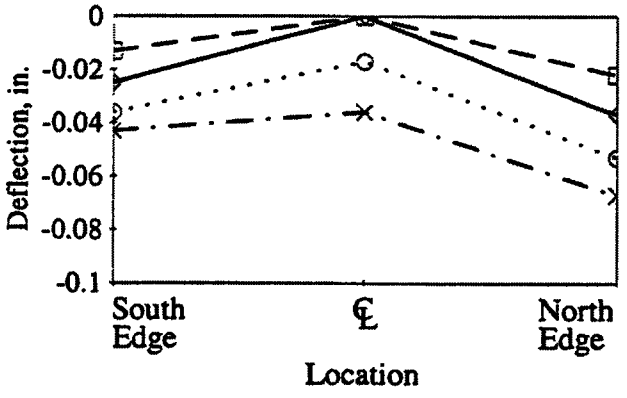

b. Load position 2.2

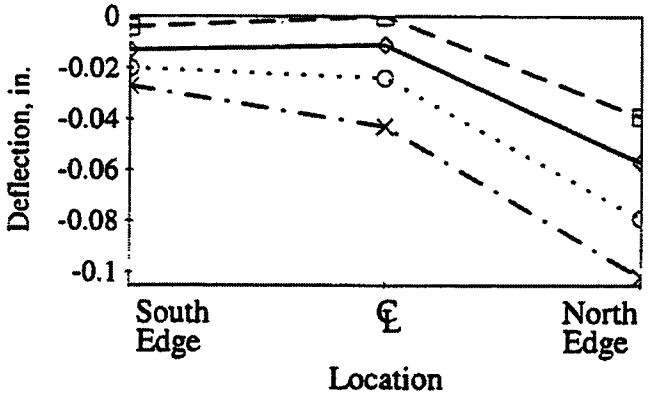

c. Load position 3.2

Figure 5.13. Bridge IV: Transverse deflection at bridge centerline.

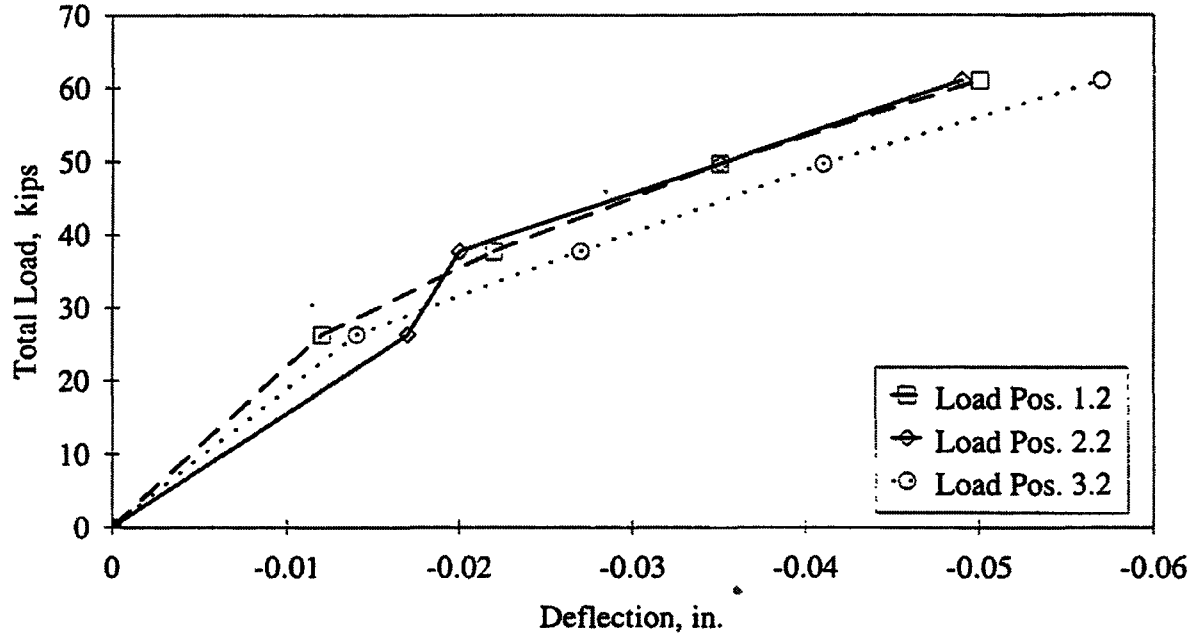

a. Centerline

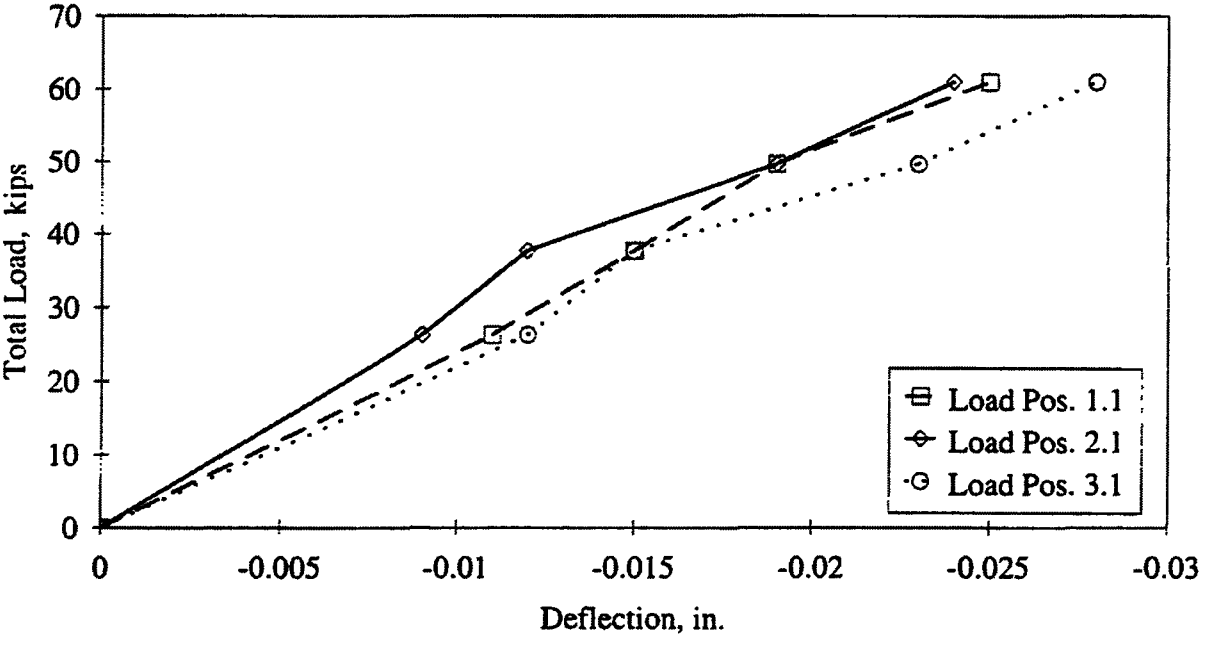

b. Quarter point

Figure 5.14. Bridge IV: Longitudinal deflections.

attributed to transverse arching of the bridge at the crown due to lateral pressure on the spandrel walls. Based on that assumption, loading from the test vehicle would increases the overburden pressure on the fill material which would also increase the horizontal pressure on the spandrel walls. The increased pressure would cause the walls to rotate and the bridge to arch. Due to the arching action, a higher percentage of the load would be distributed to the edges which translates into smaller strain values at the center and higher values near the edges.

5.5. Modified Rating

As in the previous bridges, the strain values obtained from the diagnostic load test were used to modify the theoretical rating; the procedure used was described in Sec. 1.7. In modifying the rating, the largest average strain value obtained from the three loading positions was used. As stated previously, this strain was determined to be 38 microstrain and occurred when the test vehicle was located at load position 1.2. For the same load position and load increment, the theoretical strain was calculated to be 55 microstrain.

Using these results in conjunction with the rating procedure, the theoretical rating was increased. For the HS20 rating vehicle the rating of the bridge increases from 2,295,000 N (258 tons) to 2,847,000 N (320 tons); for the Type 3 rating vehicle, the rating of the bridge increased from 1,860,000 N (209 tons) to 2,304,000 N (259 tons). A summary of the theoretical and modified rating is presented in Table 5.2. The rating calculations for the slab are presented in Appendix B.

Even though this bridge did not require posting prior to the testing, the results show that there is a reserve capacity not predicted by the analytical procedure.

Table 5.2. Bridge IV: Rating summary:

	Vehicle HS20				Vehicle Type 3			
	AASHTO LRFR		Modified Rating		AASHTO LRFR		Modified Rating	
	RF_c	R (tons)	RF_T	R (tons)	RF_c	R (tons)	RF_T	R (tons)
Arch	7.18	258.5	8.89	320.0	8.39	209.8	10.38	259.5

6. BRIDGE V: REINFORCED CONCRETE STRINGER

6.1. Bridge Description

The fifth bridge to be service load tested was a two span noncontinuous reinforced concrete girder bridge. This particular bridge was located on a secondary county road (kk ave.) in Hardin County over a branch of the Iowa River. The ADT for the bridge was 70 vehicles and consisted of local traffic. Built in 1918, Bridge V was one of a series of standard H-1 type concrete deck girder bridges constructed by the Iowa Highway Commission in the early part of the 20th century. Standard H-1 type girder bridges consisted of one to three simple spans ranging in lengths from 7,300 mm (24 ft) to 12,200 mm (40 ft). Because Bridge V was such a common bridge type, plans were easily obtained which showed the size and location of the reinforcement. Also, to ensure that the actual dimensions of the bridge matched those stated on the plans, all component dimensions were verified by field measurement. The layout of Bridge V is presented in Figure 6.1.

Bridge V consisted of two noncontinuous spans each measuring 11,430 mm (37 ft - 6 in.) from the face of the abutment to the centerline of the pier with a roadway width of 5,500 mm (18 ft). The bridge deck was 6,000 mm (15 ft - 8 in.) wide, 180 mm (7 in.) thick, and was cast monolithic with the girders. Reinforcing in the deck consisted of two layers of 13 mm (1/2 in.) square reinforcing bars spaced on 205 mm (8 in.) centers in the transverse direction and 13 mm (1/2 in.) square reinforcing bars spaced uniformly in the longitudinal direction. To ensure that the bridge remained noncontinuous, an expansion joint was provided at the joint between the two spans. The layout of the transverse reinforcement in the deck is presented in Figure 6.2.

Each span consisted of three rectangular girders spaced at 2210 mm (7 ft - 3 in.) on center. The girders had a depth measured from the bottom of the deck of 990 mm (3 ft - 3 in.) and a width of 380 mm (1 ft - 3 in.). Reinforcement in each girder consisted of two layers of square reinforcing bars. Three 32 mm (1 1/4 in.) bars were located in the bottom layer and three 29 mm (1 1/8 in.) bars were located in the top layer. Shear reinforcement in each of the girders consisted of 15 mm (1/2 in.) stirrups at various spacings throughout the

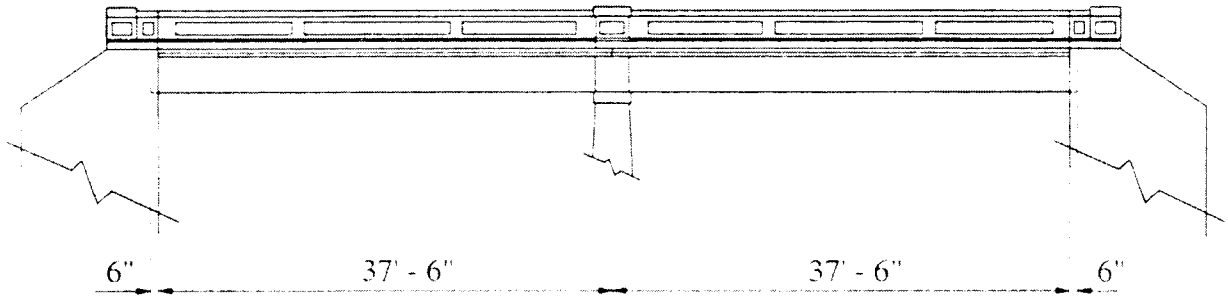

a. Elevation

b. Photograph of bridge profile

Figure 6.1. Bridge V: Layout.

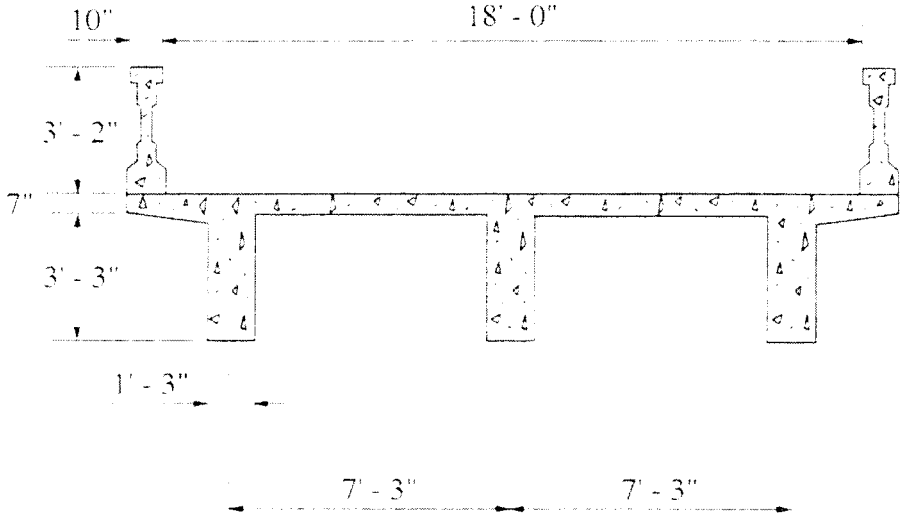

c. Typical cross section

d. Photograph of Bridge V looking South

Figure 6.1. Continued.

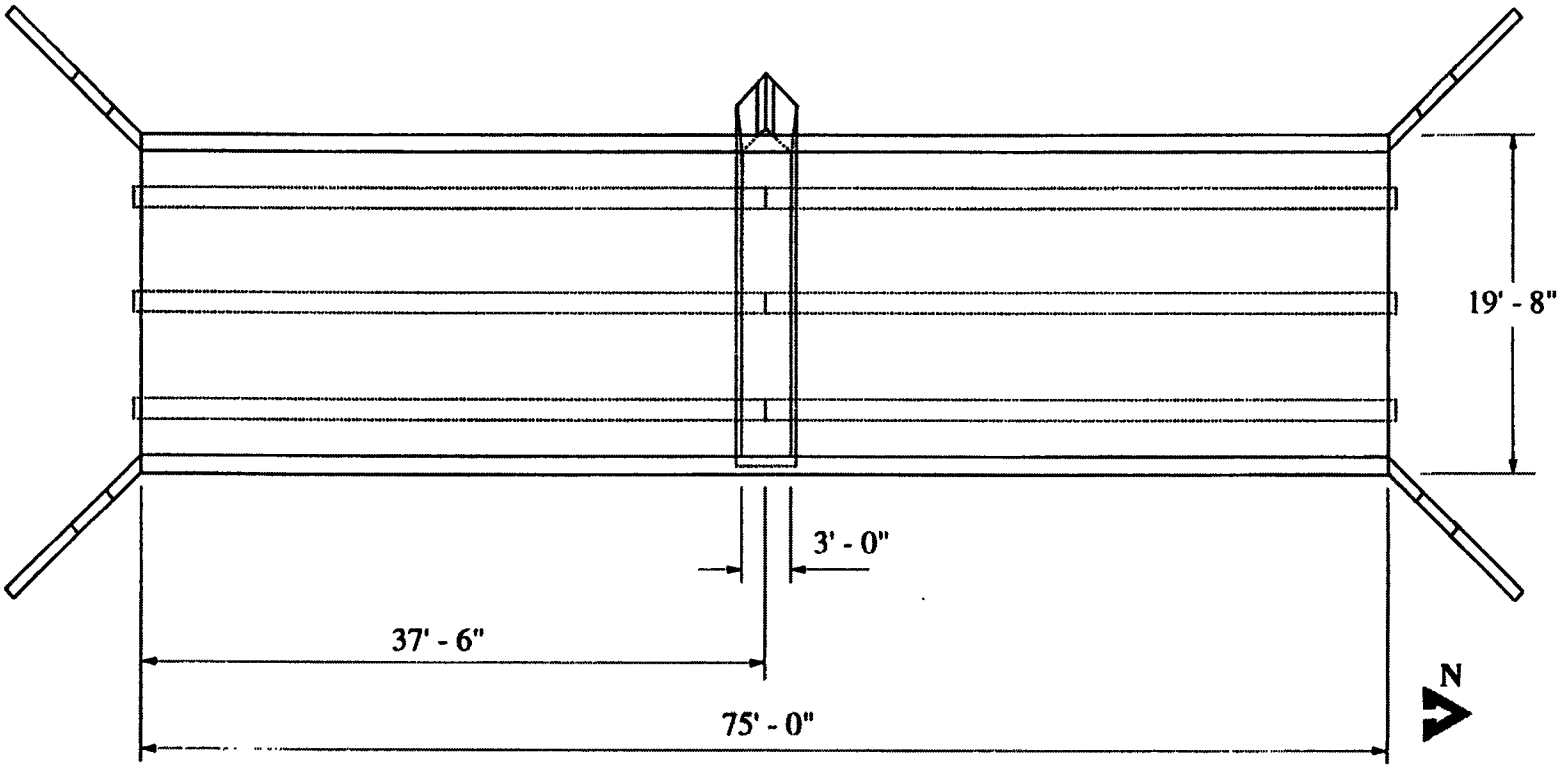

e. Plan View

Figure 6.1. Continued.

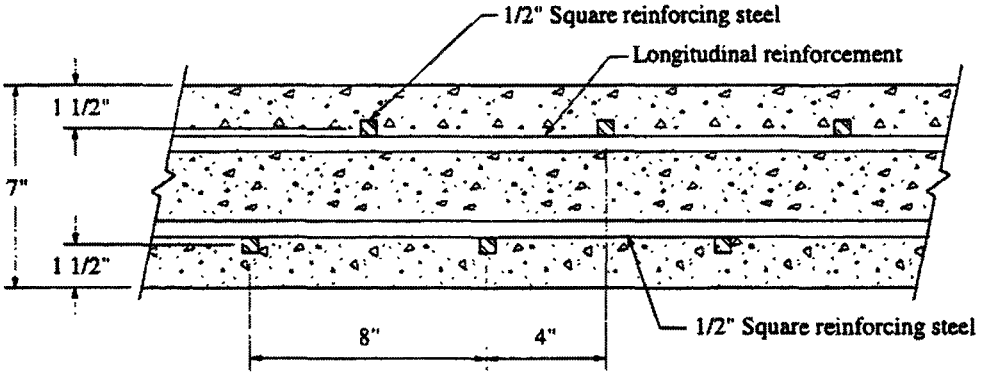

Figure 6.2. Bridge V: Deck reinforcement.

girders. For additional shear reinforcement, the top layer of reinforcing bars were bent up near the ends of each girder. Figure 6.3 shows the layout of the reinforcement in each of the girders.

The end conditions of the girders were such that each girder acted as a simply supported member. At the pier, there were expansion joints between the girders which were placed directly on the concrete with no bearing plate or pad. At the abutments, a 6 mm (1/4 in.) steel bearing plate was embedded in the abutment and in the bottom of the girder.

6.1.1. Condition Assessment

Prior to the diagnostic load test, old inspection reports were obtained and a thorough visual inspection was conducted by the researchers. The latest inspection on this bridge was conducted in 1991 and the deck and substructure were given a condition rating of 6 while the superstructure was given a condition rating of 5. The current postings of 7 tons and one lane bridge were noted in the report to remain in place.

The visual inspection conducted by the researchers revealed the bridge to be in very good condition. The only deterioration found was on the outside face of the exterior girders. At the locations of the deck drains, the concrete had spalled exposing the legs of the stirrups. A photograph of the girder deterioration at the deck drain locations is shown in Figure 6.4.

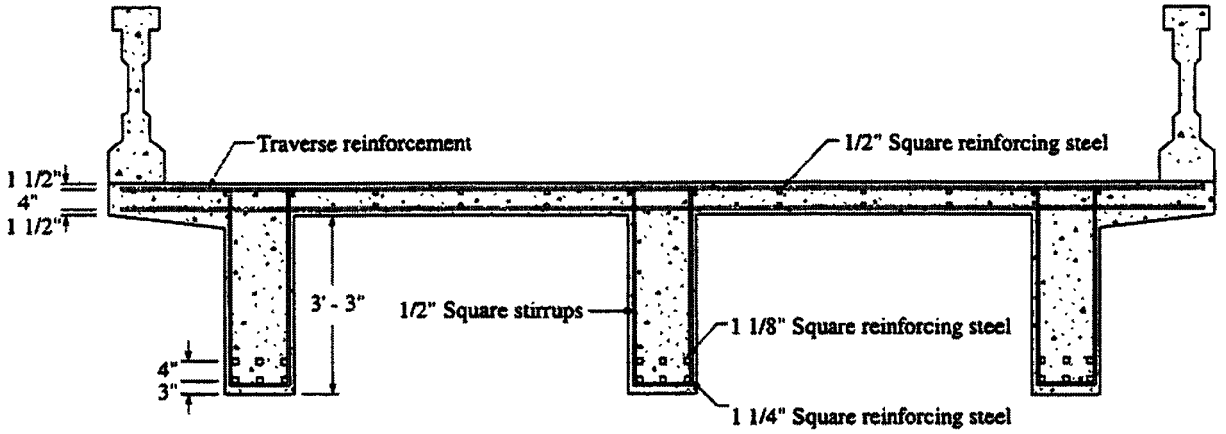

a. Centerline reinforcement

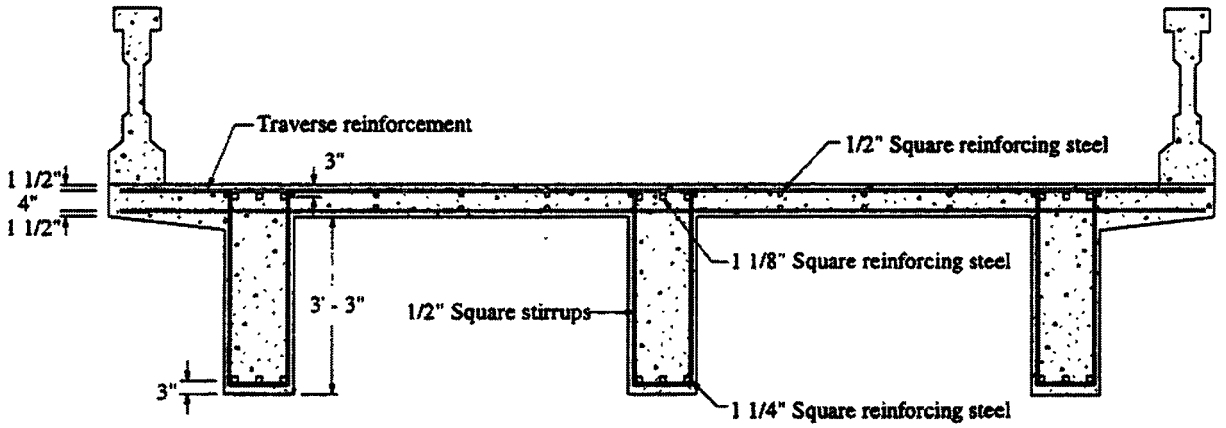

b. End reinforcement

Figure 6.3. Bridge V: Configuration and reinforcing details of girders.

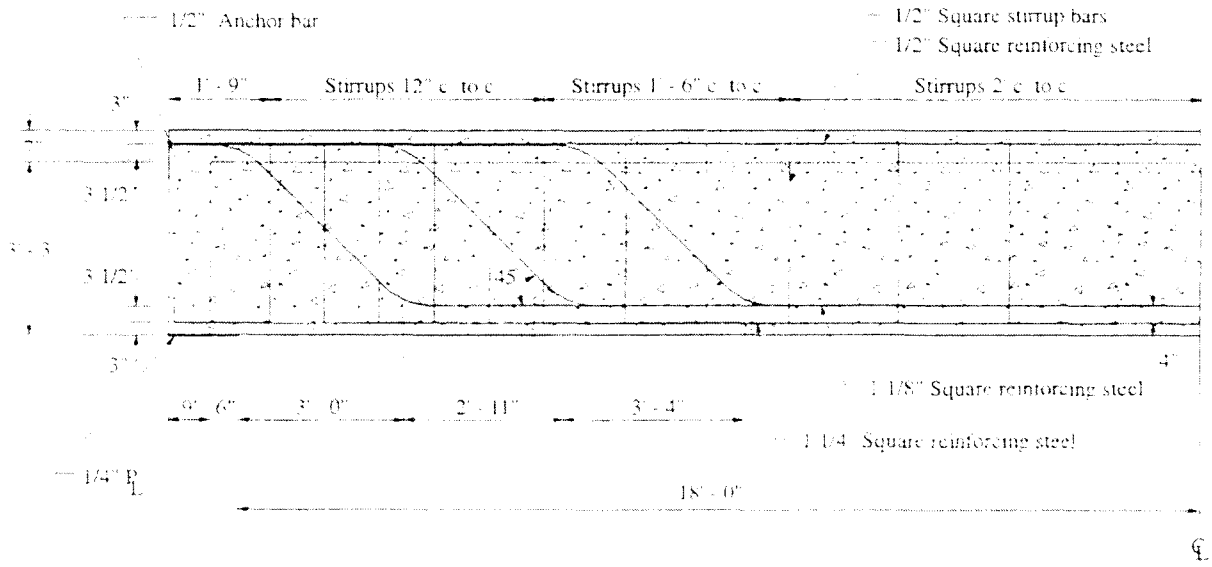

c. Half section detail

Figure 6.3. Continued.

Figure 6.4. Bridge V: Photograph of exterior girder deterioration.

6.2. AASHTO Rating

After conducting the visual inspection of the bridge and verifying the dimensions, an analytical model was constructed and the theoretical rating factors were calculated. The

rating vehicles and procedure used to obtain the theoretical rating factors were described in Secs. 1.4 and 1.7, respectively. Using the HS20-44 and the Type 3 rating vehicles, rating factors of 1.61 and 2.05, respectively, were calculated. The theoretical rating obtained from both vehicles is considerably higher than the posted rating of 7 tons. This discrepancy can not be explained due to the fact that the rating engineer's calculations and assumptions made were not available for review. The calculations used to obtain the load rating factors are presented in Appendix B. Table 6.1 shows the results of the theoretical load rating for the two rating vehicles.

Table 6.1. Bridge V: Theoretical load rating summary.

	Vehicle HS20 AASHTO LRFR		Vehicle Type 3 AASHTO LRFR	
	Rating Factor	Rating (tons)	Rating Factor	Rating (tons)
Girders	1.61	57.9	2.05	51.3

6.3. Test Setup and Procedures

As in the other bridges tested, strains and deflections were monitored at various locations on the two spans. Refer to Figure 6.5 for the strain gage and deflection transducer locations. In addition to the strain gages bonded to the bottom of each girder at the centerline, one strain gage was bonded to the bottom of girders B3 and B6 at a distance of 305 mm (1 ft) from each end. These gages were placed to determine if the support conditions exhibited any rotational restraint under the applied loading. Strain gages were also bonded to the top and bottom of the east railings at the centerline of spans one and two. The types of strain gages used and the application process were discussed in Sec. 1.6.1.

Deflections were monitored at the centerlines of the three girders in spans one and two and at the quarter points of girders B3 and B6. The deflections were obtained using the equipment and setup described in Sec 1.6.1.

The type of vehicle and loading process used in the testing of the bridge were described in Sec. 1.6.2. For this bridge, the loading was applied in three increments:

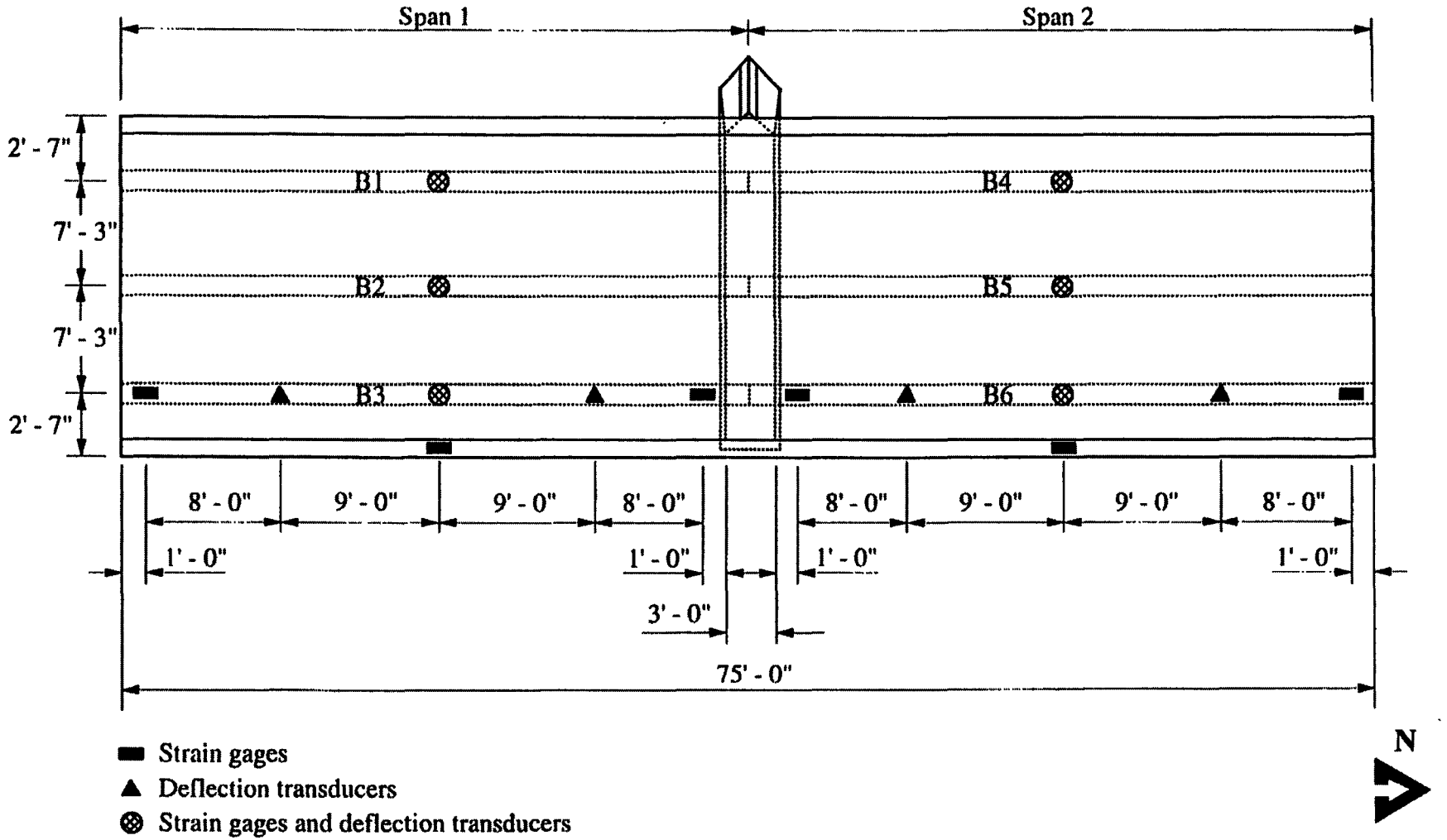

a. Plan view

Figure 6.5. Bridge V: Location of strain gages and deflection transducers.

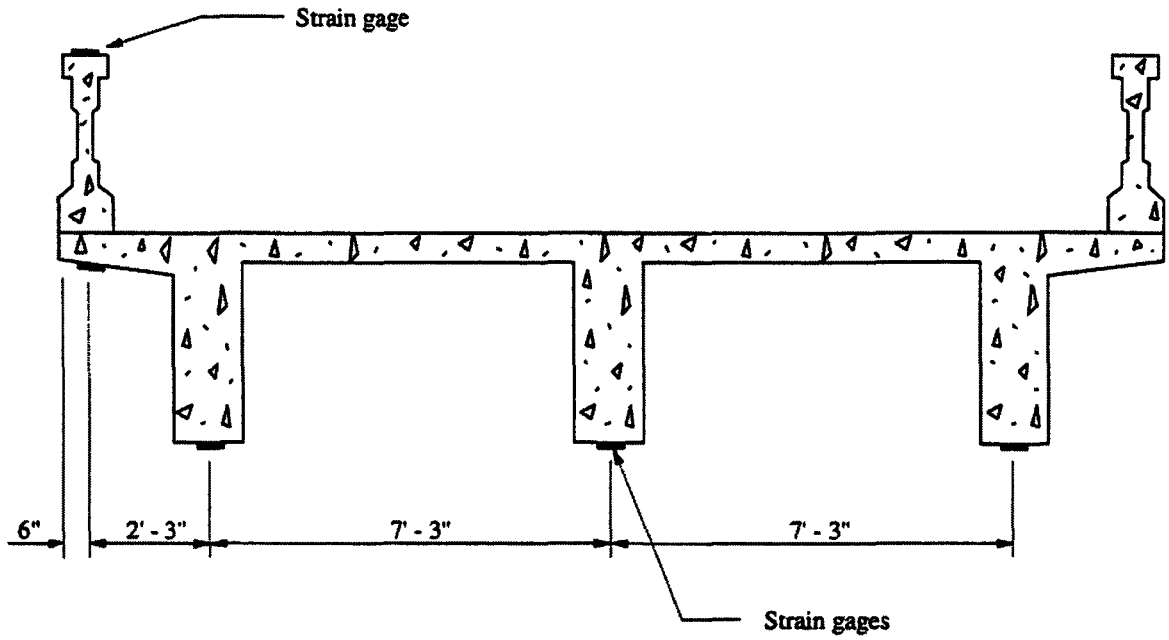

Figure 6.5. Continued.

116,500 N (26,200 lbs),178,800 N (40,200 lbs), and 275,800 N 62,000 lbs), respectively. The magnitude of the load increments and the wheel configuration of the test vehicle are presented in Figure 6.6; a photograph of the test vehicle is shown in Figure 6.7.

The strain and deflection behavior of the bridge were observed by stopping the test vehicle at various longitudinal and transverse locations. The position of the test vehicle in the various tests is shown in Figure 6.8. Longitudinally, the test vehicle was stopped at the south quarter point, center, and north quarter point in each span. At each location the test vehicle was positioned such that the front axle of the rear tandem was centered on the stopping location. It should be noted that at locations 1.6, 2.6, and 3.6, the front axle was off the bridge and the measured responses were from the rear tandem alone. Once the vehicle had been positioned, strain and deflection readings were taken. The transverse lane positioning of the test vehicle was described in Sec. 1.6.2. and is shown in Figure 6.9.

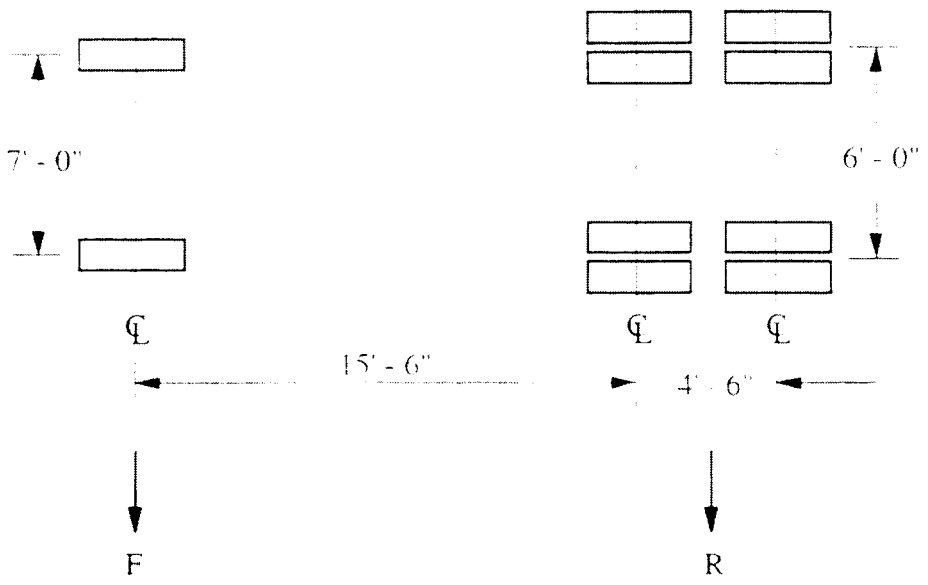

Load Increment	F (kips)	R (kips)	Total Load (kips)
1	13.0	13.2	26.2
2	15.1	25.1	40.2
3	18.3	43.7	62.0

Figure 6.6. Bridge V: Wheel configuration and weight distribution in test vehicle.

Figure 6.7. Bridge V: Photograph of test vehicle.

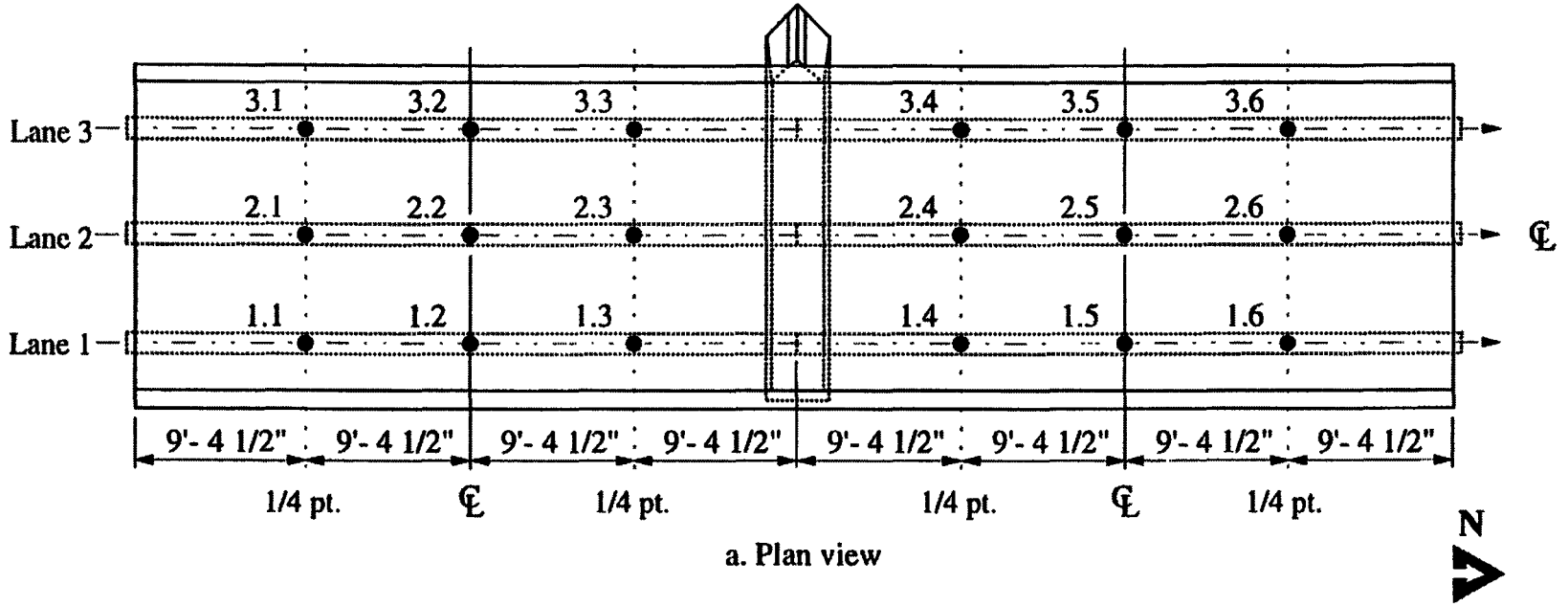

a. Plan view

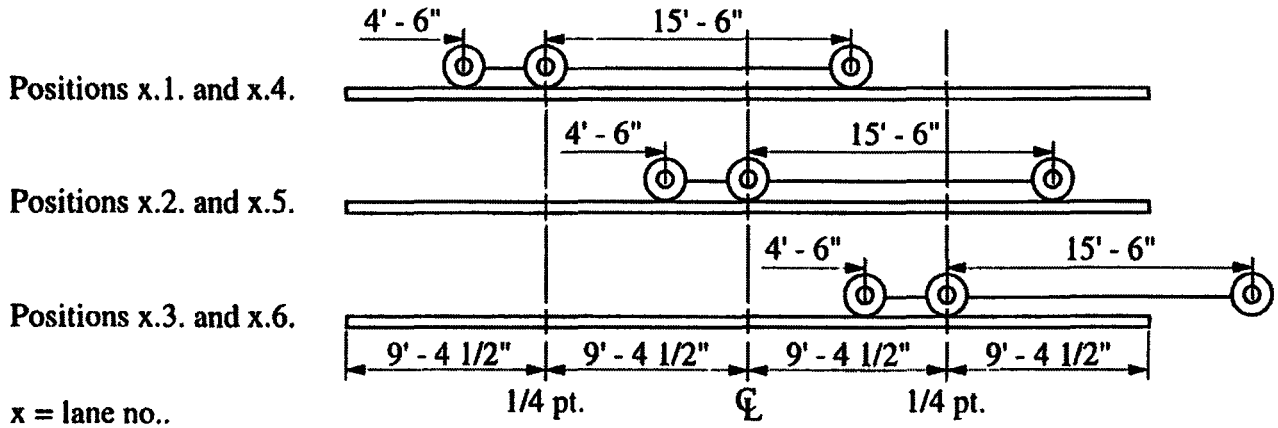

b. Truck stopping position on each span of bridge

Figure 6.8. Bridge V: Longitudinal location of test vehicle for various tests.

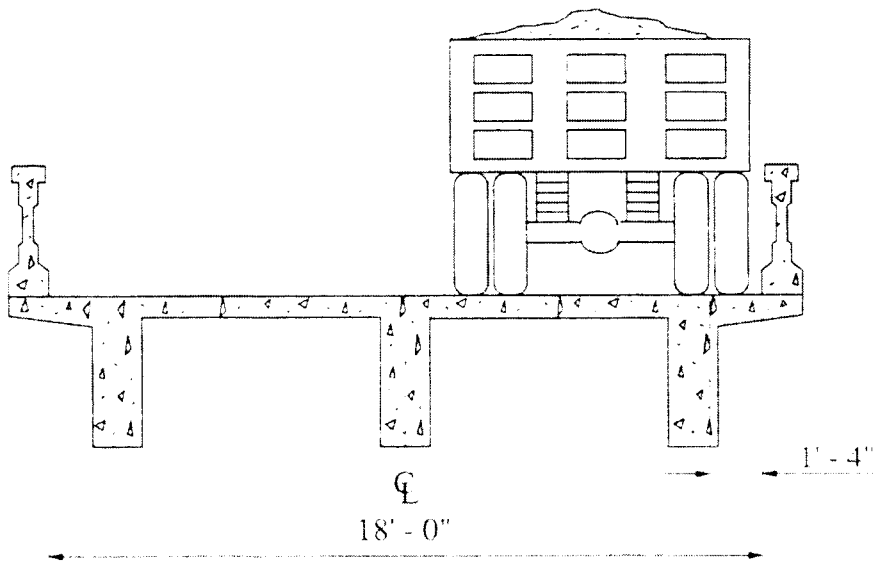

a. Lane 1

b. Photograph of test vehicle in Lane 1

Figure 6.9. Bridge V: Transverse location of test vehicle on bridge.

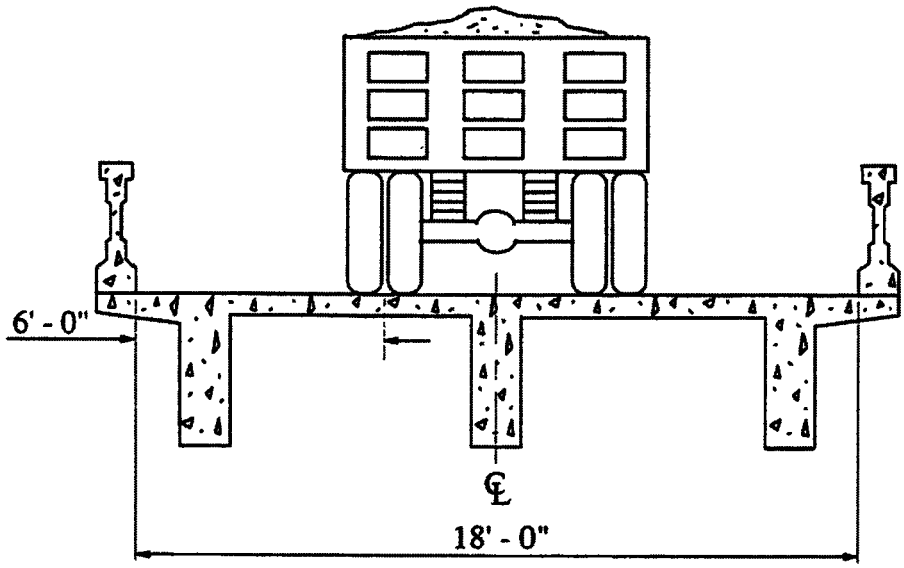

c. Lane 2

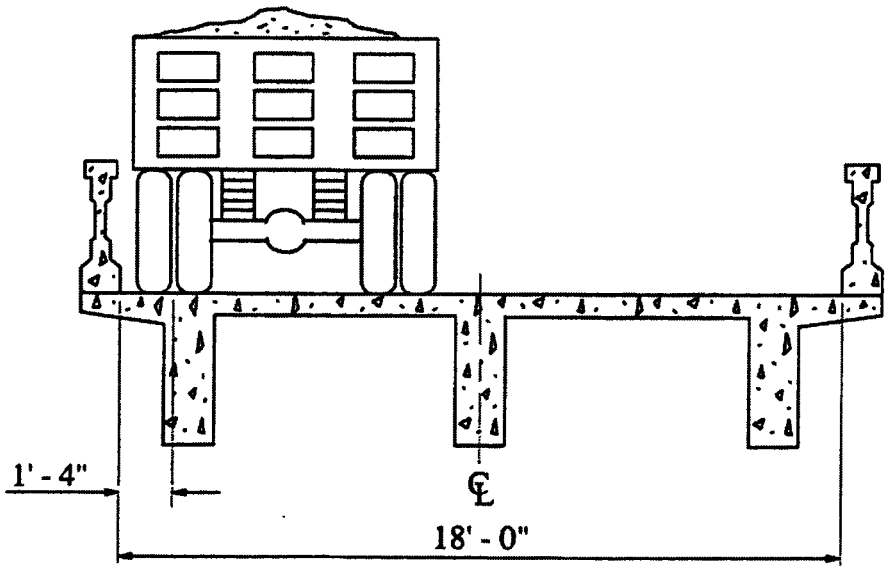

d. Lane 3

Figure 6.9. Continued.

6.4. Results and Discussion

As in the previous bridges tested, the response of the bridge remained linear for both strains and deflections. However, due to malfunctioning strain gages at the center of beams B1 and B2 of Span 1, strain values were not obtained at these locations and thus could not be compared with the strain values obtained in beams B4 and B5 of Span 2. The strains at the centerline of beams B4, B5, and B6 of Span 2 were consistent for all three loading increments and positions. Maximum strains were obtained in B5 while the strains in B4 and B6 remained considerably lower. This was as expected due to the added stiffening effect of the railings.

At load positions 1.5, 2.5, and 3.5, the maximum strain was observed in beam B5 for all three load increments. The maximum response in the member occurred at load position 2.5. At this load position, the strain values ranged from a minimum of 51 microstrain at load increment one to a maximum of 166 microstrain at load increment three. The maximum response of beams B4 and B5 occurred at load increment three and load positions 3.5 and 1.5, respectively. The maximum values obtained were 19 microstrain in B4 and 38 microstrain in B6. Graphs of the longitudinal strain in beams B4, B5, and B6 for the three load increments and positions are presented in Figure 6.10. The longitudinal strains at the center of B5 for the three load increments and positions are shown in Figure 6.11.

The strain values at the ends of beams B3 and B6 were positive for the three load increments and positions. These strains were measured at the bottom of the beams and had very small magnitudes. This strain behavior indicated that no significant end restraint existed and that the beams were allowed to rotate under the applied loading.

Figure 6.12 shows the longitudinal deflections of beams B3 and B6. The degree of the end rotations of beams B3 and B6 can be seen by observing the deflections at the quarter points and centerline of each span. At load position 1.2 and load increment one, the deflections at the south quarter point, centerline, and north quarter point of B3 were 0.20 mm (0.008 in.), 0.08 mm (0.003 in.), and 0.03 mm (0.001 in.), respectively. At load increment three, the deflections were 0.53 mm (0.021 in.), 0.84 mm (0.033 in.), and 0.33 mm (0.013 in.), respectively. From the deflections at each location, it can be seen that the end of the

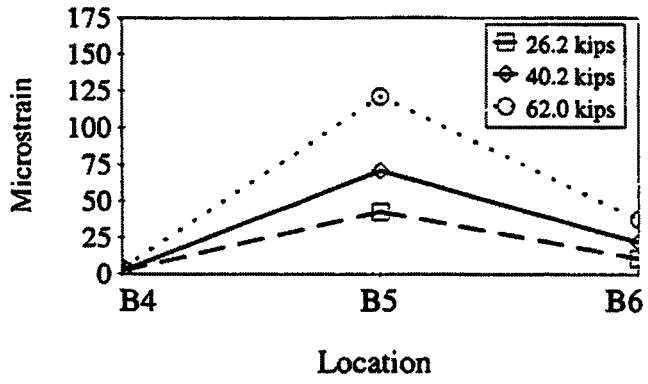

a. Load position 1.5

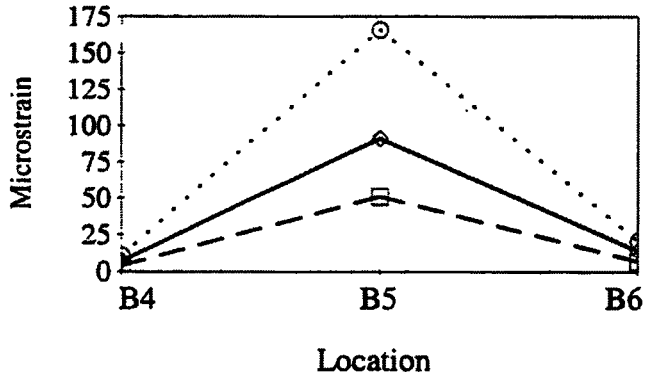

b. Load position 2.5

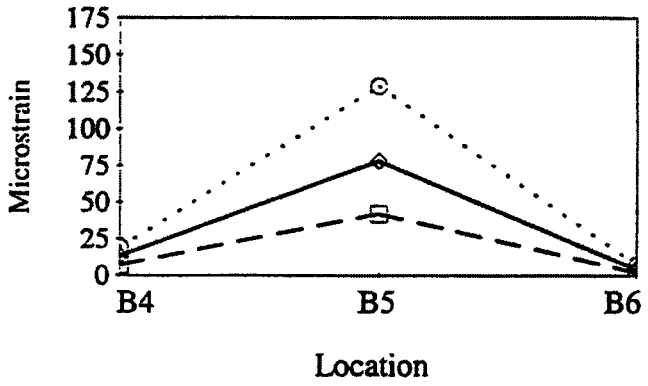

c. Load position 3.5

Figure 6.10. Bridge V: Longitudinal strains at centerline of span 2.

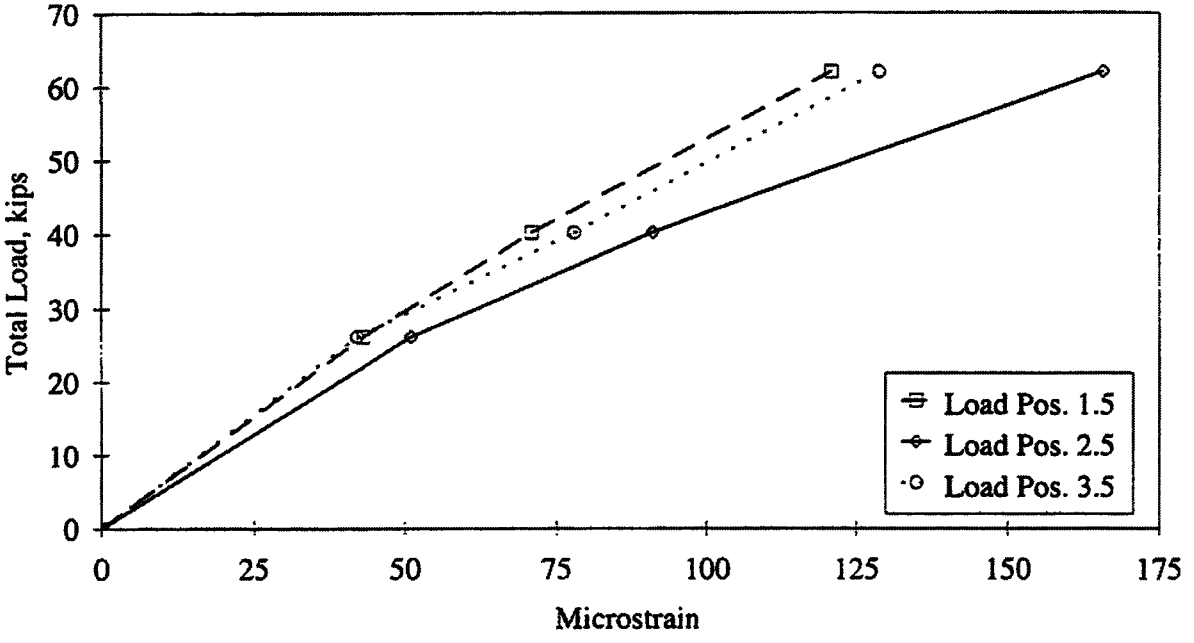

Figure 6.11. Bridge V: Longitudinal strains at centerline of beam B5.

beam bearing on the abutment is allowed to rotate more than the end bearing on the pier. This is to be expected since there is less of the beam bearing at the abutment than the pier and also because there is an embedded plate in the abutment and in the beam.

The same behavior was exhibited in beam B6. At load position 1.5 and load increment one, the deflections at the south quarter point, centerline, and north quarter point were 0.15 mm (0.006 in.), 0.18 mm (0.007 in.), and 0.28 mm (0.011 in.), respectively. At load increment three, the deflections were 0.36 mm (0.014 in.), 0.48 mm (0.019 in.), and 0.56 mm (0.022 in.), respectively.

The transverse deflections of spans 1 and 2 were approximately the same with span 2 having slightly greater deflections for all loading positions and increments. Like the strains, the largest deflections in each span were recorded for the middle girders. At load position 2.2, the deflections in B2 were maximum. The deflections ranged from 0.33 mm (0.013 in.) at load increment one to 1.17 mm (0.046 in.) at load increment three. The largest deflections

in beams B3 and B1 were obtained at load positions 1.2 and 3.2, respectively. At load position 1.2, the deflections in B3 ranged from 0.10 mm (0.004 in.) at load increment one to 0.84 mm (0.033 in.) at load increment three. At load position 3.2, the deflections in B1 ranged from 0.23 mm (0.009 in.) at load increment one to 0.76 mm (0.03 in.) at load increment three. Figure 6.13 shows the deflections of beams B1, B2, and B3 for the three loading positions and increments.

The same behavior was exhibited by beams B4, B5, and B6 in span 2. At load position 2.5, the deflections in B5 were maximum. The deflections ranged from 0.041 mm (0.016 in.) at load increment one to 1.47 mm (0.058 in.) at load increment three. The largest deflections in beams B6 and B4 were obtained at load positions 1.5 and 3.5, respectively. At load position 1.5, the deflections in B6 ranged from 0.20 mm (0.008 in.) at load increment one to 0.36 mm (0.014 in.) at load increment three. At load position 3.5, the deflections in B4 ranged from 0.15 mm (0.006 in.) at load increment one to 0.74 mm (0.029 in.) at load increment three. Figure 6.14 shows the deflections of beams B4, B5, and B6 for the three loading positions and increments.

6.5. Modified Rating

Using the strain data obtained from the diagnostic load test and the procedure described in Sec 1.7, the theoretical load rating was modified. To modify the rating, the largest strain value of 166 microstrain was used. As mentioned previously, this value occurred in beam B5 at load position 2.5 and load increment three. For the same load position and load increment, the theoretical strain calculated in the bottom of the beam was 81 microstrain. The actual value attained is over two times larger than that predicted by the analytical model. The smaller theoretical strain value is a result of a smaller effective beam section. The actual width of deck effective as a T-beam section is smaller than that suggested in AASHTO's Standard Specification for Highway Bridges [12].

Since the actual strain value in the beam is less that predicted, theoretical load rating is decreased accordingly. For the HS20 rating vehicle, the rating of the bridge decreased

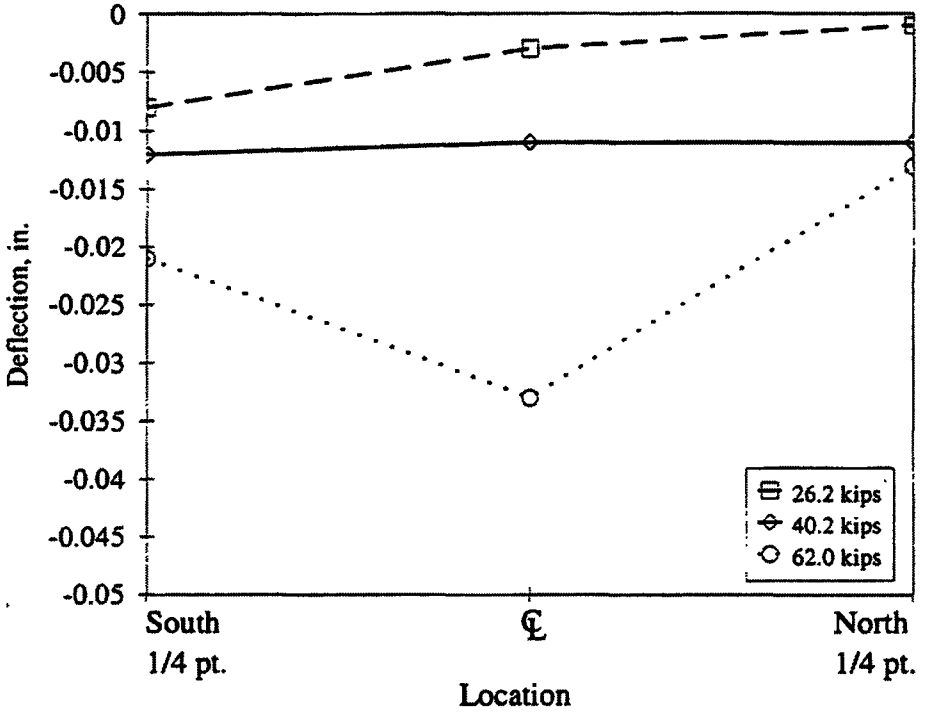

a. Beam B3: Load position 1.2

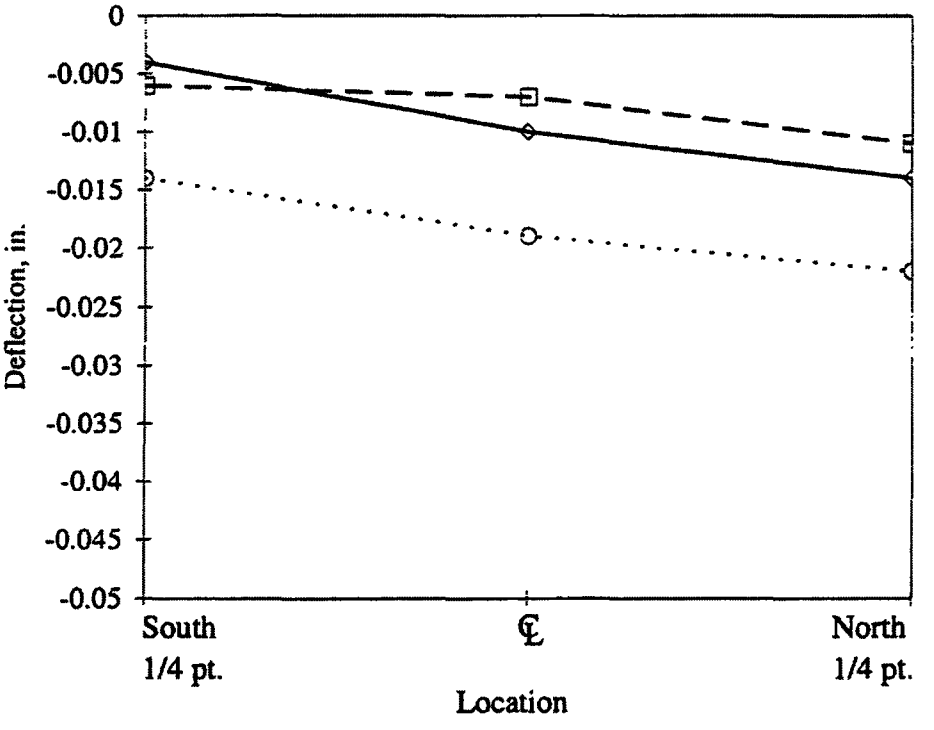

b. Beam B6: Load position 1.5

Figure 6.12. Bridge V: Longitudianl deflections of beams B3 and B6.

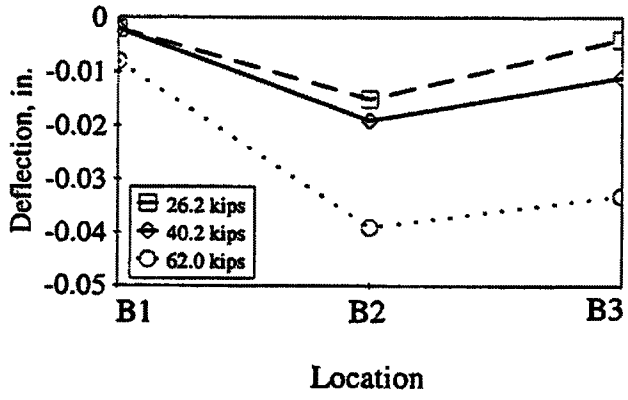

a. Load position 1.2

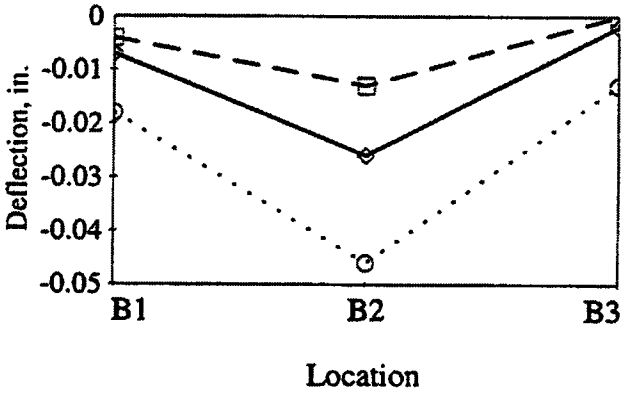

b. Load position 2.2

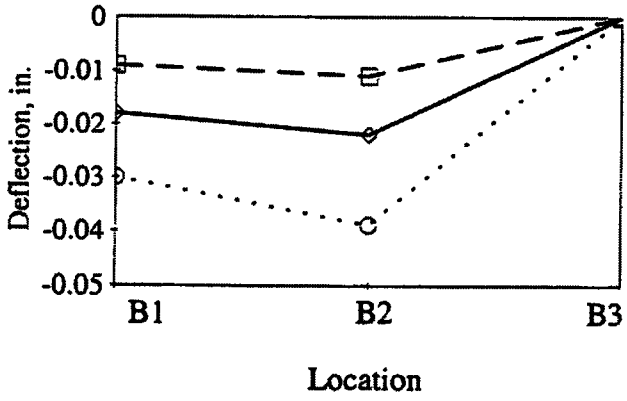

c. Load position 3.2

Figure 6.13. Bridge V: Transverse deflections at centerline of span 1.

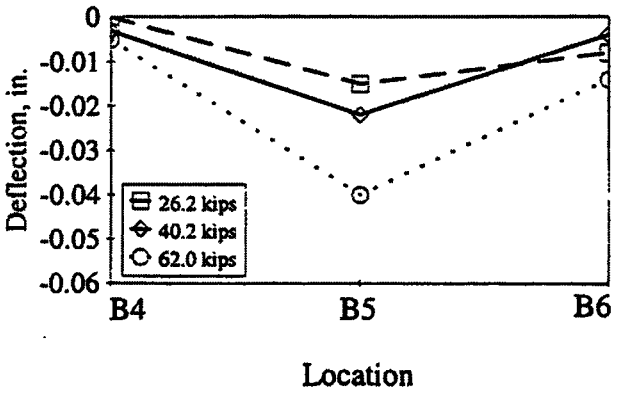

a. Load position 1.5

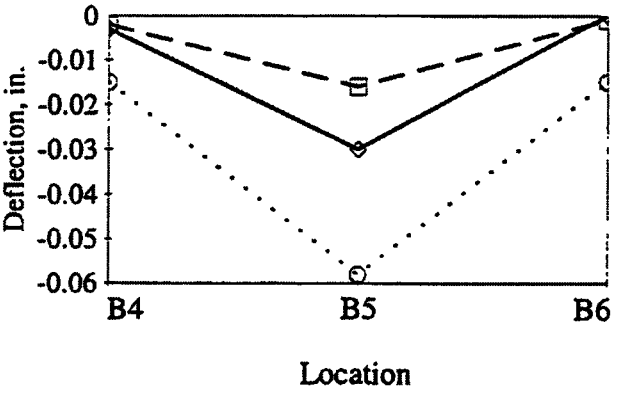

b. Load position 2.5

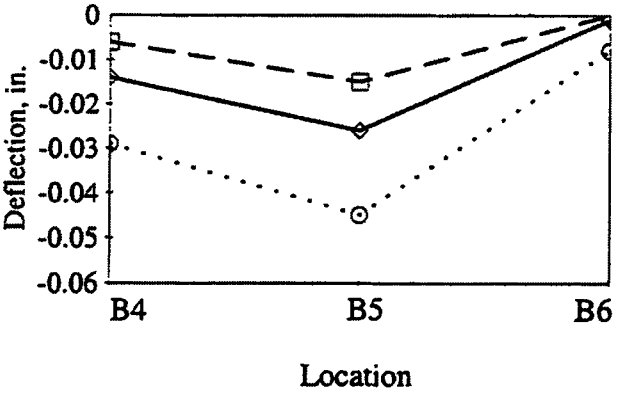

c. Load position 3.5

Figure 6.14. Bridge V: Transverse deflections at centerline of span 2.

from 507,100 N (57 tons) to 302,500 N (34 tons). For the Type 3 rating vehicle, the rating of the bridge decreased from 453,700 N (51 tons) to 266,900 N (30 tons). A summary of the theoretical and modified rating is presented in Table 6.2. The rating calculations for the bridge are presented in Appendix B.

This particular bridge demonstrates that a benefit is not always obtained from a load test. Using traditional analytical methods, the capacity of this structure could potentially be considerably overestimated. Load testing provides a way to obtain the actual response of a bridge and assign load ratings which reflect a bridges actual load carrying capacity.

Table 6.2. Bridge V: Rating summary:

	Vehicle HS20				Vehicle Type 3			
	AASHTO LRFR		Modified Rating		AASHTO LRFR		Modified Rating	
	RF_c	R (tons)	RF_T	R (tons)	RF_c	R (tons)	RF_T	R (tons)
Girders	1.61	57.9	0.95	34.2	2.05	51.3	1.21	30.3

7. BRIDGE VI: FILLED REINFORCED CONCRETE SPANDREL ARCH

7.1. Bridge Description

The final bridge to be service load tested was a filled reinforced concrete spandrel arch located in Story County over a branch of Keigley Creek. Bridge VI was one lane and located on a secondary county road (550 Ave.). The ADT for the bridge was 110 vehicles and consisted of local traffic. Built in 1913, Bridge VI is listed on the Iowa Historic Bridge Inventory and is one of 13 of this type of bridge within the state. The dimensions of the bridge were determined from field measurements and the type, size and location of the reinforcement were obtained from original plans. Figure 7.1. shows the bridge layout.

Bridge VI had a clear span of 13,720 mm (45 ft), a rise of 2,745 mm (9 ft), and a total width of 7,010 mm (23 ft). The roadway was 6,095 mm (20 ft) wide with two reinforced concrete railings 1,170 mm (3 ft - 10 in.) high and 280 mm (11 in.) wide. The arch ring was 280 mm (11 in.) thick at the crown and increased to 910 mm (3 ft) at the abutments. The roadway consisted of a soil fill material placed on top of the arch ring. The thickness of the fill ranged from 150 mm (6 in.) at the crown to 2,100 mm (6 ft - 10 in.) at the abutments. The reinforced concrete spandrel walls were constructed on either side of the arch ring to retain the fill material. Reinforcing in the arch ring consisted of two layers of 22 mm (7/8 in.) diameter bars spaced at 305 mm (12 in.) on center. The bars in the top layer were offset a distance of 150 mm (6 in.) from the bars in the bottom layer. Figure 7.2 shows the reinforcement configuration in the arch.

7.1.1. Condition Assessment

Prior to the diagnostic load test, old inspection reports were obtained and a thorough visual inspection of the bridge was conducted by the researchers. A condition rating value was not assigned to either the substructure or the superstructure after the latest inspection conducted in 1995.

The visual inspection conducted by the researchers revealed moderate deterioration. Spalling was noted on the exterior faces of the arch ring and the spandrel walls. No

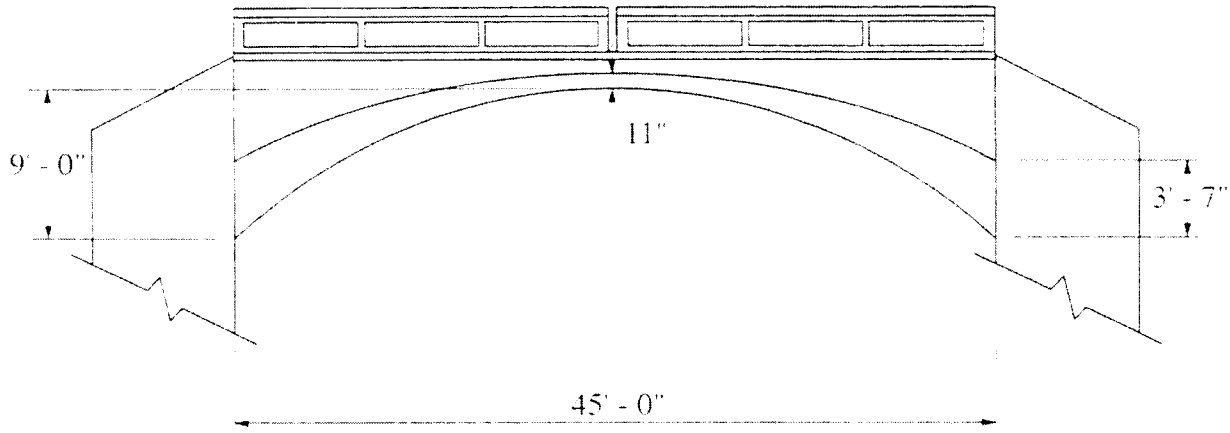

a. Elevation

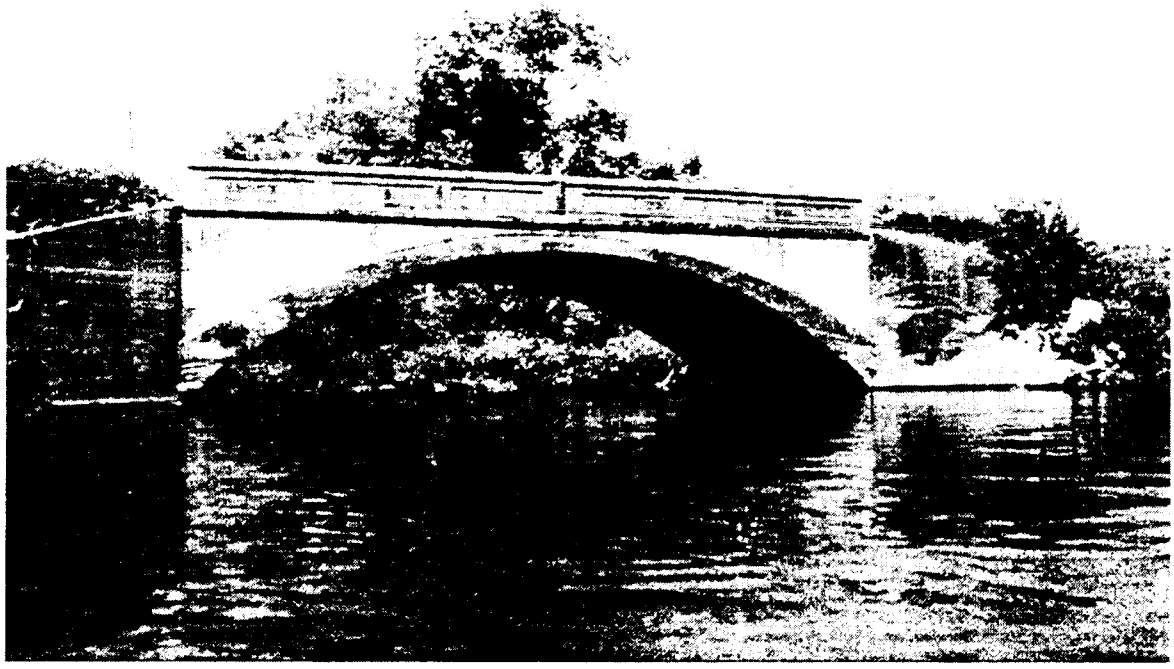

b. Photograph of bridge profile

Figure 7.1. Bridge VI: Layout

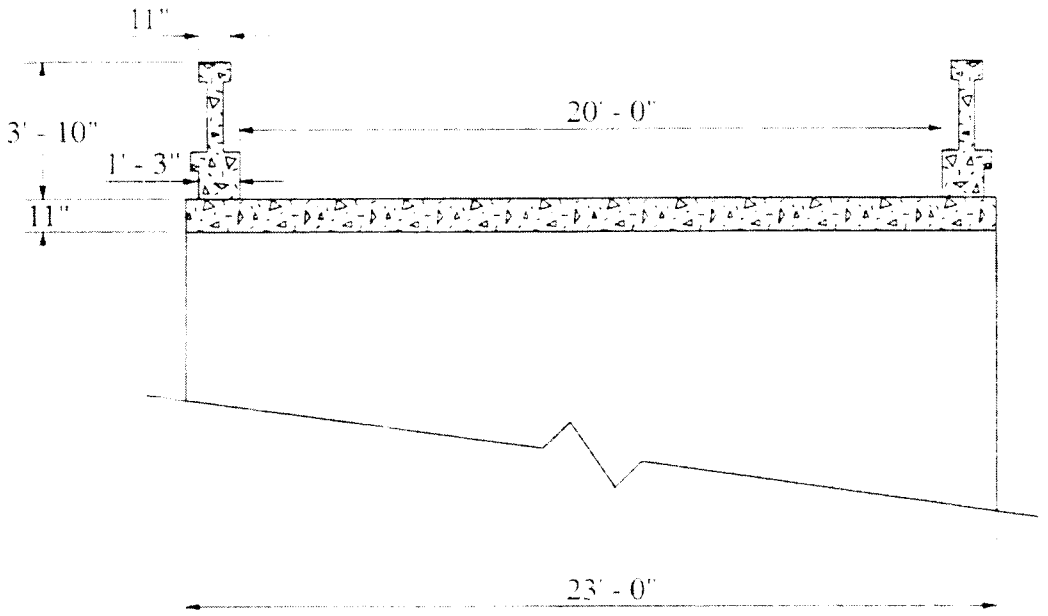

c. Centerline cross-section

d. Photograph of Bridge VI looking South

Figure 7.1. Continued.

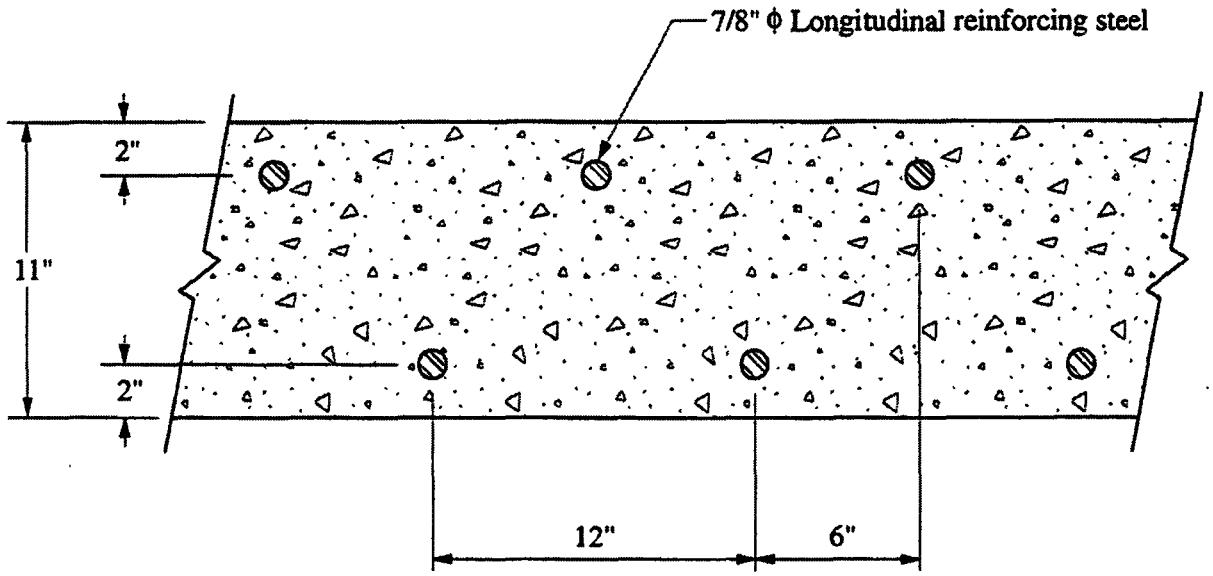

Figure 7.2. Bridge VI: Configuration and reinforcing details at crown of arch.

deterioration was noted on the underside of the arch.

7.2. AASHTO Rating

After conducting the visual inspection and determining actual dimensions, an analytical model was developed and analyzed using structural analysis software. From the analytical model, the theoretical rating factors for the vehicles described in Sec. 1.4 were calculated. The method and procedures used to obtain the rating factors were described in Sec. 1.7. Using the HS20-44 and Type 3 rating vehicles, rating factors of 5.75 and 8.44, respectively, were calculated. Like the Luten arch bridge (Bridge IV), the rating factors for this bridge were also considerabed high. The high factors can be attributed to the soil fill which causes the wheel loads to be distributed over a larger area thus resulting in lower response of the arch. The calculations used to obtain the rating factors are presented in Appendix B; theoretical load rating for the two rating vehicles are presented in Table 7.1.

Table 7.1. Bridge VI: Theoretical load rating summary.

	Vehicle HS20 AASHTO LRFR		Vehicle Type 3 AASHTO LRFR	
	Rating Factor	Rating (tons)	Rating Factor	Rating (tons)
Arch	5.75	207.0	8.44	211.0

7.3. Test Setup and Procedures

As in the previous bridges tested, strains and deflections were monitored at various locations. Strain gages were bonded to the bottom of the arch at the centerline and at the north quarter point; as shown, five strain gages were mounted on the bottom of the arch at the centerline and three at the north quarter point so that longitudinal strains could be measured. The types of strain gages used and the application process were discussed in Sec. 1.6.1.

The bridge deflections were monitored at the centerline and at the north quarter point. Three deflection transducers were mounted transversely across the bottom of the arch at the crown, one at each edge and one at the center. The same configuration was used at the north quarter point with the deflections being monitored at the edges and the centerline. The deflections were obtained using the equipment and setup described in Sec. 1.6.1; locations of the strain gages and the deflection transducers are presented in Figure 7.3.

The type of vehicle and loading process used in the testing of the bridge were described in Sec. 1.6.2. For this bridge, the loading was applied in four increments: 95,600 N (21,500 lbs), 144,100 N (32,400 lbs), 189,000 N (42,500 lbs), and 266,900 N (60,000 lbs), respectively. The wheel configuration and load distribution in the test vehicle are presented in Figure 7.4; a photograph of the test vehicle is shown in Figure 7.5.

The deflection and strain behavior of the bridge were observed by stopping the test vehicle at various longitudinal and transverse locations. Longitudinally, the test vehicle was stopped at the north quarter point, center, and south quarter point. At each location, the test vehicle was positioned such that the front axle of the rear tandem was centered on the stopping location. Once the vehicle had been positioned, strain and deflection readings were taken. The stopping locations for the various tests are shown in Figure 7.6. It should be

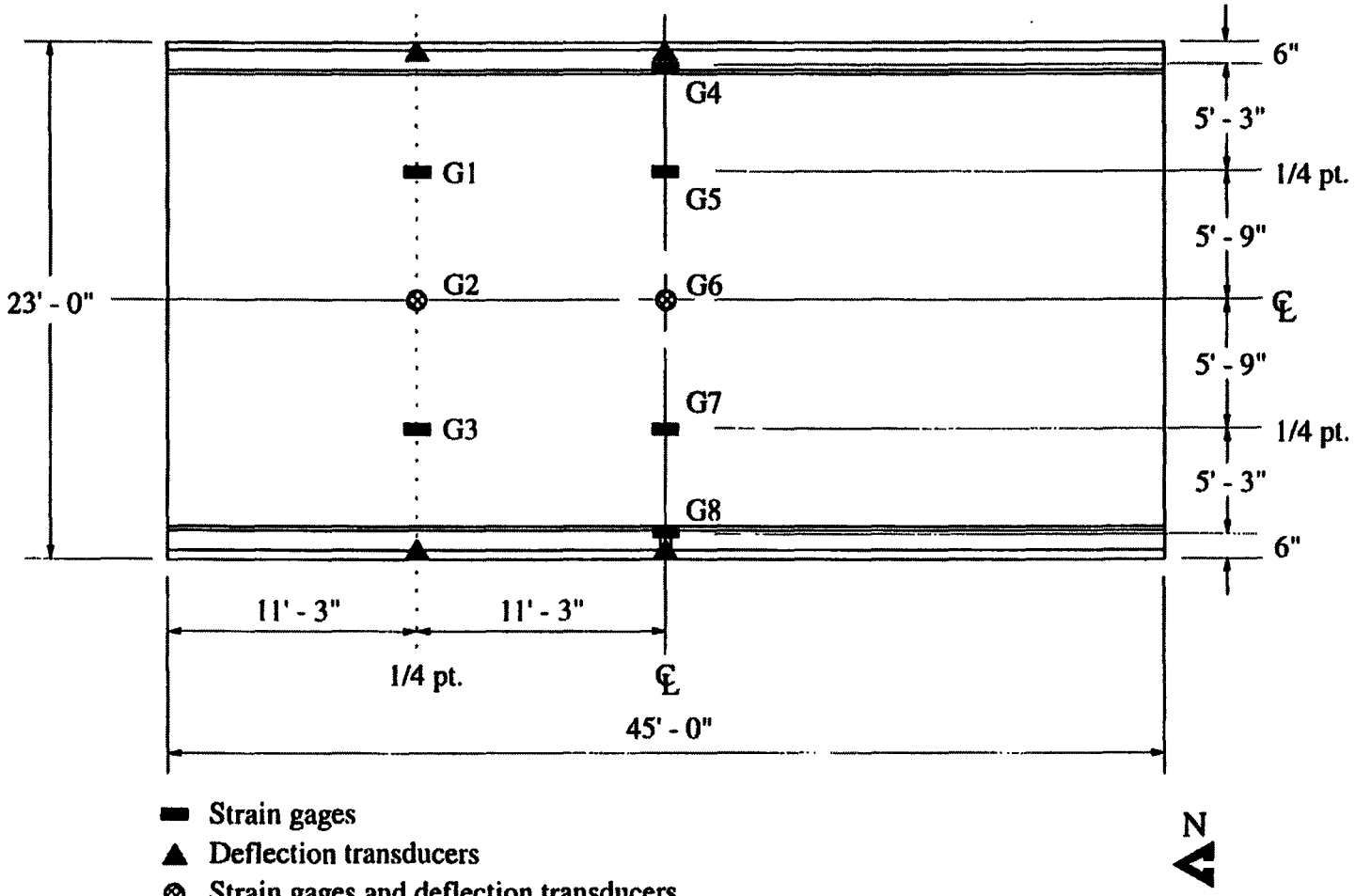

a. Plan view

Figure 7.3. Bridge VI: Location of strain gages and deflection transducers.

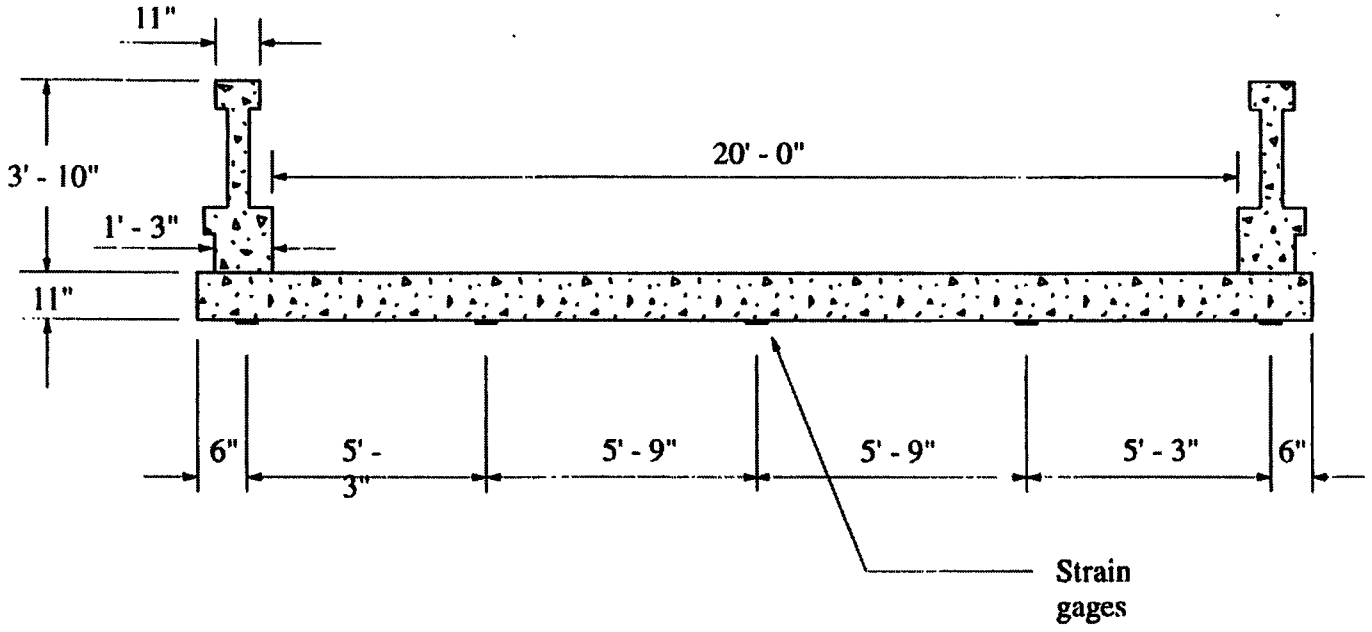

b. Centerline

Figure 7.3. Continued.

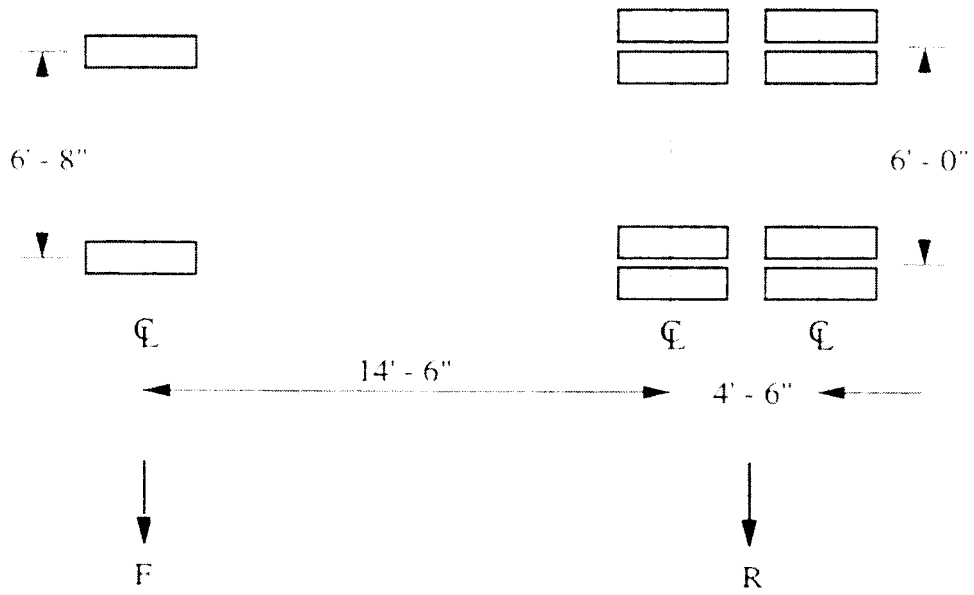

Load Increment	F (kips)	R (kips)	Total Load (kips)
1	9.3	12.2	21.5
2	12.0	20.4	32.4
3	14.5	28.0	42.5
4	16.6	43.4	60.0

Figure 7.4. Bridge VI: Wheel configuration and weight distribution in test vehicle.

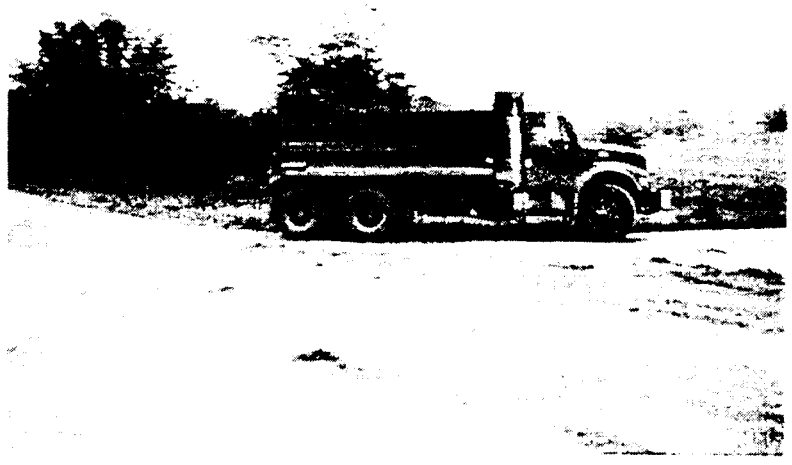

Figure 7.5. Bridge VI: Photograph of test vehicle.

noted that at load positions 1.3, 2.3, and 3.3 the front axle of the test vehicle was off the bridge thus the measured response was for the rear tandem only. The transverse lane positioning of the test vehicle was described in Sec. 1.6.2. and is shown in Figure 7.7.

7.4. Results and Discussion

Of all the bridges tested as part of this project, Bridge VI had the least response in terms of strains and deflections. Strain values remained in the single digits to low teens and deflections were measured in the hundredths for all load positions and increments. These values were also considerably lower than those obtained from the Luten arch (Bridge IV) due to the increased depth of the fill material.

The longitudinal strain at the centerline of the bridge is presented in Figure 7.8 for the four load increments and three load positions. The strain values obtained remained relatively uniform across the bottom of the arch for all load positions and load increments. At load position 1.2 and load increment four, the strains varied from a maximum of 10 microstrain at G8 to 9 microstrain, 8 microstrain, and 2 microstrain at G6, G5, and G4, respectively. The same response was exhibited for the previous three load increments. The large strain values obtained at G7 may be attributed to existing cracks in the concrete in the vicinity of the gage and thus were neglected.

At load position 2.2, the maximum strain was recorded at the centerline of the arch and then decreased toward the railings for all four load increments. This is expected since the railings increase the stiffness of the edges of the arch. At load increment four, a maximum strain of 10 microstrain was recorded at G6; 8 microstrain and 5 microstrain were recorded at G4 and G8, respectively, for this load increment.

At load position 3.2, the response of the bridge was similar to that of load position 1.2. The strains were maximum along the east edge and then decreased to a minimum at the west edge. At load increment four, a maximum strain of 13 microstrain was recorded at G4 while 9 microstrain, 7 microstrain, and 3 microstrain were measured at G5, G6, and G8, respectively. The same response was exhibited for load increments one, two, and three.

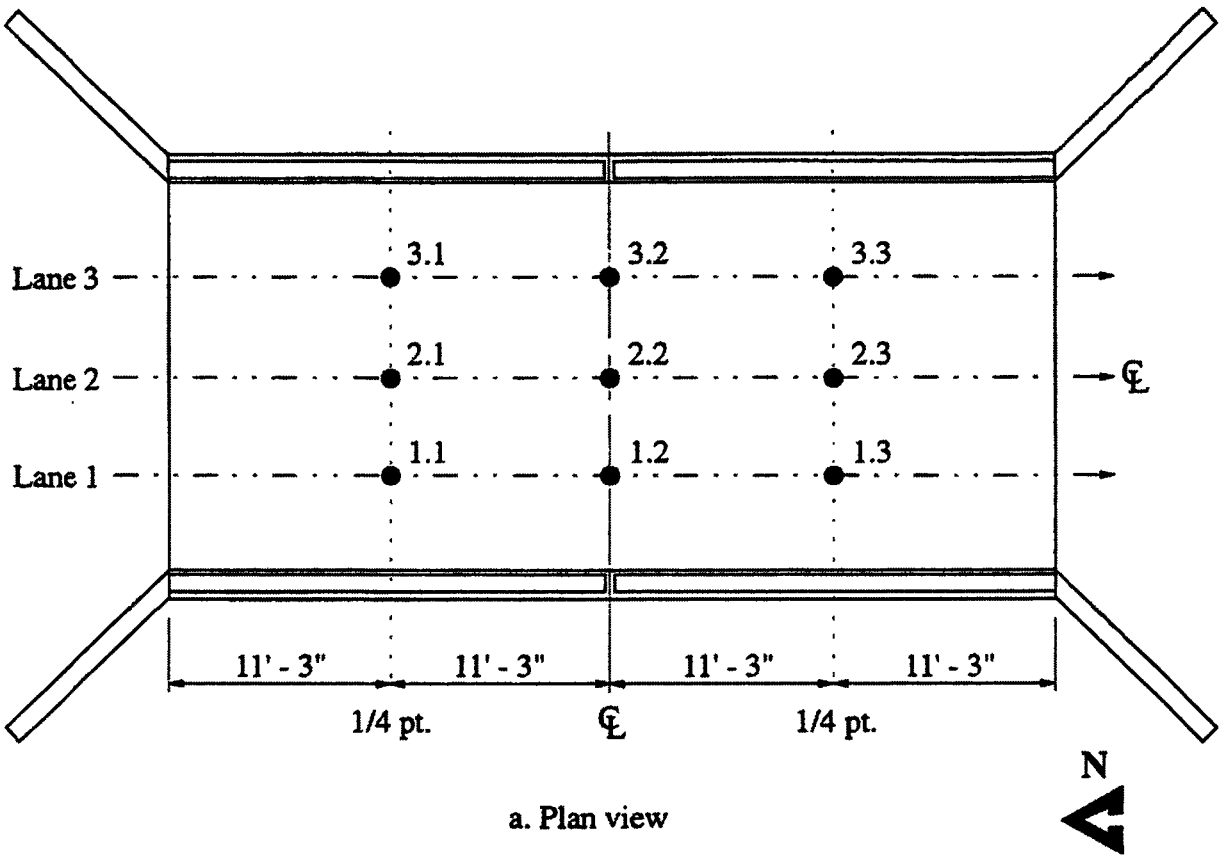

a. Plan view

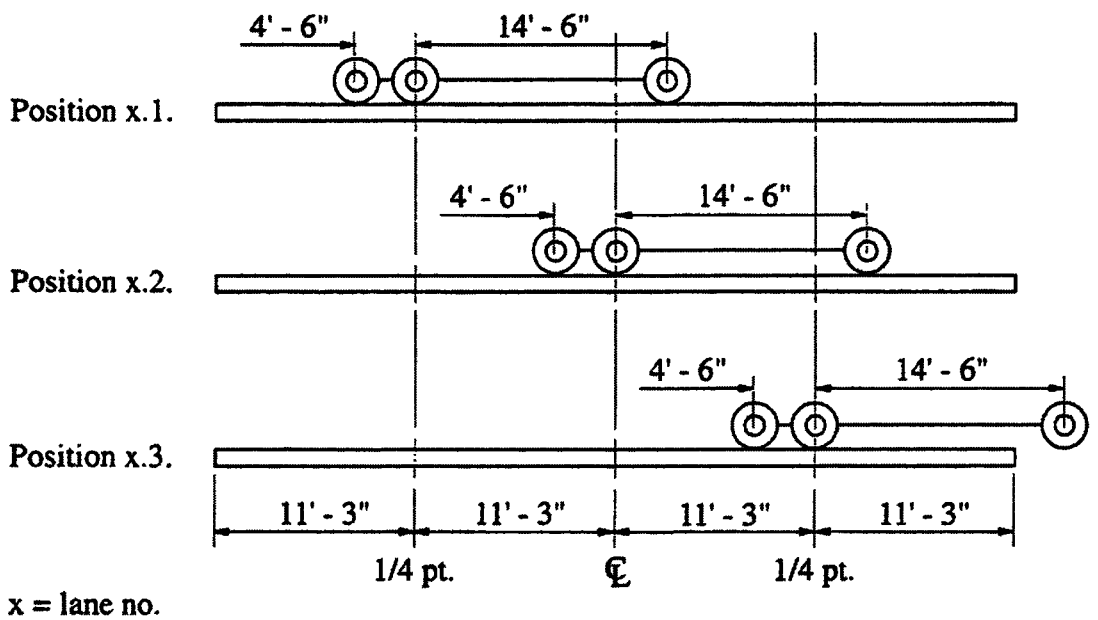

b. Truck stopping position on deck.

Figure 7.6. Bridge VI: Longitudinal location of test vehicle for various tests.

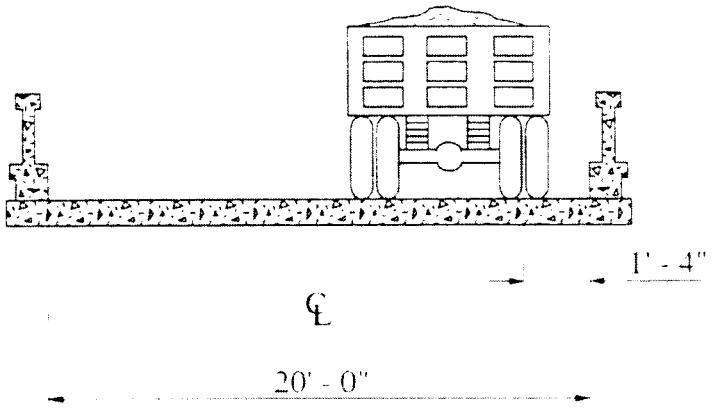

a. Lane 1

b. Photograph of test vehicle in Lane 1

Figure 7.7. Bridge VI: Transverse location of test vehicle on bridge.

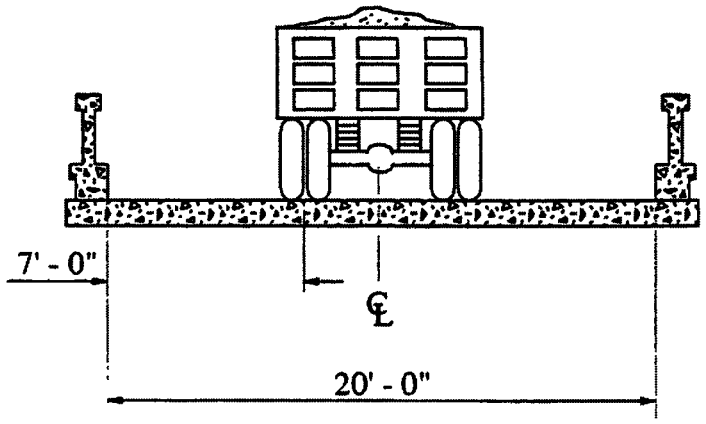

c. Lane 2

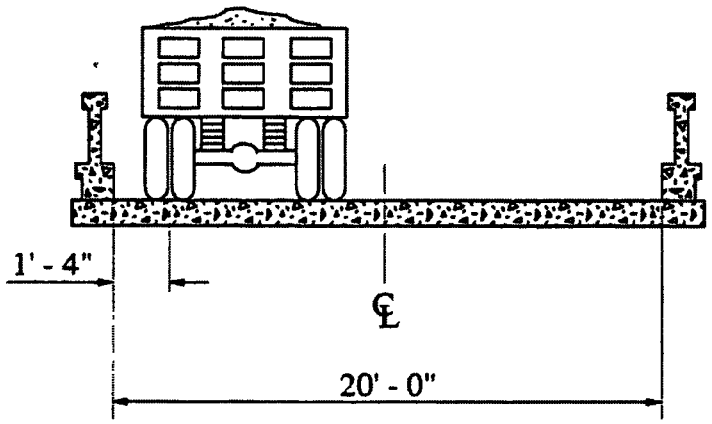

d. Lane 3

Figure 7.7. Continued.

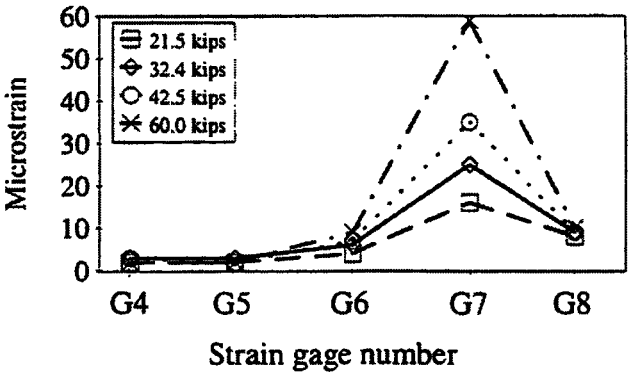

a. Load position 1.2

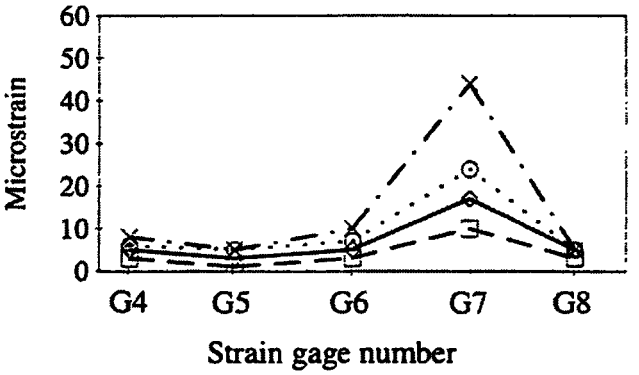

b. Load position 2.2

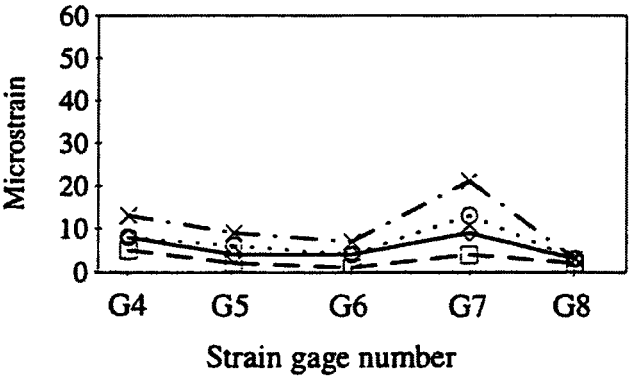

c. Load position 3.2

Figure 7.8. Bridge VI: Longitudinal strains at bridge centerline.

Like the strains at the centerline, the magnitude of the strains at the north quarter point remained in the single digits for all load positions and load increments. The average longitudinal strain at the bridge centerline is presented in Figure 7.9. These were determined by averaging the five strain readings at the crown of the arch for each load position and increment. Disregarding the strain values recorded at G7, the maximum average strain was 8 micostrain. This value occurred at load increment four and load position 3.2. This average value is 1/16th the theoretical strain (approx. 130 microstrain) at which tensile cracks begin to form in concrete.

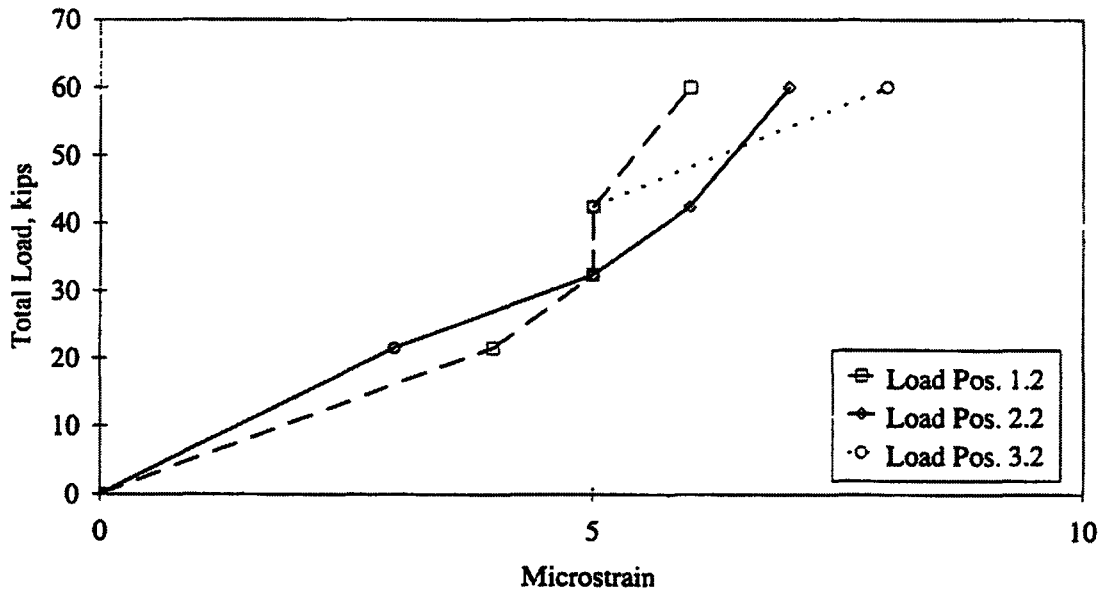

Figure 7.9. Bridge VI: Average longitudinal strains at bridge centerline.

The transverse deflection of the bridge for the various loading positions and increments is presented in Figure 7.10. Like the strains, the deflections at the crown and north quarter point of the arch were extremely small for all load positions and load increments. At load position 1.2, the maximum deflection occurred at the west edge and ranged from 0 at load increment one to 0.66 mm (0.026 in.) at load increment four. The deflection of the arch decreased to 0 at the east edge for all load increments.

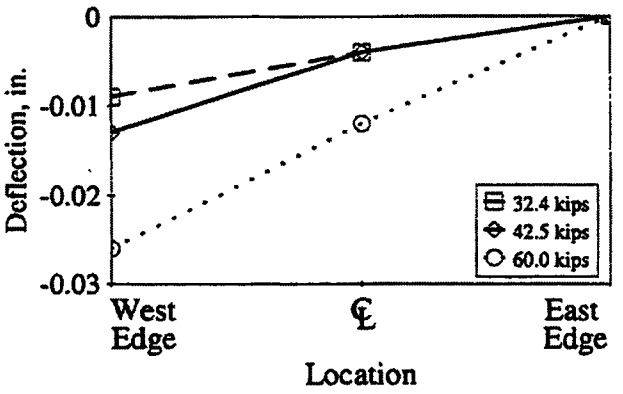

a. Load position 1.2

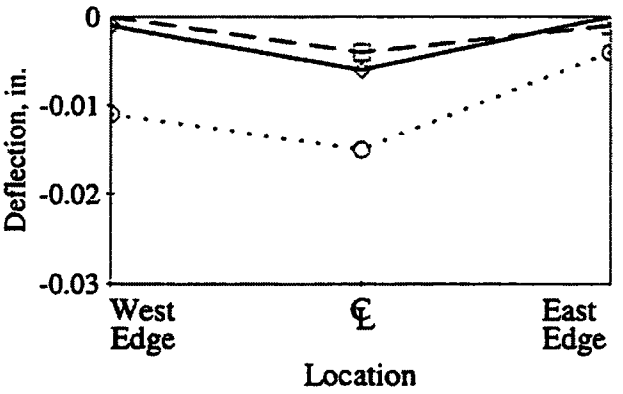

b. Load position 2.2

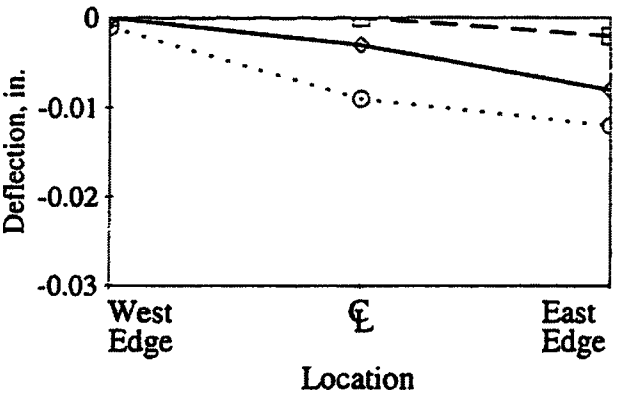

c. Load position 3.2

Figure 7.10. Bridge VI: Transverse deflections at bridge centerline.

At load position 2.2, the maximum deflection occurred at the center of the arch for all load increments. The deflections at the centerline ranged from 0 at load increment one to 0.38 mm (0.015 in.) at load increment four. Due to the presence of the railings, the deflections at the west and east edges were smaller and ranged from 0 at load increment one to 0.28 mm (0.011 in.) and 0.10 mm (0.004 in.) respectively at load increment four.

The deflection at load position 3.2 was similar to that of load position 1.2. The maximum deflection of the arch occurred at the east edge and then decreased to the west edge. At the east edge of the arch, the deflection ranged from 0 at load increment one to 0.31 mm (0.012 in.) at load increment four. At the west edge of the arch the deflection decreased to 0 for load increment one, two, and three, and 0.05 mm (0.002 in.) for load increment four.

The deflection of the arch at the north quarter point remained extremely small and ranged from 0 at load increment one to 0.10 mm (0.004 in.) at load increment four. Average deflection values at the crown and north quarter point versus the four load increments are shown in Figure 7.11.

The small strain and deflection values can most likely be attributed to the presence of the fill material. The fill material causes a greater percentage of the load to be distributed transversely and longitudinally creating more of a uniform loading condition. The small strain and deflection values obtained should be approached with caution. All instrumentation associated with data acquisition has a degree of error associated with it which should be considered.

7.5. Modified Rating

The strain values obtained from the diagnostic load test were used to modify the theoretical load rating. The procedure followed was described in Sec. 1.7.

In modifying the analytical rating, the largest average strain value at the crown of the arch was used. This value was determined to be 8 microstrain and occurred when the test vehicle was at load increment four and load position 3.2. For the same load position and load increment, the theoretical strain was calculated to be 163 microstrain.

Using these results in conjunction with the rating procedure, the theoretical rating was

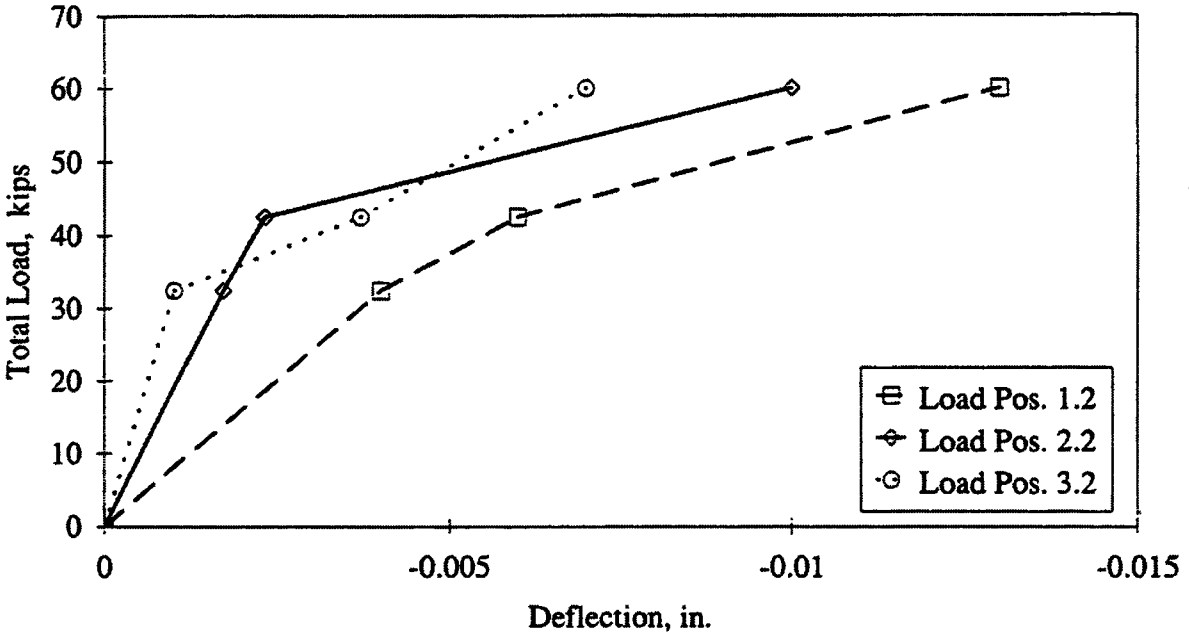

a. Centerline

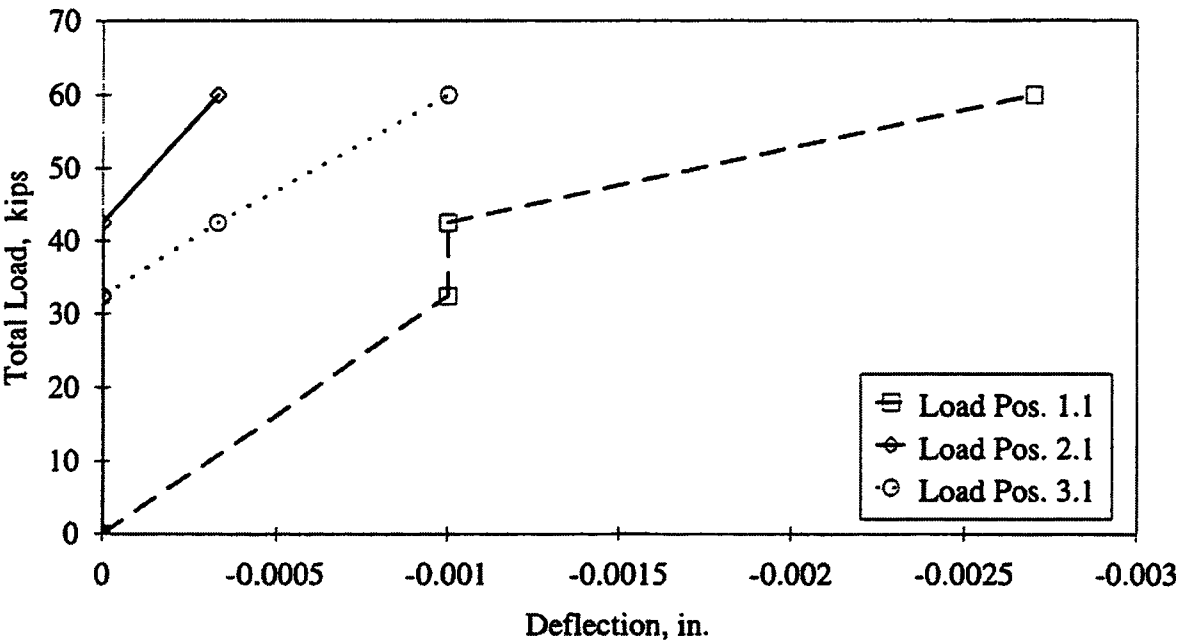

b. Quarter point

Figure 7.11. Bridge VI: Average longitudinal deflections.

increased significantly. For the HS20 rating vehicle, the rating of the bridge increased from 1,841,600 N (207 tons) to 6,814,700 N (766 tons). For the Type 3 rating vehicle, the rating of the bridge increased from 1,877,100 N (211 tons) to 8,175,800 N (919 tons). A summary of the theoretical and modified rating is presented in Table 7.2. The rating calculations for the arch are presented in Appendix B.

Modifying the rating of a bridge of this type to load levels indicated should be approached with caution. The presence of the soil fill material makes modeling the bridge very difficult. The interaction of the soil and distribution of the applied loads is very difficult to predict.

Table 7.2. Bridge VI: Rating summary:

	Vehicle HS20				Vehicle Type 3			
	AASHTO LRFR		Modified Rating		AASHTO LRFR		Modified Rating	
	RF_c	R (tons)	RF_T	R (tons)	RF_c	R (tons)	RF_T	R (tons)
Arch	5.75	207.0	21.29	766.4	8.44	211	36.76	919.0

8. SUMMARY AND CONCLUSIONS

8.1. Summary

In this investigation, six old reinforced concrete bridges were subjected to static diagnostic load tests. The results obtained were used in conjunction with an analytical rating to determine an experimental load carrying capacity of each bridge. From a review of the literature on nondestructive load testing, it was determined that many countries around the world are using this method to obtain actual load ratings and load carrying capacities. In recent years, several states have implemented nondestructive load testing programs to evaluate their bridges.

The bridges in this investigation consisted of two reinforced concrete open spandrel arches (Marsh Arches) which were scheduled for replacement, a reinforced concrete slab bridge, two reinforced concrete filled spandrel arches (one of which was a Luten Arch), and a two span reinforced concrete girder bridge. Each bridge was tested using a tandem axle dump truck at varying load increments. The test vehicle was positioned at predetermined longitudinal and transverse locations to obtain the maximum stress in the critical members. At each test location, strains and deflection data were obtained. In the bridges that were to be replaced, steel and concrete samples were obtained and video footage was taken of their demolition.

The strains obtained from the various tests were used to modify the analytical load rating of each bridge. The various bridges were rerated using the procedure developed by Lichtenstein [2] for evaluating and applying the results obtained from diagnostic load tests. The procedure involves comparing the actual strains in a particular element with those predicted by an analytical model. The value obtained is then modified based on the frequency of inspections, the accuracy of the model, and special structural features such as redundancy, fatigue, etc.

The results from the bridge testing revealed that in a majority of the bridges, the actual load carrying capacities were greater than that predicted by traditional analytical procedures. In some instances, the results were two or three times that of the theoretical

rating. However, the modified rating of the two span reinforced concrete girder bridge was less than that predicted by the analytical rating.

8.2. Conclusions

Based on testing conducted within this investigation, the following conclusions and observations can be made regarding diagnostic load testing of old reinforced concrete bridges.

1. Diagnostic load testing is a low cost effective means of obtaining better estimated load carrying capacities and rating factors of existing reinforced concrete bridges. Due to the variation in the strength of the concrete, accurate modulus of elasticity values are difficult to obtain. Variations in the modulus of elasticity of the concrete makes it difficult to obtain reliable stress values from test strains. Unless reasonably accurate modulus of elasticity values of the in-situ concrete are obtained, it may be advantages to consider proof load testing.
2. Traditional analytical ratings, in most instances, underestimate the actual load carry capacity of a bridge.
3. The presence of reinforced concrete railings and curbs adds considerable strength to a given bridge. This additional strength is typically neglected in the analytical rating of bridges.
4. In extrapolating the results obtained from diagnostic load tests to load levels greater than those placed on the bridge during the load test, care must be taken to ensure safe bridge performance at the higher load level.
5. Old reinforced concrete bridges typically have reserve capacity greater than that predicted by analytical methods despite their deteriorated condition. Most of these bridges are one lane and have large reinforced concrete railings which provides additional strength. Also, these bridges are typically over designed due to the analysis assumptions and design principles in practice at the time of their design and construction.

9. RECOMMENED FURTHER RESEARCH

On the basis of the field testing completed thus far, additional nondestructive load testing of existing bridges is proposed:

1. Since the strength of concrete is quite variable, the testing of old reinforced concrete bridges should be extended to include proof load testing. In bridges where the concrete is heavily deteriorated and the placement and size of reinforcement are unknown, proof load testing is a more accurate method for determining the maximum load carrying capacity of the bridge.
2. Additional reinforced concrete bridges need to be tested so that a data base may be developed. Using this data base, bridge engineers will be able to safely predict the load carrying capacity of similar bridges.
3. The diagnostic load testing procedure presented within this report should be extended to other types bridges, timber, steel, etc. As with the reinforced concrete bridges, a data base containing the test results of various types of steel bridges, timber bridges etc. could be developed and used to predict the behavior of similar bridges.
4. Any bridge that the state or county plans to decommission should be tested using both diagnostic test procedures and proof test procedures so that the data base on the various types of bridges in Iowa can be expanded.

10. ACKNOWLEDGEMENTS

The study presented in this report was conducted by the Bridge Engineering Center under the auspices of the Engineering Research Institute of Iowa State University. The research was sponsored by the Project Development Division of the Iowa Department of Transportation and the Iowa Highway Research Board under Research Project HR-390.

The authors wish to thank the following county engineers for their assistance with this project:

- Dave T. Anthoney - Boone County
- Harold Jensen - Story County
- Royce J. Fichtner - Marshall County
- Robert L. Haylock - Hardin County

The authors also wish to thank the project advisory committee for their guidance and input on the selection of the various types of bridges tested:

- Mark Nahra, County Engineer, Cedar County
- Dave T. Anthoney, County Engineer, Boone County
- LeRoy Bergman, Iowa DOT, Office of Local Systems
- Robert Bauer, County Engineer, Washington County
- Dennis J. Edgar, Assistant County Engineer, Blackhawk County

Appreciation is also extended to Tim Herrstrom, Denny Eppert, Boone-Perry Ready Mix, Tim Knight, Don Tice, Gilbert Coop, Rex Jennings, and Jim Peters for their assistance in testing the various bridges.

A special thanks are accorded to the following Civil Engineering undergraduate students for their assistance in various aspects of the project: Julie Manchester, Mary Walz, Ryan Paradis, and Penny Moore. In particular, the assistance of Douglas Wood, structures laboratory supervisor, made the successful completion of this project possible.

11. REFERENCES

1. American Association of State Highway and Transportation Officials. Manual for Maintenance Inspection of Bridges. Third Edition. Washington D.C.: American Association of State Highway and Transportation Officials, 1983.

2. Lichtenstein, A. G. "Bridge Rating Through Nondestructive Load Testing." National Cooperative Highway Research Program Project 12-28(13)A, Transportation Research Board, 1993.

3. Pinjarkar G., Suresh, Otto C. Guedelhoefer, Barbara J. Smith, and Robert W. Kritzler. "Nondestructive Load Testing for Bridge Evaluation and Rating", Final Report Raths, Raths and Johnson, Inc., Willowbrook, Illinois, February, 1990.

4. Conner, G.H., J. M. Stallings, T. L. McDuffie, J. R. Campbell, R. Y. Fulton, B. A. Shelton, and R. B. Mullins. "Steel Bridge Testing in Alabama." Preprinted paper presented at the Transportation Research Board 76th annual meeting (currently being considered for publication), January, 1997.

5. Moses, Fred, Jean Paul Lebet, and Rolf Bez. "Applications of Field Testing to Bridge Evaluation." Journal of Structural Engineering, ASCE, Vol. 120, No. 6, June, 1994, pp. 1745-1761.

6. Chajes, Michael J., Dennis R. Mertz, and Brett Commander. "Can Economic Bridge Testing Reduce Posting?" Better Roads, August, 1996, pp. 29-32.

7. Boothby, Thomas E., and Richard J. Craig. "Experimental Load Rating of a Historic Truss Bridge." Journal of Structural Engineering, ASCE, Vol. 2, No. 1, February, 1997, pp. 18-26.

8. Beal, D. B. "Destructive Testing of a Reinforced Concrete T-Beam Bridge." Research Report 100, Engineering Research and Development Bureau, New York Department of Transportation, December, 1982.

9. Beal, D. B. "Strength of Concrete T-Beam Bridges." ACI Symposium on Strength Evaluation of Existing Concrete Bridges, SP-88, Detroit, Michigan, 1995, pp. 143-164.

10. Imbsen, R. A., W. D. Liu, R. A. Schamber, and R. V. Nutt. " Strength Evaluation of Existing Reinforced Concrete Bridges." National Cooperative Highway Research Program Report 292, Transportation Research Board, National Research Council, Washington, D. C., June, 1987.

11. American Association of State Highway and Transportation Officials. Guide Specifications for Strength Evaluation of Existing Steel and Concrete Bridges, Washington, D. C., American Association of State Highway and Transportation Officials, 1989.

12. American Association of State Highway and Transportation Officials. Standard Specifications for Highway Bridges, 15th Edition. Washington, D. C., American Association of State Highway and Transportation Officials, 1992.

13. "Standard Test Method of Capping Cylindrical Concrete Specimens." ASTM C 617, Annual Book of ASTM Standards, American Society for Testing and Materials, Vol. 04.02, Philadelphia, PA, 1987, pp. 306-309.

14. "Standard Test Method for Compressive Strength of Cylindrical Concrete Specimens." ASTM C 39, Annual Book of ASTM Standards, American Society for Testing and Materials, Vol. 04.02, Philadelphia, PA, 1986, pp. 20-23.

15. "Standard Test Method for Obtaining and Testing Drilled Cores and Sawed Beams of Concrete." ASTM C 42, Annual Book of ASTM Standards, American Society for Testing and Materials, Vol. 04.02, Philadelphia, PA, 1990, pp. 27-28.

16. "Standard Test Methods and Definitions for Mechanical Testing of Steel Products." ASTM C 370, Annual Book of ASTM Standards, American Society for Testing and Materials, Vol. 03.01, Philadelphia, PA, 1990, pp. 204-237.

17. "Moments Shears and Reactions For Continuous Highway Bridges." American Institute of Steel Construction, New York, New York, 1966.

APPENDIX A

COUNTY ENGINEER'S QUESTIONNAIRE

QUESTIONNAIRE

BACKGROUND

After consultation with, and at the request of, several Iowa DOT and county personnel, an investigation is being considered to look at the preservation of historical concrete bridges. The research would include service load testing of the bridges and documentation of the demolition (if demolition is scheduled) for condition assessment. The results of the project would allow better understanding of the relation between load rating values and actual load capacity of concrete bridges. In our opinion, three different types of concrete bridges should be service load tested. We would appreciate your input by completing the following questionnaire.

Name_____ County_____

Fax_____ Telephone_____

1. Do you have any concrete bridges that are approximately 40-50 years old that you plan to replace in the next 5 years?

   _____Yes _____No

2. Do you have any historical concrete bridges that you plan to replace in the next 5 years?

   _____Yes _____No

3. Would you allow the bridge to be service load tested by others prior to demolition and the demolition documented to obtain information about the accuracy of the current load rating procedures?

   _____Yes _____No

Please return by February 21, 1996 to:

Terry Wipf
Civil and Construction Engineering Dept.
Iowa State University
Ames, IA 50011
Fax: 515-294-8216

APPENDIX B
LOAD RATING CALCULATIONS

BRIDGE I
BOONE MARSH ARCH BRIDGE NO. 135
Year Built: 1914

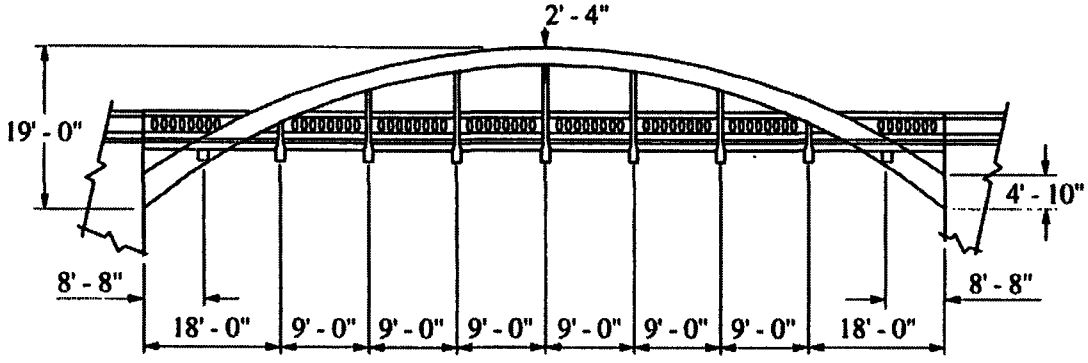

ELEVATION

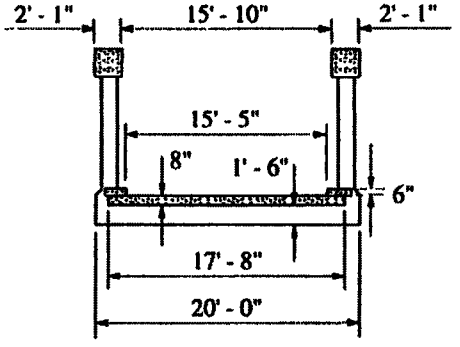

TYPICAL CROSS-SECTION

I. Rating Slab:

Span Length:

$8.0 + 8.0(1/12) = 8.67$ ft

Dead Load:

$8(1/12)(1)(0.150) = 0.100$ k/ft/ft width

Note: Due to the absence of negative moment steel, the slab will be analyzed as simply supported.

Dead Load Moment:

$$M_{DL} = \frac{wL^2}{8} = \frac{(0.100)(8.67)^2}{8}$$

$M_{DL} = 0.940$ ft-k/ft width

Live Load Moment:

$E = 4 + 0.06(s)$

E = wheel distribution

s = slab span length

$E = 4 + 0.06(8.67)$
$E = 4.52$ ft

Vehicle HS20:

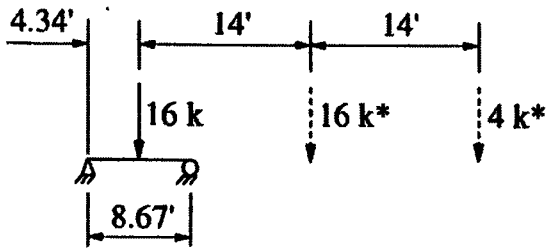

• Truck positioned to produce maximum moment

$$M_{LL} = \frac{PL}{4E}$$

M_{LL} = Maximum theoretical live load moment due to rating vehicle

$$M_{LL} = \frac{\left[\frac{(16)(8.67)}{4}\right]}{4.52}$$

$M_{LL} = 7.67$ ft-k/ft width

* Wheels off section of slab being rated

Vehicle Type 3:

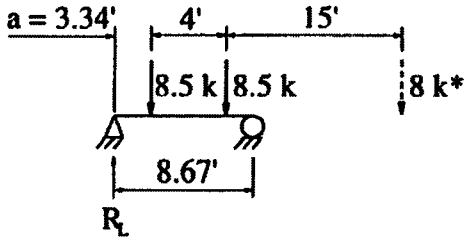

• Truck positioned to produce maximum moment

$$M_{LL} = \frac{R_L a}{E} = (3.34)\left(\frac{6.53}{4.52}\right)$$

$M_{LL} = 4.82$ ft-k/ft width

Flexural Design Strength:

Typical 1 ft section

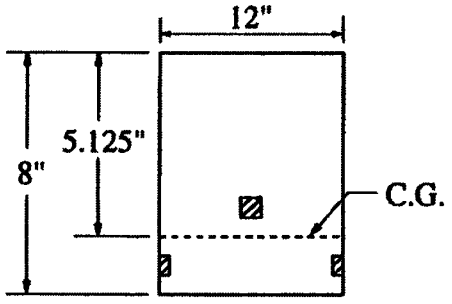

$A_s = 2(0.75)(0.75) = 1.125$ in.^{2}
$d = 8 - 1.5 - 0.75 - 0.625 = 5.125$ in.

f_y = 41 ksi (From laboratory tests)
f_c' = 4.3 ksi (From laboratory tests)

$$\rho = \frac{A_s}{bd} = \frac{1.125}{(12)(5.125)}$$

ρ = 0.0183

$\rho_{max} = 0.75\rho_b$

$$\rho_b = \frac{(0.85\beta_1 f_c')(87{,}000)}{f_y(87{,}000 + f_y)}$$

β_1 = 0.835

$$\rho_b = \frac{(0.85)(0.835)(4.3)(87{,}000)}{(41)(87{,}000 + 41{,}000)}$$

ρ_b = 0.0506

$\rho_{max} = (0.75)(0.0506)$
ρ_{max} = 0.0379

ρ = 0.0183 < ρ_{max} = 0.0379
Tension reinforcement yields

$$M_n = A_s f_y(d - \frac{a}{2})$$

$$a = \frac{A_s f_y}{0.85 f_c' b} = \frac{(1.125)(41)}{(0.85)(4.3)(12)}$$

a = 1.052 in.

$$M_n = \frac{(1.125)(41)\left(5.125 - \frac{1.052}{2}\right)}{12}$$

M_n = 17.68 ft-k/ft width

Rating:

$$RF_c = \frac{\phi M_n - \gamma_D M_{DL}}{\gamma_L M_{LL}(1 + I)}$$

ϕ = 0.7 (Heavy deterioration, careful inspection, intermittent maintenance)
γ_D = 1.2
γ_L = 1.3
I = 0.2 (Poor condition)

Vehicle HS20:

$$RF_c = \frac{(0.70)(17.68) - (1.2)(0.940)}{(1.3)(7.67)(1.2)}$$

RF_c = 0.94

Rating = (0.94)(36) = 33 T

Vehicle Type 3:

$$RF_c = \frac{(0.70)(17.68) - (1.2)(0.940)}{(1.3)(4.82)(1.2)}$$

$RF_c = 1.50$

Rating = (1.50)(25) = 37 T

II. Rating Beam:

Dead Load:

Self Weight: (1)(1.5)(0.150) = 0.225 k/ft
Slab: (0.100)(9) = 0.900 k/ft
1.125 k/ft

Dead Load Moment:

$$M_{DL} = \frac{wL^2}{8} = \frac{(1.125)(18)^2}{8}$$

$M_{DL} = 45.56$ ft-k

Live Load Moment:

Vehicle HS20:

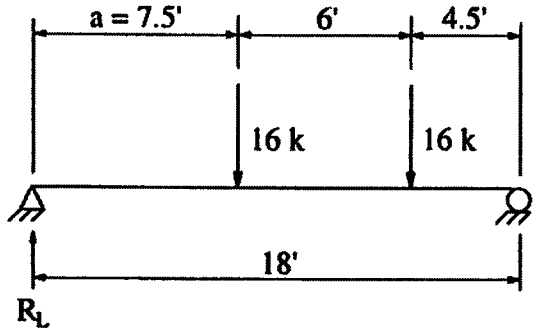

• Truck positioned to produce maximum moment

$M_{LL} = R_L a = (13.33)(7.5)$
$M_{LL} = 100.00$ ft-k

Vehicle Type 3:

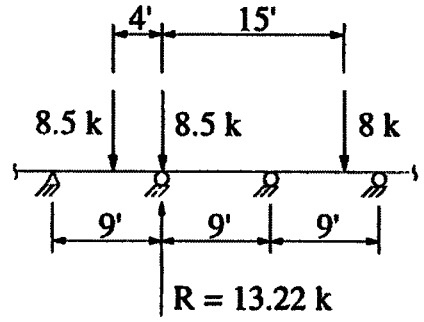

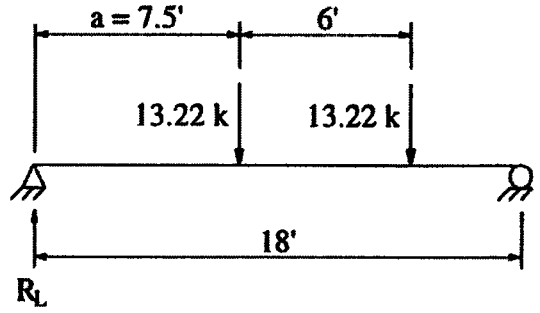

• Truck positioned to produce maximum moment

$M_{LL} = R_L a = (11.02)(7.5)$
$M_{LL} = 82.65$ ft-k

Capacity:

M_n = 299 ft-k (From laboratory test)

Rating:

$$RF_c = \frac{\phi M_n - \gamma_D M_{DL}}{\gamma_L M_{LL}(1+I)}$$

ϕ = 0.80 (Slight deterioration, careful inspection, intermittent maintenance)

γ_D = 1.2

γ_L = 1.3

I = 0.2

Vehicle HS20:

$$RF_c = \frac{(0.80)(299) - (1.2)(45.56)}{(1.3)(100)(1.2)}$$

RF_c = 1.18

Rating = (1.18)(36) = 42 T

Vehicle Type 3:

$$RF_c = \frac{(0.80)(299) - (1.2)(45.56)}{(1.3)(82.65)(1.2)}$$

RF_c = 1.43

Rating = (1.43)(25) = 35 T

Rating Modification:

$RF_T = RF_c K$

$K = 1 + K_a K_b$

Factor K_a:

$$K_a = \frac{\varepsilon_c}{\varepsilon_T} - 1$$

Theoretical Strains:

E_s = 29,000,000 psi

E_c = 3,700,000 psi

$$n = \frac{E_s}{E_c} = \frac{29,000,000}{3,700,000}$$

n = 8

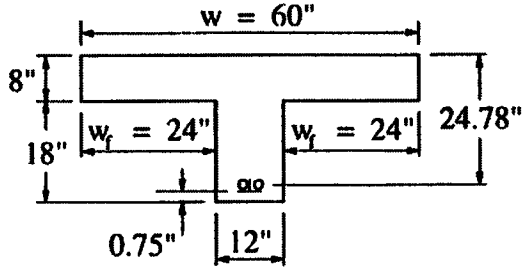

Flange Width:

i.) $w \leq 0.25L$

L = Length of beam

L = 20 ft

$w \leq 0.25(20)$
$w \leq 5$ ft

Overhanging Flange Width:

ii.) $w_f \leq 6t$

t = Slab thickness
$t = 8$ in.

$w_f \leq 6(8)$
$w_f \leq 48$ in.
$w_f = 24$ in. < 48 in.
or

iii.) $w_f \leq$ one-half clear distance to next web
$w_f \leq (0.5)(8)$
$w_f \leq 4$ ft
$w_f = 24$ in. < 4 ft
$\therefore$ Effective flange width = 5 ft

Steel:

2 L's: $2 \times 2 \times 1/4 = 2.38$ in.^{2}
f_y (L's) = 40 ksi (From laboratory tests)
2 Bars: $1.125\phi = 2$ in.^{2}
f_y (Bars) = 34 ksi (From laboratory tests)

$$A_s = 2\left(\frac{34}{40}\right) + 2.38$$

$A_s = 4.08$ in.^{2}

Moment From Test Vehicle:

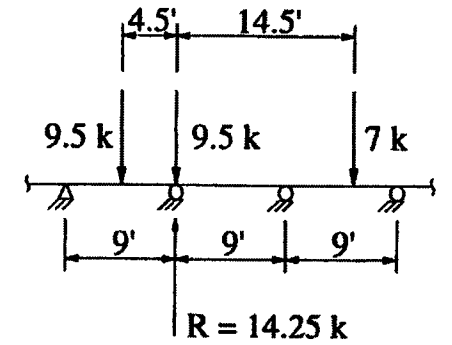

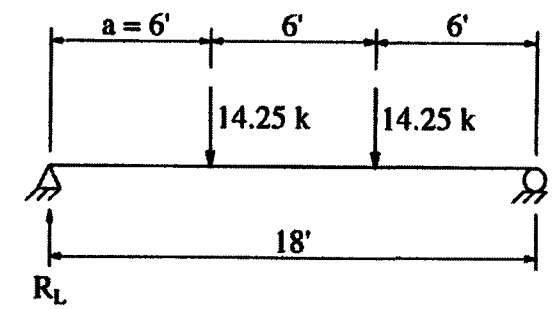

- Truck position obtained from field test

$M_T = R_L a$

M_T = Maximum theoretical live load moment due to test vehicle

$M_T = (14.25)(6)$
$M_T = 85.5$ ft-k

Stress in Steel (Cracked Section):

$$\sigma_s = \frac{M_s}{A_s jd}$$

$A_s = 4.08 \text{ in.}^2$

$j = 1 - \frac{k}{3}$

$d = 24.78 \text{ in.}$

$k = \sqrt{2\rho n + (\rho n)^2} - \rho n$

$\rho = \frac{A_s}{bd} = \frac{4.08}{(12)(24.78)}$

$\rho = 0.0137$

$n = 8$

$k = \sqrt{2(0.0137)(8) + [(0.0137)(8)]^2} - (0.0137)(8)$

$k = 0.371$

$j = 1 - \frac{0.371}{3} = 0.876$

$$\sigma_s = \frac{(85.5)(12)(1000)}{(4.08)(0.876)(24.78)}$$

$\sigma_s = 11{,}585 \text{ psi}$

$$\varepsilon_s = \frac{\sigma_s}{E_s}$$

ε_s = Calculated theoretical strain in steel

$$\varepsilon_s = \frac{11{,}585}{29{,}000{,}000}$$

$\varepsilon_s = 3.99 \times 10^{-4}$ in./in.

$\varepsilon_T = 1.43 \times 10^{-4}$ in./in.

ε_T = Strain produced by test vehicle

$$K_a = \frac{\varepsilon_s}{\varepsilon_T} - 1 = \frac{3.99 \times 10^{-4}}{1.43 \times 10^{-4}} - 1$$

$K_a = 1.79$

Factor K_b:

$K_b = K_{b1}K_{b2}K_{b3}$

Vehicle HS20:

K_{b1}: $\frac{T}{W} = \frac{M_T}{M_{LL}(1 + I)}$

$\frac{T}{W} = \frac{85.5}{100(1.2)}$

$\frac{T}{W} = 0.71$

$K_{b1} = 1.0$

Member behavior can be extrapolated to 1.33W for T/W > 0.7

Vehicle Type 3:

K_{b1}: $\frac{T}{W} = \frac{M_T}{M_{LL}(1 + I)}$

$\frac{T}{W} = \frac{85.5}{82.65(1.2)}$

$\frac{T}{W} = 0.86$

$K_{b1} = 1.0$

Member behavior can be extrapolated to 1.33W for T/W > 0.7

K_{b2}: 0.8 (Routine inspection between 1 and 2 years)

K_{b3}: 1.0 (Fatigue does not control, redundancy)

$K_b = (1.0)(0.8)(1.0)$
$K_b = 0.8$

$RF_T = RF_c(1 + K_aK_b)$

Vehicle HS20:

$RF_T = (1.18)(1 + (1.79)(0.8))$
$RF_T = 2.87$

Rating = (2.87)(36) = 103 T

Vehicle Type 3:

$RF_T = (1.43)(1 + (1.79)(0.8))$
$RF_T = 3.48$

Rating = (3.48)(25) = 87 T

III. Rating Hangers:

Dead Loads:

Curb:	(6)(1/12)(1.625)(9)(0.150)	= 1.10 k
Beam:	(0.225)(10)	= 2.25 k
Slab:	(0.900)(8.84)	= 7.96 k
Railing:	(1.80)(8.33)(0.150)	= 2.25 k
Self Weight:	(8)(1/12)(1.67)(8.83)(0.150)	= 1.48 k
		15.0 k

Live Loads:

(2 ft. from curb)

Vehicle HS20:

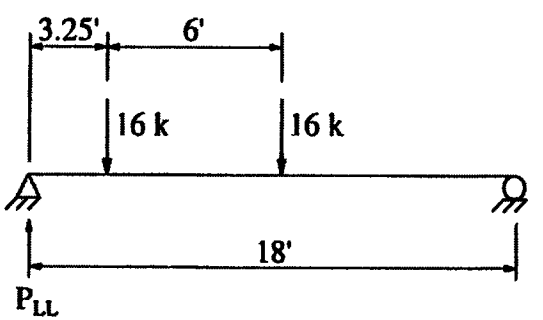

- Truck positioned to produce maximum axial force

P_{LL} = 20.9 k

P_{LL} = Maximum theoretical axial live load due to rating vehicle

Vehicle Type 3:

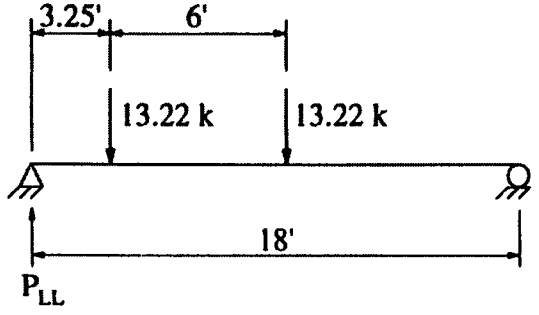

- Truck positioned to produce maximum axial force

P_{LL} = 17.3 k

Capacity:

4 L's: 2 x 2 x 1/4
Area (1) = 0.798 in.^{2} (Includes loss of section)
Total Area = 4(0.798) = 3.19 in.^{2}
f_y = 40 ksi (From laboratory tests)
$R_n = f_yA = (40)(3.19)$
R_n = 127.6 k

Rating:

$$RF_c = \frac{\phi R_n - \gamma_D D_L}{\gamma_L P_{LL}(1 + I)}$$

ϕ = 0.70 (Heavy deterioration, loss of section)
γ_D = 1.2
γ_L = 1.3
I = 0.2

Vehicle HS20:

$$RF_c = \frac{(0.70)(127.6) - (1.2)(15.0)}{(1.3)(20.9)(1.2)}$$

RF_c = 2.19

Rating = (2.19)(36) = 78 T

Vehicle Type 3:

$$RF_c = \frac{(0.70)(127.6) - (1.2)(15.0)}{(1.3)(17.3)(1.2)}$$

RF_c = 2.64

Rating = (2.64)(25) = 66 T

Rating Modification:

$RF_T = RF_cK$
$K = 1 + K_aK_b$

Factor K_a:

$$K_a = \frac{\varepsilon_c}{\varepsilon_T} - 1$$

Load Due to Test Vehicle:

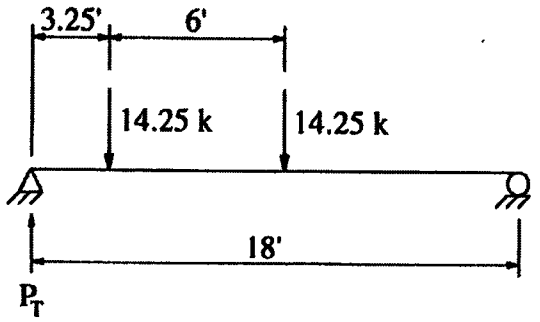

- Truck positioned to produce maximum axial force

P_T = 18.60 k

P_T = Maximum theoretical axial live load due to test vehicle

$$\frac{P_T}{\text{No. of Angles}} = \frac{18.6}{4} = 4.65 \text{ k}$$

$$\sigma_s = \frac{P}{A} = \frac{(4.65)(1000)}{0.798}$$

σ_s = 5,827 psi

$$\varepsilon_s = \frac{\sigma_s}{E_s}$$

ε_s = Calculated theoretical strain in steel

$$\varepsilon_s = \frac{5{,}827}{29{,}000{,}000}$$

$\varepsilon_s = 2.01 \times 10^{-4}$ in./in.

$\varepsilon_T = 70 \times 10^{-6}$ in./in.

ε_T = Strain produced by test vehicle

$$K_a = \frac{\varepsilon_s}{\varepsilon_T} - 1 = \frac{2.01 \times 10^{-4}}{70 \times 10^{-6}} - 1$$

K_a = 1.87

Factor K_b:

$K_b = K_{b1}K_{b2}K_{b3}$

Vehicle HS20:

$$K_{b1}: \frac{T}{W} = \frac{P_T}{P_{LL}(1 + I)}$$

$$\frac{T}{W} = \frac{18.6}{20.9(1.2)}$$

$$\frac{T}{W} = 0.74$$

$K_{b1} = 1.0$

Member behavior can be extrapolated to 1.33W for T/W > 0.7

Vehicle Type 3:

$$K_{b1}: \quad \frac{T}{W} = \frac{P_T}{P_{LL}(1 + I)}$$

$$\frac{T}{W} = \frac{18.6}{17.3(1.2)}$$

$$\frac{T}{W} = 0.90$$

$K_{b1} = 1.0$

Member behavior can be extrapolated to 1.33W and T/W > 0.7

K_{b2}: 0.8 (Routine inspection between 1 and 2 years)

K_{b3}: 1.0 (Fatigue does not control, redundancy)

$K_b = (1.0)(0.8)(1.0)$
$K_b = 0.8$

$RF_T = RF_c(1 + K_aK_b)$

Vehicle HS20:

$RF_T = (2.19)(1 + (1.87)(0.8))$
$RF_T = 5.47$

Rating = (5.47)(36) = 196 T

Vehicle Type 3:

$RF_T = (2.64)(1 + (1.87)(0.8))$
$RF_T = 6.59$

Rating = (6.59)(25) = 164 T

IV. Rating of Arches:

At Crown:

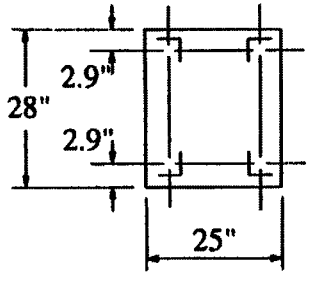

A_s = 4 L's: 3 x 3 x 5/16 = 4(1.78)
$A_s = 7.12 \text{ in.}^2$
$f_c' = 4.3$ ksi (From laboratory tests)
$f_y = 40$ ksi (From laboratory tests)

Dead Loads:

All reactions determined using structural analysis software.

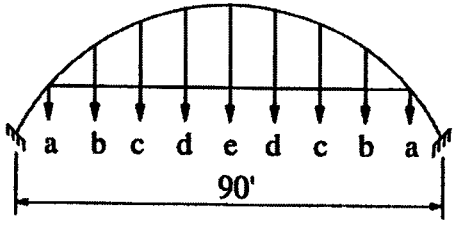

a = 13.9 k c = 14.6 k e = 15 k
b = 14 k d = 14.9 k

∴ At crown of arch:

P_{DL} = 150.44 k

M_{DL} = 39.63 ft-k

Live Loads:

Vehicle HS20:

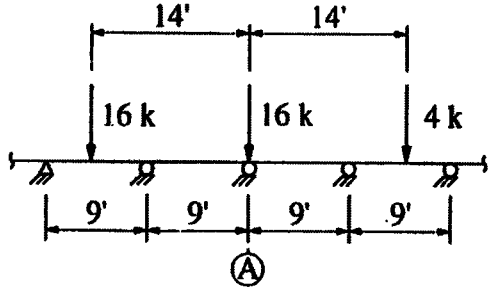

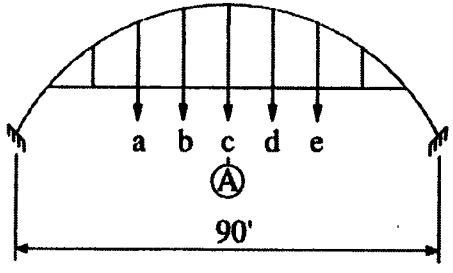

a = 11.6 k c = 20.9 k e = 2.9 k
b = 9.3 k d = 2.3 k

∴ At crown of arch:

P_{LL} = 57.04 k

M_{LL} = 81.52 ft-k

Vehicle Type 3:

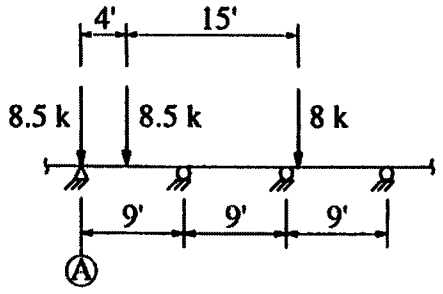

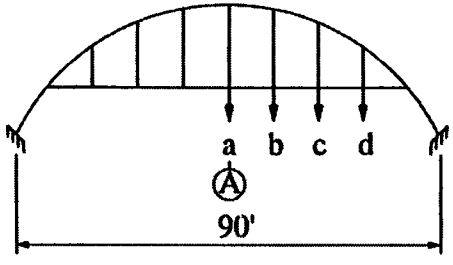

a = 17.3 k c = 9.7 k
b = 4.9 k d = 1.2 k

∴ At crown of arch:

P_{LL} = 39.85 k
M_{LL} = 65.15 ft-k

Capacity:

Assumed average Eccentricity of Axial Load on the Arch:

$$e_{AVG} = \frac{\left(\frac{M_{LL} + M_{DL}}{P_{LL} + P_{DL}}\right)_{HS20} + \left(\frac{M_{LL} + M_{DL}}{P_{LL} + P_{DL}}\right)_{Type\ 3}}{2}$$

$$e_{AVG} = \frac{\left(\frac{(81.52 + 39.63)(12)}{(150.44 + 57.04)}\right) + \left(\frac{(65.15 + 39.63)(12)}{(150.44 + 39.85)}\right)}{2}$$

$$e_{AVG} = \frac{7.01 + 6.61}{2}$$

e_{AVG} = 6.8 in.

P_n = 1,450 k
M_n = 820 ft-k
} From column interaction diagram

Rating:

$$RF_c = \frac{\phi P_n - \gamma_D P_{DL}}{\gamma_L P_{LL}(1 + I)} \text{ or } = \frac{\phi M_n - \gamma_D M_{DL}}{\gamma_L M_{LL}(1 + I)}$$

γ_D = 1.2
γ_L = 1.3
I = 0.2
ϕ = 0.70 (Heavy deterioration, careful inspection, intermittent maintenance)

Vehicle HS20:

Axial Load:

$$RF_c = \frac{(0.70)(1450) - (1.2)(150.44)}{(1.3)(57.04)(1.2)}$$

$RF_c = 9.38$

Rating = (9.38)(36) = 337 T

Moment:

$$RF_c = \frac{(0.70)(820) - (1.2)(39.63)}{(1.3)(81.52)(1.2)}$$

$RF_c = 4.14$

Rating = (4.14)(36) = 149 T

Vehicle Type 3:

Axial Load:

$$RF_c = \frac{(0.70)(1450) - (1.2)(150.44)}{(1.3)(39.85)(1.2)}$$

$RF_c = 13.42$

Rating = (13.42)(25) = 335 T

Moment:

$$RF_c = \frac{(0.70)(820) - (1.2)(39.63)}{(1.3)(65.15)(1.2)}$$

$RF_c = 5.18$

Rating = (5.18)(25) = 129 T

Rating Modification:

$RF_T = RF_cK$

$K = 1 + K_aK_b$

Factor K_a:

$$K_a = \frac{\varepsilon_s}{\varepsilon_T} - 1$$

Axial Load and Moment Due to Test Vehicle:

All reactions determined using structural analysis software.

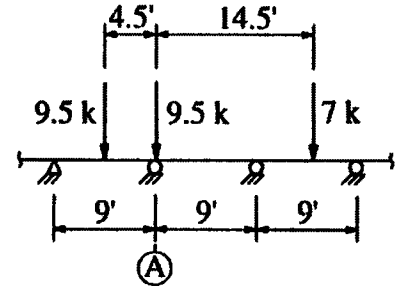

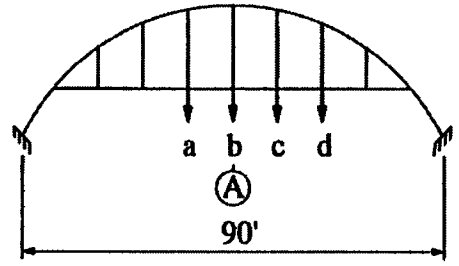

a = 6.2 k c = 3.6 k

b = 18.6 k d = 5.6 k

∴ At crown of arch:

P_T = 43.4 k

M_T = 77 ft-k

Theoretical Stress/Strain:

Analyzed as a cracked section.

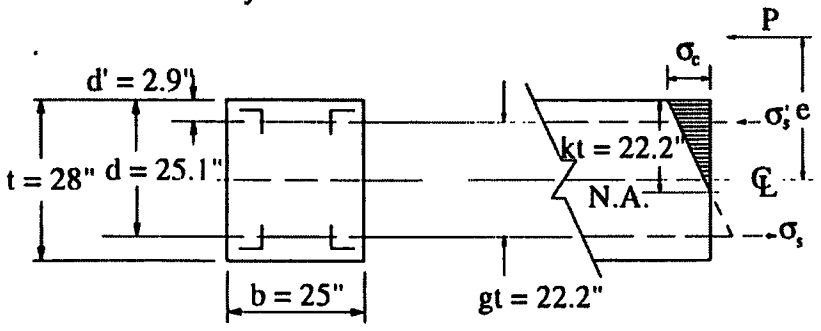

E_s = 29,000,000 psi

E_c = 3,700,000 psi

$$n = \frac{E_s}{E_c} = 8$$

P_T = 43.4 k

M_T = 77.03 ft-k

$$e = \frac{M_T + M_{DL}}{P_T + P_{DL}} = \frac{(77 + 39.6)(12)}{43.4 + 150.4}$$

e = 7.2 in.

Stress in Bottom Steel:

$$\sigma_s = n\sigma_c\left(\frac{d}{kt}\right) - 1$$

Stress in Concrete:

$$\sigma_c = \frac{P_T}{bt}\left(\frac{2k}{k^2 + 2n\rho_g k - n\rho_g}\right)$$

Determine Location of Neutral Axis:

$$k^3 - 3\left(\frac{1}{2} - \frac{e}{t}\right)k^2 + 6n\rho_g\frac{ke}{t} - 3n\rho_g\left(\frac{e}{t} + \frac{1}{2}g^2\right) = 0$$

$$\rho_g = \frac{A_s}{bt} = \frac{7.12}{(25)(28)}$$

$$\rho_g = 0.0102$$

$$g = 0.79$$

$$k^3 - 3\left(\frac{1}{2} - \frac{7.2}{28}\right)k^2 + 6(8)(0.0102)\left(\frac{7.2}{28}\right)k - 3(8)(0.0102)\left(\frac{7.2}{28} + \frac{1}{2}(0.79)^2\right) = 0$$

$$k^3 - 0.729k^2 + 0.126k - 0.139 = 0$$

$$k = 0.79$$

$$\sigma_c = \frac{(43.4)(1000)}{(25)(28)}\left(\frac{2(0.79)}{(0.79)^2 + 2(8)(0.0102)(0.79) - (8)(0.0102)}\right)$$

$$\sigma_c = 145 \text{ psi}$$

$$\sigma_s = 8(145)\left(\frac{25.1}{(0.79)(28)} - 1\right)$$

$$\sigma_s = 156 \text{ psi}$$

$$\varepsilon_c = \frac{\sigma_c}{E_c}$$

ε_c = Calculated theoretical strain in concrete

$$\varepsilon_c = \frac{145}{3{,}700{,}000}$$

$\varepsilon_c = 3.92 \times 10^{-5}$ in./in.

$$\varepsilon_s = \frac{\sigma_s}{E_s}$$

ε_s = Calculated theoretical strain in steel

$$\varepsilon_s = \frac{156}{29{,}000{,}000}$$

$\varepsilon_s = 5.38 \times 10^{-6}$ in./in.

$\varepsilon_{Tc} = 52 \times 10^{-6}$ in./in.

ε_{Tc} = Strain in concrete produced by test vehicle

$\varepsilon_{Ts} = 17 \times 10^{-6}$ in./in

ε_{Ts} = Strain in steel produced by test vehicle

$$K_a = \frac{\varepsilon_s}{\varepsilon_{Ts}} - 1 = \frac{5.38 \times 10^{-6}}{17 \times 10^{-6}} - 1$$

$K_a = -0.68$

Factor K_b:

$K_b = K_{b1}K_{b2}K_{b3}$

Vehicle HS20:

K_{b1}:

$$\frac{T}{W} = \frac{M_T}{M_{LL}(1 + I)}$$

$$\frac{T}{W} = \frac{77}{(81.52)(1.2)}$$

$$\frac{T}{W} = 0.79$$

$K_{b1} = 1.0$

Member behavior can be extrapolated to 1.33W for T/W > 0.7

Vehicle Type 3:

K_{b1}:

$$\frac{T}{W} = \frac{M_T}{M_{LL}(1 + I)}$$

$$\frac{T}{W} = \frac{77}{(65.15)(1.2)}$$

$$\frac{T}{W} = 0.98$$

$K_{b1} = 1.0$

Member behavior can be extrapolated to 1.33W for T/W > 0.7

K_{b2}: 0.8 (Routine inspection between 1 and 2 years)

K_{b3}: 0.9 (Fatigue does not control, no redundancy)

$K_b = (1.0)(0.8)(0.9)$
$K_h = 0.72$

$RF_T = RF_c(1 + K_aK_b)$

Vehicle HS20:

$RF_T = (4.14)(1 + (-0.68)(0.72))$
$RF_T = 2.11$

Rating = (2.11)(36) = 75 T

Vehicle Type 3:

$RF_T = (5.18)(1 + (-0.68)(0.72))$
$RF_T = 2.64$

Rating = (2.64)(25) = 66 T

Table B.1. Bridge I: Rating Summary:

	Vehicle HS20				Vehicle Type 3			
	AASHTO LRFR		Modified Rating		AASHTO LRFR		Modified Rating	
	RF_c	R(tons)	RF_T	R(tons)	RF_c	R(tons)	RF_T	R(tons)
Slab:	0.94	33.8			1.50	37.5		
Beams:	1.18	42.5	2.87	103.3	1.43	35.8	3.48	87.0
Hangers:	2.19	78.8	5.47	196.9	2.64	66.0	6.59	164.8
Arches:	4.14	149.0	2.11	76.0	5.18	129.5	2.64	66.0

indicates controlling component

BRIDGE II
BOONE MARSH ARCH BRIDGE NO. 134
Year Built: 1919

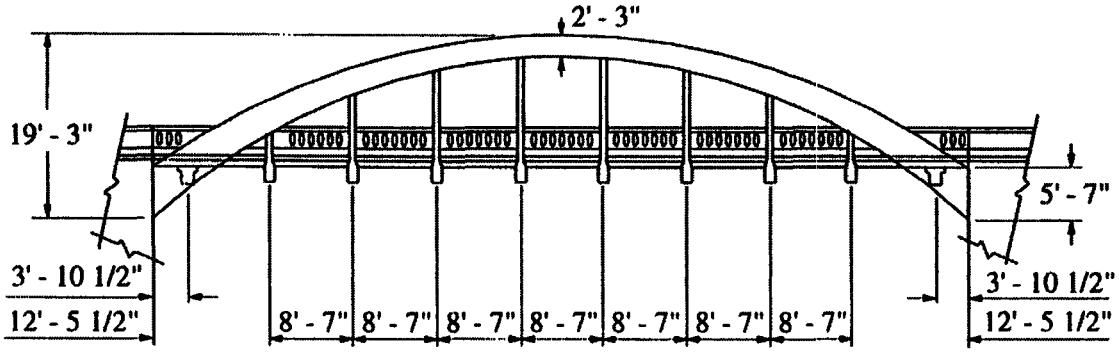

ELEVATION

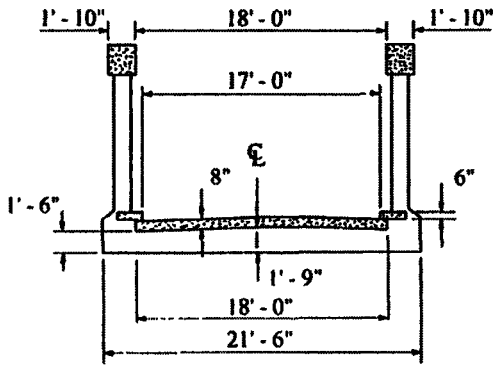

TYPICAL CROSS-SECTION

I. Rating Slab:

Effective Span = Clear Span:

8.58 - 1 = 7.58 ft

Dead Load:

8(1/12)(1)(0.150) = 0.100 k/ft/ft width

Dead Load Moment:

$+M_{DL} = M_{coef}\, wL^2$

M_{coef} = Moment coefficient obtained from AISC Moments, Shears, and Reactions for Continuous Highway Bridges [16]

$+M_{DL} = 0.078(0.100)(7.58)^2$

$+M_{DL} = 0.448$ ft-k/ft width

$-M_{DL} = M_{coef}\, wL^2 = 0.106(0.100)(7.58)^2$

$-M_{DL} = 0.609$ ft-k/ft width

Live Load Moment:

$E = 4 + 0.06(s)$

E = Wheel Distribution

s = Slab Length

$E = 4 + 0.06(7.58)$

$E = 4.45$ ft

Vehicle HS20:

$$+ M_{LL} = \frac{M_{coef}PL}{E}$$

M_{LL} = Maximum theoretical live load moment due to rating vehicle

$$+ M_{LL} = \frac{(0.2040)(16)(7.58)}{4.45} + \frac{(0.0076)(16)(7.58)}{4.45}$$

$+ M_{LL} = 5.76$ ft-k/ft width

$$- M_{LL} = \frac{M_{coef}PL}{E}$$

$$- M_{LL} = \frac{(0.1029)(16)(7.58)}{4.45}$$

$- M_{LL} = 2.80$ ft-k/ft width

Vehicle Type 3:

$$+ M_{LL} = \frac{M_{coef}PL}{E}$$

$$+ M_{LL} = \frac{(0.2040)(8)(7.58)}{4.45} + \frac{(0.0217)(8)(7.58)}{4.45}$$

$+ M_{LL} = 3.08$ ft-k/ft width

$$- M_{LL} = \frac{M_{coef}PL}{E}$$

$$- M_{LL} = \frac{(0.0956)(8)(7.58)}{4.45} + \frac{(0.0634)(8)(7.58)}{4.45}$$

$- M_{LL} = 2.17$ ft-k/ft width

Flexural Design Strength:

Due to loss of cover, the top bars are exposed.

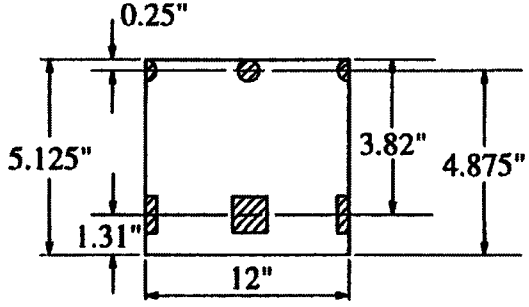

$f_c' = 4.5$ ksi (Obtained from laboratory tests)
$f_y = 47$ ksi (Obtained from laboratory tests)
1/2 in. ϕ Bars at top
5/8 in. Square bars at bottom
$A_{s_{(TOP)}} = 2(0.2) = 0.40$ in.^{2}
$A_{s_{(BOT)}} = 2(0.625)(0.625) = 0.78$ in.^{2}

Positive Moment:

Determine Minimum Steel Ratio that will Ensure Yielding of the Compression Steel:

$$\rho_{min} = \frac{0.85\beta_1 f_c' d' (87{,}000)}{f_y d(87{,}000 - f_y)} + \rho'$$

$$\beta_1 = 0.825$$

$$\rho' = \frac{A_s'}{bd} = \frac{0.40}{(12)(3.82)}$$

$$\rho' = 0.00873$$

$$\rho_{min} = \frac{0.85(0.825)(4.5)(0.25)(87{,}000)}{(47)(3.82)(87{,}000 - 47{,}000)} + 0.00873$$

$$\rho_{min} = 0.0183$$

$$\rho = \frac{A_s}{bd} = \frac{0.78}{(12)(3.82)}$$

$\rho = 0.170 < \rho_{min} = 0.183$
Compression steel does not yield

Check Maximum Steel Ratio Permitted:

$$\rho_{max} = 0.75\rho_b + \rho' \frac{f_s'}{f_y}$$

$$\rho_b = \frac{0.85\beta_1 f_c' (87{,}000)}{f_y(87{,}000 + f_y)}$$

$$\rho_b = \frac{0.85(0.825)(4.5)(87{,}000)}{(47)(87{,}000 + 47{,}000)}$$

$$\rho_b = 0.0436$$

$f_s' = 47$ ksi
$f_y = 47$ ksi

$$\rho_{max} = (0.75)(0.0436) + 0.00873\left(\frac{47}{47}\right)$$

$$\rho_{max} = 0.0414$$

$\rho = 0.0170 < \rho_{max} = 0.0414$

Determine Moment Capacity Based on Compression Steel Not Yielding:

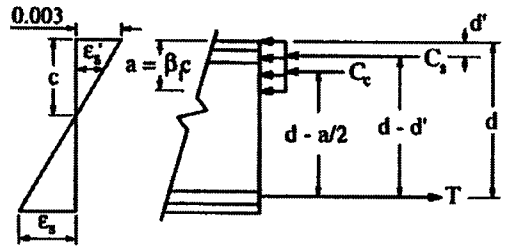

$T = A_s f_y$

$C_c = 0.85 f_c' ba$

$C_s = E_s \varepsilon_s' A_s'$

From strain equilibrium:

$$\varepsilon_s' = \left(\frac{c - d'}{c}\right)(0.003)$$

$$c = \frac{a}{\beta_1}$$

$$\varepsilon_s' = \left(1 - \frac{\beta_1 d'}{a}\right)(0.003)$$

Determine depth of stress block:

From equilibrium:

$C_c + C_s = T$

$$0.85f_c'ba + E_sA_s'\left(1 - \frac{\beta_1 d'}{a}\right)(0.003) = A_sf_y$$

or

$$(0.85f_c'b)a^2 + (0.003E_sA_s' - A_sf_y)a - (0.003E_sA_s'\beta_1 d') = 0$$

$$((0.85)(4500)(12))a^2 + (0.003(29{,}000{,}000)(0.40) - (0.78)(47{,}000))a - (0.003(29{,}000{,}000)(0.40)(0.825)(0.25)) = 0$$

$$45{,}900a^2 - 1{,}860a - 7178 = 0$$

$$a = 0.416 \text{ in.}$$

$C_c = 0.85f_c'ba = 0.85(4.5)(12)(0.416)$
$C_c = 19.09 \text{ k}$

$C_s = E_s\varepsilon_s'A_s'$

$$\varepsilon_s' = \left(1 - \frac{\beta_1 d'}{a}\right)(0.003) = \left(1 - \frac{(0.825)(0.25)}{0.416}\right)(0.003)$$

$\varepsilon_s' = 1.51 \times 10^{-3}$ in./in.

$C_s = (29{,}000)(1.51 \times 10^{-3})(0.40)$
$C_s = 17.52 \text{ k}$

$$M_n = C_c\left(d - \frac{a}{2}\right) + C_s(d - d')$$

$$M_n = \frac{19.09\left(3.82 - \frac{0.416}{2}\right) + 17.52(3.82 - 0.25)}{12}$$

$M_n = 10.95$ ft-k/ft width

Negative Moment:

Determine location of neutral axis: (Assume 5/8 in. bars are below the neutral axis)

$T = C_c - T_s$

$T = A_s F_y = (0.40)(47) = 18\ k$

$C_c = 0.85 f_c' ba = 0.85(4.5)(12)(0.825)c = 37.87c$

$$T_s = A_s' E_s \left(\frac{d' - c}{c}\right)(0.003) = (0.78)(29{,}000)\left(\frac{1.31 - c}{c}\right)(0.003) = 67.86\left(\frac{1.31 - c}{c}\right)$$

$$18 = 37.87c - 67.86\left(\frac{1.31 - c}{c}\right)$$

$$0 = 37.87c^2 + 49.86c - 88.90$$

$c = 1.0$ in.

Since the 5/8 in. bars are so close to the neutral axis, they will be neglected in the analysis.

$$\rho = \frac{A_s}{bd} = \frac{0.40}{(12)(4.875)}$$

$\rho = 0.00684$

$\rho_{max} = 0.75\rho_b$

$$\rho_b = \frac{0.85\beta_1 f_c'(87{,}000)}{f_y(87{,}000 + f_y)}$$

$\beta_1 = 0.825$

$$\rho_b = \frac{0.85(0.825)(4.5)(87{,}000)}{(47)(87{,}000 + 47{,}000)}$$

$$\rho_b = 0.0436$$

$$\rho_{max} = 0.75(0.0436)$$

$$\rho_{max} = 0.0327$$

$$\rho = 0.00684 < \rho_{max} = 0.0327$$

$\therefore$ Tension steel yields

$$M_n = A_s f_y\left(d - \frac{a}{2}\right)$$

$$a = \frac{A_s f_y}{0.85 f_c' b}$$

$$a = \frac{(0.4)(47)}{(0.85)(4.5)(12)}$$

$$a = 0.41 \text{ in.}$$

$$M_n = \frac{(0.40)(47)\left(4.875 - \frac{0.41}{2}\right)}{12}$$

$$M_n = 7.32 \text{ ft-k}$$

Rating:

$$RF_c = \frac{\phi M_n - \gamma_D M_{DL}}{\gamma_L M_{LL}(1 + I)}$$

ϕ = 0.70 (Heavy deterioration, careful inspection, intermittent maintenance)

γ_D = 1.2

γ_L = 1.3

I = 0.2 (Poor condition)

Vehicle HS20:

Positive Moment:

$$RF_c = \frac{(0.7)(10.95) - (1.2)(0.448)}{(1.3)(5.76)(1.2)}$$

$$RF_c = 0.79$$

Rating = (0.79)(36) = 28 T

Negative Moment:

$$RF_c = \frac{(0.7)(7.32) - (1.2)(0.609)}{(1.3)(2.8)(1.2)}$$

$$RF_c = 1.00$$

Rating = (1.00)(36) = 36 T

Vehicle Type 3:

Positive Moment:

$$RF_c = \frac{(0.7)(10.95) - (1.2)(0.448)}{(1.3)(3.08)(1.2)}$$

$$RF_c = 1.48$$

Rating = (1.48)(25) = 37 T

Negative Moment:

$$RF_c = \frac{(0.7)(7.32) - (1.2)(0.609)}{(1.3)(2.17)(1.2)}$$

$RF_c = 1.30$

Rating = (1.30)(25) = 32.5 T

II. Rating Beam:

Dead Load:

Self Weight: $(1)\left(\frac{1.5 + 1.75}{2}\right)(0.150) = 0.244$ k/ft

Slab: $(0.100)(8.58) = 0.858$ k/ft

1.102 k/ft

Dead Load Moment:

$$M_{DL} = \frac{wL^2}{8} = \frac{(1.10)(20)^2}{8}$$

$M_{DL} = 55.09$ ft-k

Live Load Moment:

Vehicle HS20:

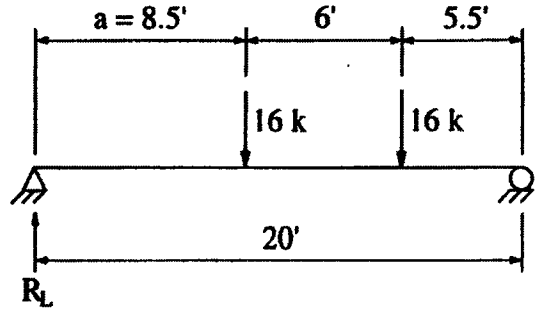

- Truck positioned to produce maximum moment

$M_{LL} = R_L a = (13.6)(8.5)$

$M_{LL} = 115.60$ ft-k

Vehicle Type 3:

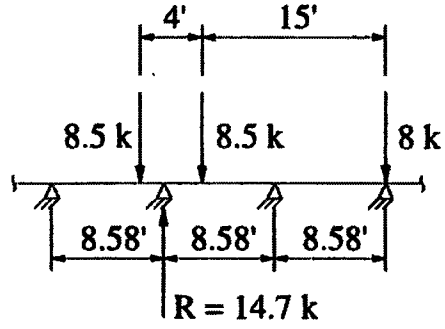

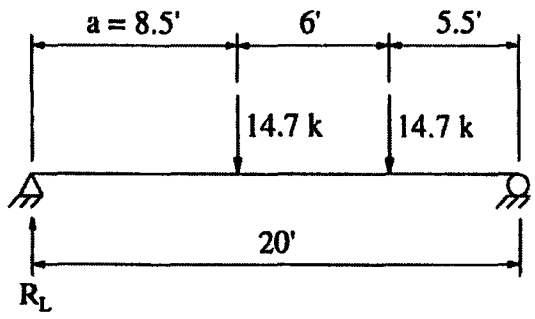

• Truck positioned to produce maximum moment

$M_{LL} = R_L a = (12.50)(8.5)$
$M_{LL} = 106.25$ ft-k

Flexural Design Strength:

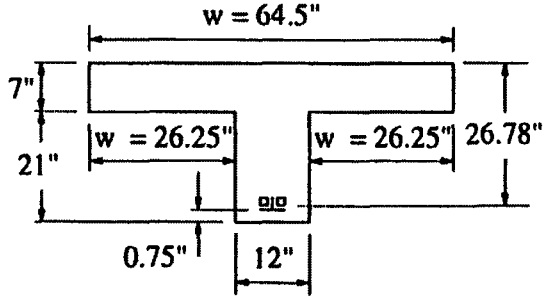

Flange Width:
i.) $w \leq 0.25L$

L = Length of beam
L = 21.5 ft

$w \leq 0.25(21.5)$
$w \leq 64.5$ in.

Overhanging Flange Width:
ii.) $w_f \leq 6t$

t = Slab thickness
t = 8 in.

$w_f \leq 6(8)$
$w_f \leq 48$ in.
$w_f = 26.26$ in. ≤ 48 in.
or
iii.) $w_f \leq$ One-half clear distance to next web
$w_f \leq 0.5(91)$
$w_f \leq 45$ in.
$w_f = 26.25$ in. < 45 in.

Steel:
2 L's: 2 1/2 x 2 1/2 x 1/4 = 2.38 in.^{2}
f_y (L's) = 42 ksi (From laboratory tests)
2 Square bars = 2 in.^{2}
f_y (Bars) = 47 ksi (From laboratory tests)

$$A_s = 2.38\left(\frac{42}{47}\right) + 2$$

$A_s = 4.13$ in.^{2}
$E_c = 3{,}800$ ksi
$E_s = 29{,}000$ ksi

$$\rho = \frac{A_s}{bd} = \frac{4.13}{(64.5)(26.78)}$$

$\rho = 0.00239$

$\rho_{max} = 0.75\rho_b$

$$\rho_b = \frac{0.85\beta_1 f_c'(87{,}000)}{f_y(87{,}000 + f_y)}$$

$\beta_1 = 0.825$

$$\rho_b = \frac{0.85(0.825)(4.5)(87{,}000)}{(47)(87{,}000 + 47{,}000)}$$

$\rho_b = 0.0436$

$\rho_{max} = 0.75(0.0436)$

$\rho_{max} = 0.0327$

$\rho = 0.00239 < \rho_{max} = 0.0327$

$\therefore$ Tension steel yields

$$M_n = A_s f_y\left(d - \frac{a}{2}\right)$$

$f_y = 47$ ksi

$f_c' = 4.5$ ksi (Obtained from laboratory tests)

$d = 26.78$ in

$$a = \frac{A_s f_y}{0.85 f_c' b}$$

$$a = \frac{(4.13)(47)}{(0.85)(4.5)(64.5)}$$

$a = 0.787$ in.

$$M_n = \frac{(4.13)(47)\left(26.78 - \frac{0.787}{2}\right)}{12}$$

$M_n = 426.82$ ft-k

Rating:

$$RF_c = \frac{\phi M_n - \gamma_D M_{DL}}{\gamma_L M_{LL}(1+I)}$$

$\phi = 0.85$ (No deterioration, intermittent maintenance)

$\gamma_D = 1.2$

$\gamma_L = 1.3$

$I = 0.2$

Vehicle HS20:

$$RF_c = \frac{362.80 - (1.2)(55.09)}{(1.3)(115.6)(1.2)}$$

$RF_c = 1.65$

Rating = (1.65)(36) = 59 T

Vehicle Type 3:

$$RF_c = \frac{362.80 - (1.2)(55.09)}{(1.3)(106.25)(1.2)}$$

$$RF_c = 1.79$$

Rating = (1.79)(25) = 44 T

Rating Modification:

$$RF_T = RF_cK$$

$$K = 1 + K_aK_b$$

Factor K_a:

$$K_a = \frac{\varepsilon_c}{\varepsilon_T} - 1$$

Theoretical Strains:

E_s = 29,000,000 psi

E_c = 3,800,000 psi

$$n = \frac{E_s}{E_c} = \frac{29,000,000}{3,800,000}$$

n = 8

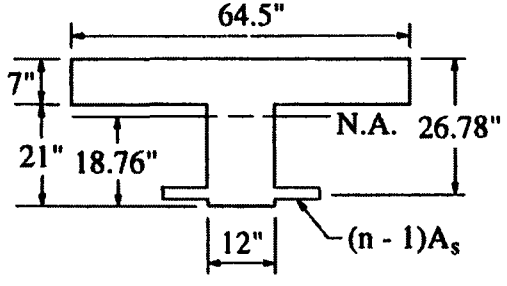

Equivalent Section:

$(n - 1)A_s = (8 - 1)(4.13)$

$(n - 1)A_s = 28.91$ in.^{2}

Location of Neutral Axis:

$\bar{y} = 18.76$ in.

Moment of Inertia:

$$I_g = \frac{bh^3}{12} + Ad^2$$

$I_g = 52,068$ in.^{4}

Moment From Test Vehicle:

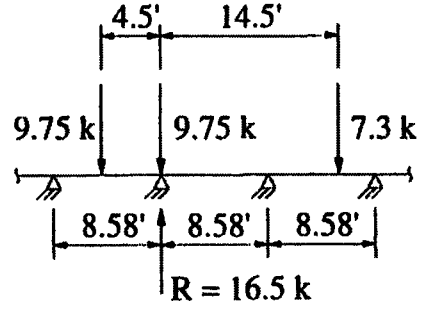

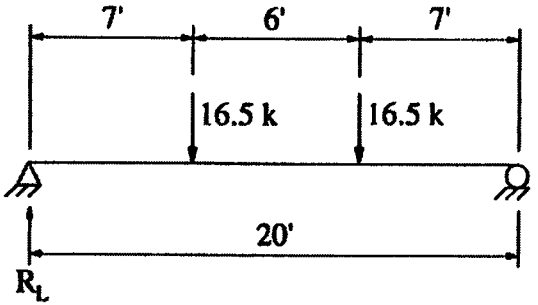

- Truck position obtained from field test

$M_T = R_L a$

M_T = Maximum theoretical live load moment due to test vehicle

$M_T = (16.5)(7)$

$M_T = 115.5$ ft-k

Theoretical Stress (Uncracked Section):

$$\sigma_c = \frac{M_T y}{I_g}$$

$$\sigma_c = \frac{(115.5)(12)(1000)(18.76)}{52{,}068}$$

$\sigma_c = 499$ psi

$$\varepsilon_c = \frac{\sigma_c}{E_c}$$

ε_c = Calculated theoretical strain in concrete

$$\varepsilon_c = \frac{499}{3{,}800{,}000}$$

$\varepsilon_c = 1.31 \times 10^{-4}$ in./in.

$\varepsilon_T = 51 \times 10^{-6}$ in./in.

ε_T = Strain produced by test vehicle

$$K_a = \frac{\varepsilon_c}{\varepsilon_T} - 1 = \frac{1.31 \times 10^{-4}}{51 \times 10^{-6}} - 1$$

$K_a = 1.57$

Factor K_b:

$K_b = K_{b1}K_{b2}K_{b3}$

Vehicle HS20:

$$K_{b1}: \frac{T}{W} = \frac{M_T}{M_{LL}(1 + I)}$$

$$\frac{T}{W} = \frac{115.5}{(115.6)(1.2)}$$

$$\frac{T}{W} = 0.83$$

$K_{b1} = 1.0$

Member behavior can be extrapolated to 1.33W for T/W > 0.7

Vehicle Type 3:

$$K_{b1}: \quad \frac{T}{W} = \frac{M_T}{M_{LL}(1 + I)}$$

$$\frac{T}{W} = \frac{115.5}{(106.21)(1.2)}$$

$$\frac{T}{W} = 0.91$$

$K_{b1} = 1.0$

Member behavior can be extrapolated to 1.33W for T/W > 0.7

K_{b2}: 0.8 (Routine inspection between 1 and 2 years)

K_{b3}: 1.0 (Fatigue does not control, redundancy)

$K_b = (1.0)(0.8)(1.0)$
$K_b = 0.80$

$RF_T = RF_c(1 + K_aK_b)$

Vehicle HS20:

$RF_T = (1.65)(1 + (1.57)(0.80))$
$RF_T = 3.72$

Rating = (3.72)(36) = 133 T

Vehicle Type 3:

$RF_T = (1.79)(1 + (1.57)(0.8))$
$RF_T = 4.04$

Rating = (4.04)(25) = 101 T

III. Rating Hangers:

Dead Loads:

Curb:	(6)(1/12)(1.75)(8.583)(0.150)	= 1.13 k
Beam:	(0.244)(10.75)	= 2.62 k
Slab:	(0.858)(9)	= 7.72 k
Railing:	(1.80)(7.58)(0.150)	= 2.05 k
Self Weight:	(7/12)(16/12)(10.8)(0.150)	= 1.26 k
		14.8 k

Live Loads:
(2 ft. from curb)

Vehicle HS20:

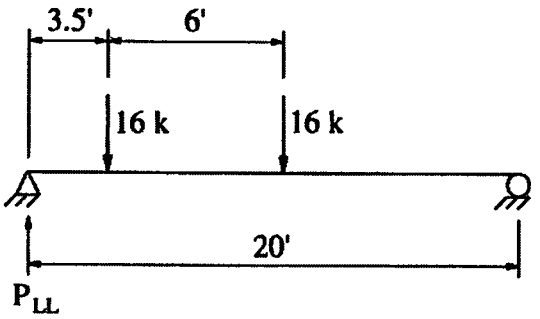

- Truck positioned to produce maximum axial force

P_{LL} = 21.6 k

P_{LL} = Maximum theoretical axial live load due to rating vehicle

Vehicle Type 3:

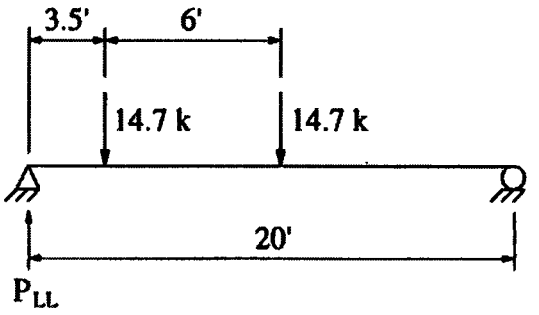

- Truck positioned to produce maximum axial force

P_{LL} = 19.8 k

Capacity:

4 L's: 2 x 2 x 1/4
Area (1) = 0.938 in.^{2}
Total Area = 4(0.938) = 3.75 in.^{2}
f_y = 42 ksi (Obtained from laboratory tests)
$R_n = f_yA = (42)(3.75)$
R_n = 157.5 k

Rating:

$$RF_c = \frac{\phi R_n - \gamma_D D_L}{\gamma_L P_{LL}(1 + I)}$$

ϕ = 0.80 (Slight deterioration, careful inspection, intermittent maintenance)

$\gamma_D = 1.2$
$\gamma_L = 1.3$
$I = 0.3$

Vehicle HS20:

$$RF_c = \frac{(0.80)(157.5) - (1.2)(14.8)}{(1.3)(21.6)(1.2)}$$

$RF_c = 3.21$

Rating = (3.21)(36) = 115 T

Vehicle Type 3:

$$RF_c = \frac{(0.80)(157.5) - (1.2)(14.8)}{(1.3)(19.8)(1.2)}$$

$RF_c = 3.50$

Rating = (3.50)(25) = 87 T

Rating Modification:

$RF_T = RF_cK$

$K = 1 + K_aK_b$

Factor K_a:

$$K_a = \frac{\varepsilon_c}{\varepsilon_T} - 1$$

Load Due to Test Vehicle:
(1.67 ft from curb)

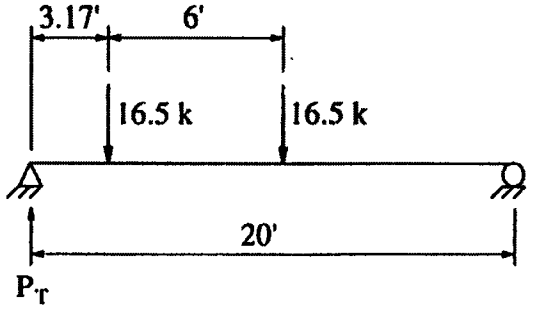

- Truck positioned to produce maximum axial force

$P_T = 22.8$ k

P_T = Maximum theoretical axial live load due to test vehicle

$$\frac{P_T}{\text{No. of Angles}} = \frac{22.8}{4} = 5.7 \text{ k}$$

$$\sigma_s = \frac{P}{A} = \frac{(5.7)(1000)}{0.938}$$

$\sigma_s = 6{,}077$ psi

$$\varepsilon_s = \frac{\sigma_s}{E_s}$$

ε_s = Calculated theoretical strain in steel

$$\varepsilon_s = \frac{6{,}077}{29{,}000{,}000}$$

$\varepsilon_s = 2.10 \times 10^{-4}$ in./in.

$\varepsilon_T = 95 \times 10^{-6}$ in./in.

ε_T = Strain produced by test vehicle

$$K_a = \frac{\varepsilon_s}{\varepsilon_T} - 1 = \frac{2.10 \times 10^{-4}}{95 \times 10^{-6}} - 1$$

$K_a = 1.21$

Factor K_b:

$K_b = K_{b1}K_{b2}K_{b3}$

Vehicle HS20:

K_{b1}: $\frac{T}{W} = \frac{P_T}{P_{LL}(1 + I)}$

$\frac{T}{W} = \frac{22.8}{21.6(1.2)}$

$\frac{T}{W} = 0.88$

$K_{b1} = 1.0$

Member behavior can be extrapolated to 1.33W for T/W > 0.7

Vehicle Type 3:

K_{b1}: $\frac{T}{W} = \frac{P_T}{P_{LL}(1 + I)}$

$\frac{T}{W} = \frac{22.8}{19.8(1.2)}$

$\frac{T}{W} = 0.96$

$K_{b1} = 1.0$

Member behavior can be extrapolated to 1.33W for T/W > 0.7

K_{b2}: 0.8 (Routine inspection between 1 and 2 years)

K_{b3}: 1.0 (Fatigue does not control, redundancy)

$K_b = (1.0)(0.8)(1.0)$

$K_b = 0.80$

$RF_T = RF_c(1 + K_aK_b)$

Vehicle HS20:

$RF_T = (3.214)(1 + (1.21)(0.80))$

$RF_T = 6.32$

Rating = (6.32)(36) = 227 T

Vehicle Type 3:

$RF_T = (3.50)(1 + (1.21)(0.80))$

$RF_T = 6.89$

Rating = (6.89)(25) = 172 T

IV. Rating of Arches:

At Crown:

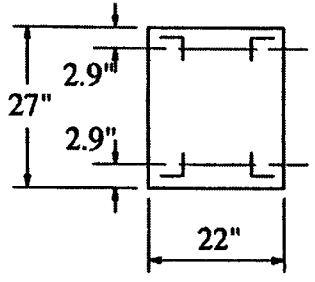

A_s = 4 L's: 3 x 3 x 5/16 = 4(1.78)

$A_s = 7.12 \text{ in.}^2$

f_c' = 4.5 ksi (From laboratory tests)

f_y = 42 ksi (From laboratory tests)

Dead Loads:

All reactions determined using structural analysis software.

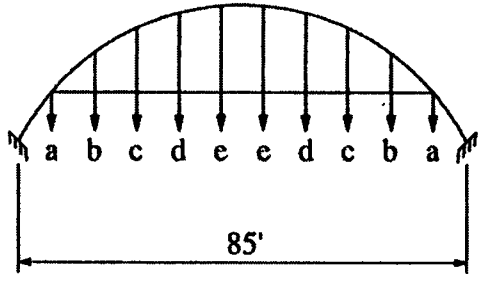

a = 10 k c = 14.3 k e = 14.8 k

b = 13.8 k d = 14.6 k

∴ At crown of arch:

P_{DL} = 138.85 k

M_{DL} = 17.77 ft-k

Live Loads:

Vehicle HS20:

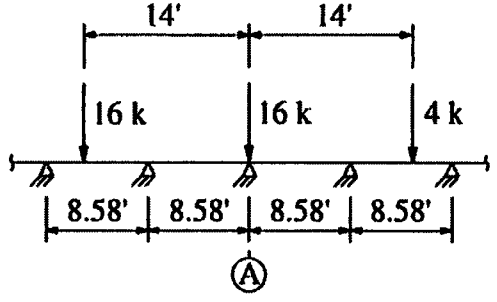

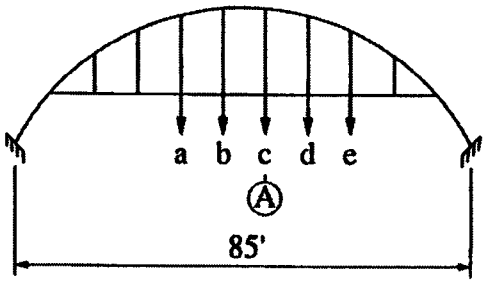

a = 15.0 k c = 21.6 k e = 3.8 k
b = 6.6 k d = 1.6 k

∴ At crown of arch:
P_{LL} = 60.1 k
M_{LL} = 61.10 ft-k

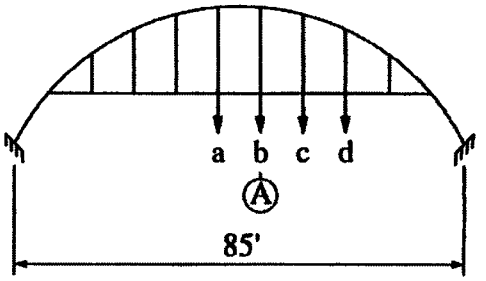

a = 1.6 k c = 1.2 k
b = 14.7 k d = 8 k

∴ At crown of arch:
P_{LL} = 29.22 k
M_{LL} = 53.22 ft-k

Vehicle Type 3:

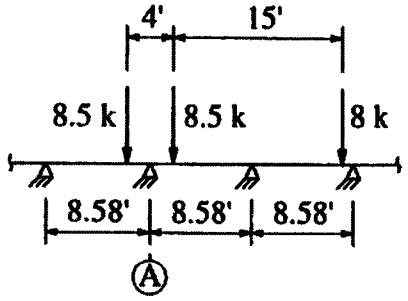

Capacity:

Assumed average Eccentricity of Axial Load on the Arch:

$$e_{AVG} = \frac{\left(\frac{M_{LL} + M_{DL}}{P_{LL} + P_{DL}}\right)_{HS20} + \left(\frac{M_{LL} + M_{DL}}{P_{LL} + P_{DL}}\right)_{Type\ 3}}{2}$$

$$e_{AVG} = \frac{\left(\frac{(61.10 + 17.77)(12)}{(60.10 + 138.85)}\right) + \left(\frac{(53.22 + 17.77)(12)}{(29.22 + 138.85)}\right)}{2}$$

$$e_{AVG} = \frac{4.76 + 5.07}{2}$$

e_{AVG} = 4.9 in.

P_n = 1,450 k
M_n = 598 ft-k
} From column interaction diagram

Rating:

$$RF_c = \frac{\phi P_n - \gamma_D P_{DL}}{\gamma_L P_{LL}(1 + I)} \text{ or } = \frac{\phi M_n - \gamma_D M_{DL}}{\gamma_L M_{LL}(1 + I)}$$

$\gamma_D = 1.2$
$\gamma_L = 1.3$
$I = 0.2$
$\phi = 0.70$ (Heavy deterioration, careful inspection, intermittent maintenance)

Vehicle HS20:

Axial Load:

$$RF_c = \frac{(0.70)(1450) - (1.2)(138.85)}{(1.3)(60.10)(1.2)}$$

$RF_c = 9.05$

Rating = (9.05)(36) = 325 T

Moment:

$$RF_c = \frac{(0.70)(598) - (1.2)(17.77)}{(1.3)(61.10)(1.2)}$$

$RF_c = 4.17$

Rating = (4.17)(36) = 150 T

Vehicle Type 3:

Axial Load:

$$RF_c = \frac{(0.70)(1450) - (1.2)(138.85)}{(1.3)(29.22)(1.2)}$$

$RF_c = 18.61$

Rating = (18.61)(25) = 465 T

Moment:

$$RF_c = \frac{(0.70)(598) - (1.2)(17.77)}{(1.3)(53.22)(1.2)}$$

$RF_c = 4.79$

Rating = (4.79)(25) = 119 T

Rating Modification:

$RF_T = RF_c K$
$K = 1 + K_a K_b$

Factor K_a:

$$K_a = \frac{\varepsilon_c}{\varepsilon_T} - 1$$

Axial Load and Moment Due to Test Vehicle:

All reactions determined using structural analysis software.

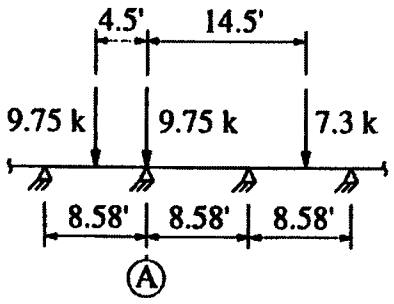

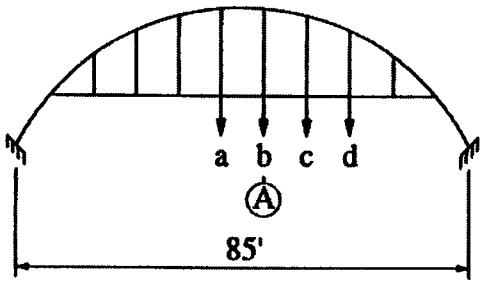

a = 5.2 k c = 1.7 k
b = 14.3 k d = 5.6 k

P_T = 32.7 k
M_T = 52.87 ft-k

Theoretical Stress/Strain:

Analyzed as an uncracked section.

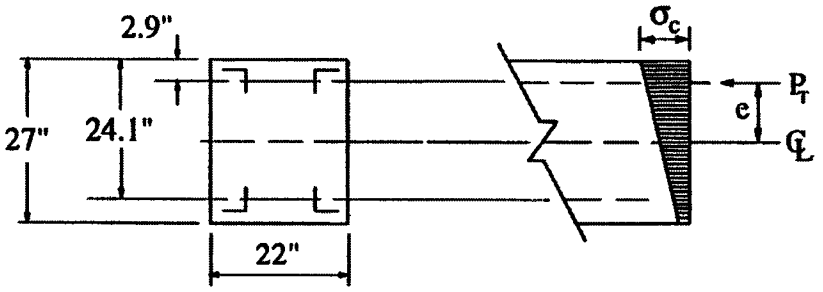

E_s = 29,000,000 psi
E_c = 3,800,000 psi
$n = \frac{E_s}{E_c} = 8$

P_T = 32.7 k
M_T = 52.87 ft-k

Transformed Section:

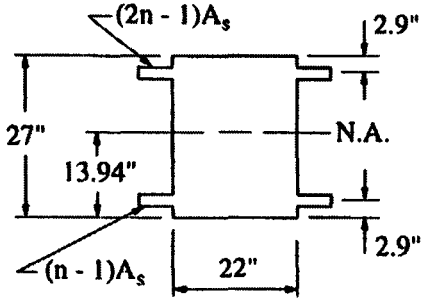

Transformed Area:

$A_{TOP} = (2n - 1)A_s = ((2)(8) - 1)(3.56)$

$A_{TOP} = 53.4 \text{ in.}^2$

$A_{BOT} = (n - 1)A_S = (8 - 1)(3.56)$

$A_{BOT} = 24.92 \text{ in.}^2$

$A_{TOT} = A_{TOP} + A_{BOT} + A_{ARCH}$

$= 53.4 + 24.92 + (22)(27)$

$A_{TOT} = 672.32 \text{ in.}^2$

Moment of Inertia:

$$I_g = \frac{bh^3}{12} + Ad^2$$

$I_g = 44{,}750 \text{ in.}^4$

Location of Neutral Axis:

$\bar{y} = 13.94$ in.

Concrete Stress/Strain:

$$\sigma_c = \frac{P_T}{A_{TOT}} + \frac{M_T y}{I_g}$$

$$\sigma_c = \frac{32.7(1000)}{672.32} + \frac{(52.87)(12)(1000)(13.94)}{44{,}750}$$

$\sigma_c = 246$ psi

$$\varepsilon_c = \frac{\sigma_c}{E_c}$$

ε_c = Calculated theoretical strain in concrete

$$\varepsilon_c = \frac{246}{3{,}800{,}000}$$

$\varepsilon_c = 6.47 \times 10^{-5}$ in./in.

$\varepsilon_T = 51 \times 10^{-6}$ in./in.

ε_T = Strain produced by test vehicle

$$K_a = \frac{\varepsilon_c}{\varepsilon_T} - 1 = \frac{6.47 \times 10^{-5}}{51 \times 10^{-6}} - 1$$

$K_a = 0.27$

Factor K_b:

$K_b = K_{b1}K_{b2}K_{b3}$

Vehicle HS20:

K_{b1}: $\frac{T}{W} = \frac{M_T}{M_{LL}(1 + I)}$

$\frac{T}{W} = \frac{52.87}{(61.1)(1.2)}$

$\frac{T}{W} = 0.72$

$K_{b1} = 1.0$

Member behavior can be extrapolated to 1.33W for T/W > 0.7

Vehicle Type 3:

K_{b1}: $\frac{T}{W} = \frac{M_T}{M_{LL}(1 + I)}$

$\frac{T}{W} = \frac{52.87}{(53.22)(1.2)}$

$\frac{T}{W} = 0.83$

$K_{b1} = 1.0$

Member behavior can be extrapolated to 1.33W for T/W > 0.7

K_{b2}: 0.8 (Routine inspection between 1 and 2 years)

K_{b3}: 0.9 (Fatigue does not control, no redundancy)

$K_b = (1.0)(0.8)(0.9)$

$K_b = 0.72$

$RF_T = RF_c(1 + K_aK_b)$

Vehicle HS20:

$RF_T = (4.17)(1 + (0.27)(0.72))$

$RF_T = 4.98$

Rating = (4.98)(36) = 179 T

Vehicle Type 3:

$RF_T = (4.79)(1 + (0.27)(0.72))$

$RF_T = 5.72$

Rating = (5.72)(25) = 143 T

Table B.2. Bridge II: Rating Summary.

	Vehicle HS20				Vehicle Type 3			
	AASHTO LRFR		Modified Rating		AASHTO LRFR		Modified Rating	
	RF_c	R(tons)	RF_T	R(tons)	RF_c	R(tons)	RF_T	R(tons)
Slab:	0.79	28.4			1.3	32.5		
Beams:	1.65	59.4	3.72	133.9	1.79	44.8	4.04	101.0
Hangers:	3.21	115.6	6.32	227.5	3.50	87.5	6.89	172.3
Arches:	4.17	150.1	4.98	179.3	4.79	119.8	5.72	143.0

indicates controlling component

BRIDGE III
BOONE COUNTY SLAB BRIDGE NO. 40
Year built: 1920

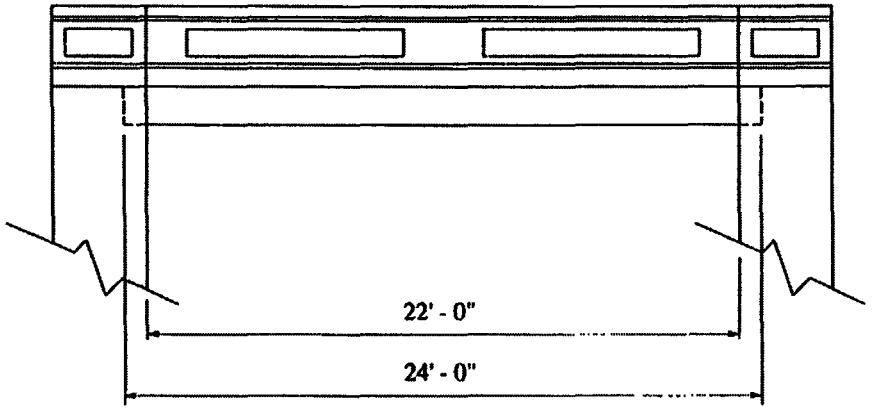

ELEVATION

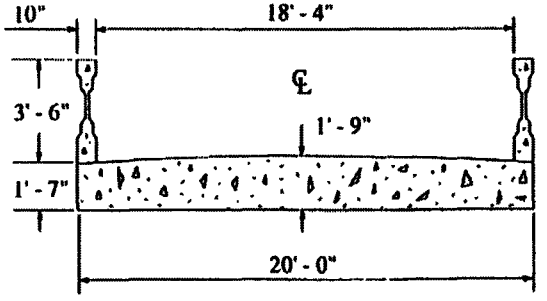

TYPICAL CROSS-SECTION

I. Rating Slab:

Dead Loads:

Railings:	[(2)(1.88)(0.150)(22)(1)]/[(22)(20)]	= 0.028 k/ft/ft width
Slab:	(0.150)(20)(1/12)(1)	= 0.250 k/ft/ft width
Gravel:	(0.120)(3)(1/12)(1)	= 0.030 k/ft/ft width
		0.308 k/ft/ft width

Dead Load Moment:

$$M_{DL} = \frac{wL^2}{8} = \frac{(0.308)(23)^2}{8}$$

L = Distance from center of supports

M_{DL} = 20.37 ft-k/ft width

Live Load Moment:

E = 4 + 0.06(s)

E = Wheel Distribution

s = Slab Length

E = 4 + (0.06)(23)

E = 5.38 ft

Vehicle HS20:

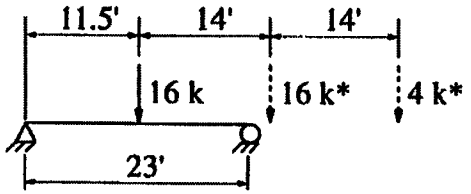

• Truck positioned to produce maximum moment

$$M_{LL} = \frac{PL}{4E}$$

M_{LL} = Maximum theoretical live load moment due to rating vehicle

$$M_{LL} = \frac{\left[\frac{(16)(23)}{4}\right]}{5.38}$$

M_{LL} = 17.10 ft-k/ft width

*Wheels off bridge

Vehicle Type 3:

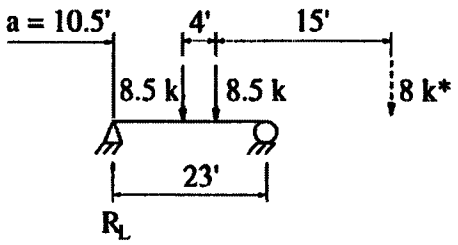

• Truck positioned to produce maximum moment

$$M_{LL} = \frac{R_L a}{E} = (7.76)\left(\frac{10.5}{5.38}\right)$$

M_{LL} = 15.2 ft-k/ft width

Flexural Design Strength:

(Typical 1 ft Section)

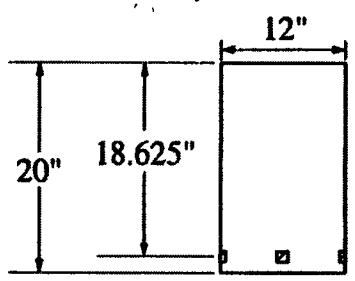

$A_s = 2(0.75)(0.75) = 1.125$ in.^{2}

Average deck thickness = (21 + 19)/2 = 20 in.
d = 20 - 1 - 0.75/2 = 18.625 in.
f_y = 33 ksi (Assumed)
f_c' = 4 ksi (Assumed)

$$\rho = \frac{A_s}{bd} = \frac{1.125}{(12)(18.625)}$$

$$\rho = 0.00503$$

$$\rho_{max} = 0.75\rho_b$$

$$\rho_b = \frac{0.85\beta_1 f_c'(87{,}000)}{f_y(87{,}000 + f_y)}$$

$$\beta_1 = 0.85$$

$$\rho_b = \frac{0.85(0.85)(4)(87{,}000)}{33(87{,}000 + 33{,}000)}$$

$$\rho_b = 0.0635$$

$$\rho_{max} = 0.75(0.0635)$$

$$\rho_{max} = 0.0476$$

$\rho = 0.00503 < \rho_{max} = 0.0476$
Tension steel yields

$$M_n = A_s f_y(d - a/2)/12$$

$$a = \frac{A_s f_y}{0.85 f_c' b}$$

$$a = \frac{(1.125)(33)}{(0.85)(4)(12)}$$

$$a = 0.91 \text{ in.}$$

$$M_n = \frac{(1.125)(33)\left(18.625 - \frac{0.91}{2}\right)}{12}$$

M_n = 56.21 ft-k/ft width

<u>Rating</u>:

$$RF_c = \frac{\phi M_n - \gamma_D M_{DL}}{\gamma_L M_{LL}(1 + I)}$$

ϕ = 0.70 (Fair condition, no redundancy, careful inspection, intermittent maintenance)
γ_D = 1.2
γ_L = 1.30
I = 0.1 (Good condition)

<u>Vehicle HS20</u>:

$$RF_c = \frac{(0.70)(56.21) - (1.2)(20.37)}{(1.30)(17.10)(1.1)}$$

RF_c = 0.61

Rating = (0.61)(36) = 21 T

Vehicle Type 3:

$$RF_c = \frac{(0.70)(56.21) - (1.2)(20.37)}{(1.30)(15.15)(1.1)}$$

$$RF_c = 0.69$$

Rating = (0.69)(25) = 17 T

Rating Modification:

$$RF_T = RF_c K$$
$$K = 1 + K_a K_b$$

Factor K_a:

$$K_a = \frac{\varepsilon_c}{\varepsilon_T} - 1$$

Theoretical Strains:

E_s = 29,000,000 psi

E_c = 3,600,000 psi

$$n = \frac{E_s}{E_c} = \frac{29{,}000{,}000}{3{,}600{,}000} = 8$$

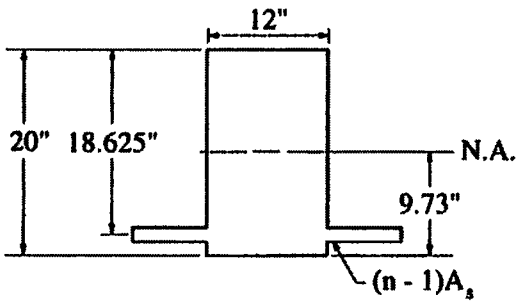

Equivalent Section:

$(n - 1)A_S = (8 - 1)(1.125) = 7.875$ in.^{2}

Centroid:

$\bar{y} = 9.73$ in.

Moment of Inertia:

$$I_g = \frac{bh^3}{12} + Ad^2$$

$I_g = 8{,}567$ in.^{4}

Moment From Test Vehicle:

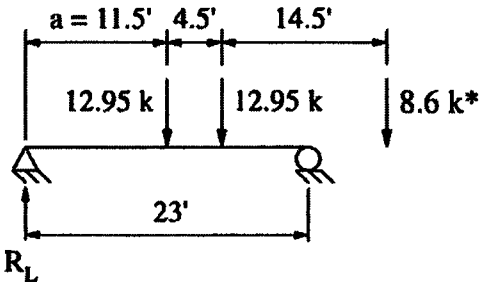

• Truck position obtained from field test

$$M_T = R_L a = (10.4)(11.5)$$

$$M_T = \frac{119.86}{5.38}$$

$$M_T = 22.23 \text{ ft-k/ft width}$$

Theoretical Stress (Uncracked Section):

$$\sigma_c = \frac{M_T y}{I_g} = \frac{(22.23)(12)(1000)(9.73)}{8,567}$$

$$\sigma_c = 303 \text{ psi}$$

$$\varepsilon_c = \frac{\sigma_c}{E_c}$$

ε_c = Calculated theoretical strain in concrete

$$\varepsilon_c = \frac{303}{3,600,000}$$

$$\varepsilon_c = 8.42 \times 10^{-5} \text{ in./in.}$$

$$\varepsilon_T = 1.3 \times 10^{-5} \text{ in./in.}$$

ε_T = Strain produced by test vehicle

$$K_a = \frac{\varepsilon_c}{\varepsilon_T} - 1 = \frac{8.42 \times 10^{-5}}{1.3 \times 10^{-5}} - 1$$

$$K_a = 5.48$$

Factor K_b:

$$K_b = K_{b1}K_{b2}K_{b3}$$

Vehicle HS20:

$$K_{b1}: \frac{T}{W} = \frac{M_T}{M_{LL}(1 + I)}$$

$$\frac{T}{W} = \frac{22.23}{(17.10)(1.1)}$$

$$\frac{T}{W} = 1.18$$

$$K_{b1} = 1.0$$

Member behavior can be extrapolated to 1.33W for T/W > 0.7

Vehicle Type 3:

$$K_{b1}: \frac{T}{W} = \frac{M_T}{M_{LL}(1 + I)}$$

$$\frac{T}{W} = \frac{22.23}{(15.15)(1.1)}$$

$$\frac{T}{W} = 1.33$$

$$K_{b1} = 1.0$$

Member behavior can be extrapolated to 1.33W for T/W > 0.7

K_{b2}: 0.8 Routine inspection between 1 and 2 years

K_{b3}: 0.9 No redundancy, fatigue does not control

$K_b = (1)(0.8)(0.9)$
$K_b = 0.72$

$RF_T = RF_c(1 + K_aK_b)$

Vehicle HS20:

$RF_T = (0.61)[1 + (5.48)(0.72)]$
$RF_T = 3.02$

Rating = (3.02)(36) = 108 T

Vehicle Type 3:

$RF_T = (0.69)[1 + (5.48)(0.72)]$
$RF_T = 3.41$

Rating = (3.41)(25) = 85 T

Table B.3. Bridge III: Rating Summary:

	Vehicle HS20				Vehicle Type 3			
	AASHTO LRFR		Modified Rating		AASHTO LRFR		Modified Rating	
	RF_c	R(tons)	RF_T	R(tons)	RF_c	R(tons)	RF_T	R(tons)
Slab	0.61	22.0	3.02	108.7	0.69	17.3	3.41	85.3

BRIDGE IV
LUTEN ARCH
Year Built: 1912

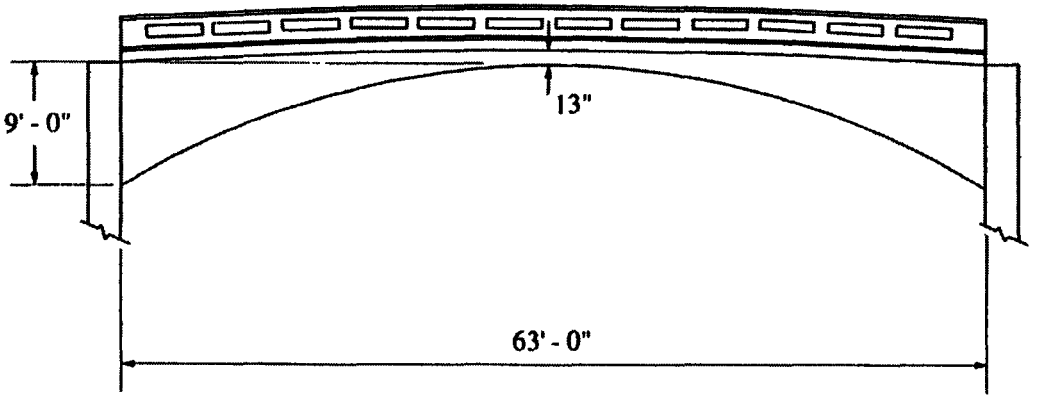

ELEVATION

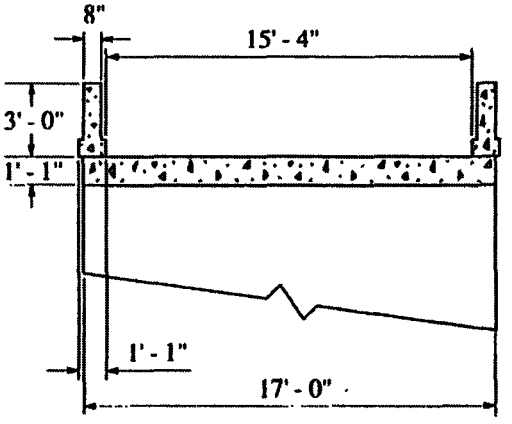

TYPICAL CROSS-SECTION

I. Rating of Arch:

At Crown:

Typical 1 ft. section

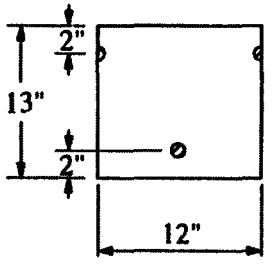

A_s = 2 Bars: 3/4 in. ϕ = 2(0.44)
A_s = 0.88 in.^{2}
f_c' = 4 ksi (Assumed)
f_y = 33 ksi (Assumed)

Dead Loads:

All reactions determined using structural analysis software.

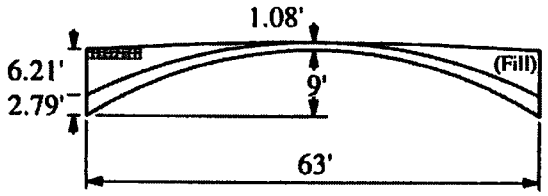

Assumed weight of fill = 120 lb/ft^3

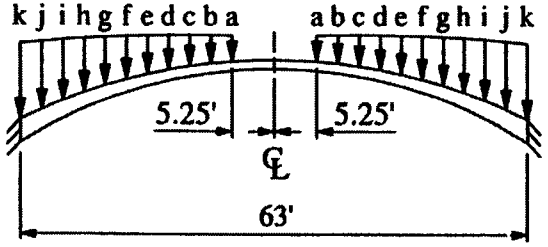

a = 20 lb/ft/ft width
b = 45 lb/ft/ft width
c = 80 lb/ft/ft width
d = 125 lb/ft/ft width
e = 180 lb/ft/ft width
f = 245 lb/ft/ft width
g = 320 lb/ft/ft width
h = 405 lb/ft/ft width
i = 505 lb/ft/ft width
j = 620 lb/ft/ft width
k = 745 lb/ft/ft width

M_{DL} = 2.58 ft-k/ft width
P_{DL} = 16.19 k/ft width

Live Loads:

Wheel load distribution (AASHTO 6.4.2):

- For fill less than 2 ft, wheel loads are distributed as if the loads were applied directly to slab.

  $E = 4 + 0.06s \leq 7.0$ ft

  s = span length, ft

- For fill greater than 2 ft but less than 8 ft, the wheel loads are distributed over squares having sides equal to 1.75 times the depth of fill. When these squares overlap, the wheel loads are evenly spread over the gross area.

  $wL = 1.75h$

  wL = Length of distribution
  h = Depth of fill

Vehicle HS20:

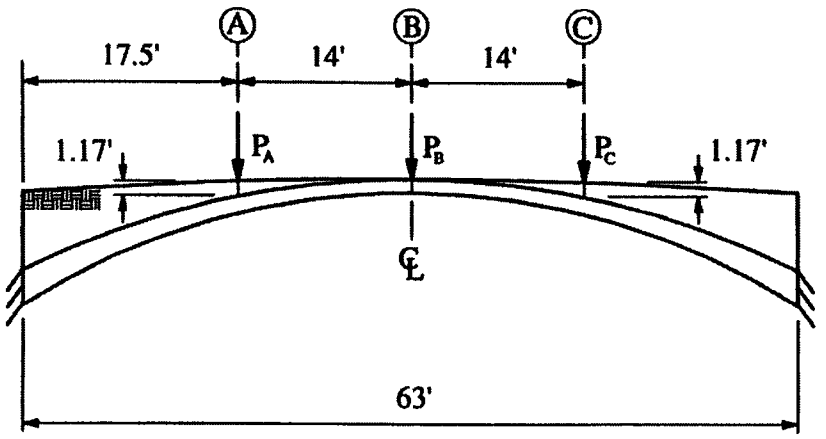

- Truck positioned to produce maximum moment

Wheel loads at A, B, and C:

Fill < 2 ft

$E = 4 + 0.06s \leq 7$ ft

$E = 4 + 0.06(63)$

$E = 7.78$ ft $= 7$ ft

$$P_A = \frac{16}{7}$$

$P_A = 2.29$ k/ft width

$$P_B = \frac{16}{7}$$

$P_B = 2.29$ k/ft width

$$P_C = \frac{4}{7}$$

$P_C = 0.57$ k/ft width

$M_{LL} = 4.33$ ft-k/ft width

M_{LL} = Maximum theoretical live load moment at crown of arch due to rating vehicle

$P_{LL} = 7.68$ k/ft width

P_{LL} = Maximum theoretical axial live load at crown of arch due to rating vehicle

Vehicle Type 3:

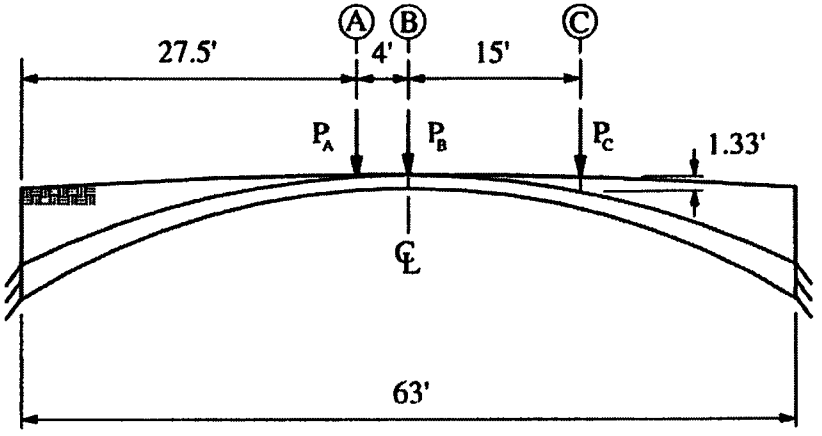

- Truck positioned to produce maximum moment

Wheel loads at A, B, and C:

Fill < 2 ft

$E = 4 + 0.06s \leq 7$ ft

$E = 4 + 0.06\,(63)$

$E = 7.78$ ft $= 7$ ft

$$P_A = \frac{8.5}{7}$$

$P_A = 1.21$ k/ft width

$$P_B = \frac{8.5}{7}$$

$P_B = 1.21$ k/ft width

$$P_C = \frac{8}{7}$$

$P_C = 1.14$ k/ft width

$M_{LL} = 3.50$ ft-k/ft width

$P_{LL} = 5.90$ k/ft width

Capacity:

Assumed average eccentricity of axial load on the arch:

$$e_{AVG}{}^{*} = \frac{\left(\frac{M_{LL}+M_{DL}}{P_{LL}+P_{DL}}\right)_{HS20} + \left(\frac{M_{LL}+M_{DL}}{P_{LL}+P_{DL}}\right)_{Type\ 3}}{2}$$

$$e_{AVG} = \frac{\left(\frac{(4.33+2.58)(12)}{7.68+16.19}\right) + \left(\frac{(3.50+2.58)(12)}{5.90+16.19}\right)}{2}$$

$$e_{AVG} = \frac{3.47 + 3.30}{2}$$

$e_{AVG} = 3.40$ in.

$P_n = 301$ k/ft width
$M_n = 86$ ft-k/ft width } From column interaction diagram

Rating:

$$RF_c = \frac{\phi P_n - \gamma_D P_{DL}}{\gamma_L P_{LL}(1+I)} \text{ or } \frac{\phi M_n - \gamma_D M_{DL}}{\gamma_L M_{LL}(1+I)}$$

$\gamma_D = 1.2$

$\gamma_L = 1.3$

$I = 0.2$ (Poor condition)

$\phi = 0.60$ (Heavily deteriorated, no redundancy, careful inspection, intermittent maintenance)

Vehicle HS20:

Axial Load:

$$RF_c = \frac{(0.60)(301) - (1.2)(16.19)}{(1.3)(7.68)(1.2)}$$

$RF_c = 13.45$

Rating $= (13.45)(36) = 484$ T

*For analysis purposes, the eccentricity within the arch is assumed to remain constant for all load cases.

Moment:

$$RF_c = \frac{(0.60)(86) - (1.2)(2.58)}{(1.3)(4.33)(1.2)}$$

$$RF_c = 7.18$$

$$\text{Rating} = (7.18)(36) = 258\ \text{T}$$

Vehicle Type 3:

Axial Load:

$$RF_c = \frac{(0.60)(301) - (1.2)(16.19)}{(1.3)(5.90)(1.2)}$$

$$RF_c = 17.51$$

$$\text{Rating} = (17.51)(25) = 437\ \text{T}$$

Moment:

$$RF_c = \frac{(0.60)(86) - (1.2)(2.58)}{(1.3)(3.50)(1.2)}$$

$$RF_c = 8.39$$

$$\text{Rating} = (8.39)(25) = 209\ \text{T}$$

Rating Modification:

$$RF_T = RF_c K$$

$$K = 1 + K_a K_b$$

Factor K_a:

$$K_a = \frac{\varepsilon_c}{\varepsilon_T} - 1$$

Axial Load and Moment Due to Test Vehicle:

All reactions determined using structural analysis software.

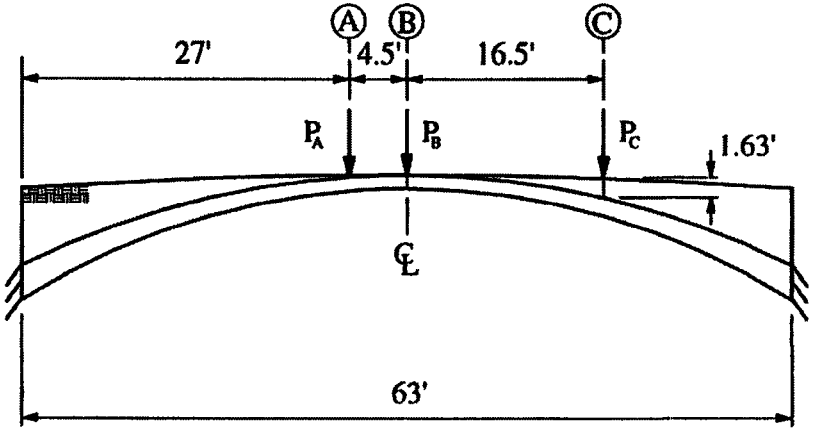

- Truck position obtained from field test

Wheel loads at A, B, and C:

Fill < 2 ft

$$E = 4 + 0.06s = 4 + 0.06\ (63)$$

$$E = 7.78\ \text{ft} = 7\ \text{ft}$$

$$P_A = \frac{10.58}{7}$$

$$P_A = 1.51\ \text{k/ft width}$$

$$P_B = \frac{10.58}{7}$$

$$P_B = 1.51\ \text{k/ft width}$$

$$P_C = \frac{9.35}{7}$$

P_C = 1.34 k/ft width

M_T = 4.22 ft-k/ft width

M_T = Maximum theoretical live load moment at crown of arch due to test vehicle

P_T = 7.06 k/ft width

P_T = Maximum theoretical axial live load at crown of arch due to test vehicle

Theoretical Stress/Strain:

(Analyzed as an uncracked section)

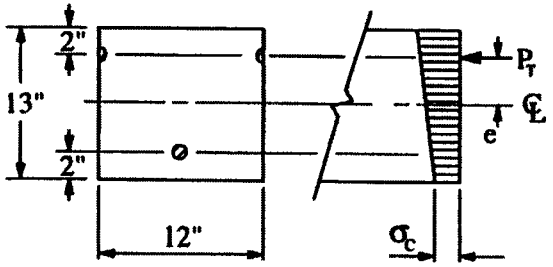

E_s = 29,000,000 psi

E_c = 3,600,000 psi

$n = \frac{E_s}{E_c} = 8$

Transformed Section:

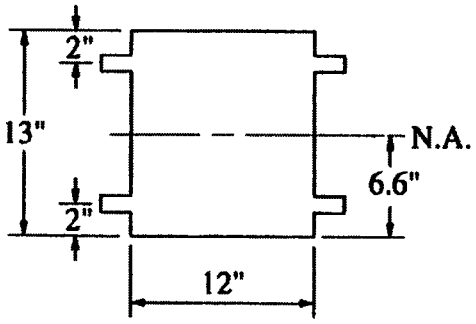

Transformed Area:

$A_{TOP} = (2n - 1)A_s = ((2)(8) - 1)(0.44)$

$A_{TOP} = 6.60$ in.^{2}

$A_{BOT} = (n - 1)A_s = (8 - 1)(0.44)$

$A_{BOT} = 3.08$ in.^{2}

$A_{TOT} = A_{TOP} + A_{BOT} + A_{ARCH} = 3.08 + 6.6 + (12)(13)$

$A_{TOT} = 165.68$ in.^{2}

Location of Neutral Axis:

$\bar{y} = 6.6$ in.

Moment of Inertia:

$$I_g = \frac{bh^3}{12} + Ad^2$$

$I_g = 2{,}392$ in.^{4}

Concrete Stress/Strain:

$$\sigma_c = \frac{P_T}{A_{TOT}} + \frac{M_T y}{I_g}$$

$$\sigma_c = \frac{(7.06)(1000)}{165.68} + \frac{(4.22)(12)(1000)(6.6)}{2{,}392}$$

$$\sigma_c = 182 \text{ psi}$$

$$\varepsilon_c = \frac{\sigma_c}{E_c}$$

ε_c = Calculated theoretical strain in concrete

$$\varepsilon_c = \frac{182}{3{,}600{,}000}$$

$$\varepsilon_c = 5.05 \times 10^{-5} \text{ in./in.}$$

$$\varepsilon_T = 38 \times 10^{-6} \text{ in./in.}$$

ε_T = Strain produced from test vehicle

$$K_a = \frac{\varepsilon_c}{\varepsilon_T} - 1 = \frac{5.05 \times 10^{-5}}{38 \times 10^{-6}} - 1$$

$$K_a = 0.33$$

Factor K_b:

$$K_b = K_{b1}K_{b2}K_{b3}$$

Vehicle HS20:

K_{b1}: $\frac{T}{W} = \frac{M_T}{M_{LL}(1 + I)}$

$$\frac{T}{W} = \frac{4.22}{(4.33)(1.2)}$$

$$\frac{T}{W} = 0.81$$

$$K_{b1} = 1$$

Member behavior can be extrapolated to 1.33W for T/W > 0.7

Vehicle Type 3:

K_{b1}: $\frac{T}{W} = \frac{M_T}{M_{LL}(1 + I)}$

$$\frac{T}{W} = \frac{4.22}{(3.50)(1.2)}$$

$$\frac{T}{W} = 1.00$$

$$K_{b1} = 1$$

Member behavior can be extrapolated to 1.33W for T/W > 0.7

K_{b2}: 0.8 Routine inspection between 1 and 2 years

K_{b3}: 0.9 Fatigue does not control, no redundancy

$K_b = (1)(0.8)(0.9)$
$K_b = 0.72$

$RF_T = RF_c(1 + K_a K_b)$

Vehicle HS20:

$RF_T = (7.18)(1 + (0.33)(0.72))$
$RF_T = 8.89$

Rating = (8.89)(36) = 320 T

Vehicle Type 3:

$RF_T = (8.39)(1 + (0.33)(0.72))$
$RF_T = 10.38$

Rating = (10.38)(25) = 259 T

Table B.4. Bridge IV: Rating Summary:

	Vehicle HS20				Vehicle Type 3			
	AASHTO LRFR		Modified Rating		AASHTO LRFR		Modified Rating	
	RF_c	R(tons)	RF_T	R(tons)	RF_c	R(tons)	RF_T	R(tons)
Arch	7.18	258.5	8.89	320.0	8.39	209.8	10.38	259.5

BRIDGE V
HARDIN COUNTY CONCRETE STRINGER BRIDGE
Year built: 1918

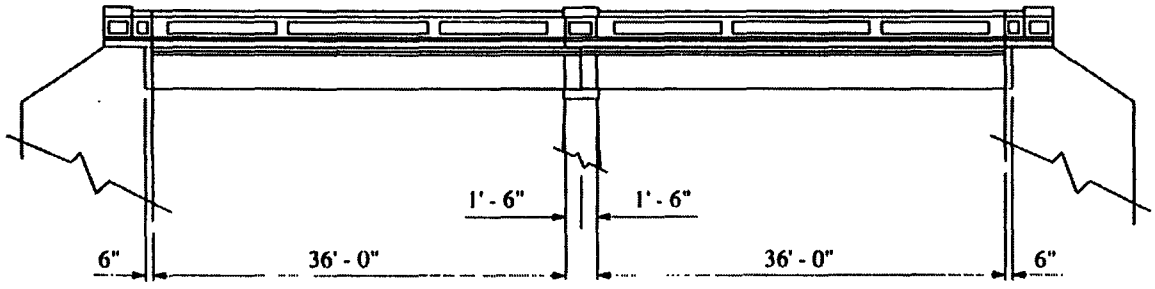

ELEVATION

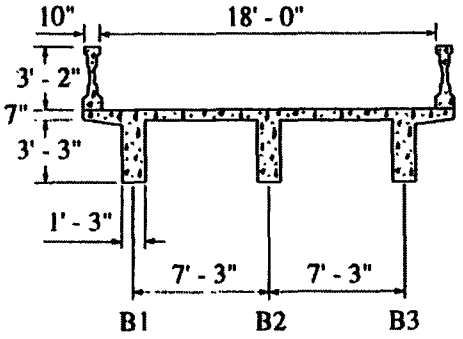

TYPICAL CROSS-SECTION

I. Rating Beam B5: (Center beam on span 2)

Dead Loads:

Deck:	(7)(1/12)(7.25)(0.150)	=	0.634 k/ft
Slab:	(15)(1/12)(39)(1/12)(0.150)	=	0.609 k/ft
Gravel:	(1)(1/12)(9.25)(0.120)	=	0.093 k/ft
			1.34 k/ft

Dead Load Moment:

$$M_{DL} = \frac{wL^2}{8}$$

L = Distance from center of supports

$$M_{DL} = \frac{(1.34)(37)^2}{8}$$

$$M_{DL} = 229.31 \text{ ft-k}$$

Live Load Moment:

Distribution factor:

$$DF = \frac{s}{6.5}$$

s = Center to center spacing of beams

s = 7.25 ft > 6 ft

Since 's' is greater than 6 ft, assume the flooring between stringers to act as a simple beam with the load on each stringer being the wheel load reaction.

Vehicle HS20:

(Rear wheels)

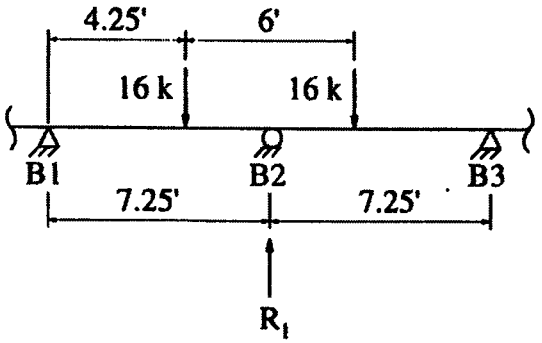

R_1 = 18.76 k

(Front wheels)

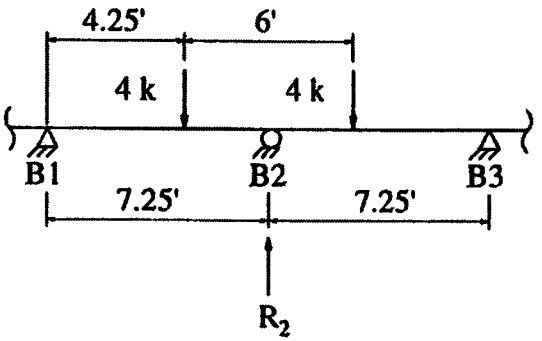

R_2 = 4.69 k

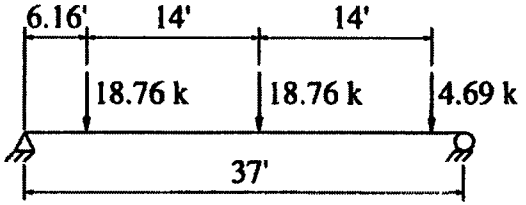

- Truck positioned to produce maximum moment

M_{LL} = 232.09 ft-k

M_{LL} = Maximum theoretical live load moment due to rating vehicle

Vehicle Type 3:

(Rear wheels)

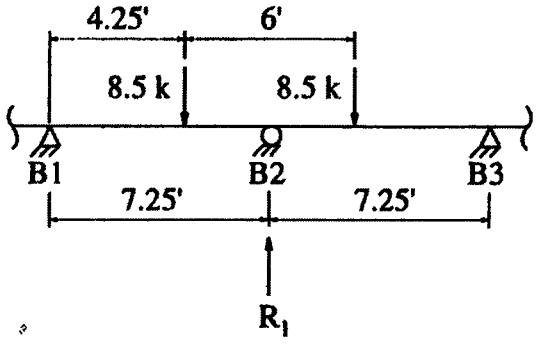

R_1 = 9.97 k

(Front wheels)

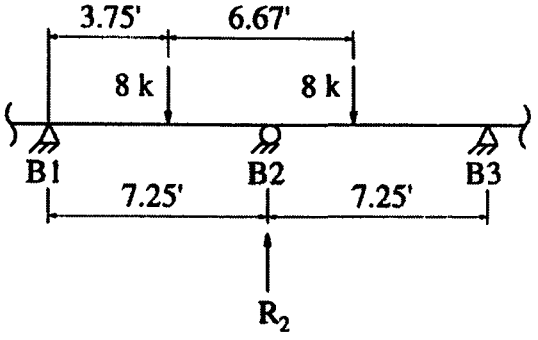

R_2 = 8.65 k

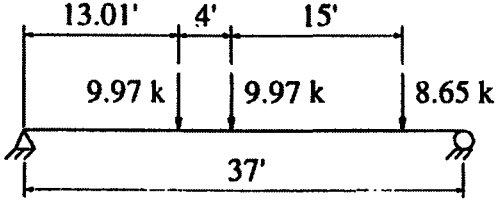

• Truck positioned to produce maximum moment

M_{LL} = 181.59 ft-k

Flexural Design Strength:

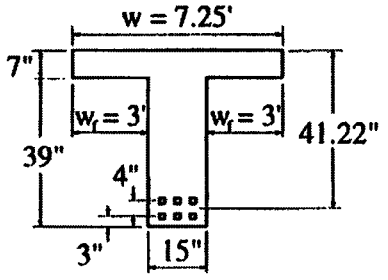

$A_{s_{(TOP)}}$: 3 Bars: 1.125 in. Square = 3.80 in.^{2}

$A_{s_{(BOT)}}$: 3 Bars: 1.25 in. Square = 4.69 in.^{2}

d = 41.22 in.

f_y = 33 ksi (Assumed)

f_c' = 4 ksi (Assumed)

Flange Width:

i.) $w \leq 0.25L$

L = Span length

L = 37 ft

$w \leq (0.25)(37)$

$w \leq 9.25$ ft

Overhanging Flange Width:

ii.) $w_f \leq 6t$

t = Slab thickness
$t = 7$ in.

$w_f \leq 6(7)$
$w_f \leq 42$ in.

$w_f = 36 < 42$ in.
or

iii.) $w_f \leq$ One-half clear distance to next web
$w_f \leq (0.5)(6)$
$w_f \leq 3$ ft

$w_f = 3$ ft

$$\rho = \frac{A_s}{bd} = \frac{8.49}{(87)(41.22)}$$

$\rho = 0.00237$

$\rho_{max} = 0.75\rho_b$

$$\rho_b = \frac{0.85\beta_1 f_c'(87{,}000)}{f_y(87{,}000 + f_y)}$$

$\beta_1 = 0.85$

$$\rho_b = \frac{0.85(0.85)(4)(87{,}000)}{33(87{,}000 + 33{,}000)}$$

$\rho_b = 0.0635$

$\rho_{max} = (0.75)(0.0635)$
$\rho_{max} = 0.0476$

$\rho = 0.00237 < \rho_{max} = 0.0476$
Tension steel yields

$M_n = A_s f_y(d - a/2)/12$

$$a = \frac{A_s f_y}{0.85 f_c' b}$$

$$a = \frac{(8.49)(33)}{(0.85)(4)(87)}$$

$a = 0.95$ in.

$$M_n = \frac{(8.49)(33)\left(41.22 - \frac{0.95}{2}\right)}{12}$$

$M_n = 951.29$ ft.-k

Rating:

$$RF_c = \frac{\phi M_n - \gamma_D M_{DL}}{\gamma_L M_{LL}(1 + I)}$$

ϕ = 0.85 (Good condition, redundancy, careful inspection, intermittent maintenance)

γ_D = 1.2

γ_L = 1.30

I = 0.1 (Good condition)

Vehicle HS20:

$$RF_c = \frac{(0.85)(951.29) - (1.2)(229.31)}{(1.3)(232.09)(1.1)}$$

RF_c = 1.61

Rating = (1.61)(36) = 57 T

Vehicle Type 3:

$$RF_c = \frac{(0.85)(951.29) - (1.2)(229.31)}{(1.3)(181.59)(1.1)}$$

RF_c = 2.05

Rating = (2.05)(25) = 51 T

Rating Modification:

$RF_T = RF_c K$

$K = 1 + K_a K_b$

Factor K_a:

$$K_a = \frac{\varepsilon_c}{\varepsilon_T} - 1$$

Theoretical Strains:

E_s = 29,000,000 psi

E_c = 3,600,000 psi

$$n = \frac{E_s}{E_c} = \frac{29,000,000}{3,600,000} = 8$$

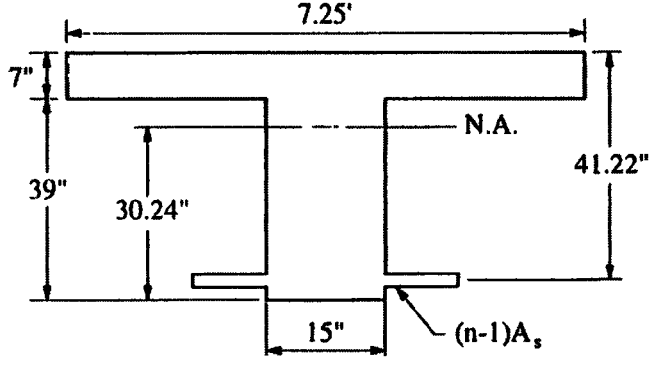

Equivalent Section:

$(n - 1)A_s = (8 - 1)(8.49) = 59.43$ in.^{2}

Centroid:

$\bar{y}$ = 29.98 in.

Moment of Inertia:

$$I_g = \frac{bh^3}{12} + Ad^2$$

I_g = 274,174 in.^{4}

Moment From Test Vehicle:

(Rear wheels)

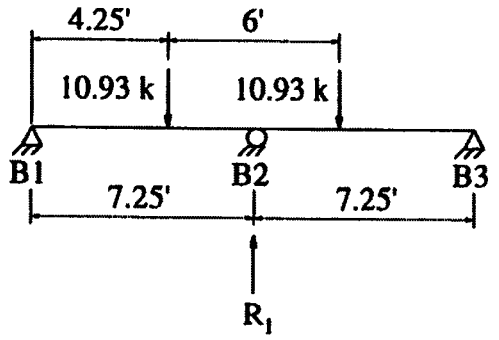

R_1 = 12.81 k

(Front wheels)

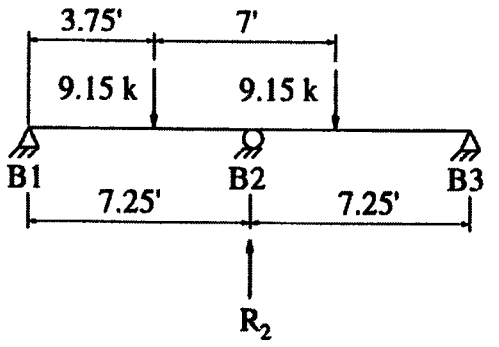

R_2 = 9.47 k

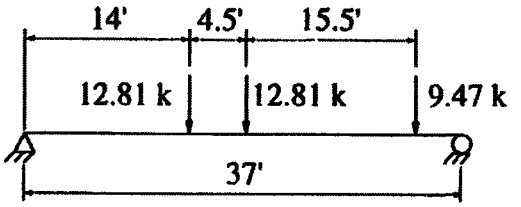

• Truck position obtained from field test

M_T = 222.45 ft-k

M_T = Maximum theoretical live load moment due to test truck

Theoretical Stress (Uncracked Section):

$$\sigma_c = \frac{M_T y}{I_g} = \frac{(222.45)(12)(1000)(29.98)}{274{,}174}$$

σ_c = 292 psi

$$\varepsilon_c = \frac{\sigma_c}{E_c}$$

ε_c = Calculated theoretical strain in concrete

$$\varepsilon_c = \frac{292}{3{,}600{,}000}$$

$\varepsilon_c = 8.11 \times 10^{-5}$ in./in.

$\varepsilon_T = 1.66 \times 10^{-4}$ in./in.

ε_T = Strain produced from test vehicle

$$K_a = \frac{\varepsilon_c}{\varepsilon_T} - 1 = \frac{8.11 \times 10^{-5}}{1.66 \times 10^{-4}} - 1$$

$K_a = -0.51$

Factor K_b:

$K_b = K_{b1}K_{b2}K_{b3}$

Vehicle HS20:

$$K_{b1}: \frac{T}{W} = \frac{M_T}{M_{LL}(1 + I)}$$

$$\frac{T}{W} = \frac{222.45}{(232.09)(1.1)}$$

$$\frac{T}{W} = 0.87$$

$K_{b1} = 1.0$

Member behavior can be extrapolated to 1.33W for T/W > 0.7

Vehicle Type 3:

$$K_{b1}: \frac{T}{W} = \frac{M_T}{M_{LL}(1 + I)}$$

$$\frac{T}{W} = \frac{222.45}{(181.59)(1.1)}$$

$$\frac{T}{W} = 1.11$$

$K_{b1} = 1.0$

Member behavior can be extrapolated to 1.33W for T/W > 0.7

K_{b2}: 0.8 Routine inspection between 1 and 2 years

K_{b3}: 1.0 Redundancy, fatigue does not control

$K_b = (1)(0.8)(1.0)$

$K_b = 0.80$

$RF_T = RF_c(1 + K_aK_b)$

Vehicle HS20:

$RF_T = (1.61)[1 + (-0.51)(0.80)]$

$RF_T = 0.95$

Rating = (0.95)(36) = 34 T

Vehicle Type 3:

$RF_T = (2.05[1 + (-0.51)(0.80)]$

$RF_T = 1.21$

Rating = (1.21)(25) = 30 T

Table B.5. Bridge V: Rating Summary:

	Vehicle HS20				Vehicle Type 3			
	AASHTO LRFR		Modified Rating		AASHTO LRFR		Modified Rating	
	RF_c	R(tons)	RF_T	R(tons)	RF_c	R(tons)	RF_T	R(tons)
Beams	1.61	57.9	0.95	34.2	2.05	51.3	1.21	30.3

BRIDGE VI
CONCRETE FILLED SPANDREL ARCH
Year Built: 1913

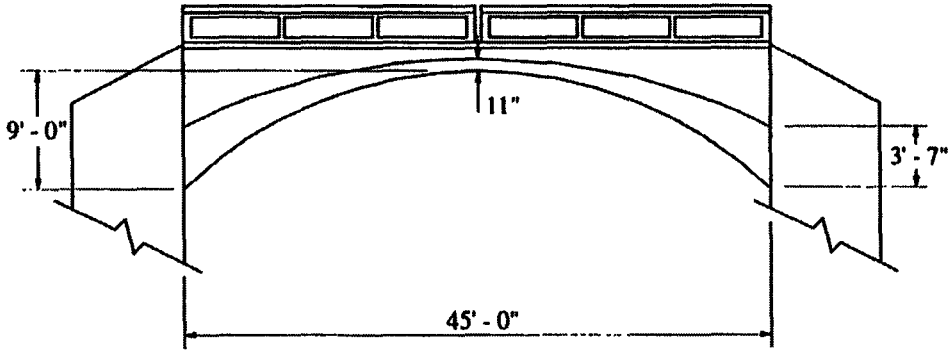

ELEVATION

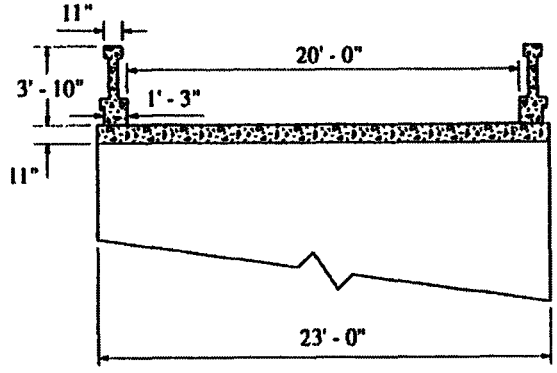

TYPICAL CROSS-SECTION

I. Rating of Arch:

At Crown:

(Typical 1 ft. section)

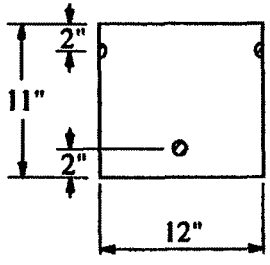

A_s : 2 Bars: 7/8 in. ϕ = 2(0.60)

A_s = 1.20 in.^{2}

f_c' = 4 ksi (Assumed)

f_y = 33 ksi (Assumed)

Dead Loads:

All reactions determined using structural analysis software.

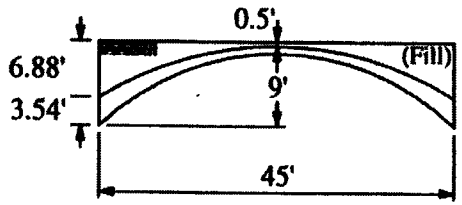

Assumed weight of fill = 120 lb/ft^3

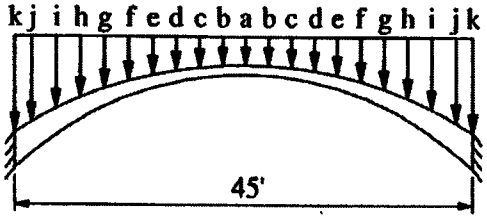

a = 60 lb/ft/ft width	g = 340 lb/ft/ft width
b = 65 lb/ft/ft width	h = 455 lb/ft/ft width
c = 90 lb/ft/ft width	i = 590 lb/ft/ft width
d = 125 lb/ft/ft width	j = 755 lb/ft/ft width
e = 180 lb/ft/ft width	k = 825 lb/ft/ft width
f = 250 lb/ft/ft width	

M_{DL} = 11.03 ft-k/ft width
P_{DL} = 64.05 k/ft width

Live Loads:

Wheel load distribution (AASHTO sec. 6.4.2):

- For fill less than 2 ft, wheel loads are distributed as if the loads were applied directly to slab.

  E = 4 + 0.06s ≤ 7.0 ft

  s = span length, ft

- For fill greater than 2 ft but less than 8 ft, the wheel loads are distributed over squares having sides equal to 1.75 times the depth of fill. When squares overlap, the wheel loads are evenly over the gross area.

these
spread

  wL = 1.75h

  wL = Length of distribution
  h = Depth of fill

Vehicle HS20:

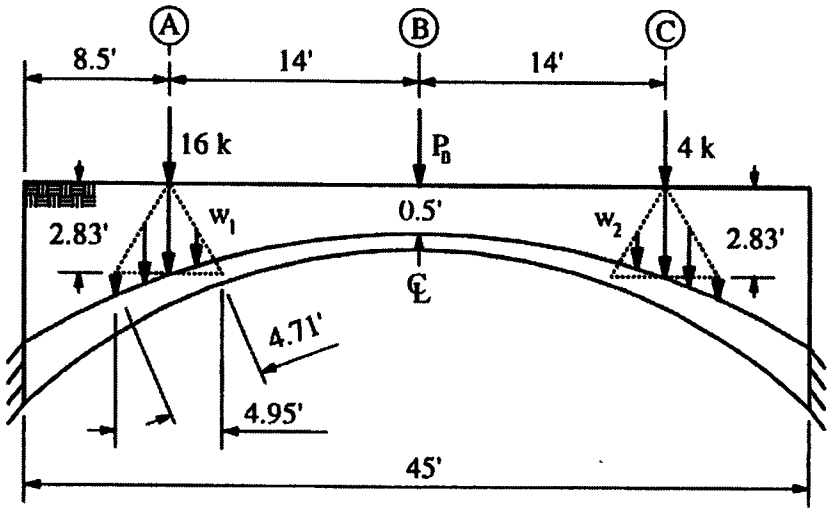

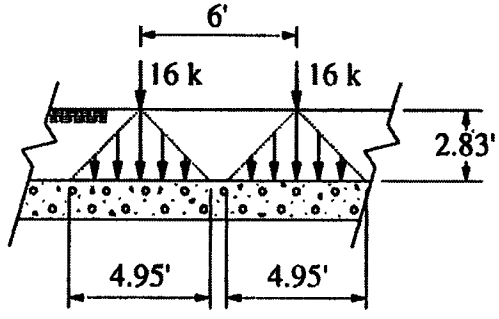

Cross-section at A

Loaded area = (4.71)(4.95)

Loaded area = 23.31 ft^2

Wheel pressure = $\frac{16}{23.31}$

Wheel pressure = 0.686 k/ft^2

w_l = Load per foot of arch = (0.686)(1)

w_l = 0.686 k/ft/ft width

Wheel load at A:

2 ft < Fill < 8 ft

h = 2.83 ft

wL = 1.75h = (1.75)(2.83)

wL = 4.95 ft

Wheel load at B:

Fill < 2 ft

E = 4 + 0.06s < 7 ft

E = 4 + 0.06(45)

E = 6.7 ft

$P_B = \frac{16}{6.7}$

P_B = 2.39 k/ft width

Wheel load at C:

2 ft < Fill < 8 ft

h = 2.83 ft

wL = 1.75h = (1.75)(2.83)

wL = 4.95 ft

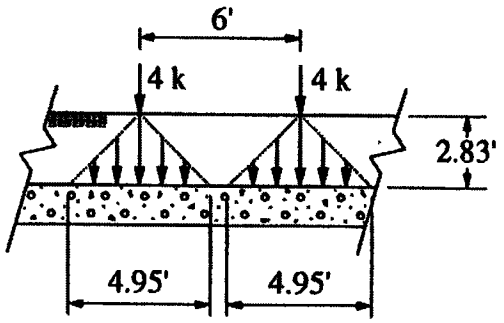

Cross-section at C

Loaded area = (4.71)(4.95)

Loaded area = 23.31 ft^2

Wheel pressure = $\frac{4}{23.31}$

Wheel pressure = 0.172 k/ft^2

w_2 = Load per foot of arch = (0.172)(1)

w_2 = 0.172 k/ft/ft width

M_{LL} = 3.24 ft-k/ft width

M_{LL} = Maximum theoretical live load moment at crown of arch due to rating vehicle

P_{LL} = 5.38 k/ft width

P_{LL} = Maximum theoretical axial live load at crown of arch due to rating vehicle

Vehicle Type 3:

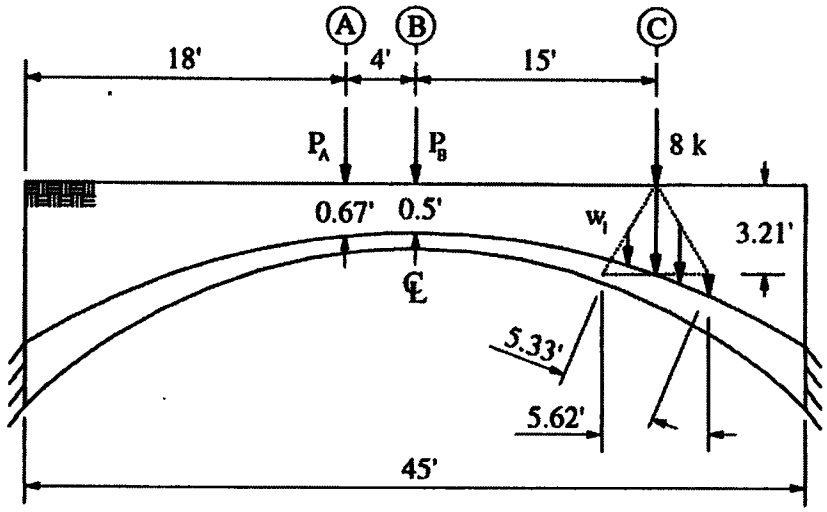

Wheel loads at A and B:

Fill < 2 ft

E = 4 + 0.06s = 4 + 0.06 (45)

E = 6.7 ft

$P_A = \frac{8.5}{6.7}$

P_A = 1.27 k/ft width

$$P_B = \frac{8.5}{6.7}$$

P_B = 1.27 k/ft width

Wheel load at C:

2 ft < Fill < 8 ft

h = 3.21 ft

wL = 1.75 h = (1.75)(3.21)

wL = 5.62 ft

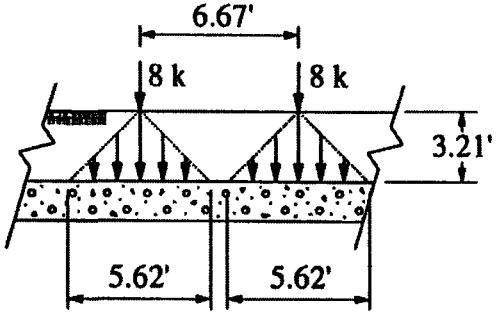

Cross-section at C

Loaded area = (5.62)(5.33)

Loaded area = 29.95 ft^2

$$\text{Wheel pressure} = \frac{8}{29.95}$$

Wheel pressure = 0.267 k/ft^2

w_l = Load per foot of arch = (0.267)(1)

w_l = 0.267 k/ft/ft width

M_{LL} = 2.21 ft-k/ft width

P_{LL} = 4.40 k/ft width

Capacity:

Assumed average eccentricity of axial load on the arch:

$$e_{AVG}^* = \frac{\left(\frac{M_{LL}+M_{DL}}{P_{LL}+P_{DL}}\right)_{HS20} + \left(\frac{M_{LL}+M_{DL}}{P_{LL}+P_{DL}}\right)_{Type\ 3}}{2}$$

$$e_{AVG} = \frac{\left(\frac{(3.24+11.03)(12)}{5.38+64.05}\right) + \left(\frac{(2.21+11.03)(12)}{4.40+64.05}\right)}{2}$$

$$e_{AVG} = \frac{2.47 + 2.32}{2}$$

e_{AVG} = 2.39 in.

P_n = 283 k/ft width
M_n = 57 ftk/ft width
} From column interaction diagram

Rating:

$$RF_c = \frac{\phi P_n - \gamma_D P_{DL}}{\gamma_L P_{LL}(1+I)} \text{ or } \frac{\phi M_n - \gamma_D M_{DL}}{\gamma_L M_{LL}(1+I)}$$

γ_D = 1.2

γ_L = 1.3

I = 0.1 (Good condition)

ϕ = 0.70 (Good condition, no redundancy, careful inspection, intermittent maintenance)

*For analysis purposes, the eccentricity in the arch is assumed constant for all load cases.

Vehicle HS20:

Axial Load:

$$RF_c = \frac{(0.70)(283) - (1.2)(64.05)}{(1.3)(5.38)(1.1)}$$

$RF_c = 15.76$

Rating = (15.76)(36) = 567 T

Moment:

$$RF_c = \frac{(0.70)(57) - (1.2)(11.03)}{(1.3)(3.24)(1.1)}$$

$RF_c = 5.75$

Rating = (5.75)(36) = 207 T

Vehicle Type 3:

Axial Load:

$$RF_c = \frac{(0.70)(283) - (1.2)(64.05)}{(1.3)(4.40)(1.1)}$$

$RF_c = 19.27$

Rating = (19.27)(25) = 481 T

Moment:

$$RF_c = \frac{(0.70)(57) - (1.2)(11.03)}{(1.3)(2.21)(1.1)}$$

$RF_c = 8.44$

Rating = (8.44)(25) = 211 T

Rating Modification:

$RF_T = RF_cK$

$K = 1 + K_aK_b$

Factor K_a:

$$K_a = \frac{\varepsilon_c}{\varepsilon_T} - 1$$

Axial Load and Moment Due to Test Vehicle:

(All reactions determined using structural analysis software)

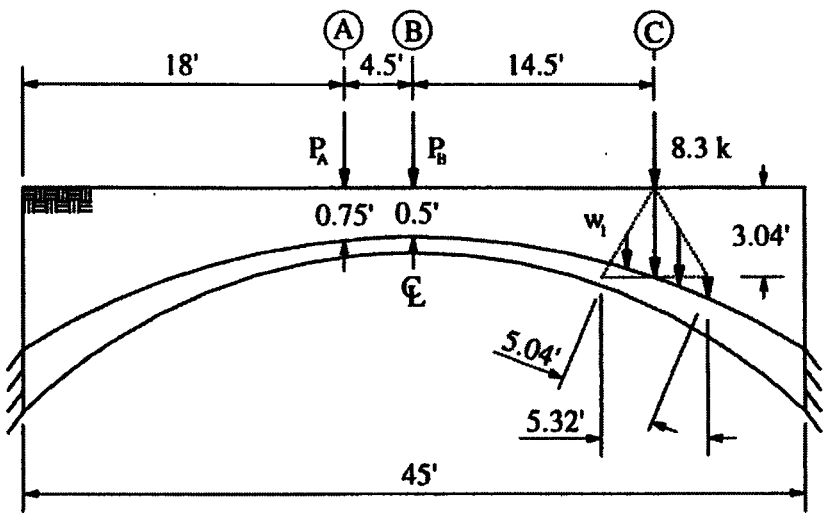

Wheel loads at A and B:

Fill < 2 ft

E = 4 + 0.06s = 4 + 0.06 (45)

E = 6.7 ft

$$P_A = \frac{10.85}{6.7}$$

P_A = 1.62 k/ft width

$$P_B = \frac{10.85}{6.7}$$

P_B = 1.62 k/ft width

Wheel load at C:

2 ft < Fill < 8 ft

h = 3.04 ft

wL = 1.75 h = (1.75)(3.04)

wL = 5.32 ft

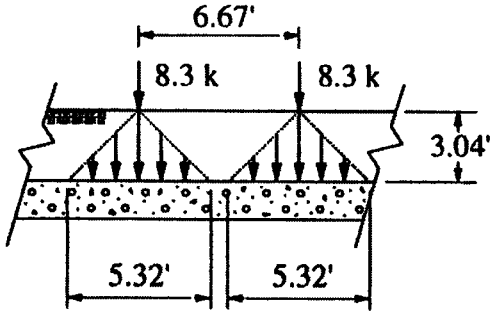

Cross-section at C

Loaded area = (5.32)(5.04)

Loaded area = 26.81 ft^2

$$\text{Wheel pressure} = \frac{8.3}{26.81}$$

Wheel pressure = 0.310 k/ft^2

w_l = Load per foot of arch = (0.310)(1)

w_l = 0.310 k/ft/ft width

M_T = 2.80 ft-k/ft width

M_T = Maximum theoretical live load moment at crown of arch due to test vehicle

P_T = 5.22 k/ft width

P_T = Maximum theoretical axial live load at crown of arch due to test vehicle

Theoretical Stress/Strain:

(Analyzed as an uncracked section)

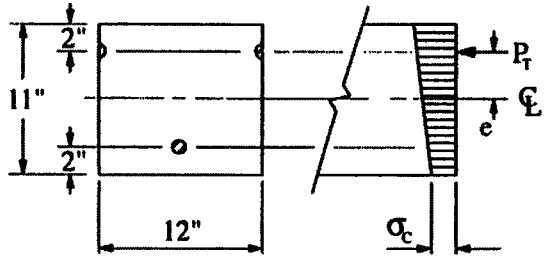

E_s = 29,000,000 psi

E_c = 3,600,000 psi

$$n = \frac{E_s}{E_c} = 8$$

Transformed Section:

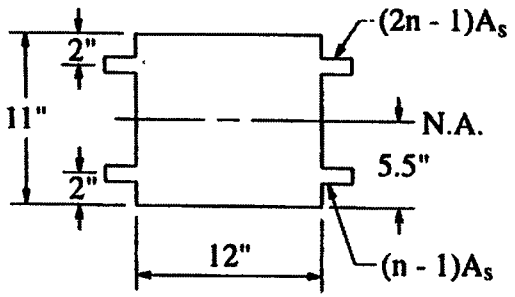

Transformed Area:

$A_{TOP} = (2n - 1)A_s = ((2)(8) - 1)(0.60)$

$A_{TOP} = 9.0 \text{ in.}^2$

$A_{BOT} = (n - 1)A_S = (8 - 1)(0.60)$

$A_{BOT} = 4.20 \text{ in.}^2$

$A_{TOT} = A_{TOP} + A_{BOT} + A_{ARCH} = 9.0 + 4.20 + (11)(12)$

$A_{TOT} = 145.2 \text{ in.}^2$

Location of Neutral Axis:

$\bar{y} = 5.62 \text{ in.}$

Moment of Inertia:

$$I_g = \frac{bh^3}{12} + Ad^2$$

$I_g = 1{,}491 \text{ in.}^4$

Concrete Stress/Strain:

$$\sigma_c = \frac{P_T}{A_{TOT}} + \frac{M_T y}{I_g}$$

$$\sigma_c = \frac{(5.22)(1000)}{145.2} + \frac{(2.80)(12)(1000)(5.62)}{1{,}491}$$

$\sigma_c = 163 \text{ psi}$

$$\varepsilon_c = \frac{\sigma_c}{E_c}$$

ε_c = Calculated theoretical strain in concrete

$$\varepsilon_c = \frac{163}{3{,}600{,}000}$$

$\varepsilon_c = 4.53 \times 10^{-5}$ in./in.

$\varepsilon_T = 8 \times 10^{-6}$ in./in.

ε_T = Strain produced from test vehicle

$$K_a = \frac{\varepsilon_c}{\varepsilon_T} - 1 = \frac{4.53 \times 10^{-5}}{8 \times 10^{-6}} - 1$$

$K_a = 4.66$

Factor K_b:

$K_b = K_{b1}K_{b2}K_{b3}$

Vehicle HS20:

K_{b1}: $\frac{T}{W} = \frac{M_T}{M_{LL}(1 + I)}$

$\frac{T}{W} = \frac{2.80}{(3.24)(1.1)}$

$\frac{T}{W} = 0.79$

$K_{b1} = 1.0$

Member behavior can be extrapolated to 1.33W for T/W > 0.7

Vehicle Type 3:

K_{b1}: $\frac{T}{W} = \frac{M_T}{M_{LL}(1 + I)}$

$\frac{T}{W} = \frac{2.80}{(2.21)(1.1)}$

$\frac{T}{W} = 1.15$

$K_{b1} = 1.0$

Member behavior can be extrapolated to 1.33W for T/W > 0.7

K_{b2}: 0.8 Routine inspection between 1 and 2 years

K_{b3}: 0.9 Fatigue does not control, no redundancy

$K_b = (1.0)(0.8)(0.9)$

$K_b = 0.72$

$RF_T = RF_c(1+K_aK_b)$

Vehicle HS20:

$RF_T = (5.75)(1 + (4.66)(0.58))$

$RF_T = 21.29$

Rating = (21.29)(36) = 766 T

Vehicle Type 3:

$RF_T = (8.44)(1 + (4.66)(0.72))$

$RF_T = 36.76$

Rating = (36.76)(25) = 919 T

Table B.6. Bridge VI: Rating Summary:

	Vehicle HS20				Vehicle Type 3			
	AASHTO LRFR		Modified Rating		AASHTO LRFR		Modified Rating	
	RF_c	R(tons)	RF_T	R(tons)	RF_c	R(tons)	RF_T	R(tons)
Arch	5.75	207	21.29	766.4	8.44	211	36.76	919